"Seismic Performance of Rehabilitated Wood Diaphragms"

by

David F. Peralta, Joseph M. Bracci and Mary Beth D. Hueste

Texas A&M University

Department of Civil Engineering

College Station, Texas 77843-3136

February 04, 2003

This research was conducted at Texas A&M University and was supported by the Mid-America Earthquake Center through the Earthquake Engineering Research Centers Program of the National Science Foundation under NSF award number EEC-9701785 and the Department of Civil Engineering and the Texas Engineering Experiment Station at Texas A&M University. Any opinions, findings and conclusions or recommendations expressed in this material are those of the authors and do not necessarily reflect those of the National Science Foundation and the other sponsors.

ABSTRACT

The objective of this research was to experimentally and analytically investigate the behavior of existing rehabilitated floor and roof wood diaphragms under in-plane lateral loads. The study focused on wood diaphragms characteristic of pre-1950's unreinforced masonry (URM) buildings found in the central and eastern regions of the United States.

Three diaphragm experimental specimens were built, tested, retrofitted and re-tested again under quasi-static reversed cyclic loading. The specimens differed in the type of sheathing, nailing pattern and the framing orientation with respect to the loading. One specimen represented a floor diaphragm, while the other two were more typical roof diaphragms, with one having a corner opening. A total of four retrofit methods were used on the specimens: (1) steel perimeter strapping and enhanced bolted connections; (2) a steel truss with enhanced bolted connections; (3) an unblocked plywood overlay and (4) a blocked plywood overlay. The in-plane lateral responses measured for the diaphragms were used to develop backbone curves, which were compared with those given in the FEMA 273 and FEMA 356 guidelines for seismic rehabilitation and some differences were found.

An analytical study of the diaphragm specimens was undertaken using two-dimensional finite element models. Inelastic quasi-static analyses were used to calibrate nailed connection slip behavior, which involves selecting hysteretic parameters for strength deterioration, stiffness degradation and pinching, to correlate with the experimentally measured diaphragm behavior under lateral loads. The analysis was extended to predict the lateral in-plane response for unretrofitted and retrofitted diaphragms of varying aspect ratios.

The experimental testing showed that all the retrofit methods provided an increase in strength and stiffness in varying degrees. The steel truss provided the most significant increase in strength and stiffness, followed by the blocked plywood overlay. The analytical data indicated that the FEMA 273 guidelines underpredict yield shear strength and overpredict stiffness, while the FEMA 356 guidelines underpredict the yield shear strength and stiffness of the diaphragm response. The results of the experimental and analytical studies were used to develop a proposed change to some of the parameters used to construct backbone curves for similar wood diaphragms according to the FEMA 356 guidelines.

ACKNOWLEDGMENTS

The members of the technical staff of the Testing, Machining and Repair Facility located in the Wisenbaker Engineering Research Center at Texas A&M University, especially Gerry Harrison, Jeff Perry and Andrew Fawcett, are appreciated for the time and energy devoted to the completion of the experimental testing. The authors also wish to thank EQE International for the information provided on existing construction in St. Louis and the undergraduate students, especially John Everett, Brian Dahm and William Beason, for their efforts in the construction of the specimens.

This research was conducted at Texas A&M University and was supported by the Mid-America Earthquake Center through the Earthquake Engineering Research Centers Program of the National Science Foundation under NSF award number EEC-9701785 and the Department of Civil Engineering and the Texas Engineering Experiment Station at Texas A&M University. Any opinions, findings and conclusions or recommendations expressed in this material are those of the authors and do not necessarily reflect those of the National Science Foundation and the other sponsors.

TABLE OF CONTENTS

Page

Page

LIST OF FIGURES

FIGURE Page

FIGURE Page

FIGURE Page

FIGURE Page

FIGURE Page

FIGURE Page

LIST OF TABLES

TABLE Page

1. INTRODUCTION

1.1 OBJECTIVES AND SCOPE

The study presented herein investigates the lateral in-plane load behavior of rehabilitated wood floor and roof diaphragms in unreinforced masonry (URM) buildings found in the Midwest region of the United States. This region has experienced some of the strongest earthquakes in the history of the country, which were caused by activity on the New Madrid seismic zone (Stelzer, 1999). Due to their importance immediately after a seismic event, the study focused on essential facility buildings constructed prior to 1950, which are considered to be at greater risk of failure than more modern buildings. From the different types of buildings in use as essential facilities, a firehouse was selected as the building prototype. Typical details for firehouses in the St. Louis, Missouri area were used to establish representative details for the region of interest. In the St. Louis area, most fire stations that were constructed prior to 1950 have diaphragms composed of nailed wood decking on wood joists. Fig. 1.1 shows a two-story URM fire station in St. Louis dated from the 1920's. The fire station is rectangular in plan and has many openings in the URM for windows and doors. Typical post 1950's construction for fire stations have diaphragms composed of steel bar joists supporting metal deck. Many structures in St. Louis have significantly deficient diaphragms based on the current state of knowledge (ATC, 1997b). One common deficiency is the lack of chord members along the edges of the diaphragm. Another deficiency is the insufficient connection between the diaphragm and the perimeter masonry walls. The expected behavior of these diaphragms under seismic excitation is highly uncertain and guidance is needed for their retrofit.

After the occurrence of the 1994 Northridge earthquake in California, it was found that the major source of damage in reinforced masonry buildings with wood roofs was failure of the out-of-plane connections between the perimeter masonry and panelized plywood roofs (Hamburger and McCormick, 1994). Nearly all types of wall

tie connections failed. A report by Bruneau (1994) identified that most of the failures found in URM buildings from earthquakes during the last 20 years are related with the diaphragm and the connections. These concerns are addressed in the present study by including representative connections in the experimental testing of the diaphragms.

FIG. 1.1 St. Louis Firehouse, circa 1920

The Mid-America Earthquake (MAE) Center is one of three national earthquake engineering research centers established by the National Science Foundation and is composed of a consortium of eight universities: the University of Illinois at Urbana-Champaign, Georgia Institute of Technology, Massachusetts Institute of Technology, the University of Memphis, University of Puerto Rico, St. Louis University, Texas A&M University and Washington University in St. Louis. The mission of the MAE Center is to develop through research, and disseminate through education and outreach, new engineering approaches necessary to minimize consequences of future earthquakes

across hazard-prone regions, including but not limited to, the eastern and central United States.

MAE Center projects initially focused on three areas: (1) Essential Facilities, (2) Transportation Networks and (3) Hazards Evaluation. The experimental part of this research presented herein forms part of the Essential Facilities Program, under Project ST-8, Performance of Rehabilitated Floor and Roof Diaphragms. Essential facilities are those buildings that support functions related to post-earthquake emergency response and disaster management. These include emergency management centers, police and fire stations, hospitals, potential shelters (including school buildings) and buildings that house emergency services. The availability and functionality of these buildings immediately following an earthquake is of the maximum importance.

The project scope includes an experimental and analytical investigation of the strength, stiffness and deformation capacities of models of existing and rehabilitated floor and roof diaphragms subject to quasi-static reversed cyclic in-plane loading. Lack of diaphragm chords, existence of openings and connection characteristics are investigated. Test results are reported consistent with parameters given in the FEMA guidelines for seismic rehabilitation of buildings, FEMA 273 (ATC, 1997a) and FEMA 356 (ASCE, 2000), which define nonlinear force-deflection behavior including expected lateral strength and stiffness. The analytical study of the diaphragms allows predicting the lateral response for a range of length-to-width aspect ratios. Recommendations to adjust the backbone curves of FEMA 356 are established. Conclusions from this research provided necessary information for other MAE Center projects focusing on essential facilities (Grubbs, 2002).

1.2 PRE-1950's URM BUILDINGS IN THE CENTRAL UNITED STATES

Construction of existing masonry buildings in the central and eastern parts of the United States dates back to the 1770's (ATC, 1997b). The majority of masonry buildings constructed before the twentieth century consisted of unreinforced clay-unit

masonry (URM); that is, without reinforcing steel within the walls. Wythes of brick were usually tied with brick headers spaced at every sixth or seventh course. Early mortars consisted of no more than lime and sand (ATC, 1997b).

The use of wood floors and roofs in masonry buildings is quite common in both existing and new construction. Buildings constructed before 1945 generally did not have plywood sheathing on the floors or roof. Sheathing in these buildings generally consisted of straight or diagonal sheathing boards (ATC, 1997b). The use of chords, members used to strengthen and stiffen diaphragms during lateral deformations, was not common either. The joist ends were cut diagonally (firecut) and supported in pocket holes in the masonry wall, having a bearing support of approximately 76 mm (3 in.). Typical pre-1950's fire stations in the St. Louis area included iron wall anchors, which were used to attach the diaphragm at about every fourth joist to the supporting URM wall (see Fig. 1.2). Some iron wall anchors have a star-shaped plate at one end that bears against the outer face of the wall and goes through the entire thickness of the wall so the other end attaches to the side face of the joist with nails (commonly referred as star anchors, see Figs. 1.3 and 1.4). Another type of wall anchor was a government anchor having a T-shaped or hooked end that is embedded in a mortar joint within the URM wall with the other end attached to the joist in the same manner as a star anchor.

Older structures, built prior to 1940, have members approaching nominal sizes, while newer buildings have lumber dimensions that are 13 mm (0.5 in.) to 25 mm (1.0 in.) smaller than the nominal size. The early nails were hand wrought. Around 1800, cut nails with a rectangular shank that tapers to a flat point were commonly used. In about 1880, wire nails began replacing the cut nails, but the use of cut nails continued well into the twentieth century (ATC, 1997b).

URM buildings have two basic structural components to resist lateral forces. The horizontal diaphragms of the building (floors and roof) distribute inertial in-plane lateral

forces to the vertical load resisting elements of the building (URM walls), which distribute the lateral forces to the foundation level.

Wood diaphragms are an assemblage of elements that typically includes three components: sheathing, framing and chords (see Fig. 1.5). The diaphragm is assumed to function as a horizontal beam that spans between the lateral load resisting walls. The moment is carried by the chords through axial action and the shear force is carried by the sheathing. Adequate nailing of the sheathing to the framing members is essential for this resistance to develop (Breyer, 1999).

In pre-1950's URM buildings roof or floor sheathing is composed of boards. Sheathing boards can be laid straight (see Fig. 1.5) or diagonal with respect to the main supporting joist members and are typically attached to the joists with two nails at the intermediate supporting members and with two or three nails at the ends of each sheathing board. The framing members that support the sheathing are composed of joist members supported vertically on the masonry wall and laterally by cross-bridging members. Bridging is typically made of short wood boards that are set nailed diagonally between joists to form an "X" pattern perpendicular to the joists. Rows of bridging are generally placed every 1.22 m to 2.44 m (4 ft. to 8 ft.) All the wood components of the diaphragm are attached together with nailed connections. Chord members are absent in this type of diaphragm construction.

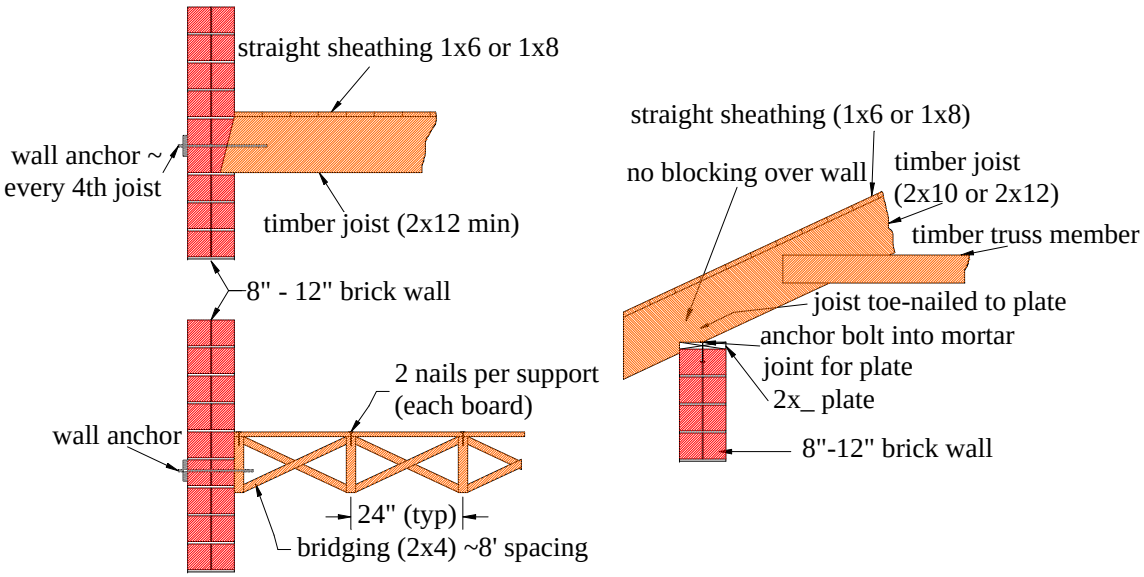

FIG. 1.2 Floor and Roof Connection Details in Pre-1950's Firehouses in St. Louis

FIG. 1.3 Typical Star Anchor (Left) and Wall Anchor (Center) Connections (photo taken in Fredrick, Maryland)

FIG. 1.4 Photograph of Star Anchor Taken from St. Louis, Missouri, URM Building

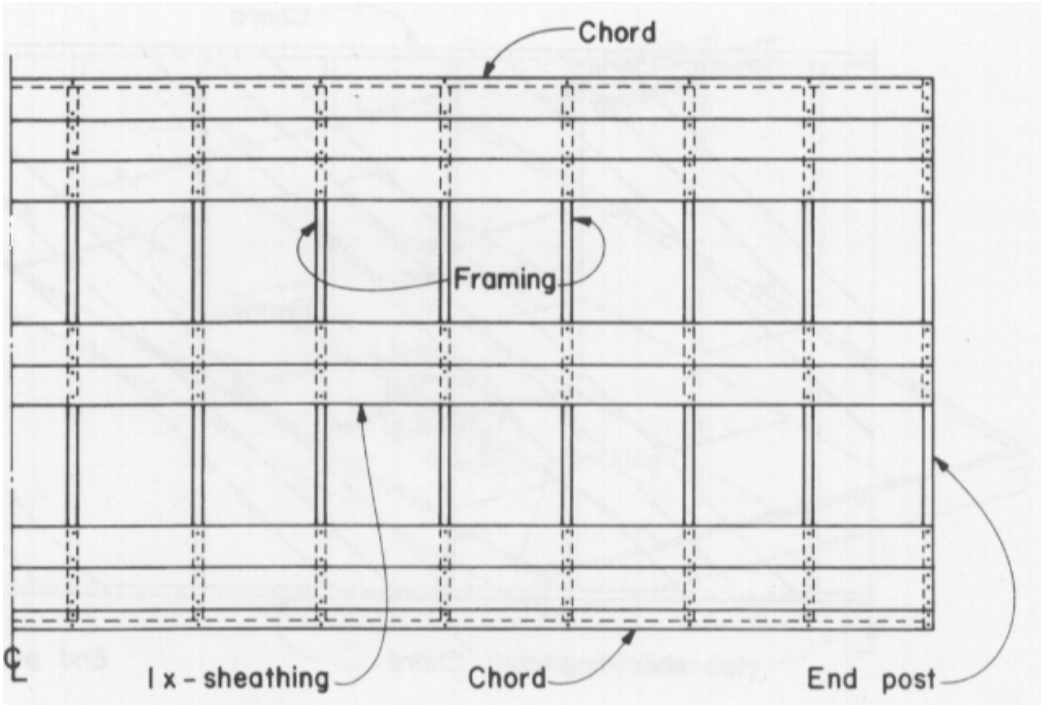

FIG. 1.5 Straight Sheathed Diaphragm Components (ATC, 1981)

1.3 RESEARCH PLAN

This research includes both an experimental and an analytical component. For the experimental component, three wood diaphragm specimens, all having a 2:1 aspect ratio, were built and attached to a pair of relatively rigid gravity and lateral load resisting frames that represented the supporting URM walls. The specimens were tested, retrofitted and retested using different rehabilitation methods including enhanced shear connectors and perimeter strapping, a steel truss attached to the bottom of the joists and connected to the support frames, and unblocked and blocked plywood overlays on top of the sheathing. The specimens were tested under quasi-static reversed cyclic loading to evaluate their in-plane lateral deformation performance.

Lateral displacement response at various points in the diaphragm, slip displacement between sheathing members, and strain response of the anchor connections were obtained. Backbone curves of the diaphragm's lateral load and displacement were constructed from the cyclic curves. The backbone curves were used to develop bilinear curves, which in turn provide the yield force and displacement of the diaphragm. Comparisons between the response of the unretrofitted diaphragms and the retrofits were made. The experimental results were also compared with the values given by the FEMA 273 and FEMA 356 seismic rehabilitation guidelines for determining the strength, stiffness and backbone curves of the diaphragms.

Detailed two-dimensional finite element meshes were developed to model the diaphragms tested in the experimental phase. An important concern for these models was to select an appropriate model of the nailed connections and parameters to simulate the nonlinear response of the diaphragm. Models for the nailed connection behavior found in the literature were used in this study. The in-plane diaphragm response was determined for monotonic and cyclic loading. To calibrate certain parameters needed for the cyclic analysis of the diaphragms, comparisons were made with the experimental results. Based on the calibrated modeling approach for diaphragms, predictions of the

in-plane response were made for similar unretrofitted and retrofitted diaphragms with a range of length-to-width aspect ratios. The predicted responses were used to develop recommendations to adjust the FEMA 356 backbone curves.

1.4 OUTLINE OF THIS STUDY

This report provides a detailed discussion of the experimental and analytical research program. Section 2 provides a review of previous research studies, which were identified as relevant to the current research program focusing on wood diaphragms. Descriptions of the test specimens and experimental loading system are given in Section 3. The response of the specimens under low-amplitude dynamic vibrations and quasi-static cyclic loading is given in Section 4. Comparisons of the measured response with the calculated in-plane strength, stiffness and deflections from the FEMA 273 and FEMA 356 guidelines are found in Section 5. Section 6 describes the finite element models of the diaphragm specimens for monotonic and cyclic quasi-static loading. Similar models were used to develop diaphragm models with different length-to-width aspect ratios, as discussed in Section 7. Predictions of the response were determined in this Section and comparisons were made for the set of diaphragms. Proposed revisions to the relevant FEMA 356 guidelines are described. Finally, Section 8 completes this report with a summary, conclusions and recommendations for further work.

2. PREVIOUS RESEARCH AND PRESENT STATE OF KNOWLEDGE

2.1 GENERAL

Since the early 1950's, a number of research institutions have conducted experimental testing of wood diaphragms to examine their behavior under lateral quasi-static and dynamic loading. A literature review of tests on straight sheathed and plywood panel diaphragms, as well as retrofits made on diaphragms of the same type, is presented below.

2.2 RESEARCH PERFORMED AT APA - THE ENGINEERED WOOD ASSOCIATION

APA - The Engineered Wood Association, formerly known as the American Plywood Association, has performed extensive research on plywood-sheathed diaphragms since the early 1950's. Fig. 2.1 shows a design table for horizontal plywood diaphragms for wind or seismic loading developed based on test results summarized below. The design table is recognized in the major model building codes currently in use. Three experimental testing programs were performed by Countryman (1952 and 1955) and Tissell (1967). The tests done by Countryman provided a design framework for the use of plywood as an efficient shear-resistant diaphragm. The research conducted by Tissell was due to changes in the manufacturing of plywood after the introduction of the U.S. Product Standard PS 1-66. The testing programs are summarized in Tables 2.1 through 2.3 and the test specimen layouts and dimensions are shown in Fig. 2.2.

Recently APA developed a plywood diaphragm applicable for design shears significantly higher than those previously published (Tissell and Elliott, 1997). Using multiple rows of fasteners in wide framing members, the diaphragm can develop the higher shear loads sometimes required for buildings in Seismic Zone 4, as specified in

the Uniform Building Code (ICBO, 1976). A table of recommended allowable shears for high loads (of wind or seismic origin) was derived based on the testing of eleven diaphragms loaded up to the limiting shear stress of the plywood (Tissell and Elliott, 1997). The research concludes that the most useful methods for obtaining higher diaphragm shear strength are: (1) increasing the number of fasteners per foot, which will require multiple rows of fasteners to prevent lumber from splitting, and (2) adding a second layer of plywood in the areas of high shear. The weakening effect of openings in diaphragms can be offset by designing for the increased shear around the openings due to the reduced plywood web area and for the tension and compression forces at each corner of the opening and at chords.

TABLE 2.1 Summary of 1952 Diaphragm Tests[1] (adapted from Countryman, 1952)

Test	Figure[2]	Framing[3]	Nailing[4] (in.)	Shear (lb./ft.)	
				Ultimate	Design
I	1-A	Blocked	8d common 3, 6, 12	1,380	360
II	1-A	Blocked	10d common 2, 4, 12	1,920	640
III	1-B	Blocked	8d common 3, 6, 12	1,756	360
IV	1-B	Unblocked	8d common 6, 6, 12	1,400	240

Note : 1 in. = 25.4 mm, 1 lb./ft. = 14.6 N/m

[1] Plywood used in all diaphragms was 13 mm (0.5 in.) Structural I C-D 32/16.
[2] Figure numbers corresponds to the diaphragms in Fig. 2.2.
[3] Framing was composed of 2x10 joists at 0.61 m (2 ft.) on center.
[4] According to nail size and nail type, nail spacing along the entire diaphragm boundary, at interior panel edges, and at interior panel nailing to intermediate joists.

TABLE 2.2 Summary of 1954 Diaphragm Tests (adapted from Countryman, 1955)

Test	Figure[1]	Framing[2]	Plywood[3]	Nailing[4] (in.)	Shear (lb./ft.)	
					Ultimate	Design
A	1-C	2x12 24” o.c. B	3/8” 24/0	8d 4, 6, 12	1,392	360
B	3-A	2x12 24” o.c. B	3/8” 24/0	10d 4, 6, 12	1,490	360
C	1-C	2x12 24” o.c. B	3/8” 24/0	8d 4, 6, 12	1,489	360
D	1-C	2x12 24” o.c. U	3/8” 24/0	8d 6, 6, 12	1,042	240
E	3-A	2x12 24” o.c. U	3/8” 24/0	8d 6, 6, 12	733	180
F	1-C	2x12 24” o.c. U	3/8” 24/0	8d 3, 3, 12	1,242	240
G	3-A	2x12 24” o.c. U	3/8” 24/0	8d 3, 3, 12	806	180
H	4-A	2x12 24” o.c. U	3/8” 24/0	8d 6, 6, 12	822	180
J	2-A	2x12 24” o.c. U	3/8” 24/0	8d 6, 6, 12	814	180
K	1-C	2x12 16” o.c. B	5/16” 20/0	6d 2, 3, 12	2,047	420
L	3-B	3x12 32” o.c. B	1/2” 32/16	10d 2.5, 4, 12	2,264	720
M	1-C	3x12 48” o.c. B	3/4” 48/24	10d 2.5, 4, 12	2,530	720
N	1-C	3x12 48” o.c. U	3/4” 48/24	10d 6, 6, 6	1,260	320
O	1-C	2x12 24” o.c. B	1/2” 32/16	8d 4, 6, 12	1,778	360
P	3-A	2x12 24” o.c. B	3/8” 24/0	8d 4, 6, 12	1,060	360

Note : 1 in. = 25.4 mm, 1 lb./ft. = 14.6 N/m

[1] Figure numbers corresponds to the diaphragms in Fig. 2.2.
[2] Size, spacing and blocked (B) or unblocked (U) framing
[3] APA Structural I Rated Sheathing, Exposure I.
[4] Common nail size, nail spacing along the entire diaphragm boundary, interior panel edges and, interior panel nailing to intermediate joists.

TABLE 2.3 Summary of 1966 Diaphragm Tests (adapted from Tissell, 1967)

Test	Figure[1]	Framing[2]	Plywood[3]	Nailing[4] (in.)	Shear (lb./ft.)	
					Ultimate	Design
1	1-D	2x8 24” o.c. B	3/8” 24/0	8d 4, 6, 12	1,350	360
2	1-D	2x8 24” o.c. B	3/8” 24/0	8d 4, 6, 12	1,155	360
3	1-D	2x8 24” o.c. B	3/8” 24/0	8d 4,6, 12	1,120	360
4	1-D	2x8 24” o.c. B	3/8” 24/0	8d 4,6, 12	1,160	360
5	1-D	2x8 24” o.c. B	3/8” 24/0	8d 4,6, 12	1,115	320
6	1-D	2x8 24” o.c. B	3/8” 24/0	8d 2, 3, 12	1,660	545
7	1-D	2x8 24” o.c. B	3/8” 24/0	8d 4, 6, 12	1,120	320
8	1-D	2x8 24” o.c. B	3/8” 24/0	8d 4,6, 12	1,125	320
9	1-D	2x8 24” o.c. B	1/2” 24/0	8d 4,6, 12	1,380	360
10	1-D	2x8 24” o.c. B	1/2” 24/0	10d 4, 6, 12	1,435	385
11	1-D	Double 2x8 48” o.c. B	1/2” 24/0	10d 2, 3, 12	1,860	590
12	1-D	Double 2x8 48” o.c. U	1-1/8” underlay T&G	8d 6, 6, 6	1,135	320
12A	1-D	Double 2x8 48” o.c. U	1-1/8” underlay T&G	8d 6, 6, 6	1,220	320
13	1-D	Double 2x8 48” o.c. B	1-1/8” underlay T&G	8d 6, 6, 6	2,050	480
14	1-D	Double 2x8 48” o.c. B	1-1/8” underlay T&G	10d 2, 3, 6	2,910	820
15	3-C	2x4 24” o.c. B	3/8” 24/0	8d 4, 6, 12	1,728	360
16	1-D	Steel Truss 48” o.c. B	3/4” 48/24	8d 2.5,4,12	2,960	600
17	2-B	Steel Truss 48” o.c. U	3/4” 48/24	#10 screw 16, 16, 16	600	190
18	2-B	Steel Truss 48” o.c. U	3/4” 48/24	#10 screw 6.5, 6.5, 16	720	190

Note : 1 in. = 25.4 mm

[1] Figure numbers corresponds to the diaphragms in Fig. 2.2.

[2] Blocked (B) or unblocked (U) framing.

[3] The plywood used was APA Structural I rated Sheathing, Exposure 1.

[4] Nail size, nail spacing along the entire diaphragm boundary, at interior panel edges and at interior panel nailing to intermediate joists.

TABLE A-1

RECOMMENDED SHEAR IN POUNDS PER FOOT FOR HORIZONTAL PLYWOOD DIAPHRAGMS WITH FRAMING OF DOUGLAS FIR, LARCH OR SOUTHERN PINE[a] FOR WIND OR SEISMIC LOADING

					Blocked Diaphragms				Unblocked Diaphragms	
					Nail Spacing (in.) at diaphragm boundaries (all cases), at continuous panel edges parallel to load (Cases 3 & 4), and at all panel edges (Cases 5 & 6)[b]				Nails Spaced 6" max. at supported edges[b]	
					6	4	2-1/2[c]	2[c]	Case 1 (no unblocked edges or continuous joints parallel to load)	All other configurations (Cases 2, 3, 4, 5 & 6)
Plywood Grade[d]	Common Nail Size	Minimum Nail Penetration in Framing (inches)	Minimum Plywood Thickness (inch)	Minimum Nominal Width of Framing Member (inches)	Nail Spacing (in.) at other panel edges (Cases 1, 2, 3 & 4)					
					6	6	4	3		
STRUCTURAL I	6d	1-1/4	5/16	2	185	250	375	420	165	125
				3	210	280	420	475	185	140
	8d	1-1/2	3/8	2	270	360	530	600	240	180
				3	300	400	600	675	265	200
	10d	1-5/8	15/32	2	320	425	640	730[c]	285	215
				3	360	480	720	820	320	240
C-D C-C and other APA grades except Species Group 5	6d	1-1/4	5/16	2	170	225	335	380	150	110
				3	190	250	380	430	170	125
			3/8	2	185	250	375	420	165	125
				3	210	280	420	475	185	140
	8d	1-1/2	3/8	2	240	320	480	545	215	160
				3	270	360	540	610	240	180
			15/32	2	270	360	530	600	240	180
				3	300	400	600	675	265	200
	10d	1-5/8	15/32	2	290	385	575	655[c]	255	190
				3	325	430	650	735	290	215
			19/32	2	320	425	640	730[c]	285	215
				3	360	480	720	820	320	240

(a) For framing of other species: (1) Find species group of lumber in AF&PA National Design Specification. (2) Find shear value from table for nail size, and for Structural I plywood (regardless of actual grade). (3) Multiply value by 0.82 for species with specific gravity of 0.42 to 0.49, and 0.65 for species with a specific gravity of less than 0.42.

(b) Space nails 12 in. o.c. along intermediate framing members.

(c) Framing shall be 3-in. nominal or wider, and nails shall be staggered where nails are spaced 2 in. or 2-1/2 in. o.c., and where 10d nails having penetration into framing of more than 1-5/8 in. are spaced 3 in. o.c. Exception: Unless otherwise required, 2-in. nominal framing may be used where full nailing surface width is available and nails are staggered.

(d) Current nomenclature for APA trademarked C-D and C-C panels is APA Rated Sheathing. C-D panels typically are classified Exposure 1 and C-C panels are classified Exterior. Structural I panels are so marked. See *APA Design/Construction Guide – Residential & Commercial* for recommended shear values for APA performance-rated wood structural panels.

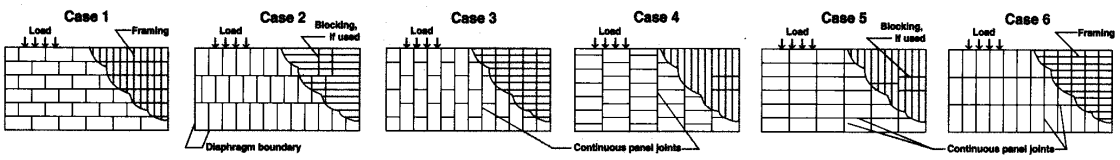

FIG. 2.1 APA Design Table for Horizontal Diaphragms (Tissell and Elliott, 1997)

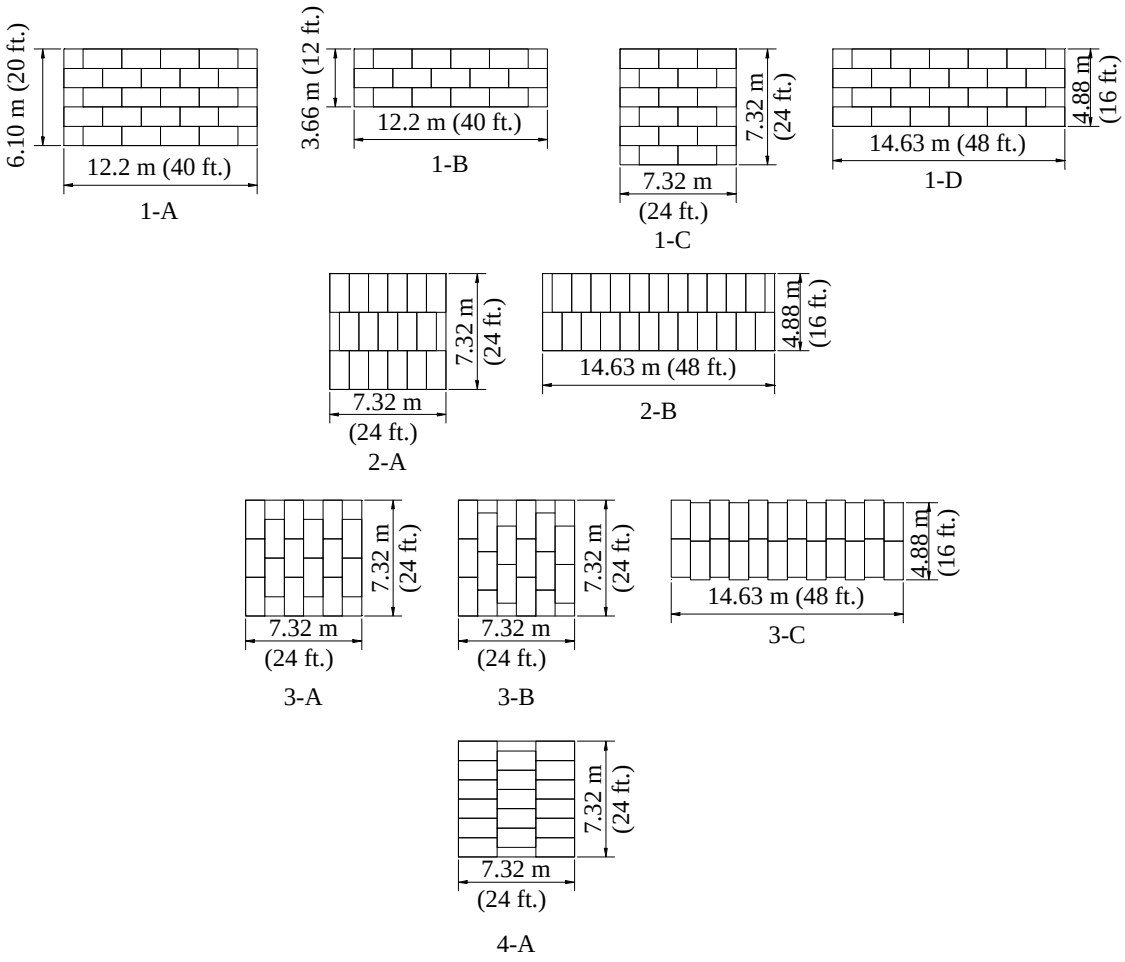

FIG. 2.2 Layout of Test Specimens (adapted from Tissell and Elliott, 1997)

2.3 RESEARCH PERFORMED AT OREGON STATE UNIVERSITY

A testing program was conducted at the Forest Products Laboratory at Oregon State University from 1952 to 1955. Tests of 16 full-scale lumber and four plywood-sheathed roof diaphragms of various sizes were conducted in order to determine the strength and stiffness at various deformation levels while varying certain characteristics of the diaphragm, including plywood thickness, lumber sheathing humidity, nailing pattern, type of boundary members, bridging, blocking, connections, openings and width-to-length ratios (Johnson, 1956). Most of the diaphragms had dimensions of 6.1 m (20 ft.) by 18.3 m (60 ft.). The lumber used was Grade No. 2, Douglas Fir surfaced on

four sides. Joists were 2x10 sections and lumber sheathing consisted of 1x6 sections. The plywood was Douglas-Fir interior unsanded C-D sheathing grade, with thicknesses of 9.5 mm (0.375 in.) and 13 mm (0.5 in.). Three sizes of common wire nails were used: 8-, 10- and 16-penny. The 10-penny nails were used to toenail the 2x10 cut-in blocks to the joists. The 16-penny nails were used to nail together 51 mm (2 in.) wide framing members to plates and other blocking and to nail stiffening members and continuous headers to joists and end posts. The 16-penny nails were used to nail together the 2x3 sheathing boards. Bolted splices were made using 19 mm (0.75 in.) diameter by 102 mm (4 in.) long machine bolts with washers. Plate splices had two bolts and six 16-penny nails on each side of the joint. All the diaphragms had 2x10 to 2x12 chord members, and diaphragm 14 had additional 2x12 chord members. Table 2.4 summarizes the details of each diaphragm specimen.

Lateral loads were quasi-statically applied in increasing monotonic displacements by hydraulic jacks at the fifth points of one chord of the specimen. Principal deformation readings were taken at mid-span of the unloaded chord and the end posts. Lateral and vertical movements of the sheathing were measured. Fig. 2.3 shows the lateral deflection response of the diaphragms tested.

Evaluation of the tests led to the following general conclusions (Johnson, 1956):

1. “The inadequacy of longitudinal lumber sheathing in resisting lateral loads was demonstrated;
2. The use of dry lumber in a longitudinally lumber sheathed diaphragm increases the strength about 40% over that obtained with green lumber;
3. The addition of 2x12 longitudinal chord members to a 2x3 laminated deck diaphragm constructed with simple 2x10 chords increased the strength by 30% (see Fig. 2.3 a);
4. The unblocked plywood-sheathed diaphragm deflected considerably more than the blocked diaphragm.”

TABLE 2.4 Construction Details of Diaphragms Tested at Oregon State University from 1952-1955 (adapted from Johnson, 1956)

Test	Dimensions (ft. x ft.)	Framing[1] (in.)	Sheathing[2] (in.)	Nailing[3] (in.)
1	20x60	2x10 24 o.c. U, G, 1	1x6 G, L	8d 2, 2
2	20x60	2x10 24 o.c. U, G, 2	1x6 G, D	8d 3, 3
3	20x60	2x10 24 o.c. U, G, N	1x6 G, D	8d 3, 3
4	20x60	2x10 24 o.c. U, D, 1	1x6 D, L	8d 2, 2
5	20x60	2x10 24 o.c. U, D, 1	1x6 D, L	8d 2, 2
6	20x60	2x10 24 o.c. U, G, 2	1x6 G, D	8d 3, 3
7	20x60	2x10 24 o.c. U, G, 2	1x6 G, D	8d 3, 3
8	20x60	2x10 24 o.c. U, G, 2	1x6 G, H	8d 3, 3
9	20x60	2x10 24 o.c. U, G, 1	0.375 Plywood	8d 6, 6, 12
10	20x60	2x10 24 o.c. B, G, 1	0.375 Plywood	8d 4, 6, 12
11	20x60	2x10 24 o.c. U, G, 1	0.375 Plywood	1.25 staples 2.625, 4, 8
12	12x60	2x10 24 o.c. B, D, N	0.5 Plywood	8d 4, 6, 12
13	20x60	2x10 24[4] o.c U, G, N	2x3 G, L	16d 1, 1
14	20x60	2x10 24[4] o.c U, G, N	2x3 G, L	16d 1, 1
15	20x60	2x10 24 o.c. U, G, 1	1x6 G, L	8d 2, 3
16	20x40	2x10 24 o.c. U, G, 1	1x6 G, L	8d 2, 3
17	20x60	2x10 24 o.c. U, G, 1	1x6 G, L	8d 2, 3
18	20x80	2x10 24 o.c. U, G, 1	1x6 G, L	8d 2, 3
19	12x60	2x10 24 o.c. U, G, 1	1x6 G, L	8d 2, 3

Note: 1 in. = 25.4 mm, 1 ft. = 304.8 mm

[1] Joist size, joist spacing, blocked (B)/unblocked (U), green (G)/dry (D) (15% moisture content, MC), 2x3 diagonal bridging: 1 center row (1) /2 rows (2) /None (N).

[2] Sheathing dimensions, green (G)/dry (D) (12% MC), diagonal (D)/herringbone (H)/ longitudinal (L).

[3] Nail size, number of nails in board sheathing at bearings and at ends of boards or nail spacing in plywood along short flange, at panel edges and intermediate bearings.

[4] Double joists 1.83 m (6 ft.) on centers.

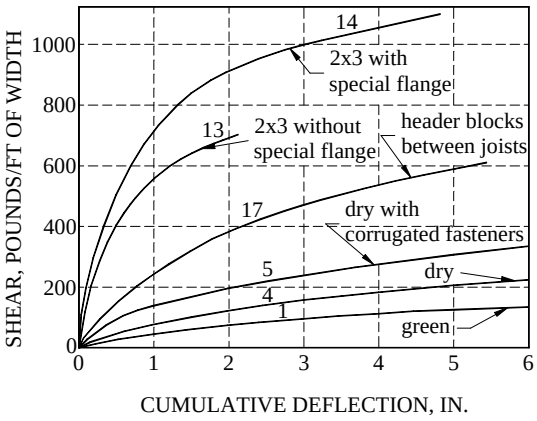

a) Maximum deflections under lateral loads for five longitudinally lumber-sheathed 20'x60' roof diaphragms

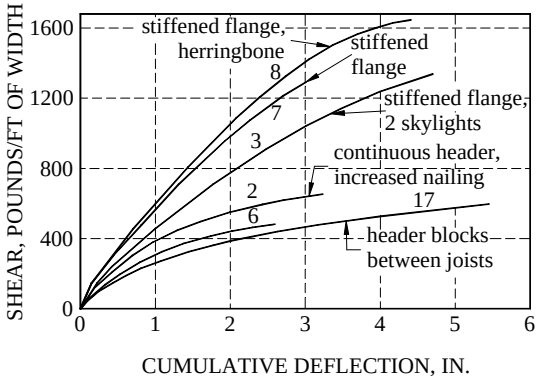

b) Maximum deflections under lateral loads for diagonally lumber-sheathed 20'x60' roof diaphragms

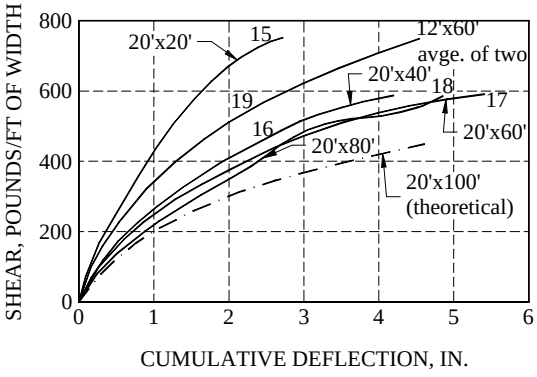

c) Maximum deflections under lateral loads for diagonally lumber-sheathed roof diaphragms of different width/lengths

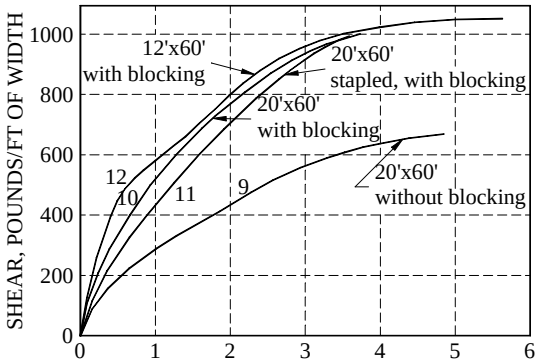

d) Maximum deflections under lateral loads for four plywood-sheathed roof diaphragms

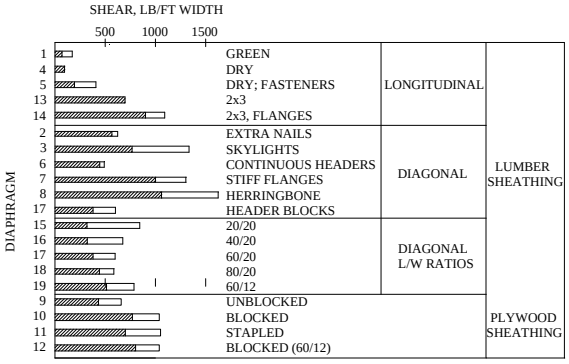

e) Final loads and loads at deflection of 1/360 length (shaded) for 20 full-scale roof diaphragms tested in 1952-1955 at the Oregon Forest Products Laboratory

FIG. 2.3 Test Results at Oregon State University (adapted from Johnson, 1956)

2.4 RESEARCH PERFORMED BY ABK

Research performed by ABK – Agbabian, Barnes and Kariotis – for the National Science Foundation developed a methodology for mitigation of seismic hazards in existing unreinforced masonry buildings (ABK, 1981). One of the experimental programs was focused on horizontal diaphragms subjected to quasi-static, cyclic, in-plane displacements and dynamic in-plane shaking.

Full-scale component tests on 14 diaphragms of 6.1 m (20 ft.) by 18.3 m (60 ft.) wood sheathed and metal deck specimens were subjected to 139 test sequences, including quasi-static and dynamic loading. Table 2.5 lists a description of the diaphragms. Dynamic tests used effective peak accelerations (EPA) of 0.1g to 0.4g. The wood sheathed diaphragms were constructed using a wood framing system fabricated with 4x12 edge and end members and 2x12 joists. All lumber sheathing was 1x6 Douglas Fir and the plywood was Douglas Fir Structural I, exterior glue, Grade C-D. The sheathing was attached to the framing system with 8d nails. The retrofit procedures consisted of the application of chords, overlays and roofing attachments.

The tests demonstrated that diaphragms have highly nonlinear and hysteretic stiffness characteristics. The dynamic test results show that the dynamic response of diaphragms is dominated by nonlinear, hysteretic characteristics for EPA's greater than 0.1g. For the most part, the diaphragm specimens were relatively undamaged for all levels of earthquake ground motion. The built-up roofing adds stiffness as long as it remains attached and detachment occurred at EPA's of approximately 0.2g. It was verified that anchorage forces develop between the diaphragms and the connecting walls. The methodology developed from this research program was later adapted for the Seismic Strengthening Provisions for Unreinforced Masonry Bearing Wall Buildings in the Uniform Code for Building Conservation (ICBO, 1997). Findings from this research program are referenced in the FEMA 273 guidelines (ATC, 1997a).

TABLE 2.5 Diaphragm Specimen Description (adapted from ABK, 1981)

Diaphragm	Description
Q	20-ga steel decking, unfilled, unchorded, button-punched seams 18 in. o.c.
R	20-ga steel decking, unfilled, chorded, button-punched seams 6 in. o.c.
C	0.5 in. plywood, unblocked, unchorded, built-up roofing
D	0.5 in. plywood, unblocked, chorded, built-up roofing, retrofit nailing
B	0.5 in. plywood, unblocked, chorded
E	1x6 straight sheathing, unchorded, built-up roofing
E_1	1x6 straight sheathing, unchorded, built-up roofing, retrofit nailing
H	1x6 straight sheathing, 0.3125 in. plywood overlay, chorded
I	1x6 diagonal sheathing, unchorded, built-up roofing
I_1	1x6 diagonal sheathing, unchorded, built-up roofing, retrofit nailing
K	1x6 diagonal sheathing, 1x6 straight sheathing overlay, chorded
N	0.5 in. plywood, blocked, chorded
P	0.75 plywood, 0.75 plywood overlay, blocked, chorded
S	20-ga steel decking, 2.5 in. concrete fill, chorded, button-punched seams 18 in. o.c.

Note: 1 in. = 25.4 mm

2.5 RESEARCH PERFORMED AT WEST VIRGINIA UNIVERSITY

A team of investigators from West Virginia University (Zagajeski et al., 1984) conducted a research investigation into the in-plane shear response of plywood timber floor diaphragms. The in-plane shear force-deformation behavior of several full-scale 4.9x7.32 m (16x24 ft.) and 4.9x4.9 m (16x16 ft.) plywood-sheathed timber diaphragms in response to dynamic, quasi-static monotonic and quasi-static cyclic loading was evaluated. In addition, the damping and natural frequency of the diaphragms and the local nail-slip response were studied. The latter study was based on the response of small-scale specimens, which simulated typical plywood panel to joist connections.

The principal objective of the experimental program was to determine how timber diaphragm details influence behavior in response to large, in-plane shear deformations. The details considered include: use of blocking; effect of openings; plywood thickness; use of corner stiffeners; and nail size used in substructure connections.

Framing members were 2x10 and 2x6 Spruce-Pine-Fir No. 2 joists and plywood panels were (13 mm) 0.5 in. C-D exterior grade, as structural grade panels were not readily available. Fasteners were 8d and 10d common nails. The nail spacings used in the plywood were 102, 152 and 203 mm (4, 6 and 8 in.) A total of 25 tests were conducted by systematically varying the above parameters. Blocking was spaced at 1.63 m (5 ft. 4 in.) intervals. In a second test series, the blocking arrangement was placed along all plywood boundaries perpendicular to the joists. Corner openings were considered in some diaphragms.

Diaphragms were instrumented to measure applied load, lateral shear displacement, inter-panel nail slip, slip between the test diaphragm and steel load frame and support displacement. The load was applied using a 89 kN (20 kips) capacity MTS actuator. Quasi-static and dynamic loading were applied to the specimens. The dynamic loading was a sinusoidal load with a frequency of 5 Hz.

The experimental results demonstrated that the in-plane shear response is controlled by the nail-slip characteristics of the joints between adjacent plywood panels and between panels and boundary elements. An equivalent viscous hysteretic damping ratio of 15% to 20% of the critical damping was determined from the tests. It was found that blocking significantly improves behavior. The effect of a thicker plywood panel is negative in the nail-slip response, because of a reduction in nail penetration depth into the supporting joists.

2.6 RESEARCH PERFORMED AT THE UNIVERSITY OF OTTAWA

Recently, a research program was conducted at the University of Ottawa to investigate the flexible-floor and rigid wall interaction in old URM buildings (Paquette and Bruneau, 2000). The research included pseudo-dynamic testing of a full-scale one-story URM specimen with a wood roof. The diaphragm consisted of wood joists sheathed with diagonal boards and a straight board overlay. The diaphragm was

anchored to the walls with through-wall bolts as specified in the Uniform Code for Building Conservation (ICBO, 1997). The rectangular shaped specimen was built with two wythes solid brick walls and type O mortar was used. The specimen had two load-bearing shear walls, each with two openings. The test set-up used one actuator at the diaphragm center-span. The specimen was subjected to a synthetic ground motion for La Malbaie, Canada with a peak ground acceleration of 0.453g. The wood diaphragm showed a nonlinear inelastic hysteretic response. The diaphragm developed minor damage as some nails popped out at the ends of the diaphragm.

2.7 CUREE - CALTECH WOODFRAME PROJECT

The Consortium of Universities for Research in Earthquake Engineering (CUREE) and the California Institute of Technology partnered together in a four-year project starting in 1999. The motivation for the project came from the large amount of damage to wood residential buildings, which occurred during the 1994 Northridge earthquake. The intent of the project was to develop reliable and economical methods of improving woodframe building performance in earthquakes. To achieve that intent a wide range of issues were investigated, ranging from detailed studies of economic losses to experiments studying the earthquake behavior of full-scale buildings. Tests on plywood panel diaphragms were performed to study the factors that contribute to the stiffness (i.e., the sheathing nailing, and presence of chords, openings, blocking, and adhesives). Several findings from the tests and recommendations have been made as follows (CUREE, 2002):

1. Shear wall testing demonstrated the adverse effects of unbalanced nailing patterns on shear wall capacity. The same principle is applicable to the case of diaphragms. The nailing pattern around each panel should be symmetric (the number of nails in a line along each of the panel’s parallel edges should be equal).

2. The use of adhesives between the joists and plywood increased the diaphragm shear stiffness up to a maximum of 46%. The effect of adhesives should be included in the shear deformation portion of an equation estimating diaphragm deflections.
3. Flexural stiffness of two specimens dropped 42% and 71% with the removal of the diaphragm chord.
4. Blocking increased the shear stiffness by 10% to 300%. The addition of blocking is an effective method for reducing the deflections, by increasing the shear stiffness of the diaphragm. The combination of blocking and adhesives is even more effective.
5. Walls at the diaphragm perimeter were observed to significantly increase the stiffness of diaphragms without chords and moderately increase the stiffness of diaphragms with chords. Additional research is recommended to actively include the walls in the design of diaphragms.
6. Diaphragm openings can have a significant effect on the diaphragm global stiffness and local shear stiffness.

2.8 SUMMARY

Some differences can be mentioned from the investigations presented in the previous sections. In the APA tests (Countryman, 1952, 1955, Tissell, 1967) the purpose was to demonstrate the feasibility for using plywood as a shear resistant material. The specimens covered a range of length-to-width aspect ratios, ranging from 1:1 to 3:1. Unidirectional, cyclic static loading was used. The experimental program performed at Oregon State University (Johnson, 1956) focused on straight and diagonal sheathing diaphragms and some plywood sheathed diaphragm specimens. The specimens had length-to-width aspect ratios ranging from 1:1 to 4:1. Unidirectional, cyclic 5-point static loading was used for the tests. The tests conducted by ABK (ABK, 1981) included steel decking, plywood diaphragms, straight and diagonal sheathed diaphragms and used only a length-to-width aspect ratio of 3:1. Three-point quasi-static cyclic loads and dynamic loads were used in the tests. The results and developments from this research program are used in the Uniform Code for Building Conservation

(ICBO, 1997) and FEMA 273 guidelines (ATC, 1997a) for wood diaphragms. The research performed at West Virginia University (Zagajeski et al, 1984) used plywood sheathed diaphragms. The specimen length-to-width aspect ratios used were 1:1 and 1.5:1. Dynamic, monotonic and cyclic quasi-static loads were applied to the diaphragms. The research included analytical modeling of the diaphragm behavior considering the nonlinearity from the nail-slip. Recently, the University of Ottawa (Paquette and Bruneau, 2000) conducted a pseudo-dynamic test of a full-scale one-story rectangular-shaped URM building with a wood diaphragm composed of diagonal sheathing and a straight sheathing overlay to investigate the flexible-floor and rigid wall interaction under ground motions.

3. EXPERIMENTAL PROGRAM

3.1 GENERAL

This section provides a general description of the experimental testing program, including specimen layouts and details, retrofit details, load test assembly, instrumentation, data acquisition and loading protocol. A total of three specimens were constructed, tested, retrofitted and retested in the Texas Engineering Experiment Station's Testing, Machining and Repair Facility at Texas A&M University.

3.2 DESCRIPTION OF DIAPHRAGM SPECIMENS

3.2.1 General Description

A total of three diaphragm specimens were constructed with elements and connection details of typical pre-1950's wood floor and roof diaphragms, as described in Section 1. Many materials and construction details used for the diaphragm specimens were common to all three diaphragms tested. These common details are described in this section, while the following sections describe details that are unique for each specific diaphragm.

The materials of the test diaphragms were of commonly available lumber grades and sizes. Diaphragm specimens were constructed at a reduced scale of approximately 1:2 and had length-to-width dimensions of 7.32 m by 3.66 m (24 ft. x 12 ft.), or an aspect ratio of 2:1, for all the diaphragm specimens. A general view of the experimental test setup for each diaphragm is shown in Fig. 3.1. The figure shows the load path starting from the actuator to the loading frame, to the diaphragm, to the wall ("star") anchors, to the support frames and finally to the reaction floor.

The diaphragms had a framing structure composed of an arrangement of 2x10 beam joists (2x10 Southern Pine Grade II lumber) running in the long direction for the first specimen and short direction for the other two specimens. The diaphragm sheathing

was composed of 1x4 center matched (tongue & groove) Southern Pine class C boards running in the short direction for the first specimen and square edged 1x6 Southern Pine Grade II lumber boards running staggered in the long direction for the other two specimens. Actual dimensions of the boards are shown in Fig. 3.2. Bridging members composed of 2x4 angled boards were placed in rows spaced at 2.43 m (8 ft.). Bridging boards were nailed in pairs between the beam joists using 10d common nails. Replicated wall ("star") anchors (discussed in Section 1.2) were used to connect the diaphragm assemblage to the gravity and lateral load support system, which was represented in these tests by the rigid steel reaction frames. Steel anchors were fabricated in the laboratory based on the dimensions of an actual star anchor taken from a building in St. Louis (see Fig. 1.4).

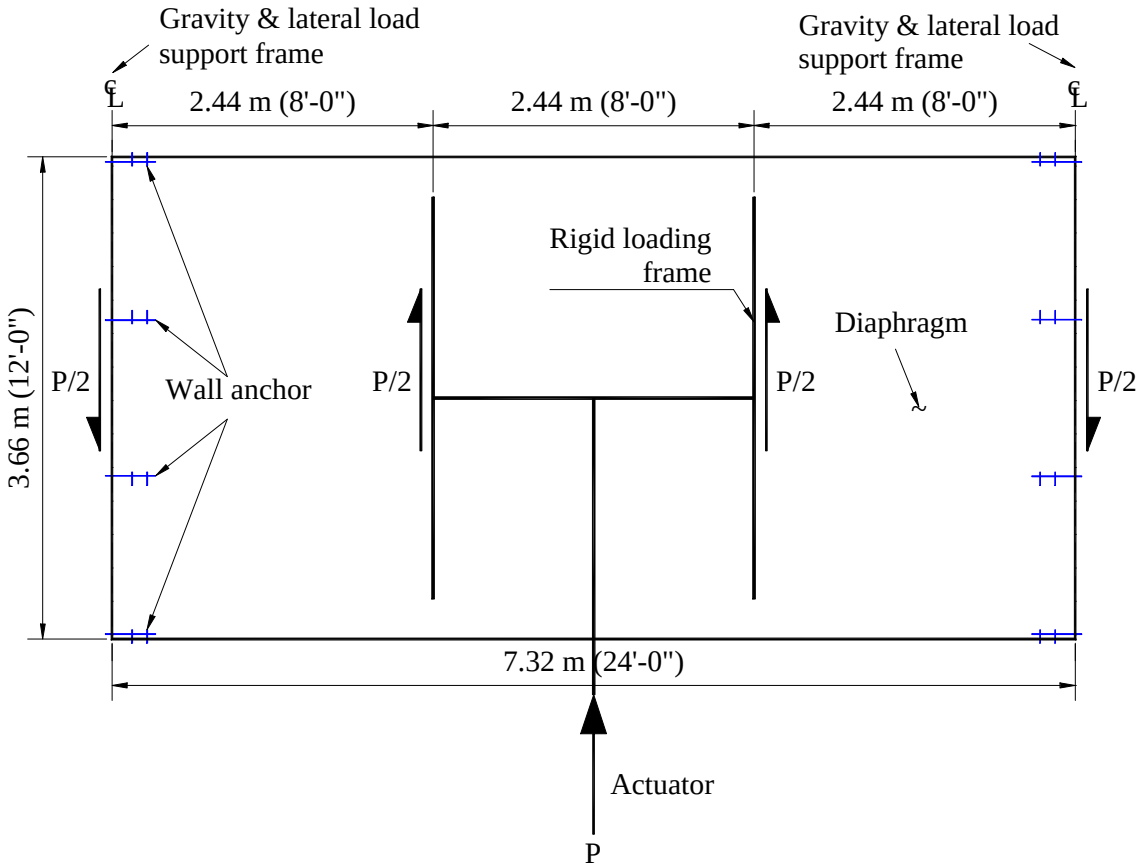

FIG. 3.1 General Diaphragm Specimen Dimensions and Load Path – Plan View

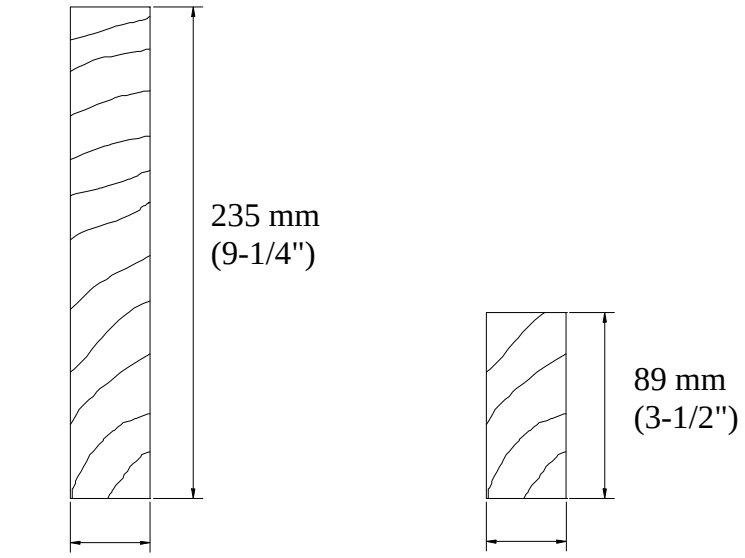

(a) Framing Cross Section

(b) Nails

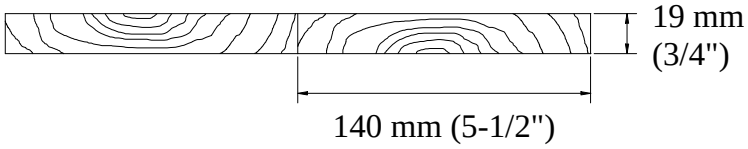

Square-edged 1x6 Boards Cross Section

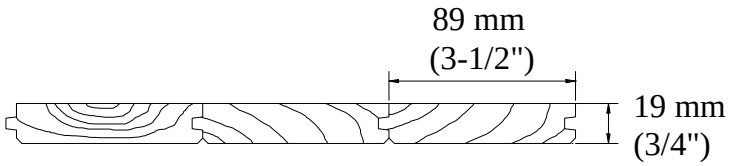

Center matched (T&G) 1x4 boards

(c) Sheathing Cross Section

FIG. 3.2 Nominal Lumber Dimensions and Nail Types

Three specimens were constructed: (1) a tongue & groove (T&G) single straight sheathed diaphragm, labeled MAE-1; (2) a square edged single straight sheathed diaphragm (MAE-2); and (3) a square edged single straight sheathed diaphragm with a corner opening (MAE-3). After initial testing, all three specimens were retrofitted and retested again. Each specimen was built with new materials, with the exception of the steel truss, which was used to retrofit diaphragms MAE-1 and MAE-2.

3.2.2 Tongue & Groove Single Straight Sheathed Diaphragm

This section describes the construction of a single straight sheathed diaphragm using tongue & groove boards and two retrofit procedures made on the same diaphragm in order to reinforce the connections of the diaphragm to the reaction frames and increase the in-plane lateral stiffness of the diaphragm, based on the findings of the original testing.

3.2.2.1 Diaphragm MAE-1

The framing of the diaphragm MAE-1 was composed of nominal 2x10 beam joists spanning 7.32 m (24 ft.) and spaced 406 mm (16 in.) on center (o.c.). The beam joists were supported at their ends on the two gravity and lateral load support frames and one gravity load support frame at their midspan (see Figs. 3.3). The beam joists had a bearing length of approximately 76 mm (3 in.) on the bottom flange of the steel beam of the support frame (described later in Section 3.3), similar to the bearing length provided in typical unreinforced masonry (URM) construction (see Section 1.2). The beam joist ends were cut diagonally with a slope of 1:3 to make the “fire-cuts” typically found in URM buildings (see Fig. 3.3c).

The framing of the diaphragm was sheathed with center matched (tongue & groove) 1x4 by 3.66 m (12 ft.) boards of Southern Pine (Grade C) oriented at right angles to the joists (see Fig. 3.3). Blind-nailing (nails toe-nailed through the tongue) was used to secure the sheathing to the beam joists at every intersection using one 10d

finishing head type nail per beam joist. Power-driven nails were used to attach the sheathing to the beam joists. The framing was supported and attached to the gravity and lateral load support frame with a simulated star anchor at every fourth beam joist, making a total of four anchors for each support frame (see Fig. 3.3c).

To experimentally represent the wall ("star") anchors found in pre-1950's URM construction, replica anchors were fabricated by welding a 15.9 mm (0.625 in.) diameter threaded rod fillet ASTM GR 36 to a 6.4 mm x 25.4 mm (0.25 in. x 1 in.) ASTM GR 36 strapping plate (see Fig. 3.3d). The flat plate portion of the anchor had two holes through which 8d nails were inserted to attach the star anchor to the joist. Also a 90-degree bend, using a very small bend radius, at the end of the plate was made for embedment into a notch made in the side face of the joist. The other end of the anchor had a heavy washer and was bolted to the web of the steel beam of the supporting frame.

Three rows of bridging boards were symmetrically placed running in the short direction at 2.44 m (8 ft.) o.c. (see Fig. 3.3b). The bridging consisted of two 2x4 angled boards placed between the beam joists that were toe nailed to the beam joists with two 8d common wire nails at each end.

(a) Photograph

FIG. 3.3 Tongue & Groove (T&G) Single Straight Sheathed Diaphragm MAE-1

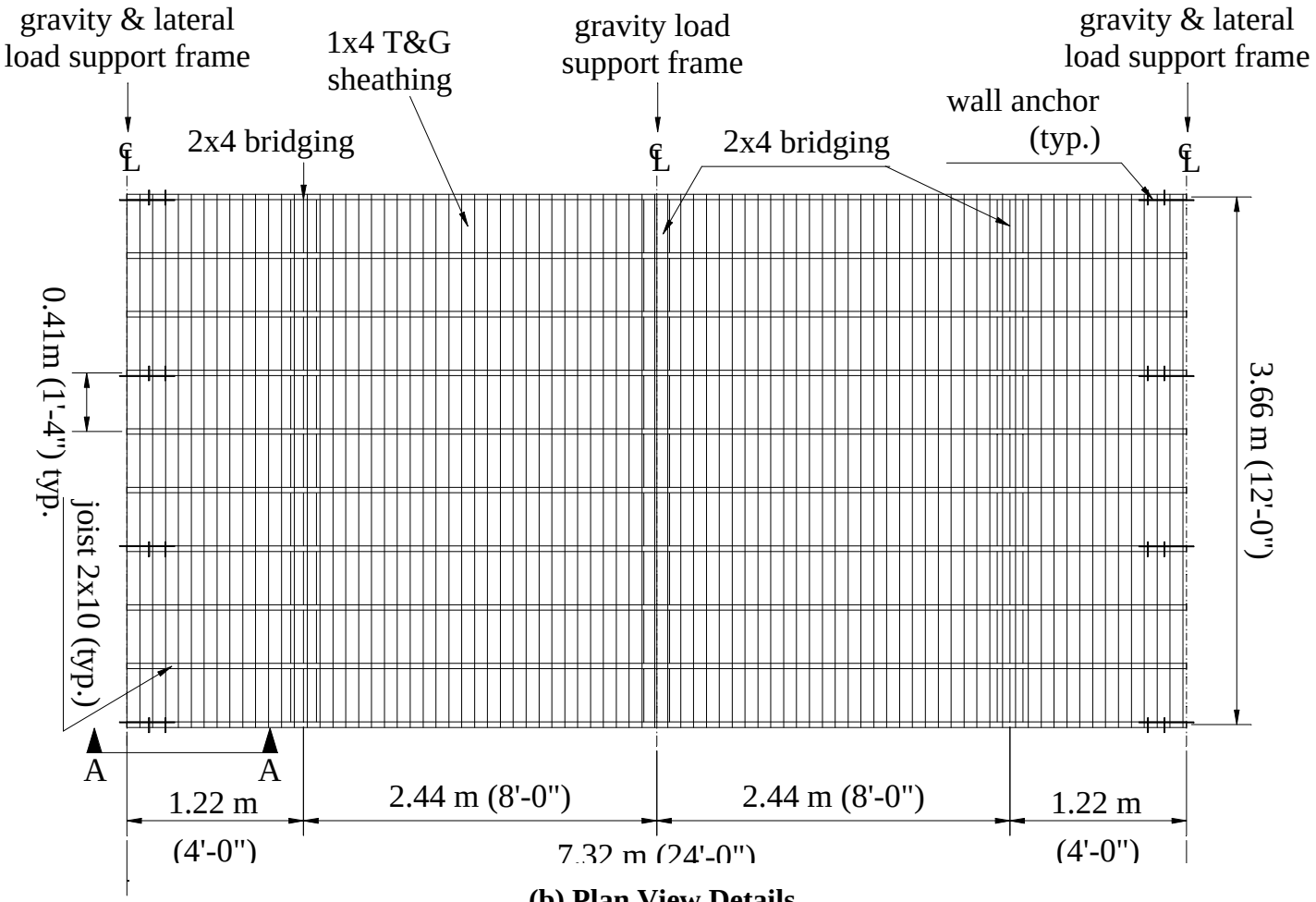

(b) Plan View Details

FIG. 3.3 Continued

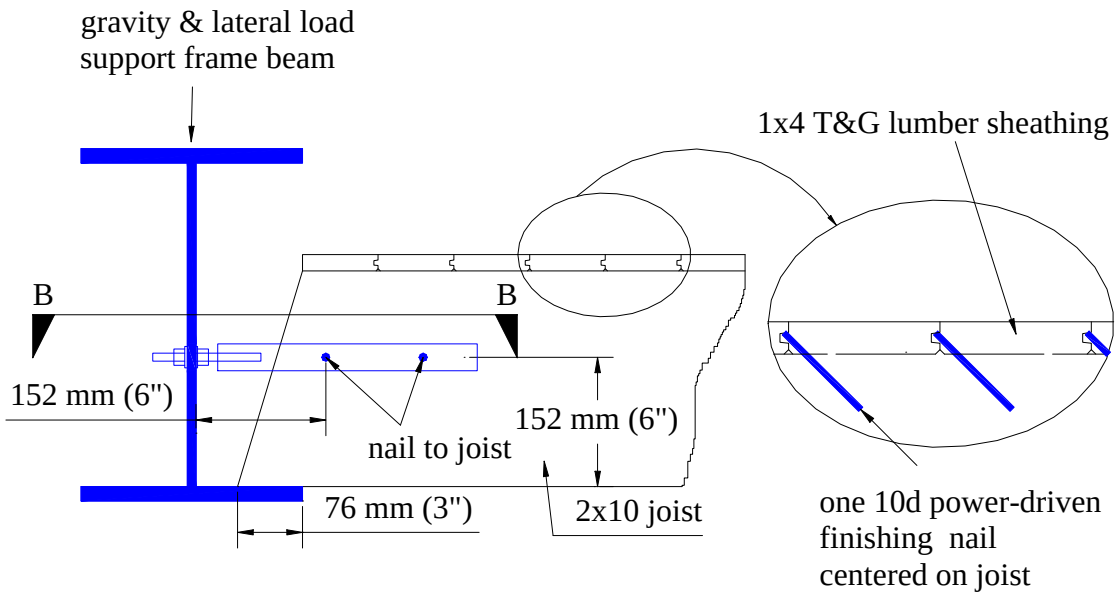

(c) Section A-A - Connection and nail details

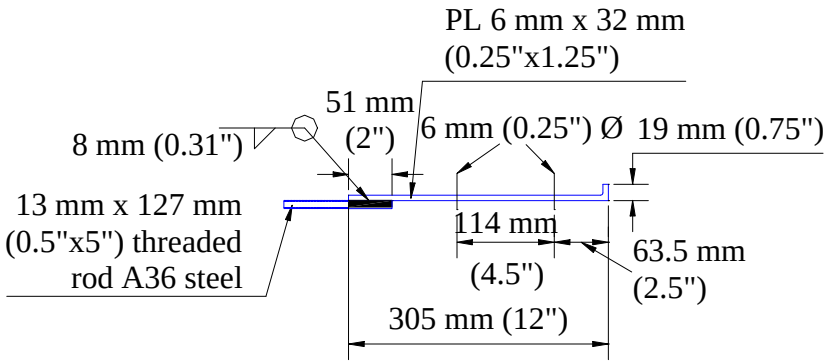

(d) Section B-B - Anchor Details

FIG. 3.3 Continued

3.2.2.2 Connection Retrofit Diaphragm MAE-1A

As will be discussed later in detail, specimen MAE-1 had inadequate connectivity between the diaphragm and lateral load resisting system. In addition the response was relatively flexible, which may lead to significant out of plane bending of URM walls. Therefore, the first retrofit of diaphragm specimen MAE-1 was designed to improve the attachment between the diaphragm and the lateral load support system. This retrofit was based on connection retrofit details used for several projects in California for which structural drawings were provided by the project engineer. These retrofit projects also included plywood overlays, while the retrofitted specimen MAE-1A did not. For MAE-1A, a steel strap was added around the perimeter of the specimen and additional connections were provided to the lateral support, as shown in Figs. 3.4a and 3.4b. The purpose of the steel strap was to improve the shear transfer between the diaphragm and the support frame through the existing and added connections. In addition, the strap provided a "chord" to help resist tension stresses due to bending of the diaphragm. Calculations of the additional shear strength provided by the steel strap are given in Section 5.1.2.1.1. This test was performed to assess whether this retrofit solution was effective in reducing the lateral deformations of the specimen.

The perimeter steel strap was attached to the supporting frames with angle connections placed on top of the diaphragm, above the existing anchor connections, as shown in Fig. 3.4c. In addition, short straps 457 mm (1 ft. 6 in.) in length were placed every 1.22 m (4 ft.) oriented at a right angle with respect to the perimeter strap (see Fig. 3.4b). The short straps were attached to the perimeter straps by welding a small splice plate at the intersection of the two straps. The cross-sectional dimensions of the strapping were 51 mm by 6.4 mm (2 in. by 0.25 in.). The short straps parallel to the joist ends were attached to the deck and joists with 6 mm ϕ x 76 mm (0.25 in. ϕ x 3 in.) lag screws spaced every 102 mm (4 in.). The short straps running perpendicular to the joists were attached to the decking only using #10 x 25 mm (1 in.) wood screws every 89 mm (3.5 in.). Bolted angles were used to attach the strapping to the supporting frame. As

shown in Fig. 3.4, two 16 mm ϕ x 38 mm (0.625 in. ϕ x 1.5 in.) bolts connected 5x5x1/2 angles 254 mm (10 in.) in length to the steel frame, simulating the face of the URM wall. A 3x4x1/4 angle of 254 mm (10 in.) in length was connected to the 5x5x1/2 angle with one 16 mm ϕ x 38 mm (0.625 in. ϕ x 1.5 in.) bolt and to the perimeter strap and diaphragm with four #10 x 25 mm (1 in.) wood screws every 51 mm (2 in.) and one 6 mm ϕ x 76 mm (0.25 in. ϕ x 3 in.) lag screw to the joist. The perimeter straps running in the joist direction were attached to the decking and joists with 6 mm ϕ x 76 mm (0.25 in. ϕ x 3 in.) lag screws spaced every 178 mm (7 in.) and every 89 mm (3.5 in.) on the splice plates. The perimeter straps running perpendicular to the joists were attached every 102 mm (4 in.) using #10 x 25 mm (1 in.) wood screws and one 6 mm ϕ x 76 mm (0.25 in. ϕ x 3 in.) lag screw on every joist intersection. The strapping running in the long direction of the diaphragm required a splice plate placed 1.22 m (4 ft.) from the end. All details are provided in Fig. 3.4b.

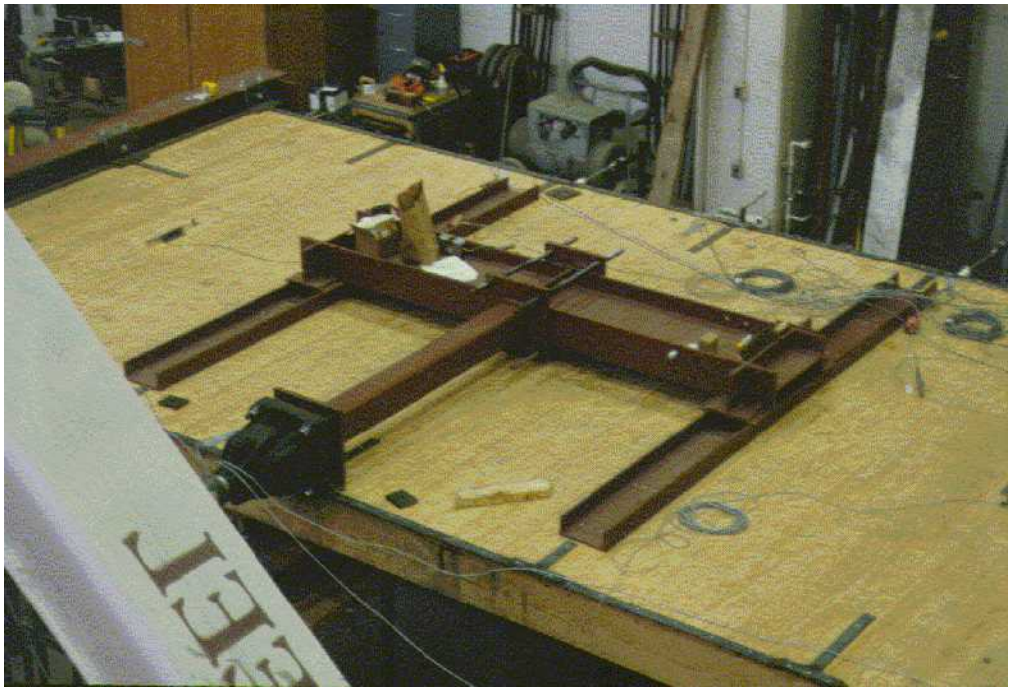

(a) Photograph

FIG. 3.4 Connection Retrofit Diaphragm MAE-1A

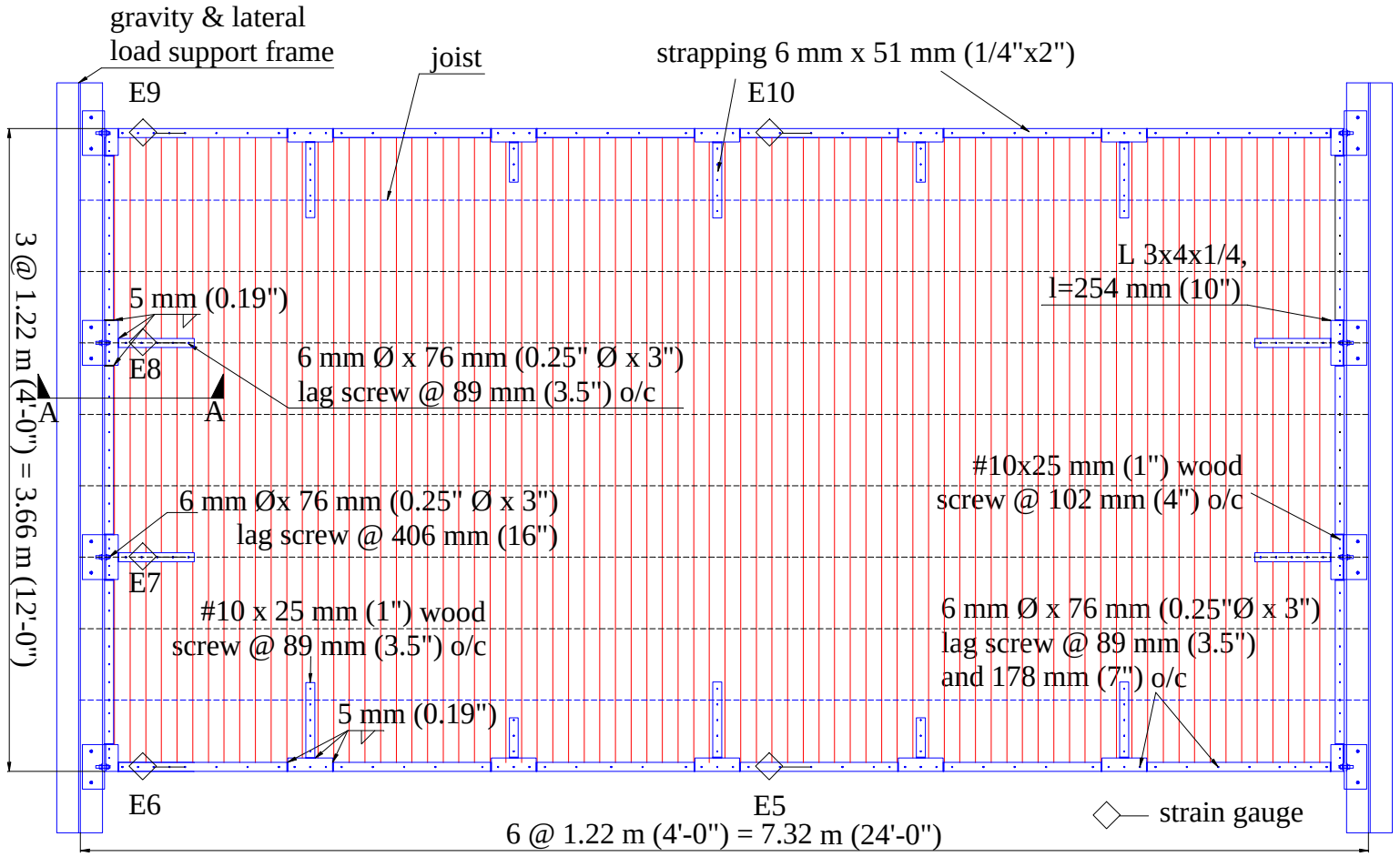

(b) Plan View Details

FIG. 3.4 Continued

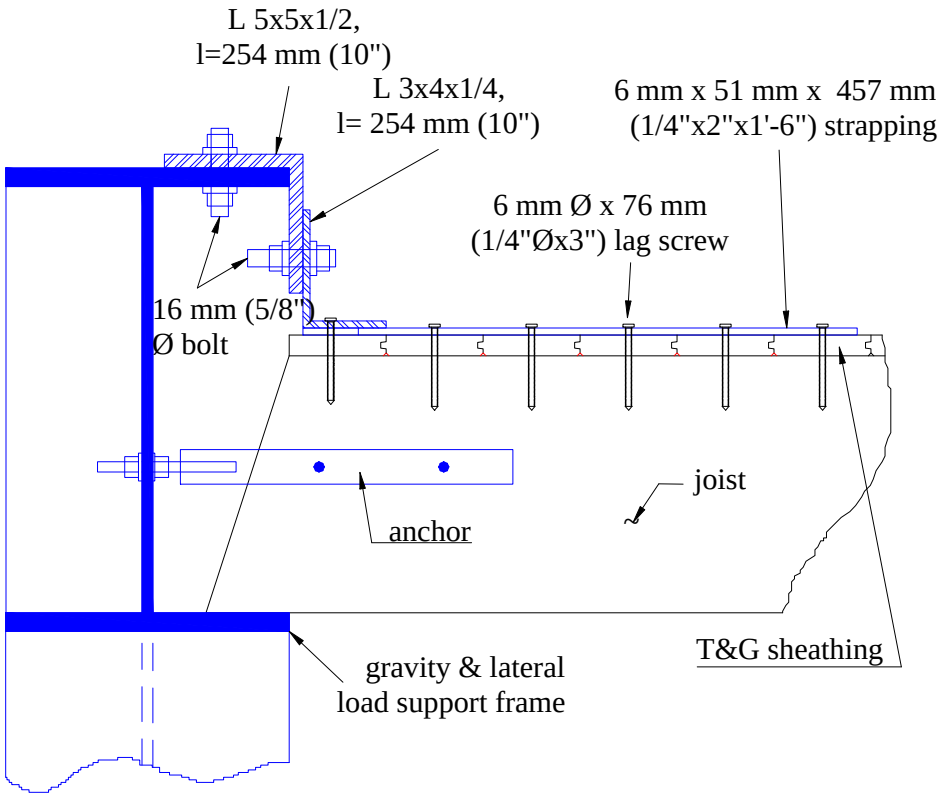

(c) Section A-A - Connection Detail

FIG. 3.4 Continued

3.2.2.3 Steel Truss Retrofit Diaphragm MAE-1B

The second retrofit of this specimen (MAE-1B), was aimed at significantly increasing the diaphragm stiffness and reducing lateral deformations. A steel truss system was placed underneath the diaphragm and attached to the bottom of the joists, as shown in Fig. 3.5. Section 5.1.2.3 provides details on the design of the truss members. The strapping from retrofitted diaphragm MAE-1A, and the added connections to the supporting frame were kept in place. All eight members of the truss were WT4x6.5 sections, oriented with the flange against the underside of the beam joists. The ends of the truss members were bolted to gusset plates with four 16 mm (0.625 in.) bolts. The gusset plates were 6 mm (0.25 in.) thick and attached to the wood joists with 8 mm ϕ x

76 mm (0.3125 in. ϕ x 3 in.) lag screws spaced every 51 mm (2 in.). Collector elements oriented parallel to the load were also attached to the joists by four lag screws of the same dimensions at every joist intersection. It was necessary to use steel spacers to fill the gap at the intersections between the collector elements and the joists. The gusset plates located at the ends of the truss were securely attached to the supporting frames by a bolted double angle connection, as shown in Fig. 3.5c. Four 22 mm (0.875 in.) diameter bolts were used on each leg of the angle connection. For reasons of construction time and cost, the truss configuration was not crossed braced in the middle. The bracing was not required on the specimen because the lateral loading was applied directly on top of the collector elements parallel to the loading. However, cross bracing would be necessary when applying this retrofit to a URM building, where bi-directional loading needs to be considered.

(a) Photograph from Bottom

FIG. 3.5 Steel Truss Retrofit Diaphragm MAE-1B

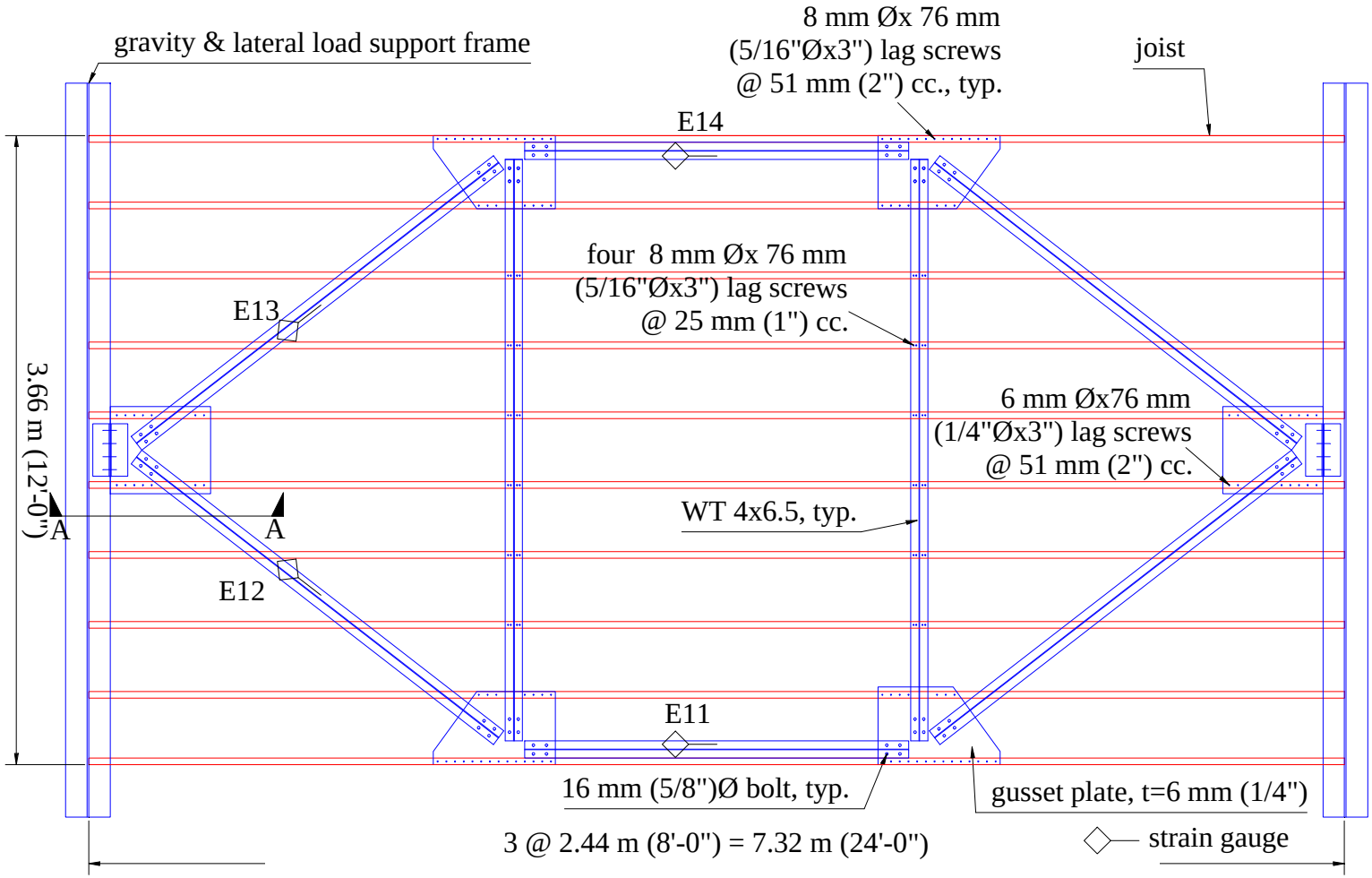

(b) Plan View Detail (Sheathing and Steel Strap Retrofit not Shown)

FIG. 3.5 Continued

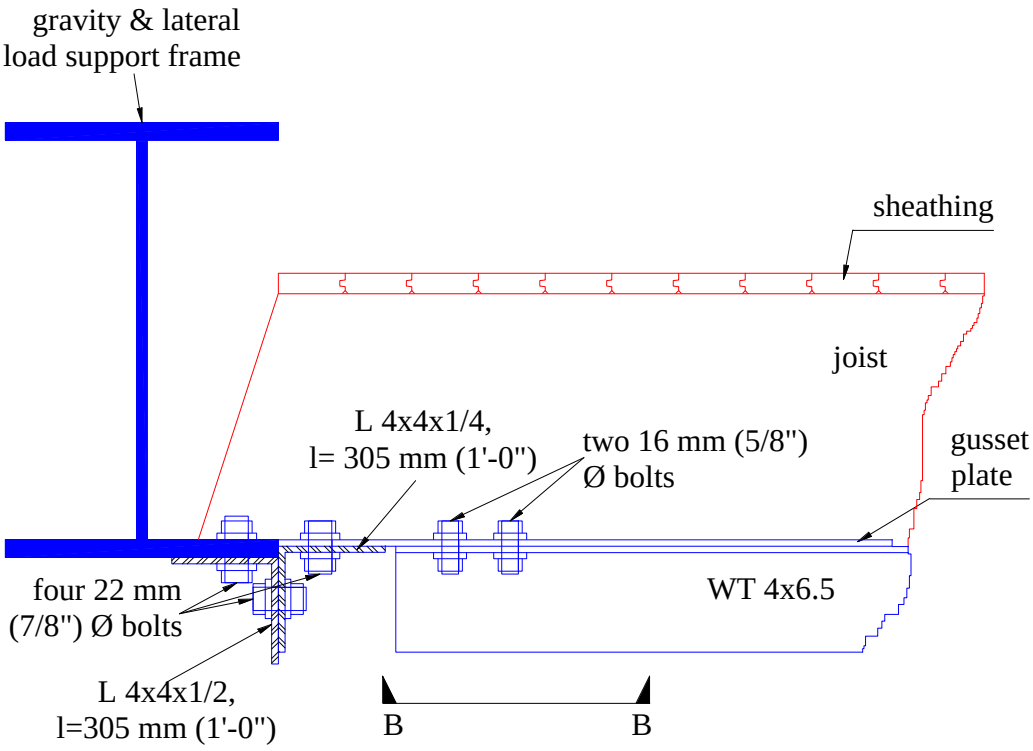

(c) Section A-A - Connection Details (Steel Strap Retrofit not Shown)

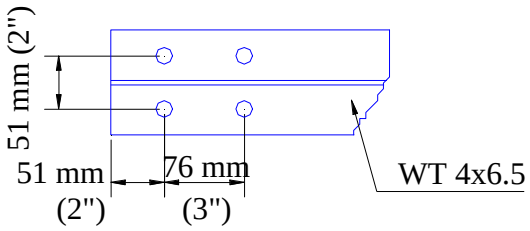

(d) Section B-B – Truss Member Connections

FIG. 3.5 Continued

3.2.3 Square Edged Single Straight Sheathed Diaphragm

This section describes the construction of a single straight-sheathed diaphragm using square edged boards and three retrofits using an underside steel truss, an unblocked plywood overlay and a blocked plywood overlay.

3.2.3.1 Diaphragm MAE-2

Specimen MAE-2 was designed to represent a typical roof diaphragm in pre-1950's URM buildings. MAE-2 had the same plan dimensions as specimen MAE-1, 7.32 m x 3.66 m (24 ft. x 12 ft.), as well as the same beam joist size (2x10) and the same gravity and lateral support frames. In addition, W12x26 steel beams were added to the support frames along the long sides of the diaphragm. The top flange of the W12x26 steel beams were made flush with the bottom flange of the gravity and lateral support frame beams at their intersection and the flanges were attached using four 16 mm ϕ x 51 mm (0.625 in. ϕ x 2 in.) bolts at each connection location. The gravity support frame at the center of the diaphragm used for testing MAE-1A was not needed and was removed. Beam joists were aligned in the short direction of the diaphragm, having a length of 3.66 m (12 ft.). The ends of the beam joists had 76 mm (3 in.) of bearing support on the new steel beams. Firecuts were not made on the beam joists in this specimen, because the structural behavior of the diaphragm was not affected by their presence. Sheathing was provided using 1x6 square edge straight boards, staggered symmetrically with respect to the diaphragm midspan. The maximum length of the boards was 3.66 m (12 ft.), as shown in Fig. 3.6a. Three 8d common nails were used at the supports end and two at interior joist support locations for each sheathing board. Threaded bars of 16 mm (0.625 in.) diameter by 254 mm (10 in.) long were used to anchor the joists to the reaction frames by passing through the end joists at about mid-height of the joists and spaced every 1.22 m (4 ft.), as shown in Fig. 3.6b. The anchors also passed through a 127 mm x 127 mm x 3mm by 305 mm long (5"x5"x1/8"x12") tube to simulate the support conditions of the anchor into the wall, because an end joist would be nearly flush with the adjoining wall in an actual building. The minimum edge distance of the anchors to the joist ends was 38 mm (1.5 in.).

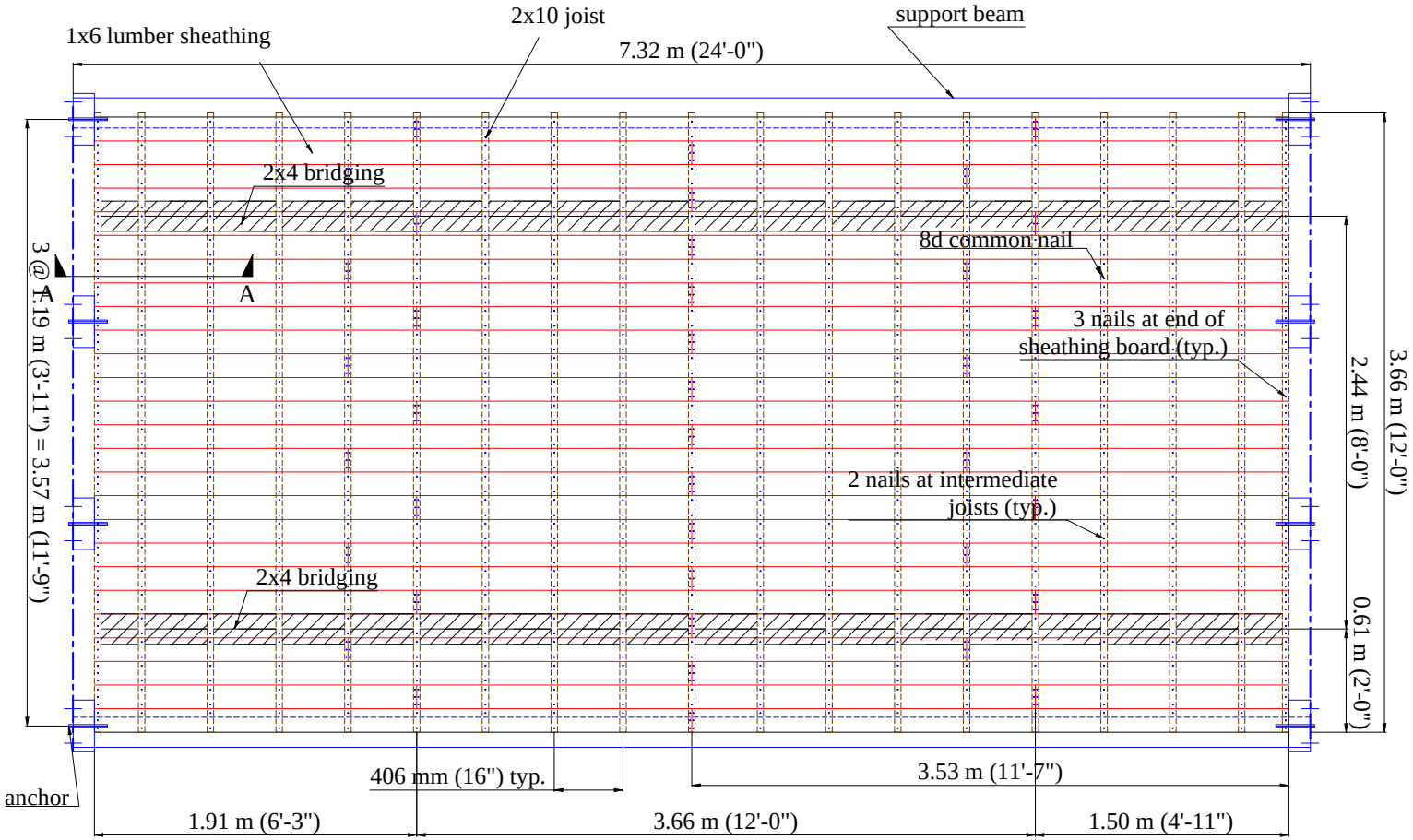

(a) Plan View Details

FIG. 3.6 Square Edged Single Straight Sheathed Diaphragm MAE-2

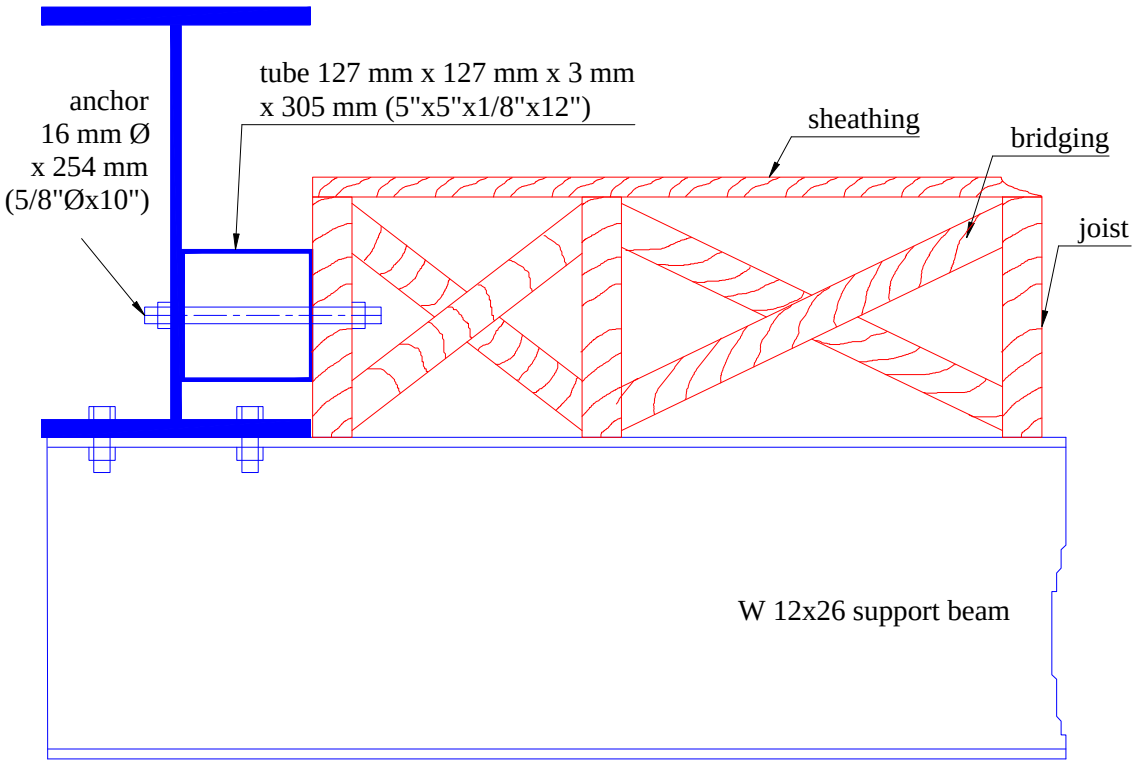

(b) Section A-A - Connection Detail

FIG. 3.6 Continued

3.2.3.2 Steel Truss Retrofit Diaphragm MAE-2A

As in specimen MAE-1, the experimental behavior of diaphragm MAE-2 was also very flexible, which is discussed in detail later. Therefore, the purpose of this retrofit scheme was to significantly increase the lateral stiffness of the diaphragm. Therefore, diaphragm MAE-2A used the same steel truss used in the retrofitted diaphragm MAE-1B with some minor modifications, as shown in Fig. 3.7. The design of the steel truss is detailed in Section 5.1.2.3. The collector elements of the truss were replaced by 6 mm x 51 mm (0.25 in. x 2 in.) steel plates attached to the joists by 8 mm ϕ x 76 mm (0.3125 ϕ x 3 in.) lag screws spaced every 102 mm (4 in.). The gusset plates

were rotated in order to make a new set of holes to connect the brace elements to the gusset plates. Fig. 3.7c shows the connection detail of the truss to the support frames.

3.2.3.3 Unblocked Plywood Overlay Retrofit Diaphragm MAE-2B

After removing the steel truss from diaphragm MAE-2A, an unblocked plywood overlay was nailed to the diaphragm for improving the diaphragm's in-plane lateral stiffness. The design was based on provisions from APA (Tissell and Elliott, 1997) and is detailed in Section 5.1.2.1.3. The thickness of the plywood overlay was 9.5 mm (0.375 in.) and the panels were arranged as shown in Fig. 3.8. Each plywood panel was nailed with 8d common nails spaced at 152 mm (6 in.) at the supported panel edges and 305 mm (1 ft.) along intermediate joists. A gap of 3 mm (0.125 in.) was left between panels along all edges in accordance with APA plywood sheathing installation recommendations (APA, 1985).

(a) Photograph from Bottom

FIG. 3.7 Steel Truss Retrofit Diaphragm MAE-2A

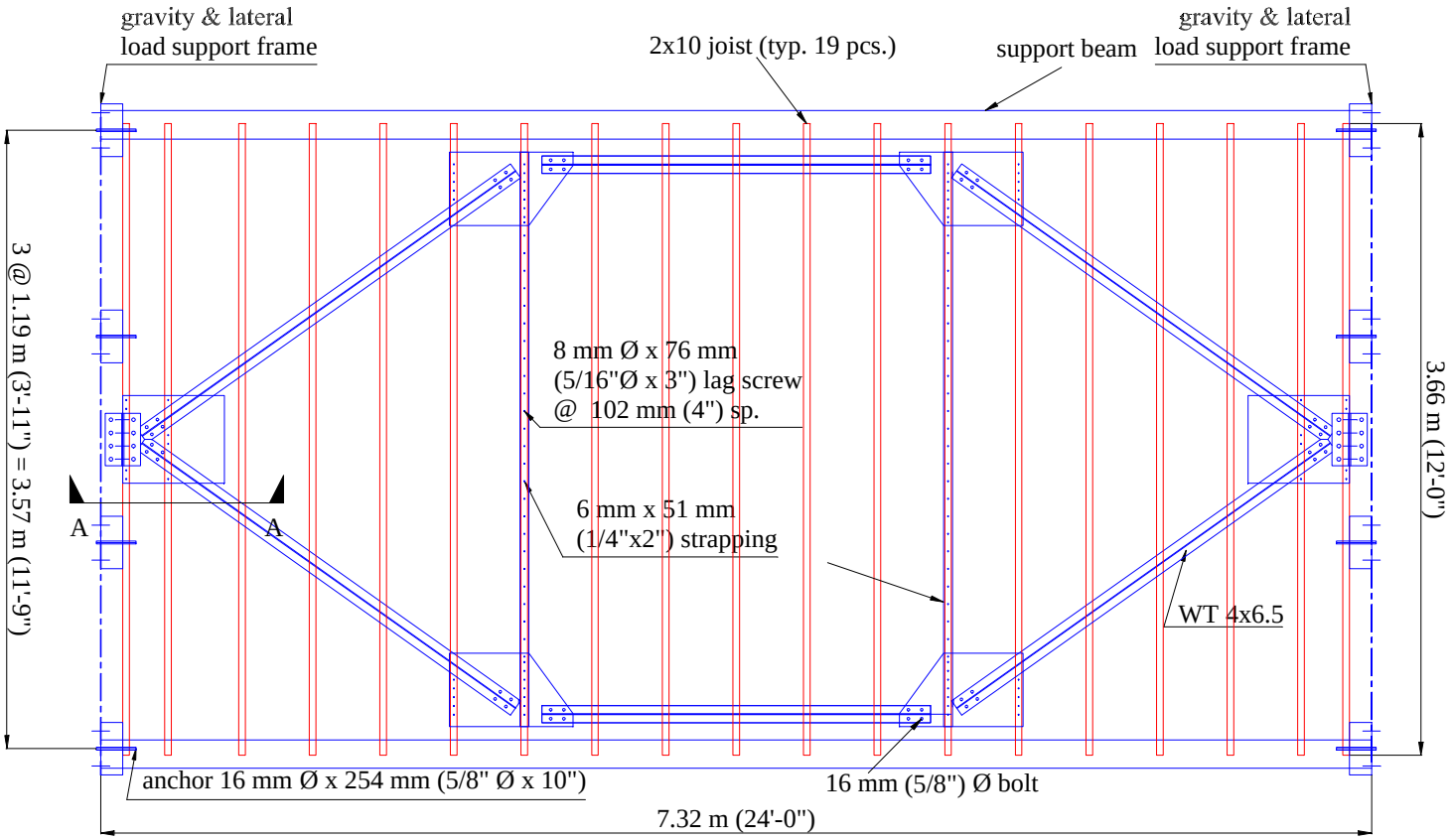

(b) Plan View Details (Sheathing not Shown)

FIG. 3.7 Continued

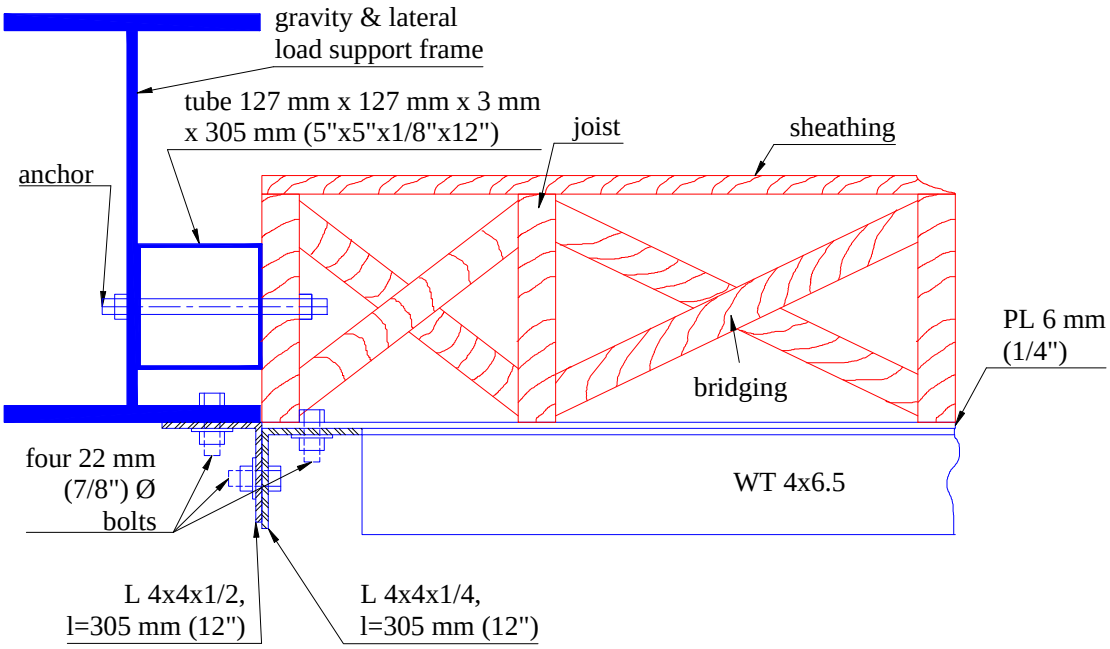

(c) Section A-A -Connection Detail

FIG. 3.7 Continued

3.2.3.4 Blocked Plywood Overlay Retrofit Diaphragm MAE-2C

After testing diaphragm MAE-2B, blocking was added to the diaphragm using 2x4 boards that were approximately 368 mm (14.5 in.) long (see Fig. 3.9). The design was based on the specifications from APA (Tissell and Elliott, 1997) and details of the calculations are given in Section 5.1.2.1.3. The blocking boards were placed underneath the unsupported (long) edges of the panels and nailed between the joists with 8d common nails. With the blocking in place, nails were added to the plywood overlay to reduce the spacing to 51 mm (2 in.) at the diaphragm boundaries and 76 mm (3 in.) at the other panel edges (both directions). No additional nails were added along the intermediate supporting joists.

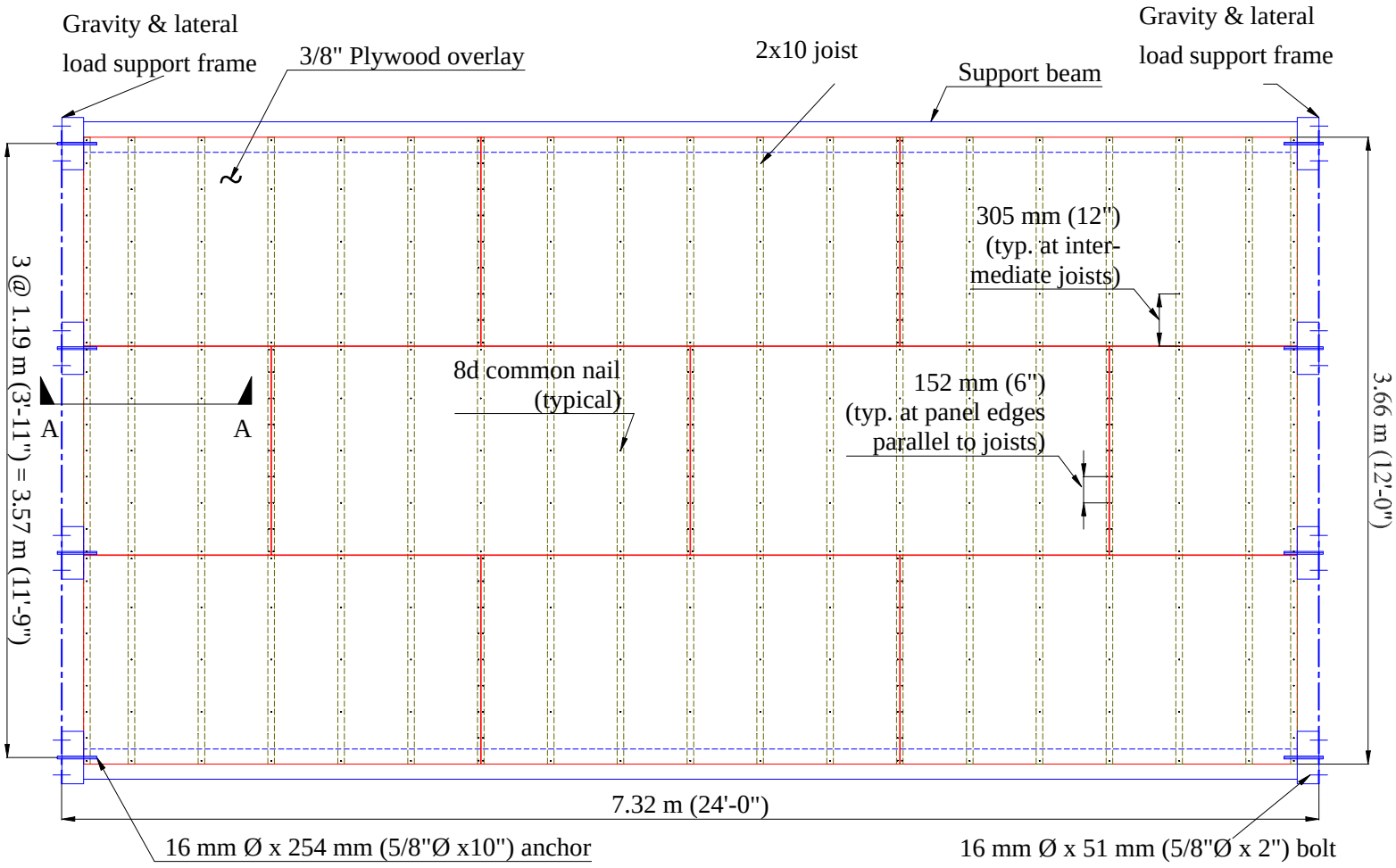

(a) Plan View Details

FIG. 3.8 Unblocked Plywood Overlay Retrofit Diaphragm MAE-2B

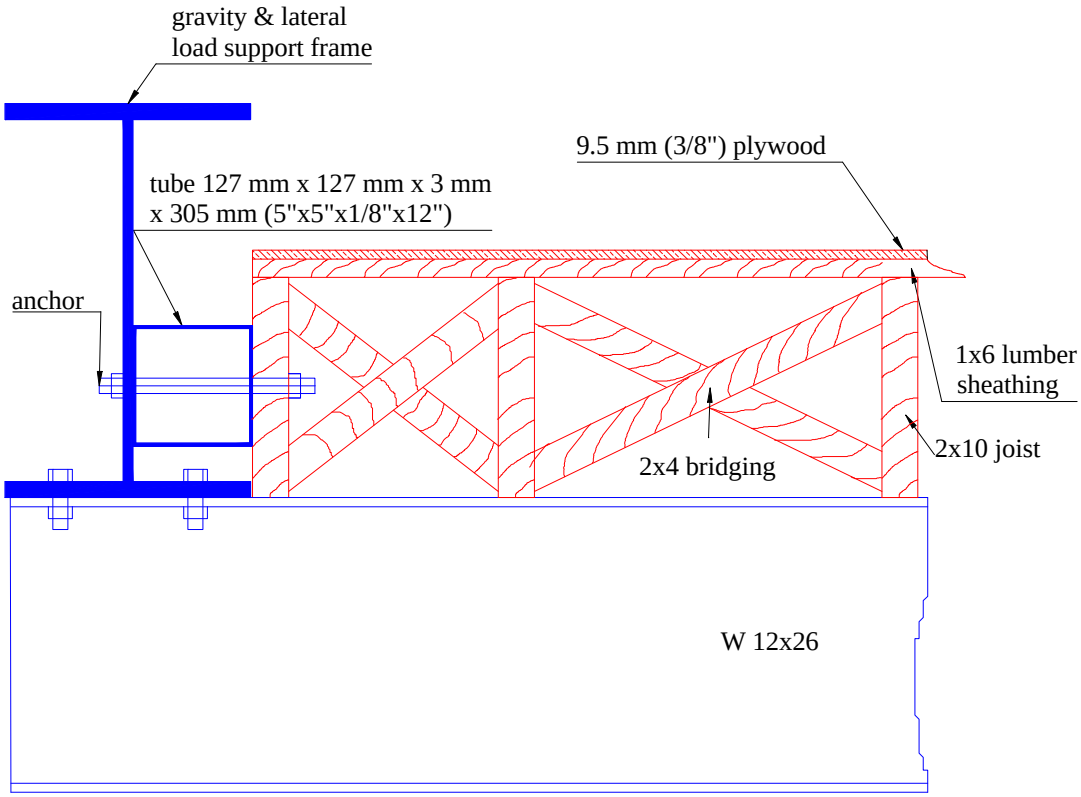

(b) Connection Detail

FIG. 3.8 Continued

FIG. 3.9 Blocked Plywood Overlay Retrofit Diaphragm MAE-2C

3.2.4 Square Edged Single Straight Sheathed Diaphragm with Corner Opening

This section describes the construction of a single straight-sheathed diaphragm with a corner opening. Two retrofits for this diaphragm using unblocked and blocked plywood overlays are also described.

3.2.4.1 Diaphragm MAE-3

The geometry, construction and materials used in diaphragm MAE-3 were the same as those used for diaphragm MAE-2 with the addition of a 0.81 m x 1.57 m (2 ft. 8 in. x 5 ft. 2 in.) opening located at one corner of the diaphragm, as shown in Fig. 3.10. This opening was intended to be representative of a typical stairwell opening. Two joists were shortened and nailed to a transverse 1.57 m (2 ft. 8 in.) long joist to frame the opening, as shown in Fig. 3.10b. The sheathing was also shortened at the required locations and the boards were staggered appropriately. Along the edge of the diaphragm with the opening, only three anchors were used to attach the diaphragm to the support frame, as shown in Fig. 3.10b.

3.2.4.2 Unblocked Plywood Overlay Retrofit Diaphragm MAE-3A

Similar to diaphragm MAE-2, diaphragm MAE-3 was retrofitted by adding an unblocked plywood overlay, as shown in Fig. 3.11, to increase the in-plane lateral stiffness of the diaphragm. The design followed specifications from APA (Tissell and Elliott, 1997) and the calculations are given in Section 5.1.2.1.3. Plywood panels of 9.5 mm (0.375 in.) thickness and 1.22 m x 2.44 m (4 ft. x 8 ft.) dimensions were nailed using 8d common nails. The nail arrangement consisted of 152 mm (6 in.) spacing on the supported panel edges parallel to the loading and 305 mm (1 ft.) spacing at the interior joists, as shown in Fig. 3.11. A gap of 3 mm (0.125 in.) was used between

(a) Photograph

FIG. 3.10 Single Straight Sheathed Diaphragm with Corner Opening MAE-3

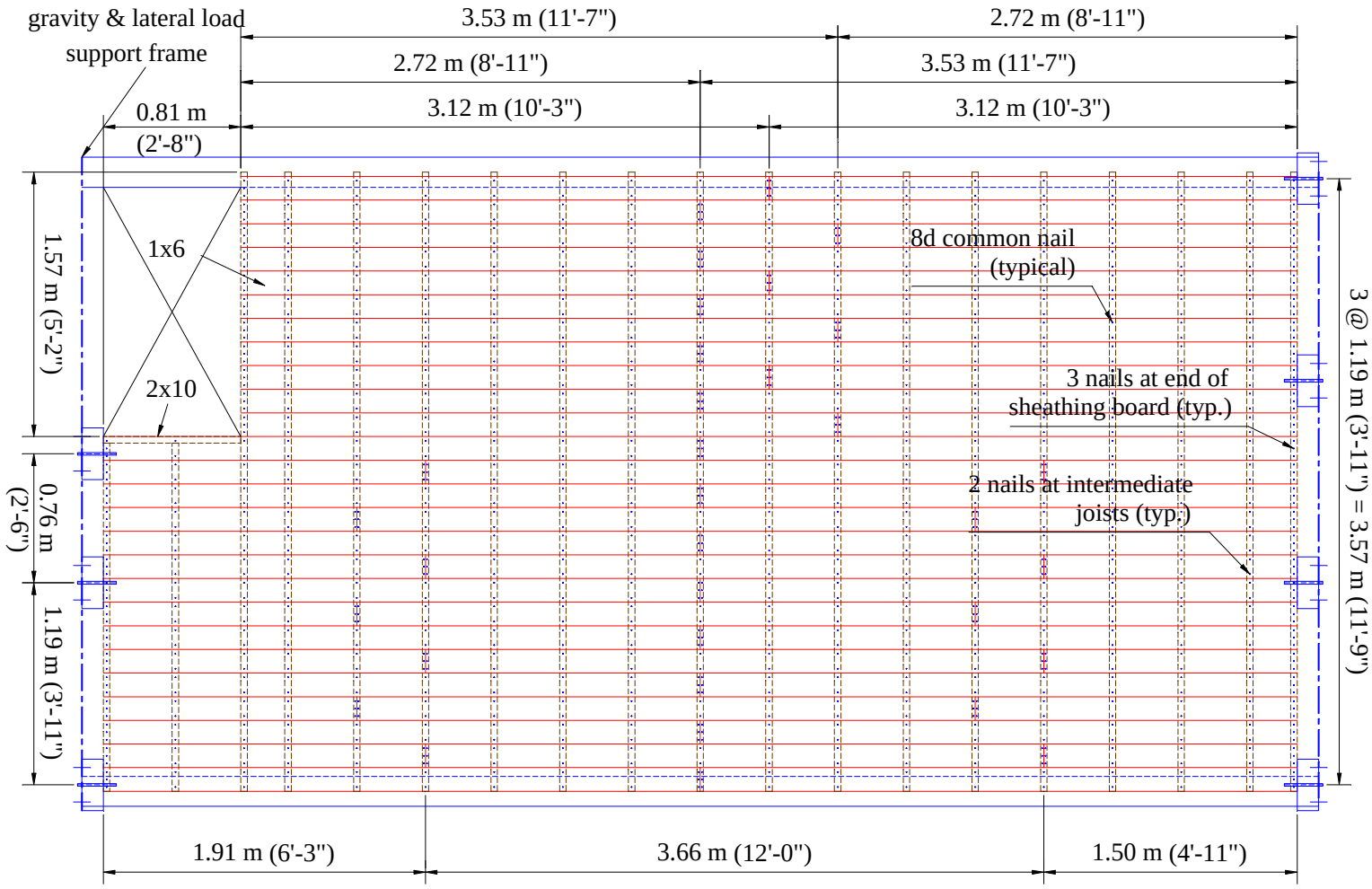

(b) Plan View Details

FIG. 3.10 Continued

panels in both directions. The panels were arranged following the same pattern as in diaphragm MAE-2B, cutting the panels to accommodate the corner opening.

3.2.4.3 Blocked Plywood Overlay Retrofit Diaphragm MAE-3B

Diaphragm MAE-3B was similar to diaphragm MAE-3A, with the addition of 2x4 blocking boards placed at the bottom of the sheathing, running below the unsupported (long) edges of the panels. The specifications from APA (Tissell and Elliott, 1997) were used for the design and the calculations are given in Section 5.1.2.1.3. The length of the blocking boards was cut to fit the face-to-face separation between joists, approximately 368 mm (14.5 in.) and nailed to the joists using 8d common nails. With the blocking in place, nails were added to reduce the nail spacing to 51 mm (2 in.) along the edges of the diaphragm and 76 mm (3 in.) at the panel edges, similar to diaphragm retrofit MAE-2C. Additionally, a 6 mm x 51 mm x 1.52 m (0.25 in. x 2 in. x 5 ft.) steel strap was attached on top of the diaphragm, along the short side of the opening to reinforce the corner (see Fig. 3.12). Blocking boards were added and nailed to the joists to secure the strapping with 8 mm ϕ x 76 mm (0.3125 in. ϕ x 3 in.) lag screws running every 51 mm (2 in.). Table 3.1 provides with a summary of the diaphragms and their retrofits including the main characteristics of the sheathing, supports and type of retrofit.

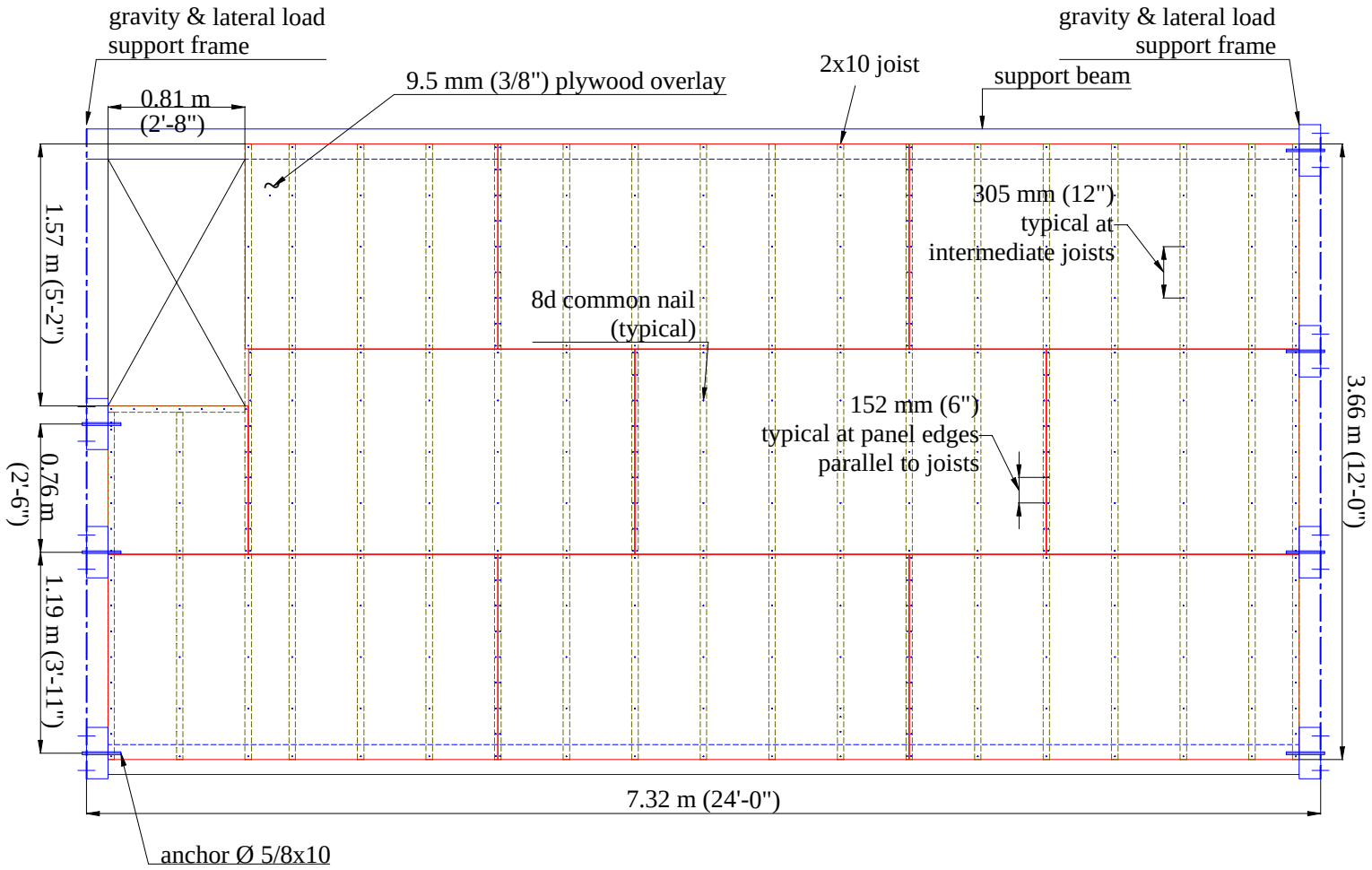

FIG. 3.11 Unblocked Plywood Overlay Retrofit Diaphragm MAE-3A

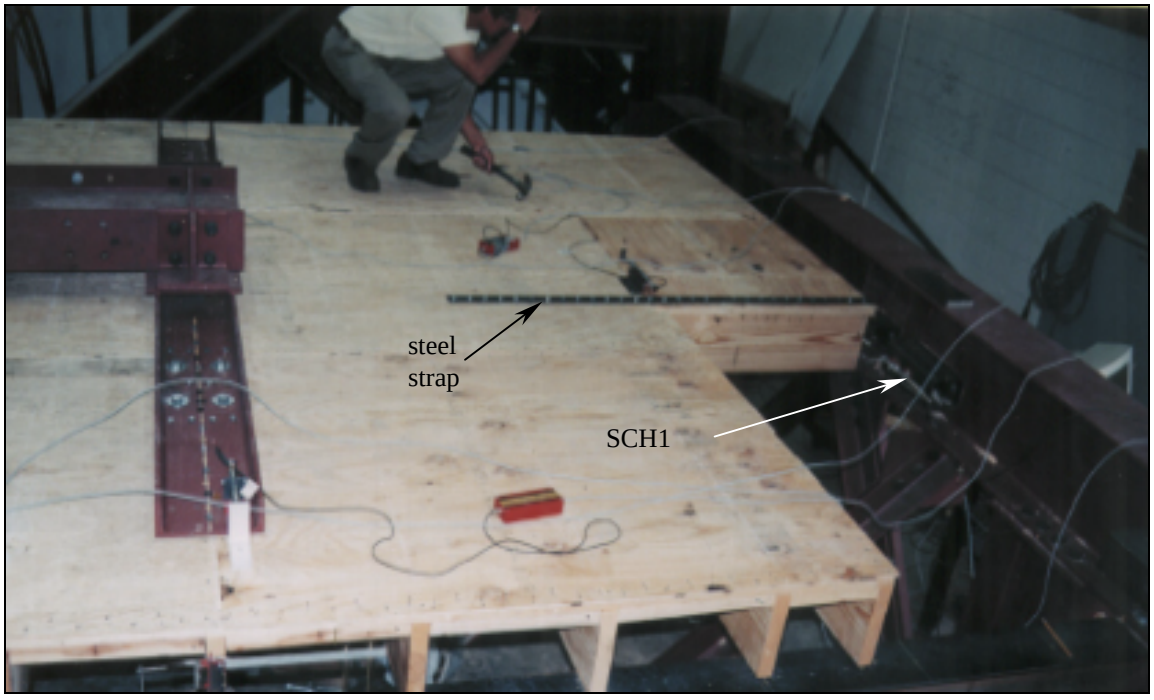

FIG. 3.12 Blocked Plywood Overlay Retrofit Diaphragm MAE-3B

TABLE 3.1 Diaphragm Specimen Description

Diaphragm	Description
MAE-1	1x4 T&G sheathing, star anchors
MAE-1A	MAE-1 plus enhanced bolted connections and perimeter steel strapping
MAE-1B	MAE-1A plus steel truss
MAE-2	1x6 straight sheathing, bolted connections, unchorded
MAE-2A	MAE-2 plus steel truss
MAE-2B	MAE-2 plus 3/8” unblocked plywood overlay
MAE-2C	MAE-2 plus 3/8” blocked plywood overlay
MAE-3	1x6 straight sheathing, bolted connections, unchorded, corner opening
MAE-3A	MAE-3 plus 3/8” unblocked plywood overlay
MAE-3B	MAE-3 plus 3/8” blocked plywood overlay, steel strap at opening

3.3 EXPERIMENTAL SETUP

This section describes the experimental test setup used for all diaphragm specimens, including the support frames, loading frame, actuator instrumentation and data acquisition.

The two lateral and gravity load support steel frames mentioned in the previous sections were designed for the maximum actuator load capacity of 500 kN (110 kips). Fig. 3.13 shows a plan view of a typical specimen, supports and loading system. A W16x67 wide flange section was used for the beam and columns members of the lateral and gravity load support frames (see Fig. 3.14). The beam in each frame was connected to the two supporting columns with eight 22 mm (0.875 in.) diameter bolts distributed in two rows on both sides of the beam web, attaching the bottom flange of the beam to a plate welded to the top of the column. The columns were welded to a base plate 25 mm (1 in.) in thickness, which was connected to the reaction floor with four 51 mm (2 in.) diameter threaded bars (see Fig. 3.14). To provide in-plane and out-of-plane stiffness to the support frames, double angle diagonal braces were attached to the frame through gusset plates and three 22 mm (0.875 in.) diameter bolts at each end of the braces (see Figs. 3.14 and 3.15).

Diaphragm MAE-1 required an additional gravity support frame at its center, as shown in Fig. 3.14a. Diaphragms MAE-2 and MAE-3 required additional gravity support beams running along the long edges of the diaphragm, as shown in Fig. 3.14b.

3.3.1 Loading System

Fig. 3.13 shows the position of the actuator and the loading frame with respect to the diaphragm. A 500 kN (110 kips) capacity hydraulic actuator was used to apply quasi-static load in the plane of the diaphragm. For this purpose, the actuator was attached to a steel loading frame connected to the top of the diaphragm. As shown in Figs. 3.13 and 3.14, the loading frame had a H-shaped geometry in plan, composed of

two MC9x25.4 by 3.05 m (10 ft.) long channels spaced 2.44 m (8 ft.) center-to-center and joined together by a W18x55 by 2.74 m (9 ft.) long beam on top of the channels. Both channels and the beam webs were oriented parallel to the plane of the diaphragm, with the channel webs directly in contact with the top surface of the diaphragm. The channels of the loading frame were attached to the diaphragm by 9.5 mm diameter x 102 mm (0.375 in. diameter x 4 in.) lag screws and 16 mm diameter x 102 mm (0.625 in. diameter x 4 in.) long bolts. The lag screws were distributed along the length of the channels in 8 rows spaced every 406 mm (16 in.), with 4 lag screws per row spaced at 51 mm (2 in.). The loading frame transferred the load from the actuator to the diaphragm system. Wood blocking made flush with the bottom of the diaphragm sheathing and nailed to the adjacent joists was required in the load transfer region of the diaphragm (along the channels) in order to utilize the full length of the lag screws and bolts into the diaphragm. This blocking was used for load transfer in all the specimens. A vertical offset of 229 mm (9 in.) between the axis of the actuator and the top surface of the diaphragm sheathing was required in order to avoid interference of the actuator and diaphragm specimen during testing. One end of the actuator was supported by a stiff reaction column, while the other end was attached to the loading frame and supported vertically by a light steel frame, as shown in Fig. 3.15.

3.3.2 Instrumentation

The applied lateral displacements and resulting forces were measured directly through the actuator's built-in displacement transducer and load cell. Specimen response was obtained from accelerometers for the forced vibration tests and linear variable displacement transducers (LVDT) and strain gauges for the quasi-static tests. These instruments were used to measure the contribution of each element's (joists, sheathing boards, anchors, etc.) response to the overall specimen response. The common arrangement of these instruments for all diaphragm tests is shown in Fig. 3.13. The instruments were placed symmetrically on the diaphragm, with the actuator acting as the axis of symmetry. Displacement transducers SCH1, SCH2, SCH3, SCH4 and

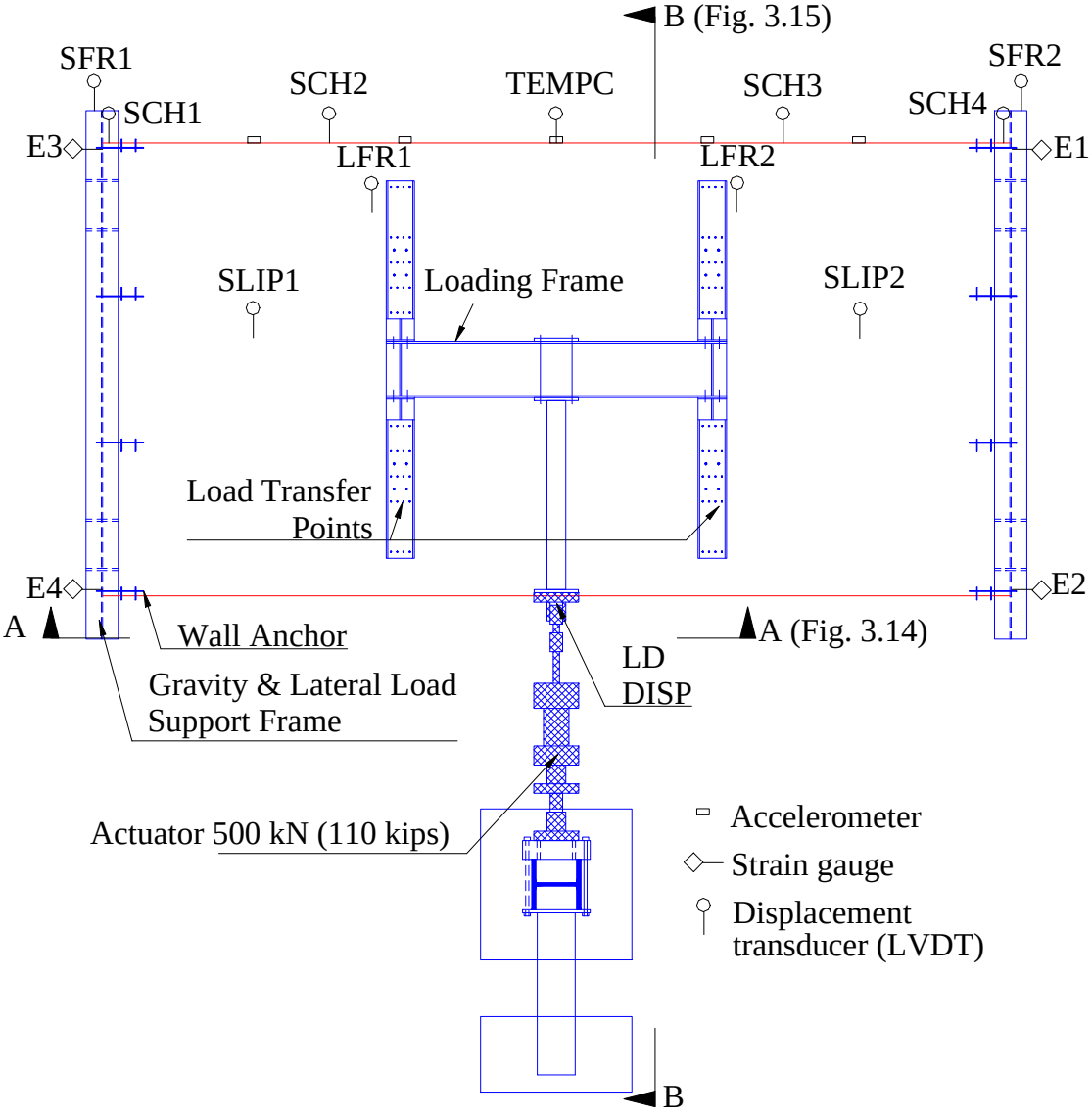

FIG. 3.13 Common Test Setup and Instrumentation for All Diaphragms

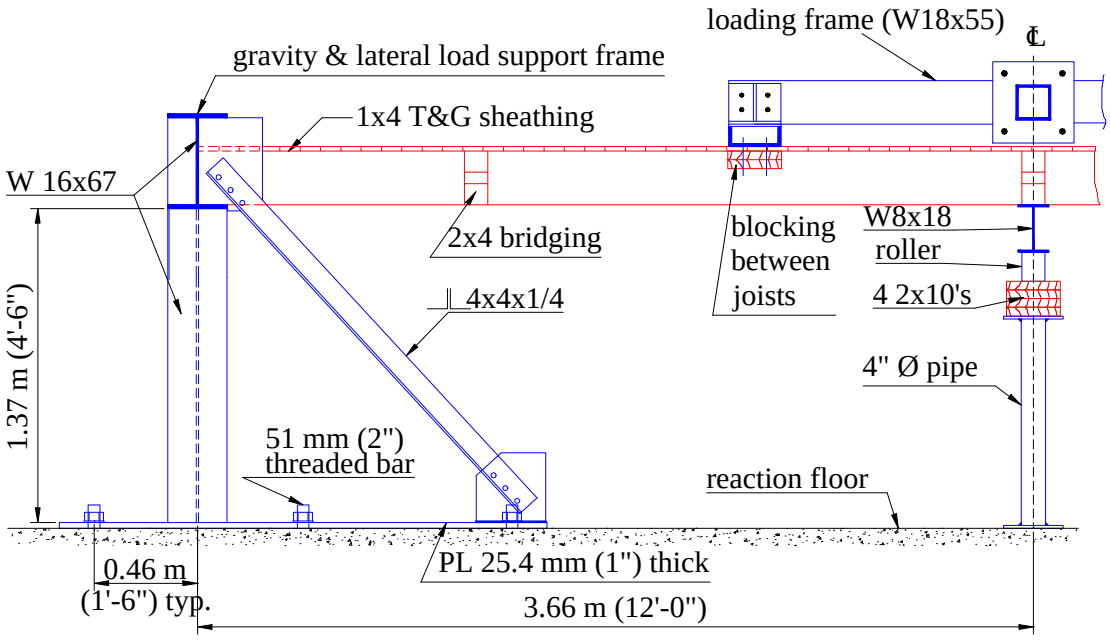

(a) Specimen MAE-1

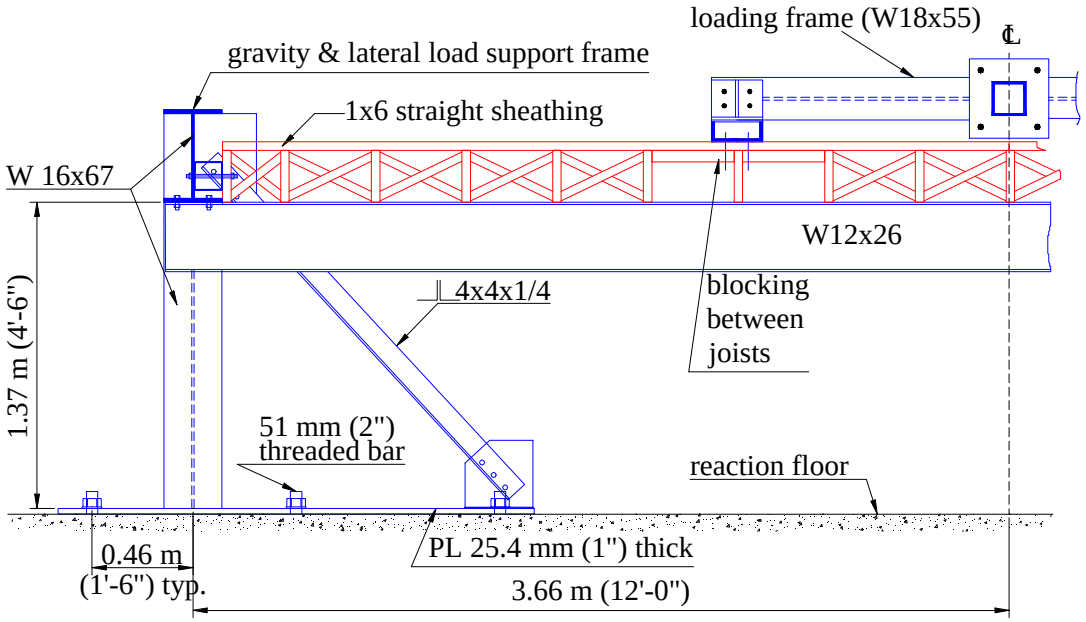

(b) Specimens MAE-2 & MAE-3

FIG. 3.14 Elevation View of Test Setup (Section A-A in Fig. 3.13)

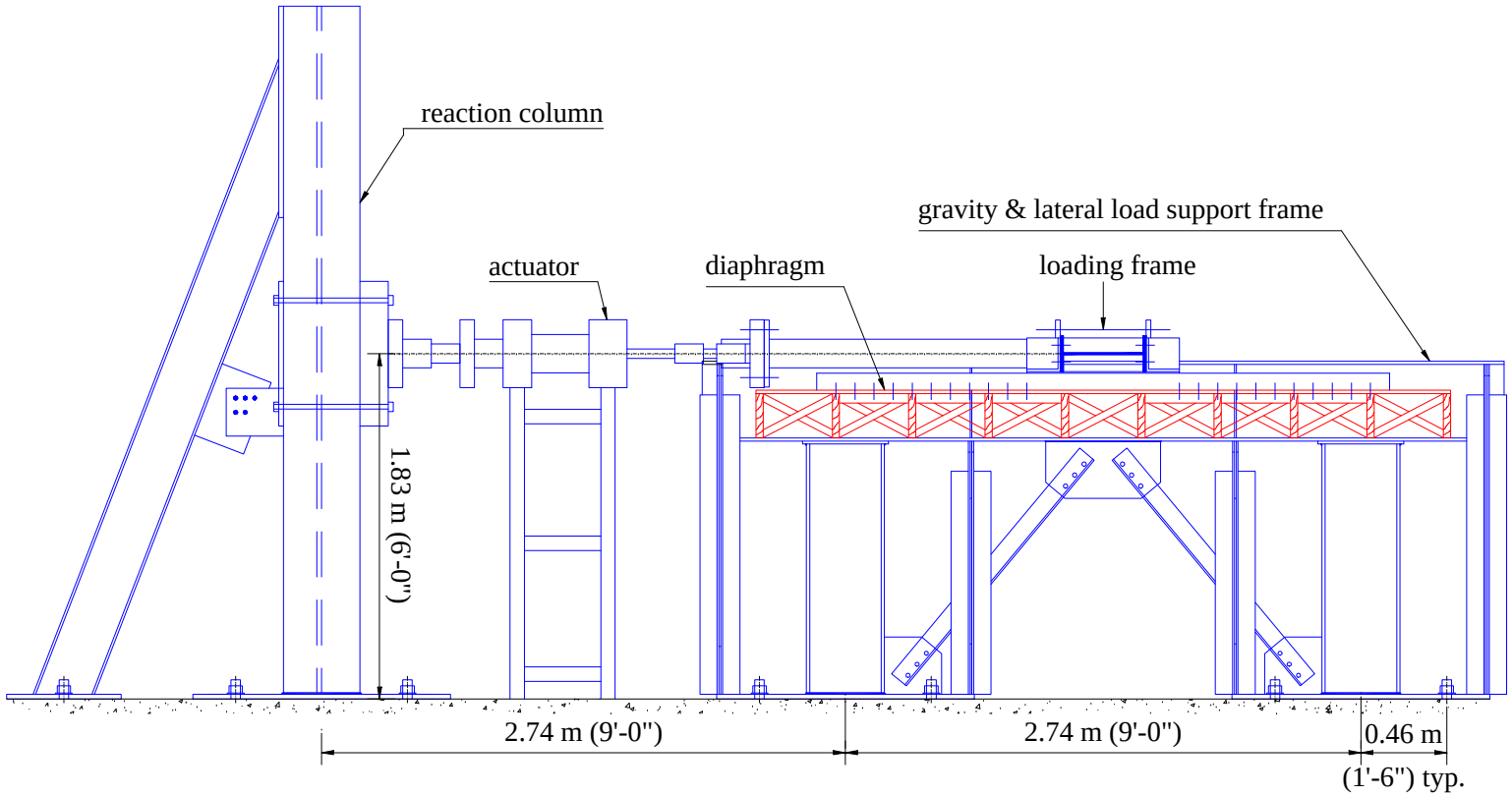

(a) Specimen MAE-1

FIG. 3.15 Loading System Setup (Section B-B in Fig. 3.13)

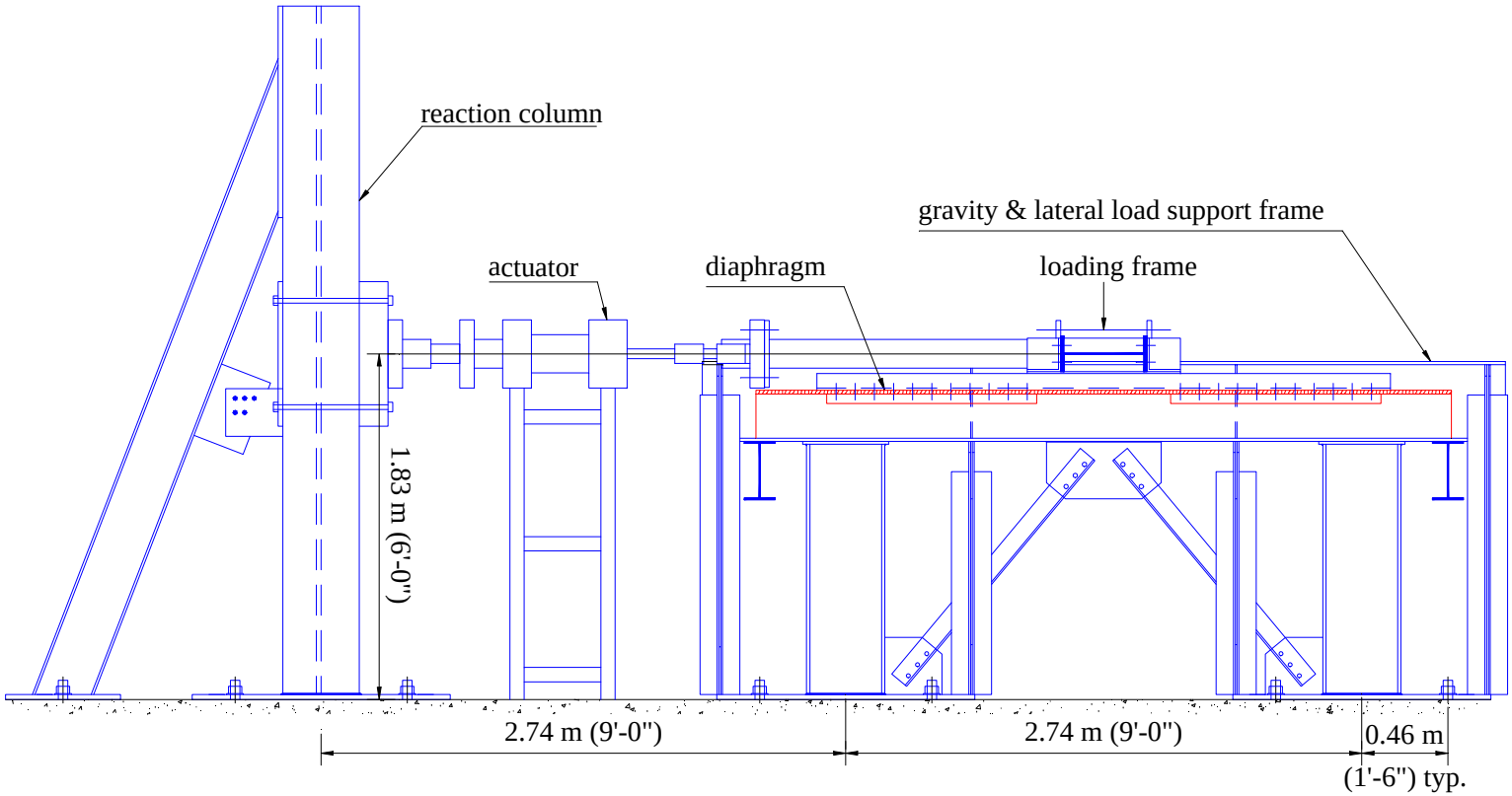

(b) Specimen MAE-2 and MAE-3

FIG. 3.15 Continued

TEMPC measured lateral displacements on the long edge of the diaphragm opposite to the actuator and were distributed evenly every 1.83 m (6 ft.). SCH1 and SCH4 had a stroke limit of 51 mm (2 in.) and were used to measure relative deformations between the diaphragm edge and the lateral framing. SCH2, SCH3 and TEMPC had a stroke limit of 102 mm (4 in.) and were used to measure the diaphragm lateral deformation relative to the ground. Displacement transducers SFR1 and SFR2 measured lateral displacements on the supporting frames with respect to the ground and had a stroke limit of 51 mm (2 in.). For this purpose, the transducers were placed at the level of the centroidal axes of the joists and were attached to vertical tubes fixed to the floor, as can be observed in Fig. 3.16. Displacement transducers LFR1 and LFR2 measured the lateral slip displacements of the loading frame with respect to the diaphragm and were attached on top of the diaphragm sheathing with a stroke limit of 25 mm (1 in.). Displacement transducers SLIP1 and SLIP2 measured the relative slip between adjacent boards and were also attached on top of the diaphragm, as shown in Fig. 3.17, with a stroke limit of 25 mm (1 in.). Strain gauges E1, E2, E3 and E4 measured the strain in the anchors located at the corners of the diaphragm. In the retrofitted specimen MAE-1A, six additional strain gauges (E5, E6, E7, E8, E9 and E10) were placed along the strap, two on the longitudinal straps and four on the left strap, as shown in Fig. 3.4b. In addition to the instrumentation just mentioned, four additional strain gauges (E11, E12, E13 and E14) were placed on the retrofitted specimen MAE-1B, at the middle of each brace web, as shown in Fig. 3.5b.

Diaphragms MAE-2, MAE-2B and MAE-2C had the same instrumentation as diaphragm MAE-1. Diaphragm MAE-2A had the same instrumentation as diaphragm MAE-1B. Diaphragms MAE-3, MAE-3A and MAE-3B had similar arrangement as MAE-1 except the attachment location of transducer SCH1 was changed to the bottom flange of the supporting frame, next to the supported opening corner, as shown in Fig. 3.12.

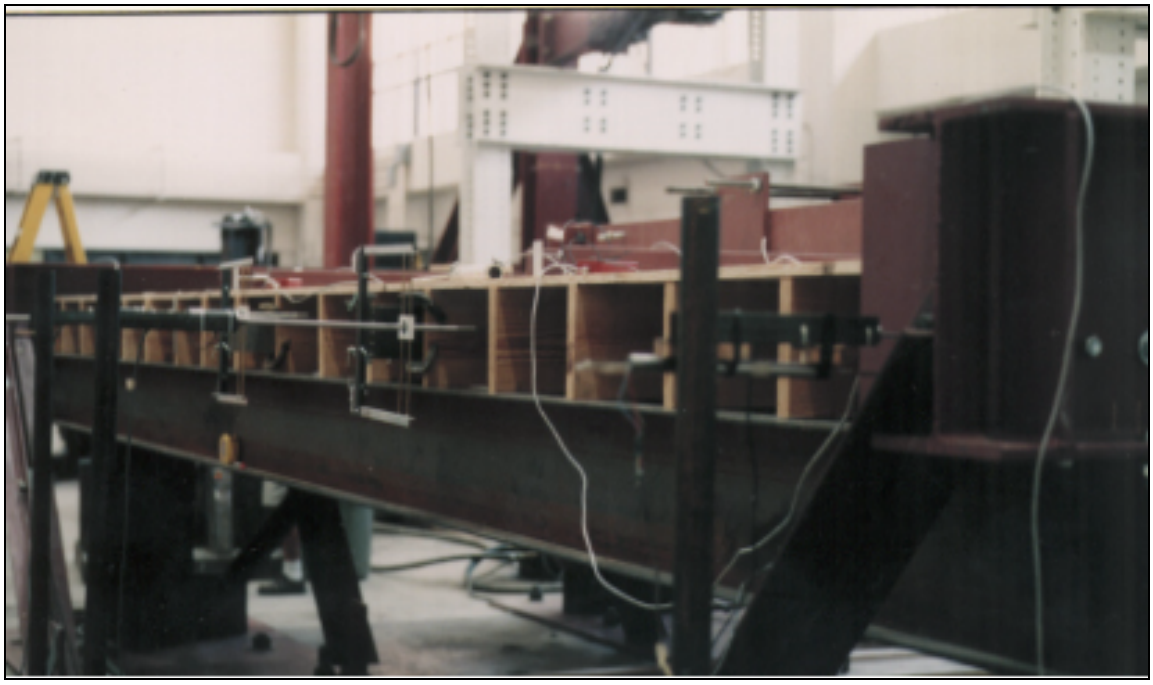

FIG. 3.16 Displacement Transducers SCH1 to SCH5 on Diaphragm MAE-2

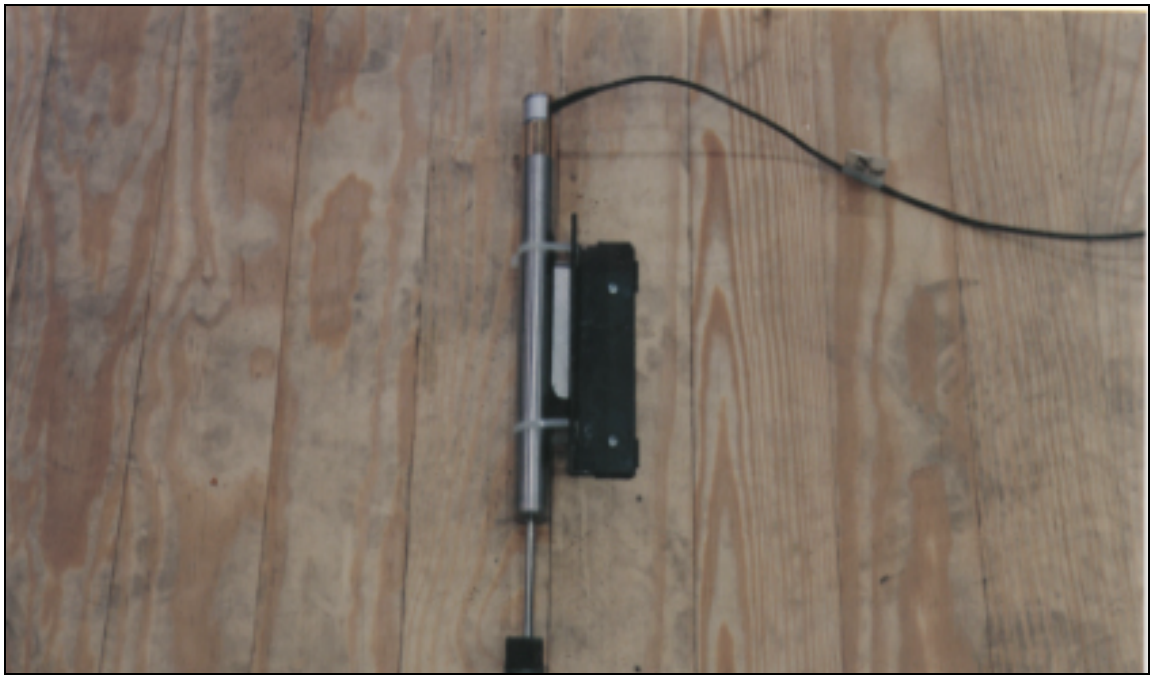

FIG. 3.17 Displacement Transducer SLIP1 on Top Face of Diaphragm MAE-1

3.3.3 Data Acquisition

A PC base data acquisition system (LabView) was used to record all data from the instrumentation to an ASCII text file on the PC hard drive. Sufficient sampling (recording) rates were selected for all tests to avoid aliasing.

3.4 LOAD PROTOCOL

Two types of loads were applied to the diaphragm specimens. The first one was a small-amplitude forced vibration test where an impulse load was applied to the diaphragm and the time history deformation response was recorded for post-processing to determine the first mode frequency of vibration of the diaphragm. The purpose of this test was to determine the initial fundamental dynamic characteristics (frequency and mode shape) of the diaphragm. This test was made only on diaphragm MAE-1, as explained in Section 4.1. The second type of test was quasi-static cyclic loading, where a displacement was applied with the actuator in incremental displacement amplitudes. The purpose of the quasi-static test was to determine the elastic and inelastic cyclic behavior of the diaphragm, deformation levels and critical failure mechanisms for each diaphragm specimen and its components. All specimens underwent quasi-static testing.

3.4.1 Forced Vibration Testing

The equipment used for forced vibration testing consisted of five accelerometers placed along the long edge of the diaphragm and connected to the data acquisition system. To force the diaphragm into free vibrations, three persons simultaneously pushed the diaphragm. The accelerometers were spaced every 1.83 m (6 ft.) and

attached at mid-height of the joist. The impact point was located at the midspan on the opposite edge of the diaphragm. Data from the instrumentation was recorded at a time step of 0.001 seconds and the maximum number of points recorded was 4,096. The measured response was post-processed to determine the fundamental frequency of the specimen using the Fast Fourier Transform. The original time response was filtered to remove high frequency contents (caused by scattering vibrations from the push and vibration from machines in the laboratory basement) using a Butterworth filter with a half-power equal to 5 and a cut-off frequency of 10 Hz to obtain a smooth time response.

3.4.2 Quasi-Static Testing

Displacement-controlled quasi-static reversed cyclic testing was performed on each diaphragm applying two cycles for each lateral displacement amplitude: 3.2, 6.4, 9.5, 12.7, 19.1, 25.4, 38.1, 50.8, 63.5 and 76.2 mm (0.125, 0.25, 0.375, 0.5, 0.75, 1.0, 1.5, 2.0, 2.5 and 3.0 in.), as shown in Fig. 3.18. These displacement amplitudes were determined to be appropriate for determining the elastic and inelastic lateral response of the diaphragm specimen. The sampling rate ranged from 4 to 0.5 points per second for the lowest and highest amplitude cycles, respectively and the load rate was kept constant at 25 mm (1 in.) per minute.

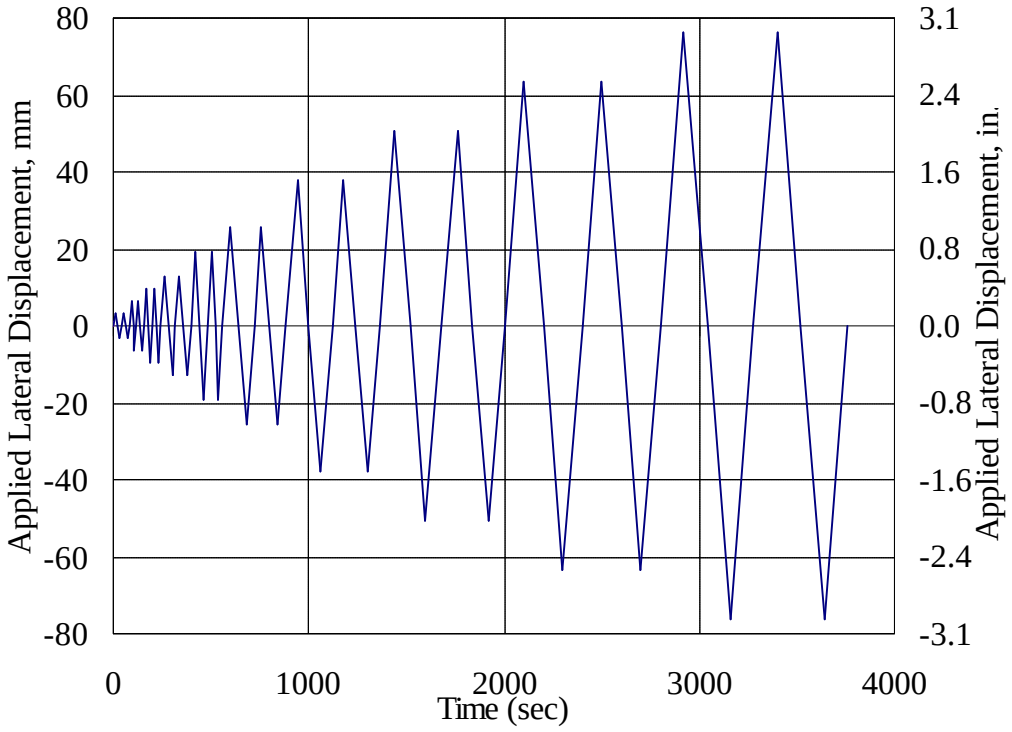

FIG. 3.18 Load History for Quasi-Static Testing

4. TEST RESULTS

4.1 GENERAL

This section presents the results of the forced vibration and quasi-static tests of the diaphragm specimens. Forced vibration tests were performed only on the first diaphragm (MAE-1 and MAE-1A), because the other diaphragms were too stiff to produce a significant vibration response. All diaphragms were tested under displacement-controlled quasi-static reversed cyclic loading.

The lateral displacements of the diaphragm specimen measured in the quasi-static tests were composed of three independent lateral displacement components: (1) displacement of the gravity and lateral load support frame (Δ_{SFR}), (2) displacement of the anchor connections between the diaphragm and the support frame (Δ_{AC}), and (3) displacement of the diaphragm at point i (Δ_{Di}) with respect to the diaphragm connections, as shown in Fig. 4.1. Displacement transducers at the diaphragm midspan and loading points (point i), at the diaphragm edge (point j) and at the support frame (point k) measured displacements relative to the reaction floor. Because of this, the diaphragm displacements recorded by the transducers included the aforementioned displacement components. Since the parameters of interest are the diaphragm and anchor behaviors, the curves presented here will consider only these two displacement components (Δ_{AC} and Δ_{Di}).

For each specimen, four typical response curves are presented. The graphs labeled “Load-Displacement at Loading Points” show the actuator load versus the average lateral displacement of the diaphragm at the connections of the loading apparatus (Δ_{LP}) (transducers SCH2 and SCH3 in Fig. 3.13). The graphs labeled “Load-Slip Displacement at Connection” show the actuator load versus average lateral displacement of the anchor connections (Δ_{AC}) (transducers SCH1 and SCH4 in Fig. 3.13). Next, the plots labeled “Load-Slip Displacement Between Boards” show the

actuator load versus the average slip displacement between sheathing boards or panels (Δ_{SB}) (transducers SLIP1 and SLIP2 in Fig. 3.13). Finally, the plots labeled "Load-Anchor Strain" show two curves representing the actuator load versus the average strain of the anchors on opposite ends of the diaphragm. The lateral displacements are calculated as follows (see instrumentation layout in Fig. 3.13):

$$\Delta_{LP} = \frac{d_{SCH2} + d_{SCH3}}{2} - \Delta_{SFR} \tag{4.1}$$

$$\Delta_{MP} = d_{TEMPC} - \Delta_{SFR} \tag{4.2}$$

$$\Delta_{AC} = \frac{d_{SCH1} + d_{SCH4}}{2} - \Delta_{SFR} \tag{4.3}$$

$$\Delta_{SFR} = \frac{d_{SFR1} + d_{SFR2}}{2} \tag{4.4}$$

where:

δ_{SCHi} = Displacement of transducer SCHi
δ_{SFRi} = Displacement of transducer SFRi
δ_{TEMPC} = Displacement of transducer TEMPC
Δ_{LP} = Average overall lateral displacement of the diaphragm at the loading points
Δ_{MP} = Overall lateral displacement of diaphragm at midspan
Δ_{AC} = Average lateral displacement of the anchor connections
Δ_{SFR} = Average lateral displacement of the support frames.

The slip displacement between boards and the anchor strains are calculated as follows:

$$\Delta_{SB} = \frac{d_{SLIP1} + d_{SLIP2}}{2} \tag{4.5}$$

$$e_{AT} = \frac{e_1 + e_3}{2}, \quad e_{AB} = \frac{e_2 + e_4}{2} \tag{4.6}$$

where:

Δ_{SB} = Average lateral slip displacement between boards
δ_{SLIPi} = Displacement of transducer SLIPi

ε_{AT}, ε_{AB} = Average strain of anchors located at the same end of the support frames

ε_1, ε_2, ε_3, ε_4= Anchor strains at the strain gauge locations (see Fig. 3.13).

A positive load and displacement in the diaphragm response corresponds to actuator contraction (pulling the diaphragm). Positive strain corresponds to this direction.

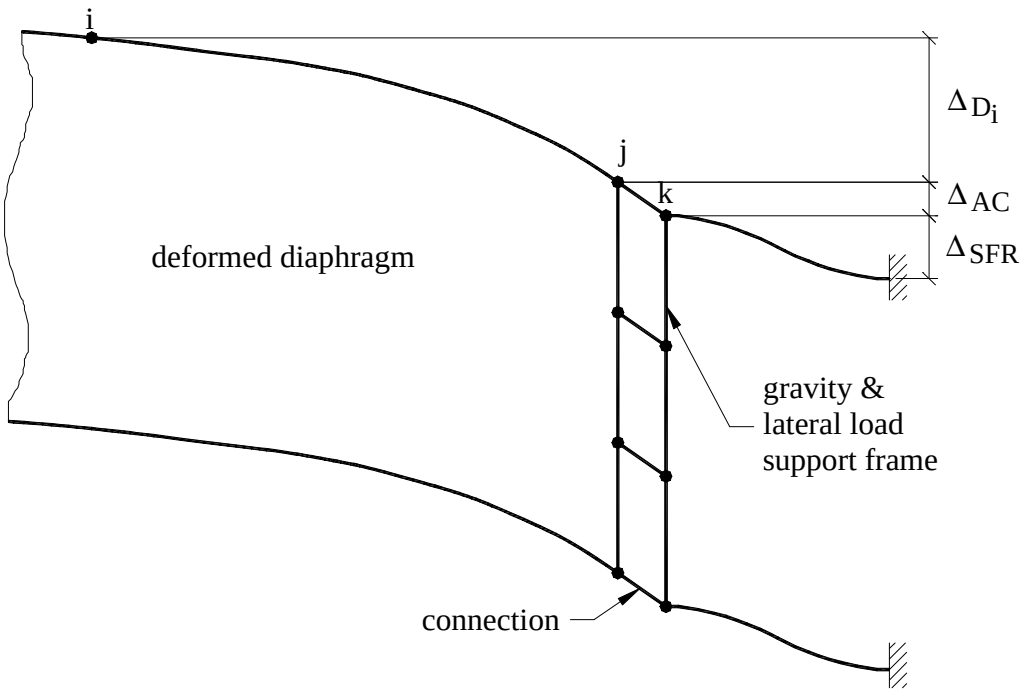

FIG. 4.1 Lateral Displacements Measured in the Tests

To determine the shape of the diaphragm at maximum loading, a parabola of order *n* was interpolated using the measured average lateral displacement of the diaphragm at the anchor connection (Δ_{AC}), loading point (Δ_{LP}) and midpoint (Δ_{MP}). The equation of a parabola with axis at the y axis and vertex at the origin is (see Fig. 4.2):

$$y = k\,x^{n} \tag{4.7}$$

where:

$$k = \frac{\Delta_{MP} - \Delta_{AC}}{\left(\frac{L}{2}\right)^{n}} \qquad n = \frac{\ln\left(\frac{\Delta_{MP} - \Delta_{LP}}{\Delta_{MP} - \Delta_{AC}}\right)}{\ln\left(\frac{48}{139}\right)}$$

L = diaphragm length

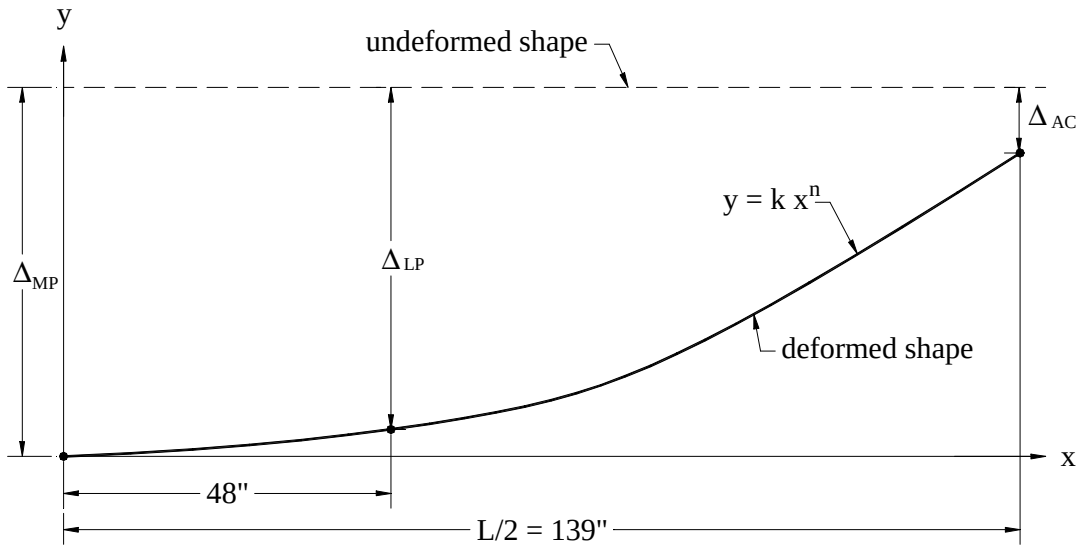

FIG. 4.2 Interpolation of Parabolic Curve for the Deformed Diaphragm

4.2 BACKBONE CURVES AND PARAMETER DEFINITIONS

The essential features of the in-plane shear force-displacement response of wood diaphragms are illustrated in Fig. 4.3. Idealized lateral force versus deformation pushover curves (backbone curves) are developed from the experimental force versus

displacement cyclic curves at the diaphragm midpoint by plotting a series of linear segments through the intersection of the first cycle curve for the (*i*)th deformation step with the second cycle curve of the (*i*-1)th deformation step, for all *i* steps, (ATC, 1997a) as shown in Fig. 4.3.

The yield displacement (Δ_y), yield force (V_y), effective stiffness (K) and post-yield stiffness (K_2) were calculated from equivalent bilinear curves. These curves were constructed from the backbone curves that characterize the behavior of the diaphragms for the nonlinear static procedure (NSP) defined in FEMA 273. The method used to estimate the yield deformation and load was based on an equivalent bilinear system with the same energy absorption as the real system (Mahin and Bertero, 1976). For the construction of the bilinear curves, the region under the bilinear curve and the backbone curve should have the same area. The intersection of the segments in the bilinear curve defines the yielding point, as shown in Fig. 4.3. The initial stiffness (K_i) of the diaphragm was taken as the slope of the first segment of the backbone curve. This parameter is used in the linear static procedure (LSP) defined in FEMA 273 and, together with the effective stiffness (K) to determine the effective fundamental period for the NSP.

A significant residual displacement (Δ_R) can occur due to inelastic response when the load is reduced to zero. When the load is reversed, the loop can show an initial low shear stiffness. It gradually increases as the load increases until the response is similar to the initial load cycle. This phenomenon is known as pinching and is attributed to the slack in nail joints associated with local damage to the wood in the vicinity of the connectors (Zagajeski et al., 1984).

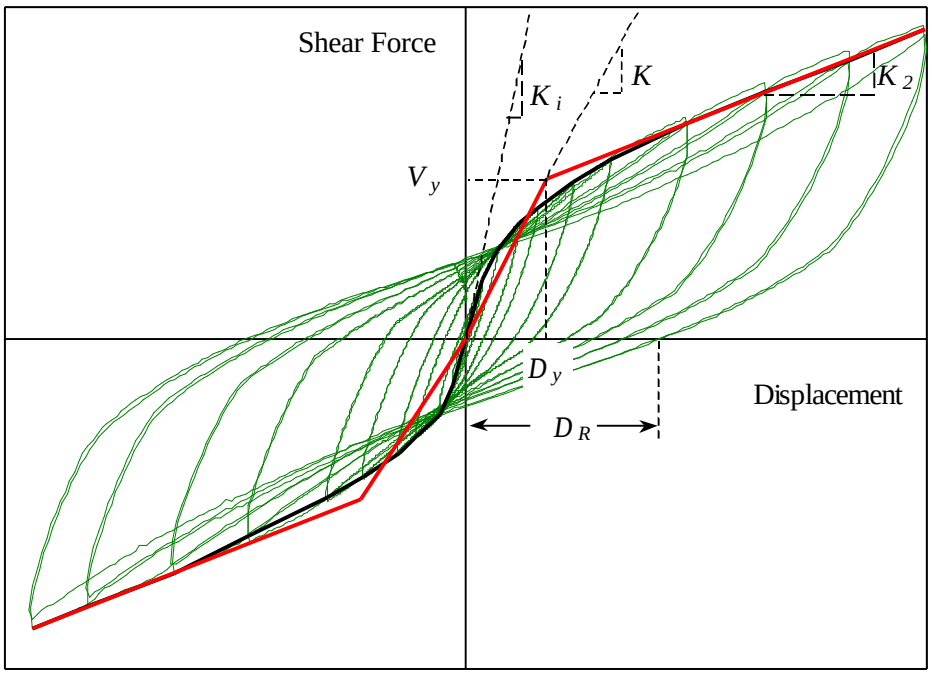

Fig. 4.3 Backbone Curve and Parameter Definition for Experimental Data

4.3 TONGUE & GROOVE SINGLE STRAIGHT SHEATHED DIAPHRAGM

4.3.1 Diaphragm MAE-1

Forced vibration tests were first performed on the T&G sheathed diaphragm with the loading frame connected to the diaphragm. The acceleration time responses at five different points on the diaphragm were recorded and later processed, as explained in Section 3.4.1, to obtain the filtered frequency responses and the corresponding smooth time responses.

A lateral impulse loading was applied to the diaphragm by having three persons simultaneously push the diaphragm in the same direction and put into free vibrations. Fig. 4.4 shows the filtered time and frequency responses for the accelerometer at the diaphragm midpoint of MAE-1. The resulting frequency response shows the fundamental peak frequency at 3.2 Hz. The damping ratio can be found applying the

logarithmic decrement method (Chopra, 1995) on the filtered time response as shown below:

$$z = \frac{1}{2pj} \ln \left[\frac{\ddot{u}_i}{\ddot{u}_{i+j}} \right] \tag{4.8}$$

where:

z = damping ratio
j = number of cycles of motion between the acceleration amplitudes
$\ddot{u}_i, \ddot{u}_{i+j}$ = acceleration at cycle i, i+j

The damping ratio was estimated by taking the average of the damping values obtained by applying Eq. 4.8 on the first and fifth peak and valley of the responses recorded in the accelerometers. The resulting average damping ratio was 11% for specimen MAE-1. The damping value reported for plywood diaphragms, as mentioned in section 2.5, was 15% to 20%.

After the forced vibration test, diaphragm MAE-1 was tested under displacement-controlled quasi-static reversed cyclic loading up to the maximum displacement amplitude of the actuator, 76 mm (3.0 in.). Fig. 4.5 shows the actuator load versus average displacement curve of the diaphragm at the loading points. Up to a lateral displacement of 2.8 mm (0.11 in.) an initial tangent stiffness (K_i) of 2 kN/cm (1.1 kips/in) was maintained during loading. On the next displacement increment, the tangent stiffness reduced to 0.9 kN/cm (0.5 kips/in), remaining nearly constant until a maximum load of 9 kN (2 kips). The residual displacement (Δ_R) grew on each cycle, with a maximum of 16.5 mm (0.65 in.) on average.

Fig. 4.6 shows the actuator load versus average displacement at the anchor connections of the diaphragm with a maximum displacement of 10 mm (0.4 in.). Comparing this displacement with the maximum lateral displacement at the diaphragm

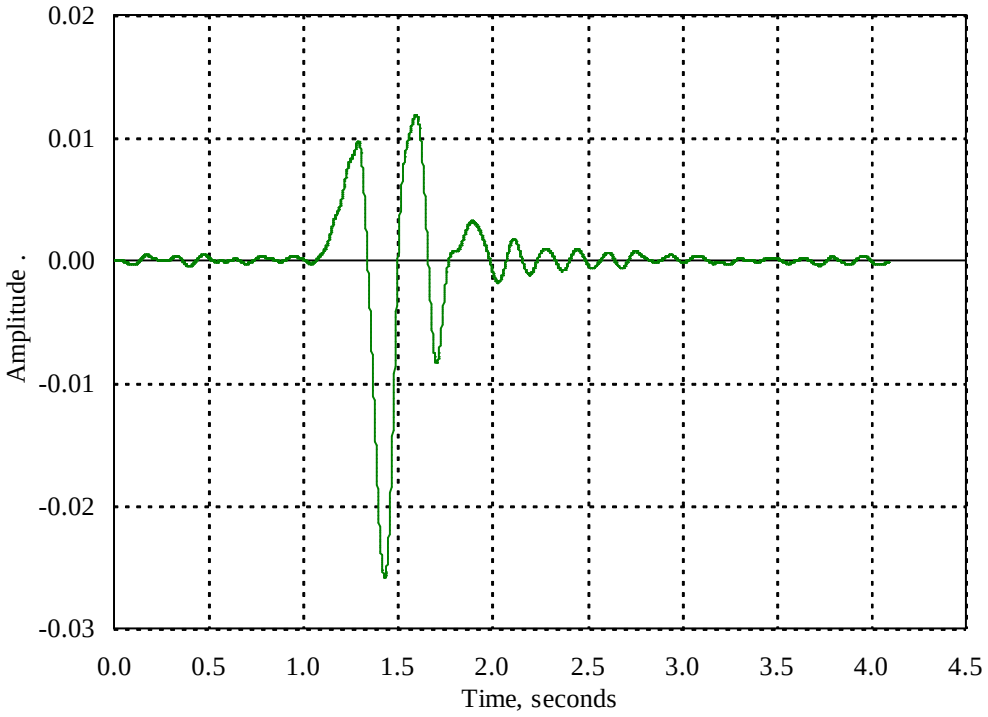

(a) Filtered Time Response

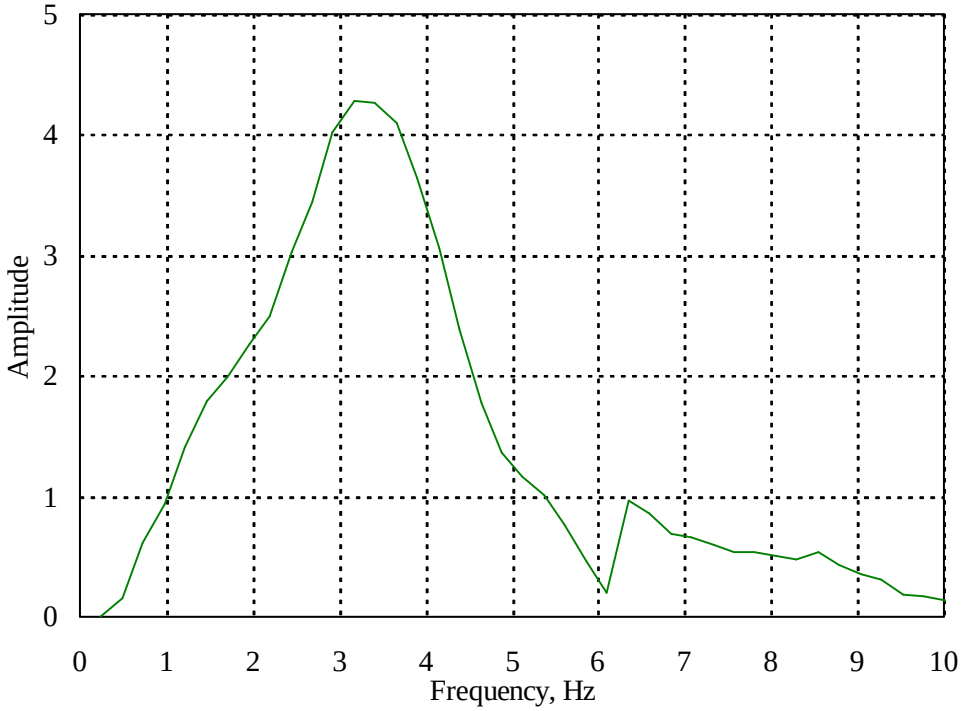

(b) Frequency Response

FIG. 4.4 Forced Vibration Response of Diaphragm MAE-1

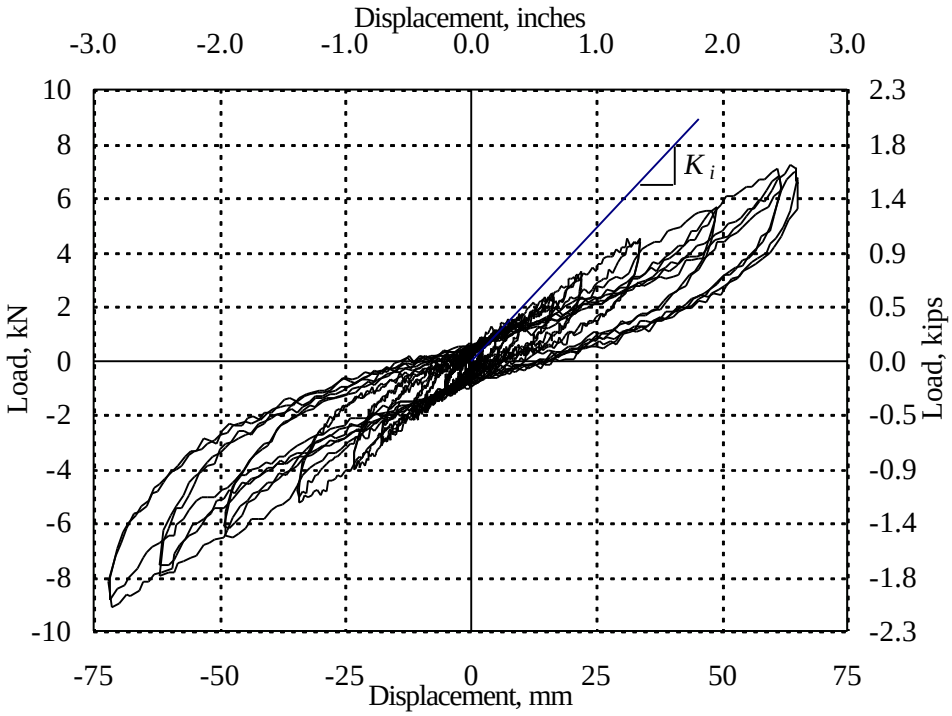

FIG. 4.5 Diaphragm MAE-1. Load-Displacement at Loading Points

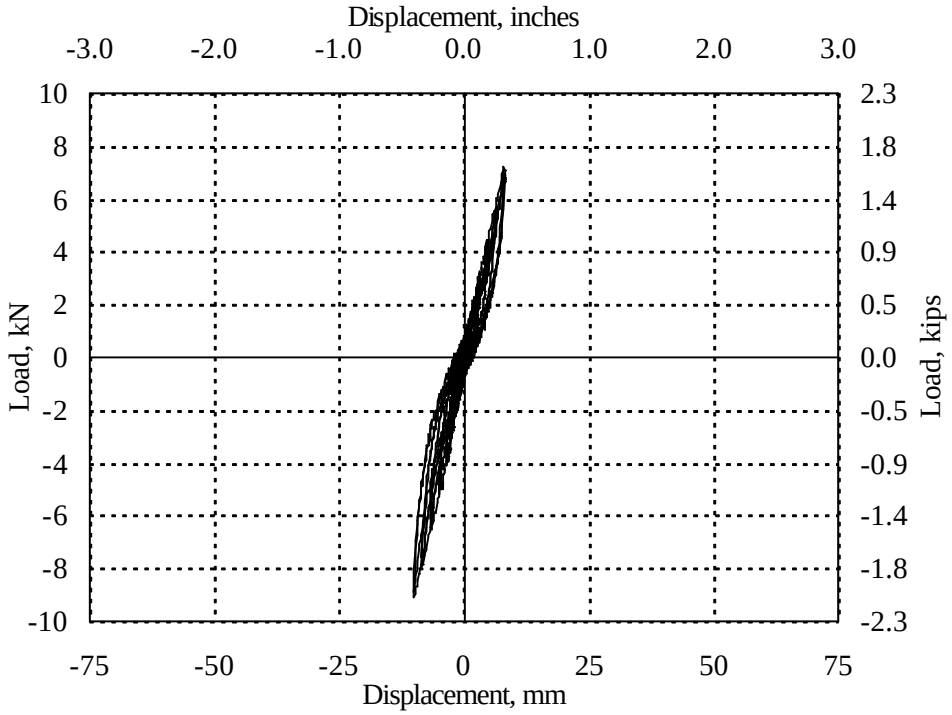

FIG. 4.6 Diaphragm MAE-1. Load-Slip Displacement at Connection

midpoint, (Δ_{MP}) 71 mm (2.8 in.), shows that the lateral displacement of the anchor connection contributed 14% to the overall lateral displacement.

An indication of the nail behavior in this diaphragm is given by Fig. 4.7, which shows the actuator load versus average slip displacement between T&G sheathing boards. The measured slip is composed by two parts: (1) the lateral displacement of the joists between the two adjacent sheathing boards (δ_j); and (2) the lateral deformation of the nails (nail slip) at the same location (δ_{ns}). The lateral displacement of the joist (δ_j) can be approximated from Eq. 4.7, replacing the average displacements measured in the diaphragm. Using Eq. 4.7 to determine the slope of the parabola, evaluating it at the transducer location (x = 96 in., see Fig. 3.13) and multiplying by the width of one sheathing board, 89 mm (3.5 in.), a lateral joist displacement (δ_j) of 2.3 mm (0.089 in.) resulted. Subtracting it from the slip between sheathing boards (Δ_{SB}) equal to 1.4 mm (0.055 in.), a nail slip (δ_{ns}) of 0.9 mm (0.034 in.) resulted.

Fig. 4.8 shows the curves of actuator load versus average strain of the anchor connection. The strains were due to bending and axial actions, but the data available was insufficient to clarify their amount of participation. The primary factor for the nonlinear behavior in these curves is the out of phase response between the actuator (vertical axis) and the strains in the anchor (horizontal axis). The reasons for the effect are stated below. First, the actuator load and anchor connections were not at the same horizontal plane. This vertical eccentricity could have introduced torsional moments to the anchors twisting them without increasing the strains. This behavior can be reflected in the slope of the loops that are almost vertical at higher loads during loading and unloading. Second, the way the anchors were connected to the joists caused the anchors to behave differently under compression and tension. As observed in Fig. 3.3, the joist

was able to bear against the anchor when it was under compression, but separate from the anchor when in tension, after reversing the load. Third, the nail-slip between the sheathing and the joists could generate a residual deformation that might affect the anchor connections.

The actuator load versus anchor strain curve of the strain gauges closer to the actuator (ε_{AB}) shows that the compression strain was higher than the tension strain for every cycle. On the last cycle, the compression strain was 420 μs, twice the magnitude of the tension strain but lower than the yield strain (1200 μs). It was not possible to verify if the compression strains were due to axial or flexural actions. To determine deformation from bending actions, two strain gauges per anchor were required, placed on opposite sides of the anchor, where the maximum deformations might occur.

It should be emphasized that there were no signs of damage to the wood components or anchor connections of the diaphragm. The lack of damage was attributed to the high flexibility of the diaphragm, which allowed high deformations under small loads. Permanent lateral deformations of the nails were not visible.

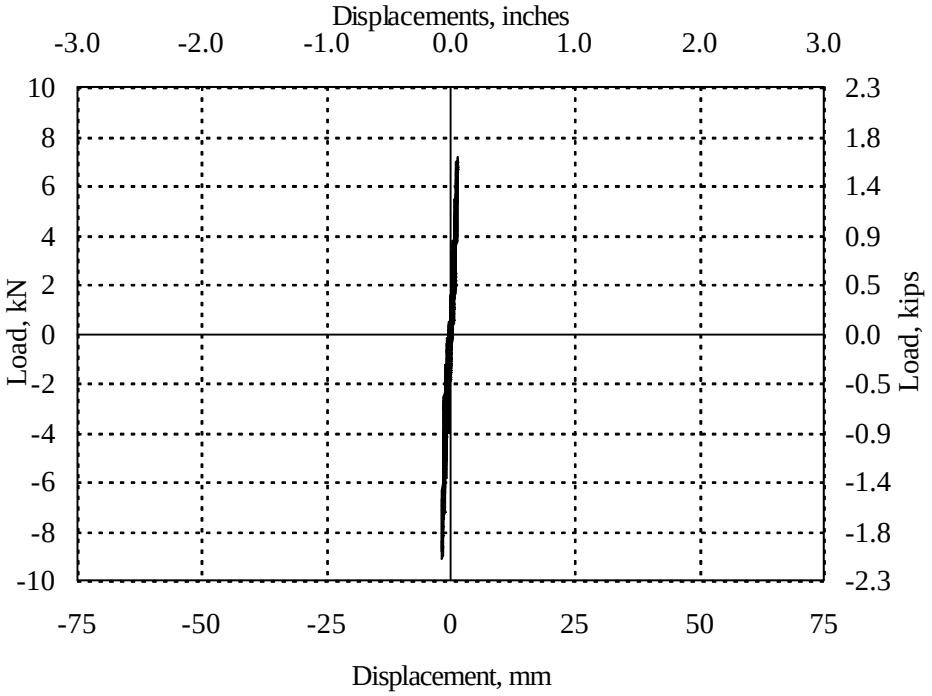

FIG. 4.7 Diaphragm MAE-1. Load-Slip Displacement Between Tongue & Groove Sheathing

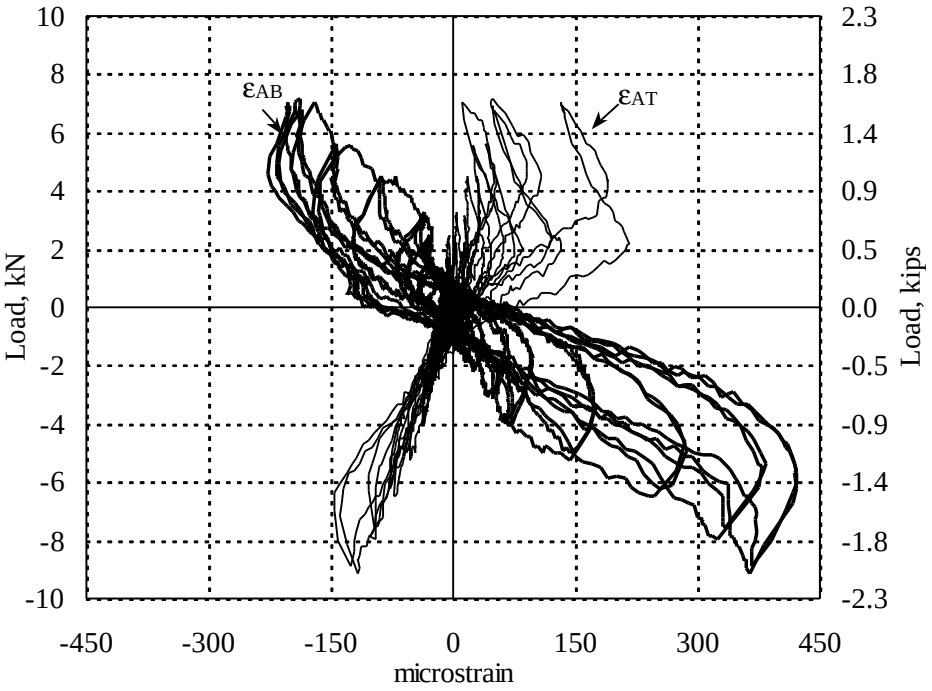

FIG. 4.8 Diaphragm MAE-1. Load-Anchor Strain

4.3.2 Connection Retrofit Diaphragm MAE-1A

A forced vibration test was performed for the connection retrofit diaphragm MAE-1A. The instrumentation was the same as in the previous test for MAE-1 and the impulse force was again manually applied to excite the desired fundamental frequency. The filtered time history response and the corresponding frequency response for the midpoint diaphragm accelerometer are shown in Fig. 4.9. The frequency response shows the fundamental frequency at 3.7 Hz. The logarithmic decrement method was used, as described in MAE-1, and a damping ratio of 15.5% for diaphragm MAE-1A was obtained.

A quasi-static test was then performed using additional instrumentation to monitor the strapping elements, as described in Section 3.3.2. In general the behavior of diaphragm MAE-1A was stiffer and stronger than MAE-1, as shown when comparing Figs. 4.10 and 4.5. The peak actuator load increased to 18 kN (4 kips), about two times the peak load of the unretrofitted case, for a mid-point diaphragm maximum overall lateral displacement of 76 mm (3.0 in.). The increase in shear strength came from the lag screws used to secure the longitudinal strapping in the sheathing boards and also from the additional shear connections. Fig. 4.10 also shows more clearly that the load versus deformation behavior is approximately bi-linear, with an initial tangent stiffness (K_i) of 12 kN/cm (6.7 kips/in.) followed by a post-yield tangent stiffness of 1.3 kN/cm (0.8 kips/in.). The additional bolted connections to the support frames used in this retrofit reduced the lateral displacement of the anchors to 5 mm (0.2 in.), as shown in Fig. 4.11, which is 6.7% of the total lateral displacement at the diaphragm midpoint.

The maximum slip displacement between T&G sheathing (Δ_{SB}) was 2.9 mm (0.115 in.), as shown in Fig. 4.12. Using Eq. 4.7 to interpolate a parabola for the deformed diaphragm and proceeding as explained in MAE-1, a lateral joist displacement (δ_j) of 2.5 mm (0.099 in.) resulted. After obtaining the difference between the two values, a nail slip (δ_{ns}) of 0.4 mm (0.016 in.) was computed.

The average strain behavior of the anchor connection is shown in Fig. 4.13. Only the values of strain gauge ε_2 were used for ε_{AB}, due to instrumentation errors with ε_4. Similarly as in diaphragm MAE-1, the out of phase response between the actuator and the anchors can contribute to the nonlinear behavior, but to a smaller degree, because of the presence of the bolted connections on top of diaphragm MAE-1A. Also, the anchor connections showed a higher strain under compression (550 μs) versus 160 μs under tension. Under tension, the joist separated from the anchor, while it bore on the anchor strap under compression. It was not clear if compression forces developed in the anchor section. The effect of the nail-slip on the behavior of the anchor was reduced by the presence of the perimeter strapping.

Fig. 4.14 shows actuator load versus strain curves at the ends and midpoints of the steel strapping on the long edge of the diaphragm, with a maximum of 170 μs and 95 μs, respectively. In this case, the strain gauges were at mid width of the strapping section, measuring the axial deformations directly. Eq. 4.9 gives the axial force developed in the strapping :

$$F = E\varepsilon A \tag{4.9}$$

where E is the Young's modulus of the material, ε is the measured axial strain and A is the area of section.

For the steel strapping, a Young's modulus of 20,020 kN/cm^2 (29,000 ksi) and an area of 3.2 cm^2 (0.5 in.^{2}) gives a maximum force of 11 kN (2.5 kips). Assuming the joist underneath the strapping developed the same strain, Eq. 4.9 can be used to calculate the force developed in the joist. Using a Young's modulus of 1,312 kN/cm^2 (1,900 ksi) for Southern Pine and an area of 89.7 cm^2 (13.9 in.^{2}), a force of 20 kN (4.5 kips) was obtained. Then a total force of 31 kN (7 kips) was developed in the chord of the diaphragm, resisted by the anchor and bolted connections on the chord ends. After a visual inspection of the diaphragm, no signs of visible damage were found in the sheathing, joists anchor connections, strapping or bolted connections.

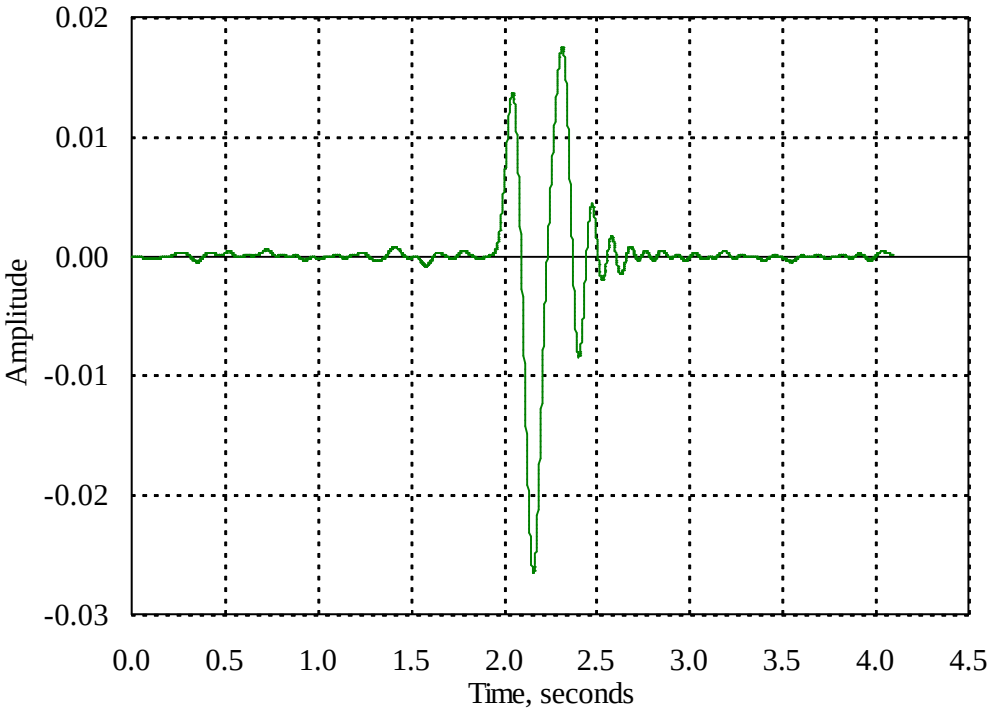

(a) Filtered Time Response

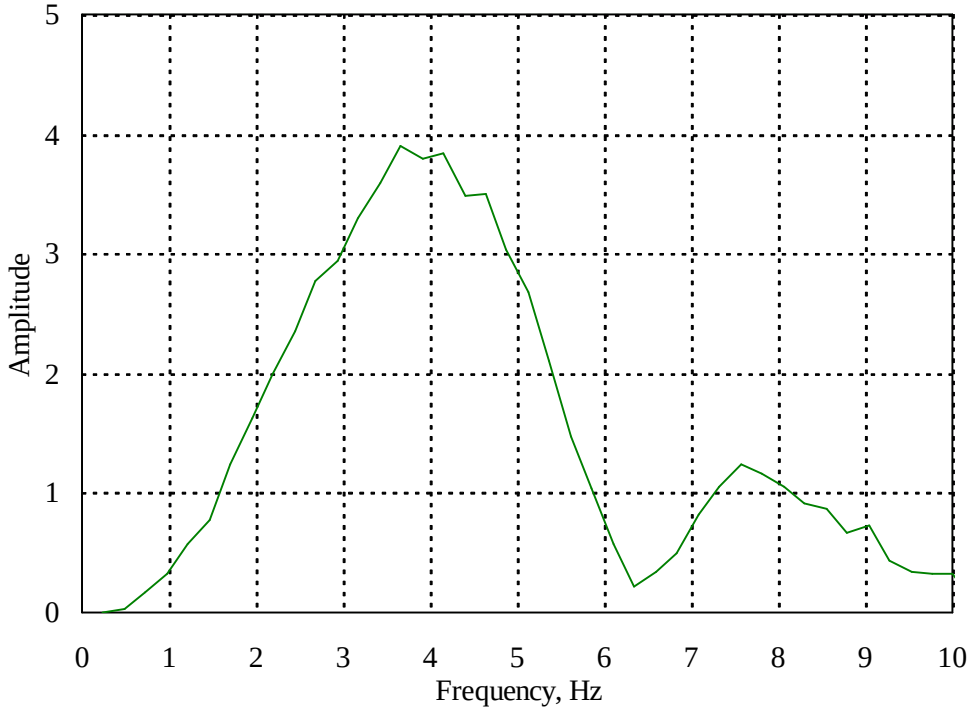

(b) Frequency Response

FIG. 4.9 Forced Vibration Response of Diaphragm MAE-1A

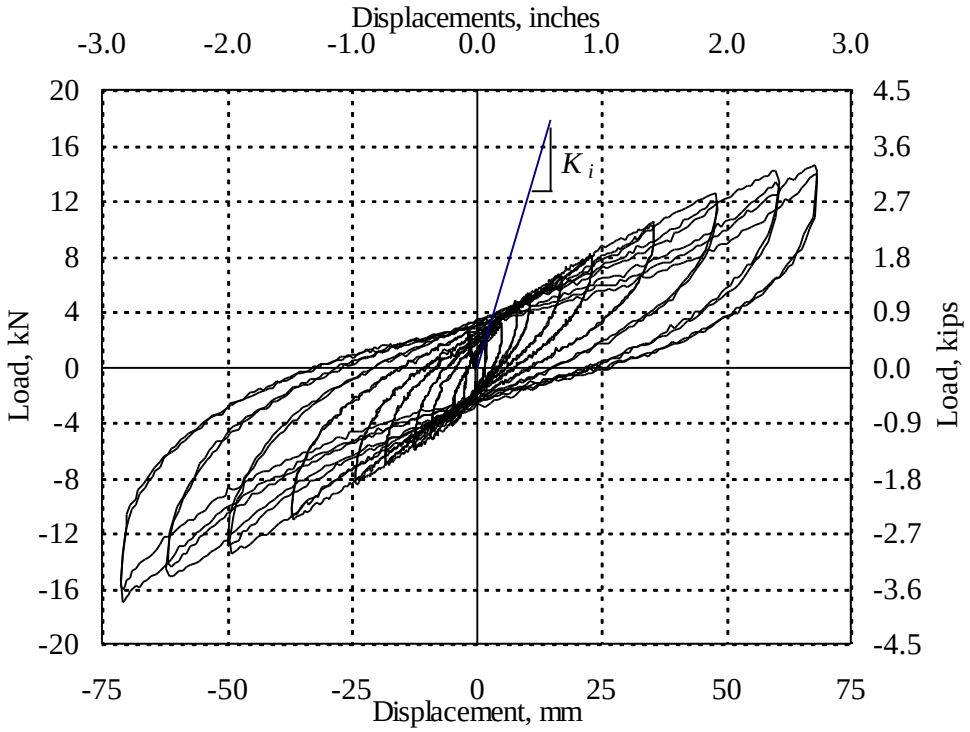

FIG. 4.10 Diaphragm MAE-1A. Load-Displacement at Loading Points

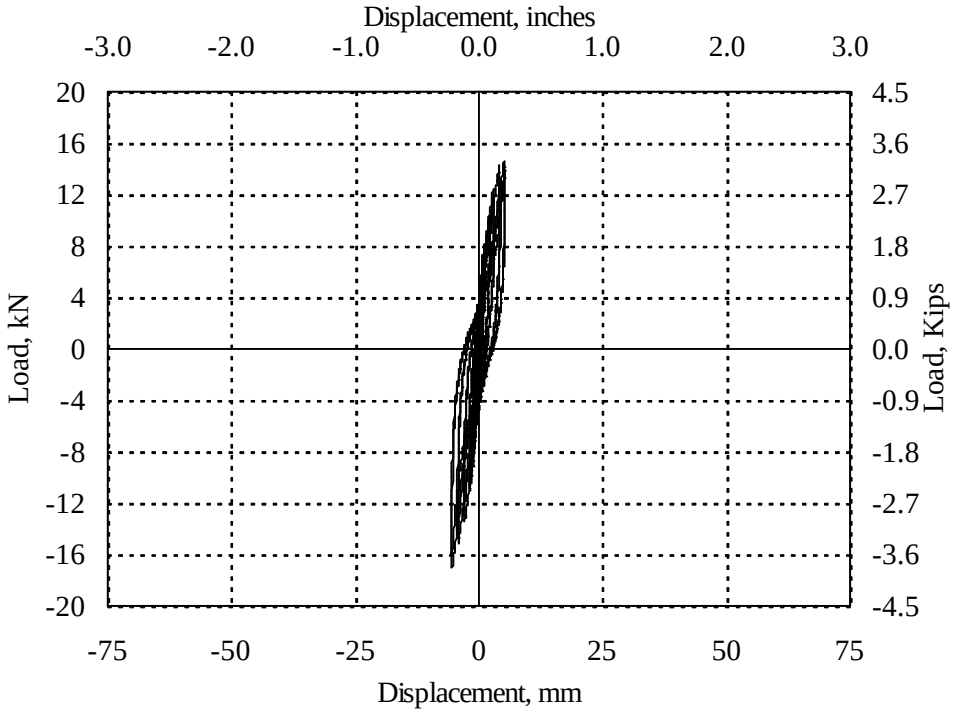

FIG. 4.11 Diaphragm MAE-1A. Load-Slip Displacement at Connection

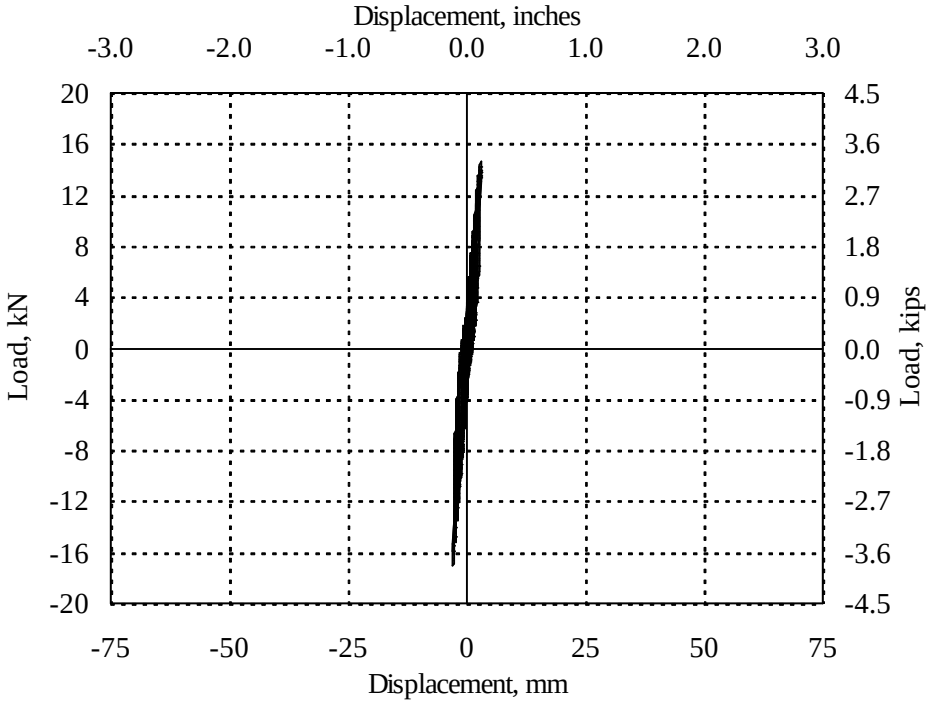

FIG. 4.12 Diaphragm MAE-1A. Load-Slip Displacement Between Tongue & Groove Sheathing

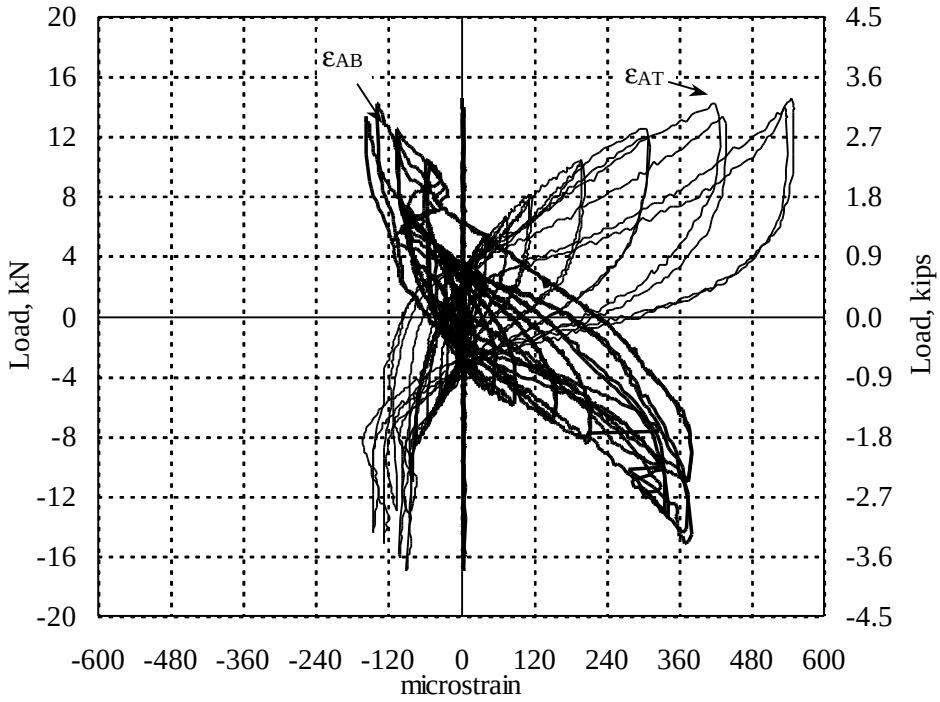

FIG. 4.13 Diaphragm MAE-1A. Load-Anchor Strain

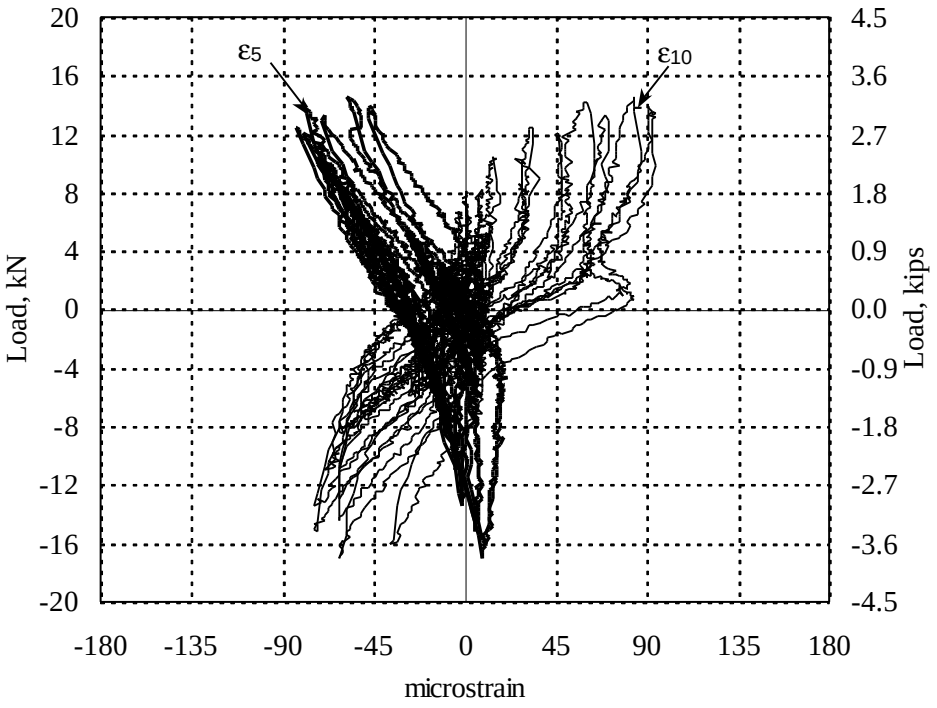

(a) Midpoints of Strap

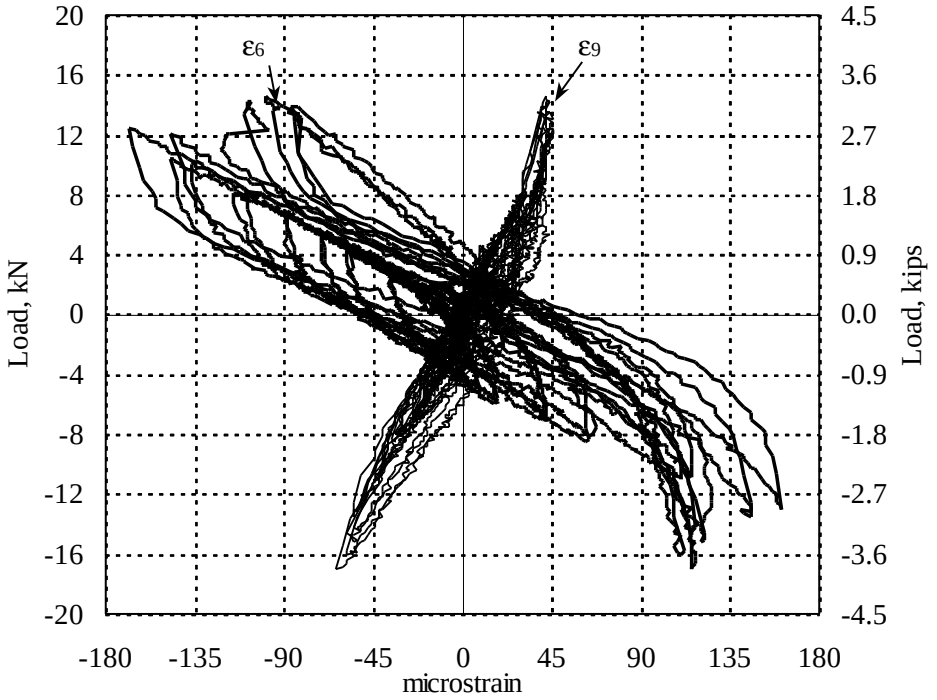

(b) Ends of Strap

FIG. 4.14 Diaphragm MAE-1A. Load-Strap Strain

4.3.3 Steel Truss Retrofit Diaphragm MAE-1B

Quasi-static testing with the same characteristics as the previous tests was conducted on diaphragm MAE-1B, using additional instrumentation to monitor the strains in the steel truss members, as described in Section 3.3.2. The displacement sequence applied for this test included a new cycle at 32 mm (1.25 in.). As observed in Fig. 4.15, the initial stiffness (K_i) of this diaphragm was 108 kN/cm (61.4 kips/in.) and the peak actuator load was 169 kN (38 kips).

The higher lateral loads applied to this retrofit generated a large overturning moment (from the vertical eccentricity between the actuator, sheathing and the steel truss), which tended to twist the joists along their longitudinal axes. This resulted in smaller displacements read by the instruments along the diaphragm edge, because the displacement transducers were positioned at the joist midheight. For example a maximum displacement of 36 mm (1.4 in.) was measured at the diaphragm midpoint for the last applied displacement of 64 mm (2.5 in.). The test was terminated at this cycle because of this, and not because of specific failure to the diaphragm sheathing.

Fig. 4.16 shows the actuator load versus average displacement at the anchor connection (Δ_{AC}) with a maximum lateral displacement of 4 mm (0.16 in.), which is about 10% of the maximum diaphragm displacement at the loading points, 38 mm (1.5 in.).

The maximum slip displacement measured between T&G sheathing (Δ_{SB}) was 3 mm (0.11 in.), as shown in Fig. 4.17. The measured diaphragm midpoint displacement (Δ_{MP}) was lower than the diaphragm displacement at the loading points, so it was corrected using the values in the other direction. Using Eq. 4.7 and the same approach described for MAE-1, the lateral joist displacement (δ_j) was computed to be 1.4 mm (0.054 in.). Taking the difference between these two values, a nail slip of 1.4 mm (0.056 in.) resulted.

The curves of actuator force versus average strain of the anchor connections are shown in Fig. 4.18. Only strain gauge ε_2 was used for the values of ε_{AB}. The rolling of the joists introduced torsion to the anchor connections. This behavior might be reflected when the loops show load increase without any strain variation. The anchor connections developed higher strains in compression, 312 μs over 170 μs in tension. A better contact between the anchor and the joist was attributed for the difference. Having only one strain gauge per anchor, it was not possible to determine the contribution of bending and axial actions in the measured strain.

Fig. 4.19 shows the strains in the truss members, which had a maximum of 221 μs in the horizontal braces under tension forces. Using Eq. 4.9, a maximum axial force of 55 kN (12.3 kips) was computed for the horizontal brace. Based in the equilibrium relationship between the brace forces and the external load (see Fig. 5.2), a force of 165 kN (36.9 kips) was transferred from the actuator load of 169 kN (38 kips). Then the sheathing absorbed a force of 4.9 kN (1.1 kips). The design load for the horizontal brace was 125 kN (28 kips). The diagonal braces showed a maximum strain of 188 μs giving only a load of 46.8 kN (10.5 kips).

At an applied displacement cycle of 38 mm (1.5 in.), major bending cracks, caused by the diaphragm shears and overturning moment from the vertical eccentricity of the load, appeared in the upper part of the joist webs, close to the sheathing. Most of the cracks began propagating from the nails that attached blocking members to the joists. Fig. 4.20 shows a photo of a typical joist after it was disassembled from the diaphragm. The blocking members were used to attach the loading frame to the sheathing. The cracks were visible from both sides of the joist and were distributed mostly underneath the loading frame, as shown in Fig. 4.21. The joist anchors did not suffer damage, possibly because the bolted connections on top of the diaphragm prevented major twisting of the anchor connections. No visible damage was found in the T&G boards or nails.

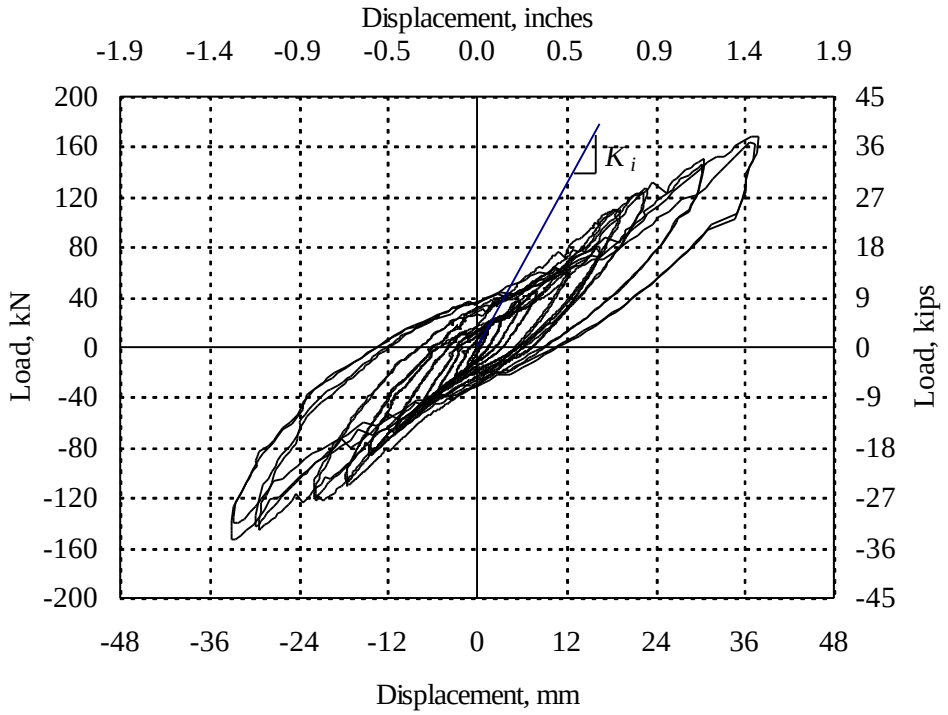

FIG. 4.15 Diaphragm MAE-1B. Load-Displacement at Loading Points

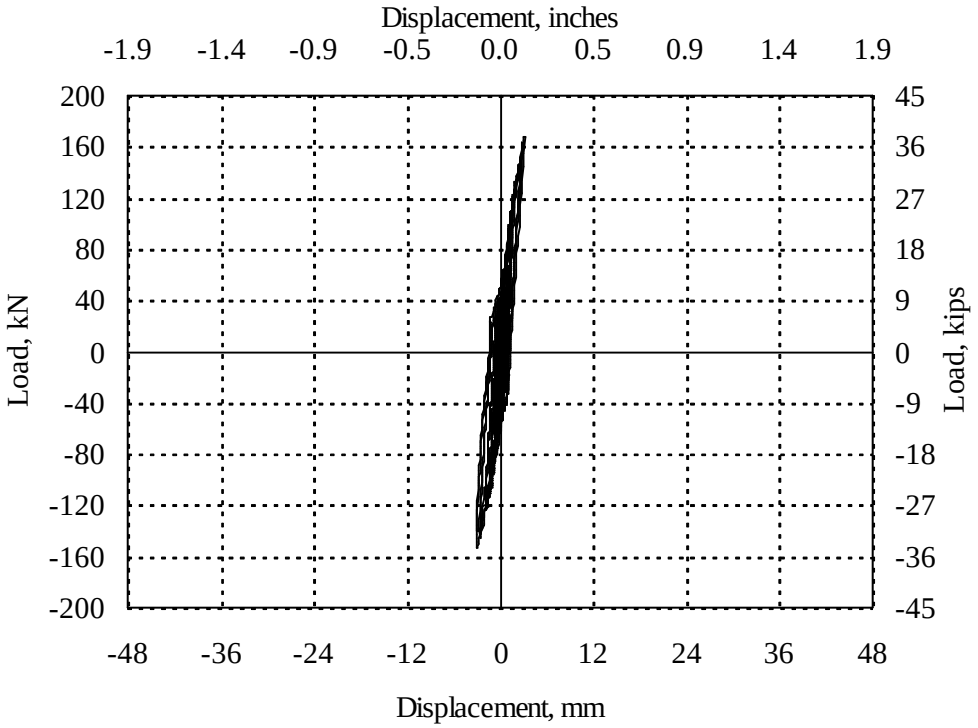

FIG. 4.16 Diaphragm MAE-1B. Load-Slip Displacement at Connection

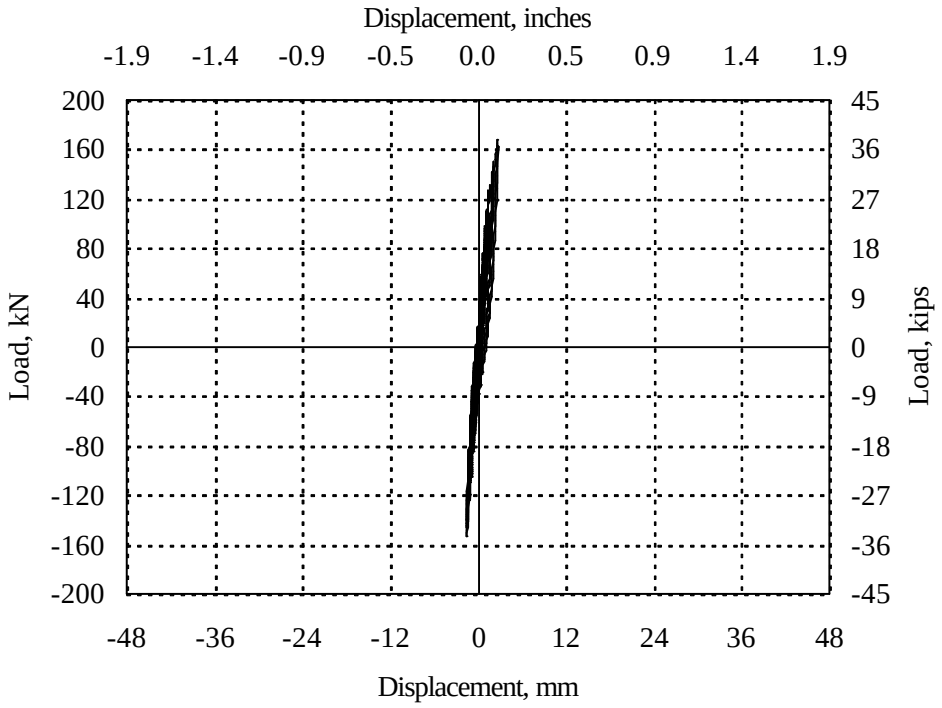

FIG. 4.17 Diaphragm MAE-1B. Load-Slip Displacement Between Tongue & Groove Sheathing

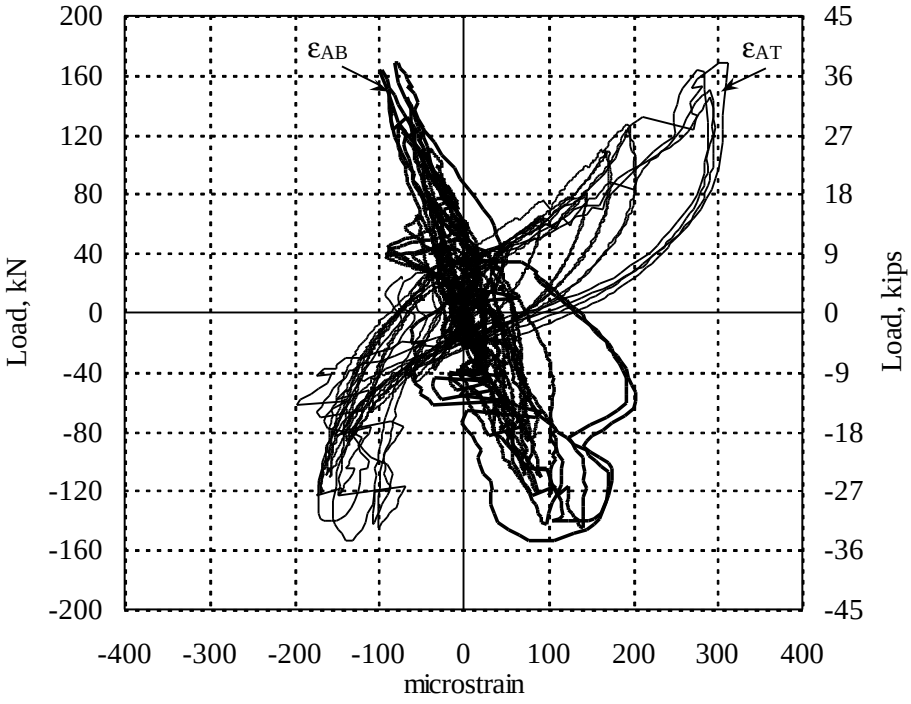

FIG. 4.18 Diaphragm MAE-1B. Load-Anchor Strain

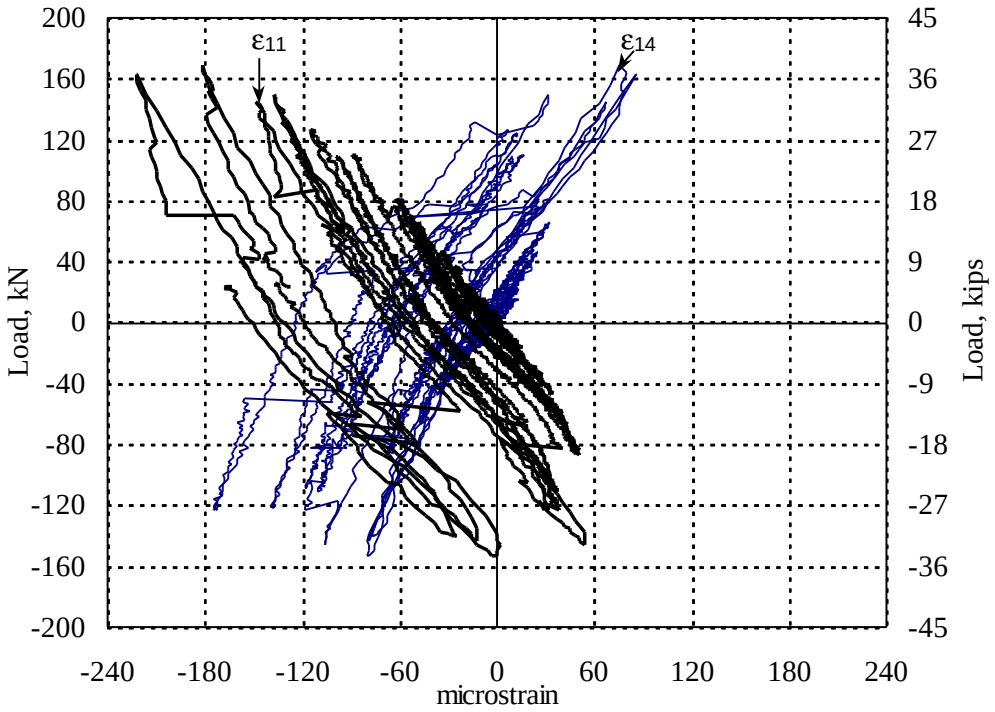

a) Horizontal Braces

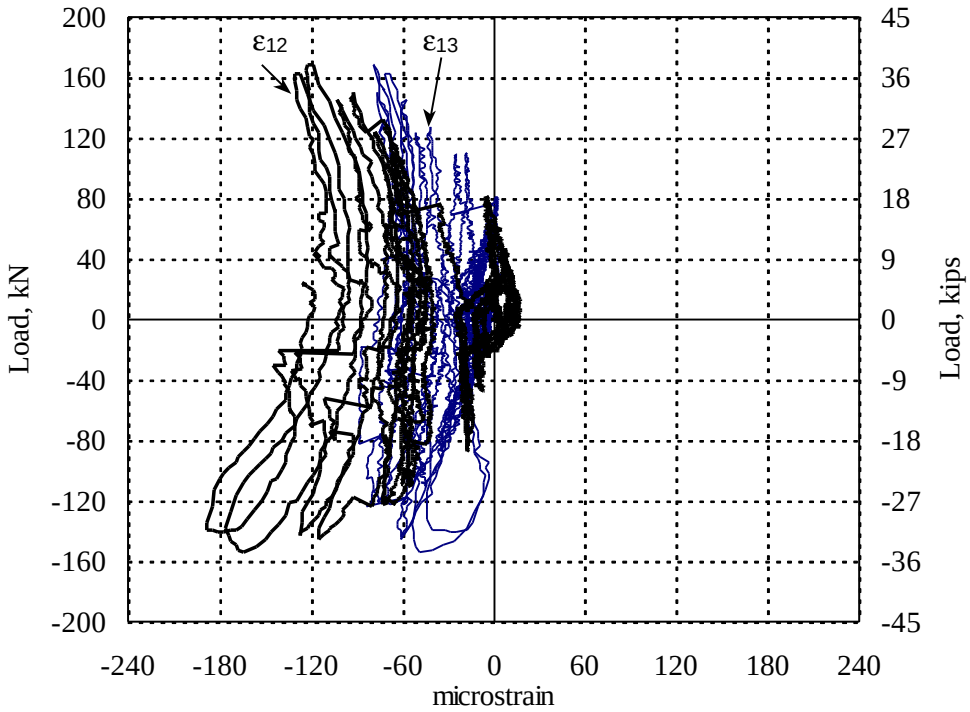

b) Diagonal Braces

FIG. 4.19 Diaphragm MAE-1B. Load-Truss Strain

FIG. 4.20 Crack in Joist of Diaphragm MAE-1B (After Disassembly)

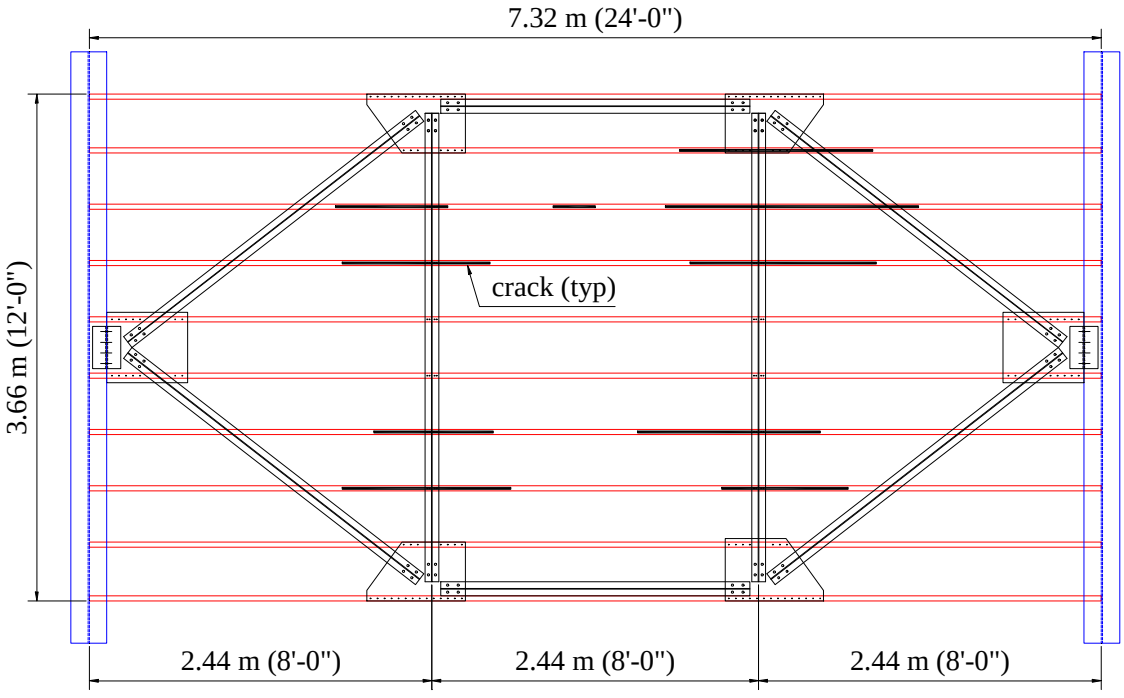

FIG. 4.21 Crack Locations in the Joists After Testing Diaphragm MAE-1B

4.3.4 Comparison of Responses

Table 4.1 shows the fundamental frequencies obtained from each forced vibration test. The table also shows the calculated initial stiffness of the diaphragm using a single-degree of freedom lumped mass model:

$$K_i = 4p^2 mf^2 \tag{4.10}$$

where:

K_i = initial stiffness of diaphragm (kN/cm)
m = mass of diaphragm (kN s^2/cm)
f = fundamental frequency (Hz)

TABLE 4.1 Diaphragm Initial Stiffness from Forced Vibration Tests

Diaphragm	Frequency[1] (Hz)	Weight[2] kN (kips)	Initial Stiffness[3] kN/cm (kips/in.)
MAE-1	3.2	8.9 (2.0)	3.6 (2.1)
MAE-1A	3.7	9.4 (2.1)	5.1 (2.9)

[1] measured
[2] estimated
[3] calculated from Eq. 4.10

The weights of diaphragm MAE-1 and the loading apparatus were estimated to be approximately 9 kN (2 kips) total and, for MAE-1A, the steel strapping and bolted connections weighed an estimated 0.45 kN (0.1 kips). The table shows that the measured frequency of MAE-1A is 16% higher than MAE-1. This trend follows Eq. 4.10, which shows that for systems of comparable mass, the stiffer system has a higher fundamental frequency. But when comparing the initial stiffness (K_i) obtained from the forced vibrations tests and from the quasi-static tests, the values do not match. For diaphragm MAE-1, the dynamic over static initial stiffness ratio was 1.9, while in MAE-1A the ratio was 0.43. A cause of the discrepancy could be that the lumped model was

not appropriate. Other reasons could originate from the difficulty in estimating the initial stiffness from the quasi-static test data, because at the beginning the points were not following a smooth curve.

Figs. 4.22 to 4.24 show the diaphragm backbone curves (according to FEMA 273) constructed from the data at the diaphragm midpoint, except for diaphragm MAE-1B that used the data at the loading points because the data at midpoint was distorted by the overturning moment. A superposition of the backbone curves is shown in Fig. 4.25 for comparison. Diaphragm MAE-1B was significantly stiffer and stronger than MAE-1 and MAE1-A.

A summary of the maximum response parameters measured during testing of diaphragm MAE-1 and its retrofits, MAE-1A and MAE-1B, is given in Table 4.2. It can be observed that the initial stiffness (K_i) of retrofitted diaphragms MAE-1A and MAE-1B was six and 55 times higher than in MAE-1, respectively. Table 4.3 shows the yielding parameters from the bilinear curves and the ratios of variation between MAE-1A and MAE-1 and MAE-1B and MAE-1. As the ratios show, the yield force (V_y), effective stiffness (K) and post-yield stiffness (K_2) for MAE-1A and MAE-1B increased with respect to MAE-1. The yield displacement (Δ_y) for MAE-1A and MAE-1B decreased to 60% and 80% of MAE-1, respectively.

As calculated in the previous sections, from the average slip between T&G boards, it was possible to obtain the average nail slip, which varied from 0.9 mm (0.034 in.) in diaphragm MAE-1 to 0.4 mm (0.016 in.) and 1.4 mm (0.056 in.) in diaphragms MAE-1A and MAE-1B, respectively. The addition of steel strapping and lag screws resulted in a 50% reduction of nail slip in MAE-1A even though the shear demand had doubled. The increase of nail-slip in MAE-1B with respect to MAE-1A was 3.5 times, while the actuator force increased ten times.

The lateral displacement at the anchor connection (Δ_{AC}) was 14%, 7% and 11% of the overall lateral displacement at the diaphragm midpoint (Δ_{MP}) for diaphragms MAE-1, MAE-1A and MAE-1B, respectively. The additional bolted connections on top of diaphragm MAE-1A reduced the ratio Δ_{AC}/Δ_{MP} by 50% and by 21% in MAE-1B, with the addition of the truss connections. In all three cases, the anchors had higher strains in one direction of the loading when compared to the other direction (1.9 times in MAE-1, 3.4 times in MAE-1A and 1.8 times in MAE-1B). This occurred because the joist was able to bear against the anchor in one direction (greater strains) but separated from the anchor when the direction of the load was reversed (see Fig. 3.3). The anchors were subjected to bending, axial forces and possibly torsion and because only one strain gauge was used on the anchor, it was not possible to obtain the contribution of each action to the strains.

The behavior of the anchor connections is shown in Fig. 4.26. It is observed that the maximum displacement of the anchors (Δ_{AC}) in the retrofitted diaphragms MAE-1A and MAE-1B was reduced to 65% and 40% of MAE-1, respectively. The additional bolted connections used on top of diaphragms MAE-1A and MAE-1B reduced the anchor displacement in spite of the higher loads applied to the diaphragm.

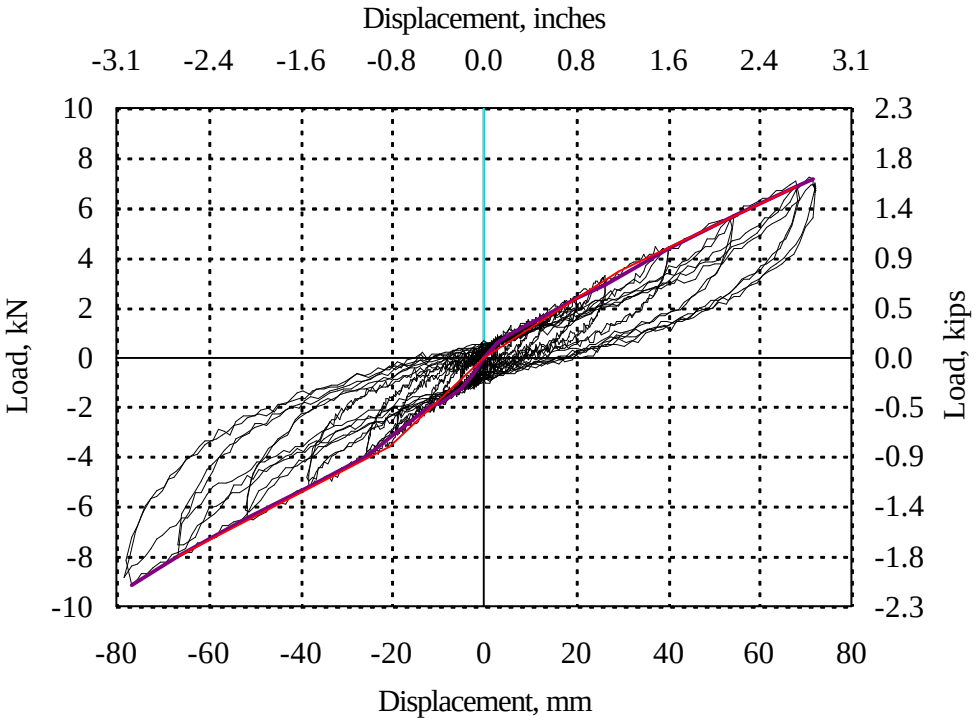

FIG. 4.22 Backbone Curve at Midpoint of Diaphragm MAE-1

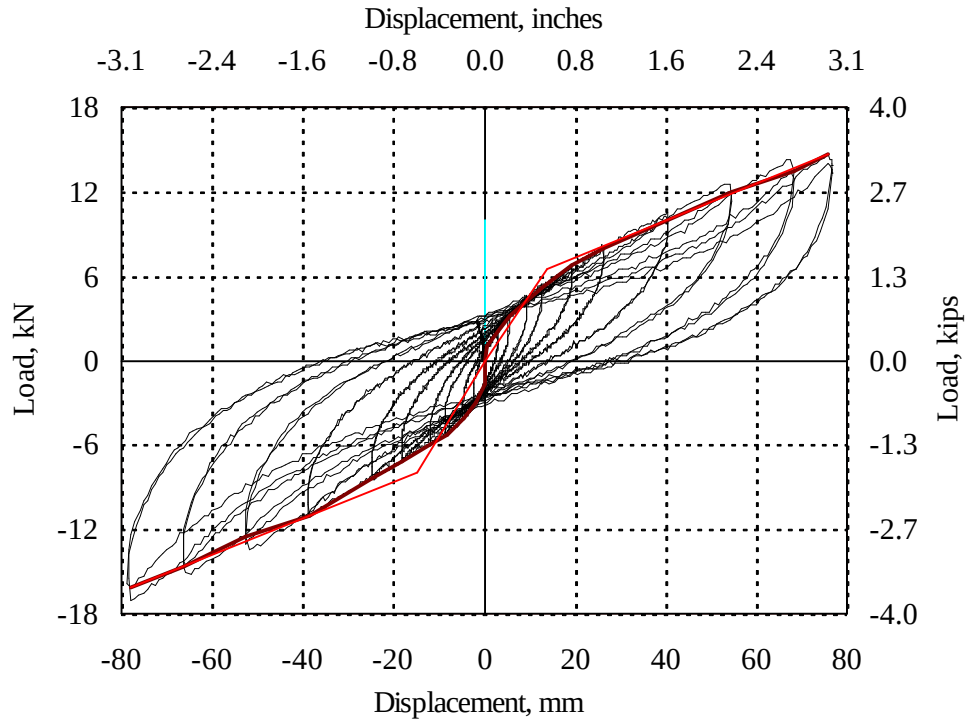

FIG. 4.23 Backbone Curve at Midpoint of Diaphragm MAE-1A

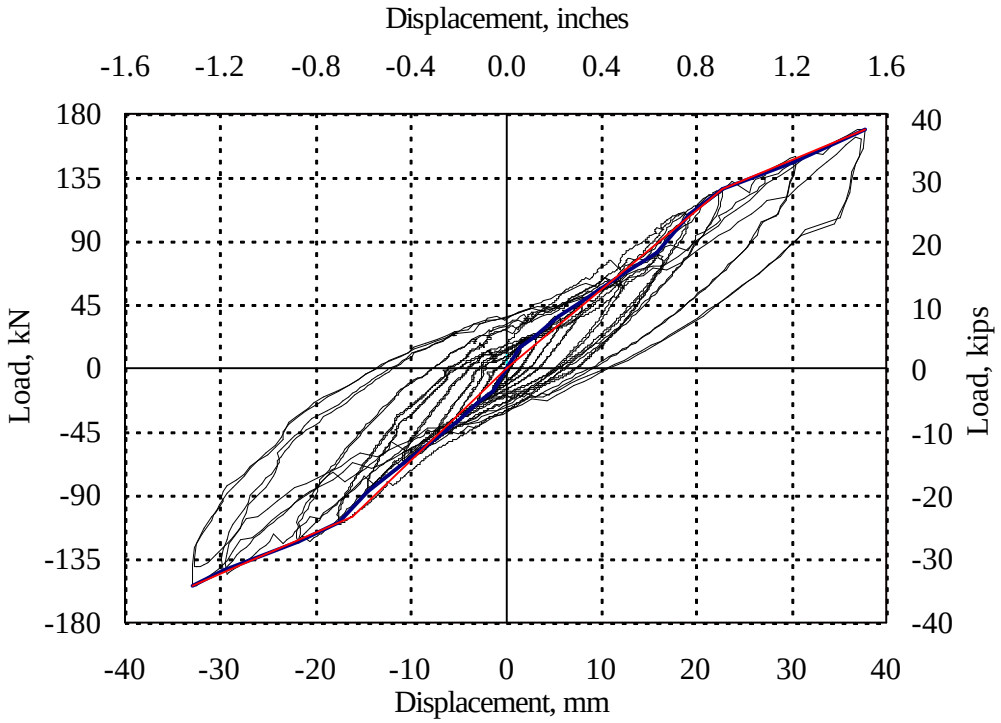

FIG. 4.24 Backbone Curve at Loading Points of Diaphragm MAE-1B

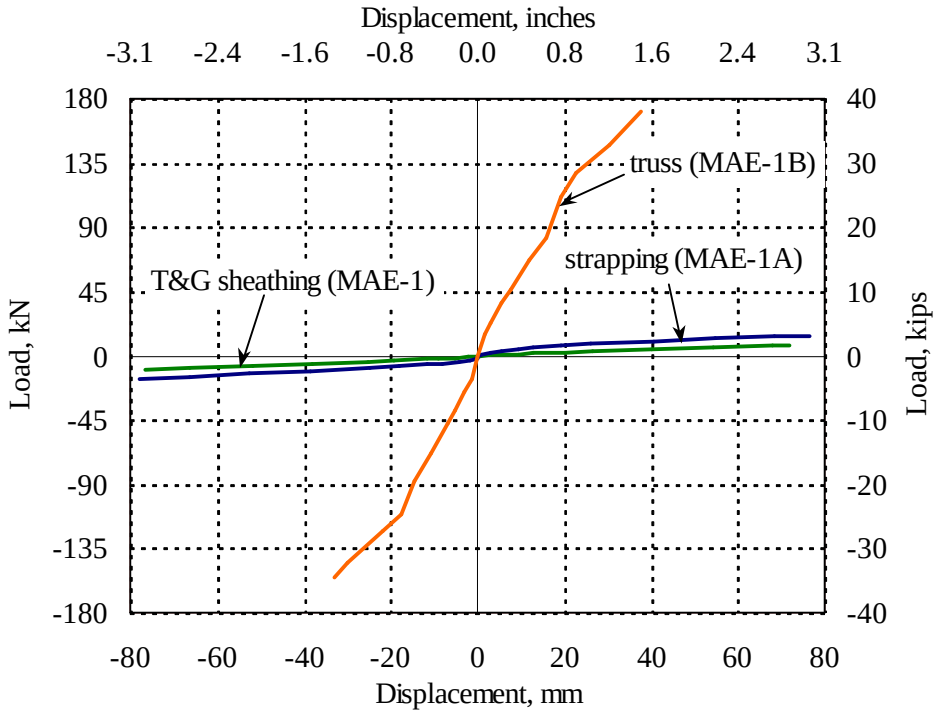

FIG. 4.25 Comparison of Backbone Curves for Diaphragm 1

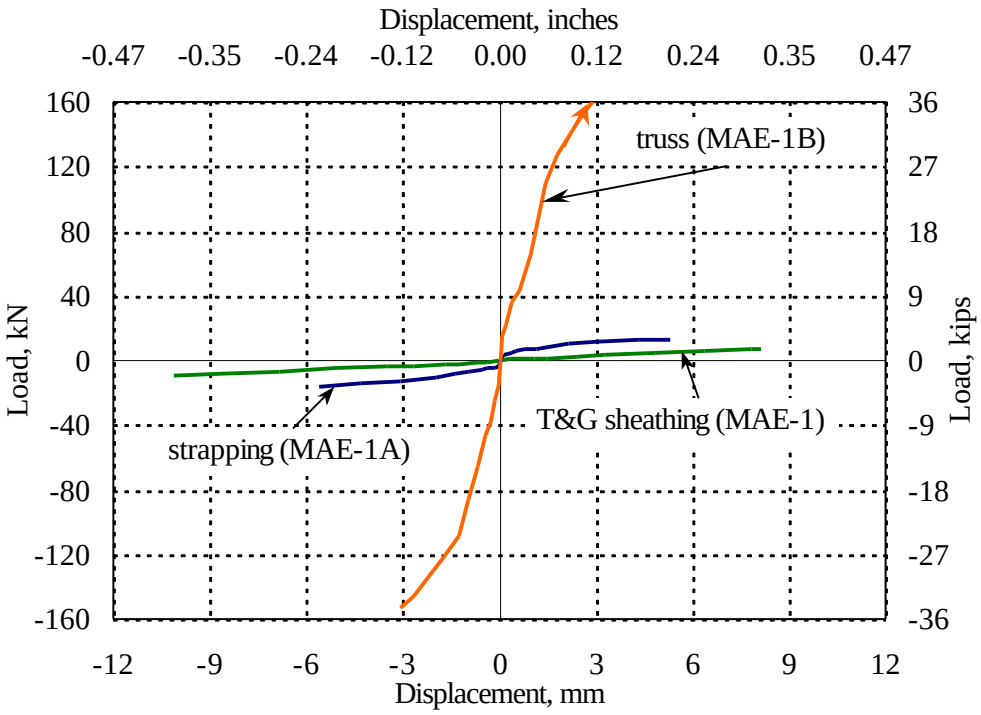

FIG. 4.26 Backbone Curves at Anchor Connection of Diaphragm 1

TABLE 4.2 Response Parameters for Specimen 1 and Its Retrofits

Parameter	MAE-1	MAE-1A	MAE-1B
Δ_{AMP}, mm (in.)	76 (3.0)	76 (3.0)	64 (2.5)
Δ_{MP}, mm (in.)	71 (2.8)	76 (3.0)	36 (1.4)
Δ_{LP}, mm (in.)	66 (2.6)	69 (2.7)	38 (1.5)
Δ_{AC}, mm (in.)	10 (0.40)	5 (0.20)	4 (0.16)
Δ_{SB}, mm (in.)	2 (0.06)	3 (0.12)	3 (0.11)
ε_{AC}, μs	420	500	360
F_{max}, kN (kips)	9 (2.0)	17 (3.8)	169 (38.0)
ε_{SMP}, μs	-	94	568
ε_{SEP}, μs	-	168	493
ε_{T}, μs	-	-	221
K_i, kN/cm (kips/in.)	2 (1.1)	12 (6.7)	108 (61.4)

Δ_{AMP} = Maximum displacement amplitude applied on the test
Δ_{MP} = Maximum overall lateral displacement at diaphragm midpoint
Δ_{LP} = Maximum lateral displacement at the loading points
Δ_{AC} = Maximum lateral displacement at the anchor connection
Δ_{SB} = Maximum slip displacement between boards
ε_{AC} = Maximum strain in anchor connections
F_{max} = Maximum actuator load
ε_{SMP} = Maximum strain at strap midpoints
ε_{SEP} = Maximum strain at strap ends
ε_{T} = Maximum strain in the truss members
K_i = Initial stiffness (from backbone curve)

TABLE 4.3 Parameters from Bilinear Curves of Specimen 1 and Its Retrofits

Parameter	MAE-1	MAE-1A	MAE-1B	1A/1	1B/1
V_y, kN (kips)	4 (0.8)	7 (1.6)	116 (26.0)	2.0	32.5
Δ_y, mm (in.)	25 (1.0)	15 (0.6)	20 (0.8)	0.6	0.8
K, kN/cm (kips/in.)	1.4 (0.8)	5.1 (2.8)	59.3 (33.8)	3.5	41.2
K_2, kN/cm (kips/in.)	0.9 (0.5)	1.3 (0.8)	28.6 (16.3)	1.6	32.6

V_y = Yielding actuator force
Δ_y = Yielding displacement
K = Effective stiffness
K_2 = Post-yield stiffness

4.4 SQUARE EDGED SINGLE STRAIGHT SHEATHED DIAPHRAGM

4.4.1 Diaphragm MAE-2

Diaphragm specimen MAE-2 was subjected to quasi-static reversed cyclic loading up to a maximum displacement of 76 mm (3 in.). In this diaphragm, the joists were oriented in the actuator direction and therefore they slid along their vertical supports generating friction and noise. The actuator load versus average displacement at the loading points curve (Fig. 4.27) showed an initial tangent stiffness (K_i) of 36 kN/cm (20.6 kips/in.). The stiffness degraded gradually on subsequent cycles and at 31 kN (7 kips) of actuator load the tangent post-yield stiffness remained constant at 4 kN/cm (2.3 kips/in.). The residual displacement grew on each cycle of loading having a maximum of 25 mm (1 in.). The shear strength for this diaphragm was governed by the nail couple developed in the sheathing boards, which resisted a maximum actuator load of 56.7 kN (12.8 kips) for a diaphragm mid-point overall lateral displacement of 80 mm (3.15 in.).

The maximum lateral displacement of the anchor connection (Δ_{AC}) was 1.3 mm (0.05 in.), which was only 1.6% of the overall lateral displacement at the diaphragm midpoint (Δ_{MP}), as shown in Fig. 4.28. An indication of the nail slip behavior is shown

in Fig. 4.29, which shows the load versus average slip displacement between two adjacent sheathing boards with a maximum slip of 4.8 mm (0.19 in.).

The joist orientation and connections in diaphragm MAE-2 were different from diaphragm MAE-1 and therefore the connection responses were not the same. The connections had wall anchors connected perpendicular to the joists in MAE-2. As a result only the sheathing along the long edges of the diaphragm could act as chords and transmit axial forces to the connections. The connection consisted of a threaded bar inserted through a hole to the beam web of the support frame, the adjacent steel tube and the joist (see Fig. 3.6b). During loading, the connections were subjected to shear, bending and possibly axial actions, but only the overall strain was recorded on one side of the connection. The connections did not show deformations until approximately 40 kN (9 kips), possibly because a sufficient load was required to overcome the friction forces between the wood joist and the connecting tube before deforming the anchors. The oversized hole in the steel tube may have contributed to this behavior. After the anchor bore on the hole of the steel tube, the strain increased elastically until the load was reversed. In the unloading phase, the anchor did not show strain loss until approximately –31.2 kN (-7 kips), probably after the connection bore on the opposite side of the tube hole and then the connection bent in the negative direction, as the strains in Fig. 4.30 indicate. It was observed also that all the connections in diaphragm MAE-2 deformed in the same direction (see Fig. 4.30). The maximum strain was 640 μs, indicating the connection had not yielded.

Fig. 4.31 shows the deformed diaphragm during the test. Fig. 4.31a shows that the sheathing boards of the diaphragm slipped with respect to each other at 51 mm (2 in.) of applied displacement. The offset line shown in the center of this photo was straight in the undeformed position. Fig. 4.31b shows the deformed shape of the diaphragm for 76 mm (3 in.) of applied displacement. No cracks were detected in the joists or sheathing and permanent deformation of the nails was not visible.

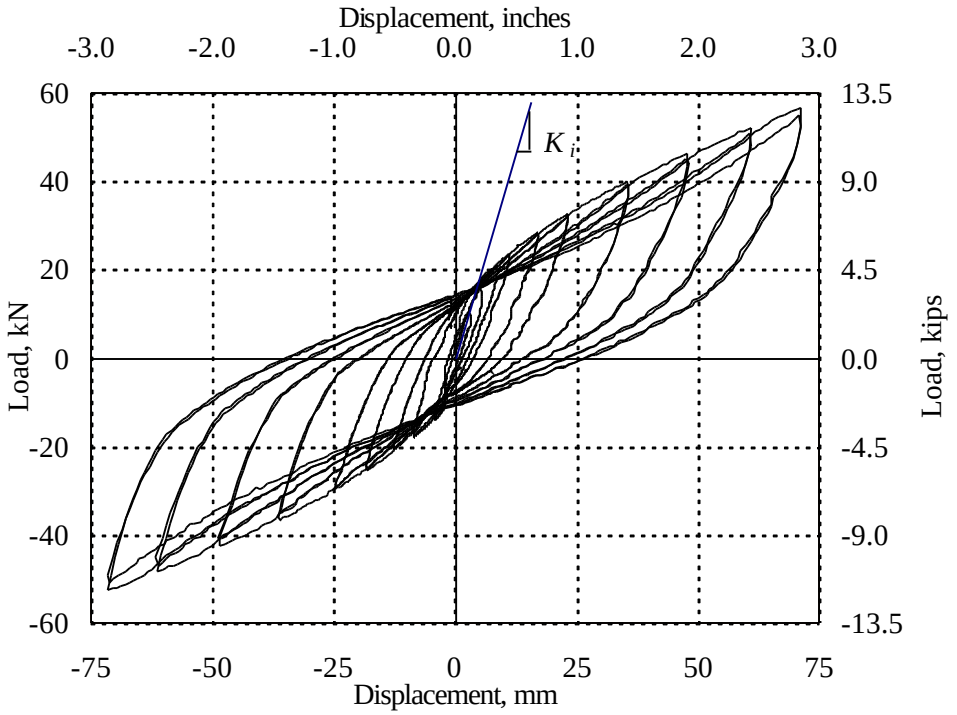

FIG. 4.27 Diaphragm MAE-2. Load-Displacement at Loading Points

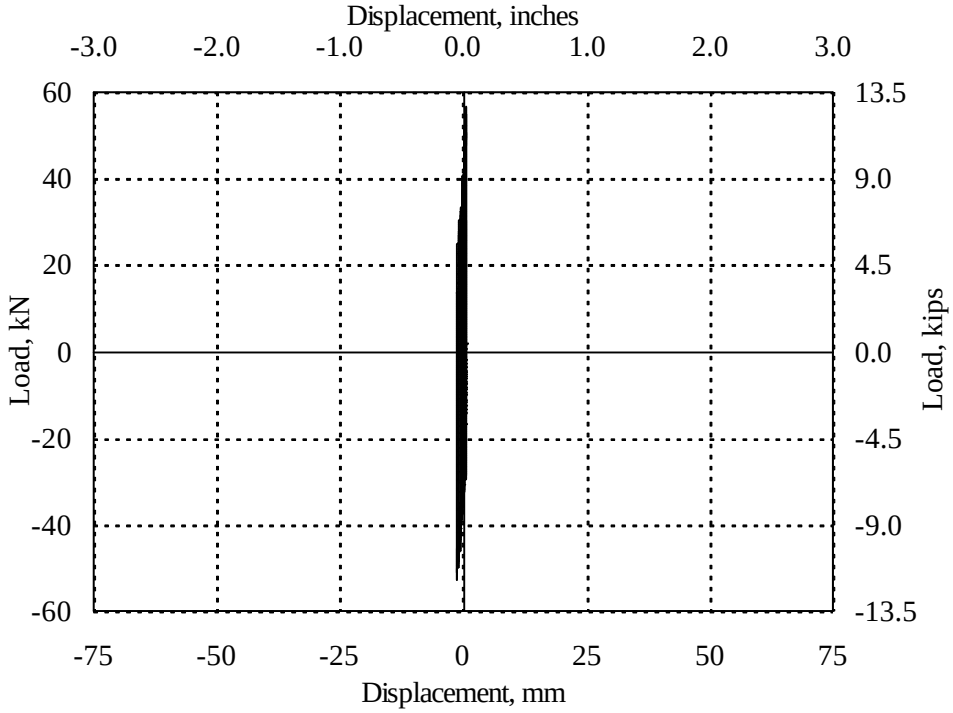

FIG. 4.28 Diaphragm MAE-2. Load-Slip Displacement at Connection

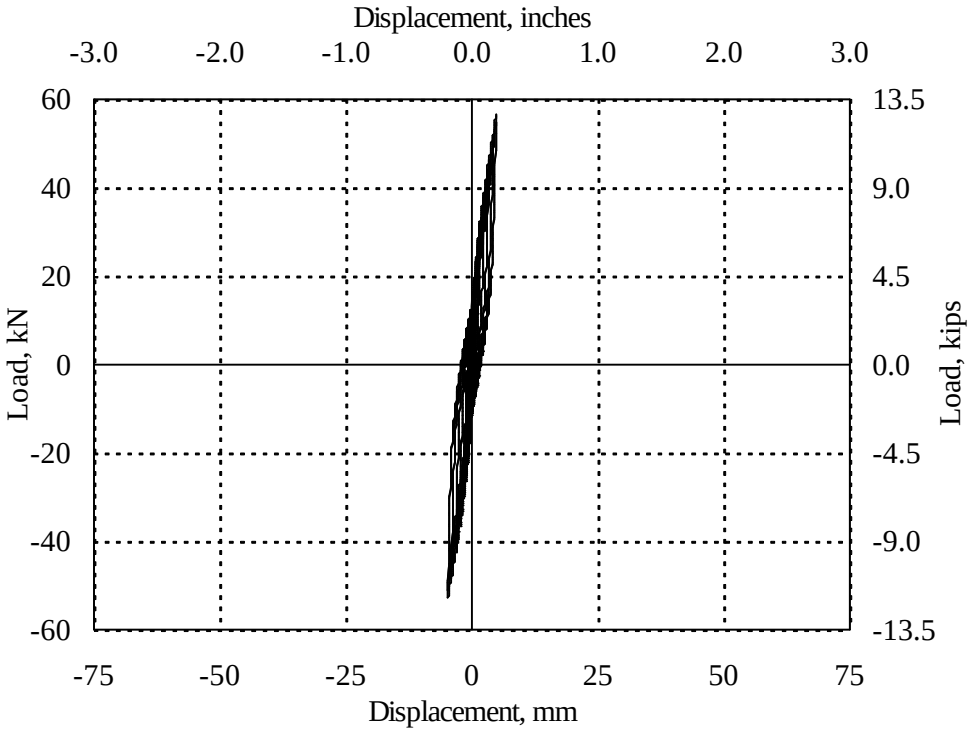

FIG. 4.29 Diaphragm MAE-2. Load-Slip Displacement Between Boards

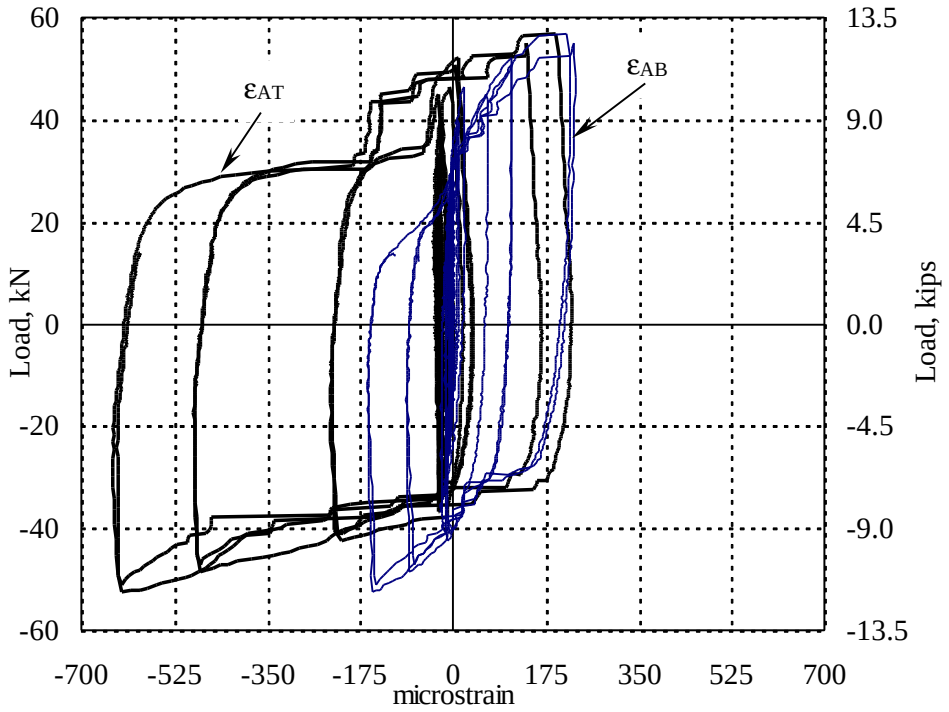

FIG. 4.30 Diaphragm MAE-2. Load-Strain at Anchors

(a) Slip of Sheathing Boards at 51 mm (2 in.) **(b) Deformed Diaphragm at 76 mm (3 in.)**

FIG. 4.31 Deformations in Diaphragm MAE-2 During Quasi-Static Test

4.4.2 Steel Truss Retrofit Diaphragm MAE-2A

The steel truss retrofit diaphragm specimen MAE-2A was tested under a quasi-static reverse cyclic loading up to an applied lateral displacement of 25 mm (1.0 in.). At 13 mm (0.5 in.) of applied lateral displacement and 125 kN (28 kips) of actuator peak load, one long edge of the diaphragm lifted up about 50 mm (2 in.), pivoting around the joist ends of the opposite edge (see Fig. 4.32). The uplifting occurred for the first time during testing of diaphragm MAE-2A and was caused by the overturning moment that resulted from the eccentricities between the actuator load,

and the center of resistance of the diaphragm and truss members. The displacement transducers recorded much lower displacements than the corresponding applied displacements when uplifting occurred (see Fig. 4.32).

Fig. 4.33 shows the actuator force versus the average displacement at the loading points of the diaphragm. The curve exhibits an initial tangent stiffness (K_i) of 270 kN/cm (154 kips/in.) and rapidly decays to a tangent post-yield stiffness of 54 kN/cm (31 kips/in.). The residual displacement grew considerably on each cycle, with a maximum of 6 mm (0.25 in.). The maximum actuator load applied was 156 kN (35 kips) and the maximum mid-point lateral displacement was 11 mm (0.42 in.). The rehabilitated diaphragm could have resisted more loads but the overturning provoked an early failure.

Fig. 4.34 shows the actuator load versus average displacement at the anchor connection with a maximum displacement of 1.8 mm (0.07 in.), about 13% of the maximum diaphragm displacement of 14 mm (0.55 in.) at the midpoint. The nail slip in the sheathing boards were low for the level of load resisted, as shown Fig. 4.35, with a maximum average slip displacement between sheathing boards of 0.8 mm (0.03 in.).

The anchors behaved similarly as described in diaphragm MAE-2, where the first cycles showed no strain until the load was 75.7 kN (17 kips). In the next cycles the higher loads deformed the anchor until a maximum strain of 695 μs, as shown in Fig. 4.36. The unloading phase did not show a loss of strain until a load of -71 kN (–16 kips), possibly after the anchor bore in the opposite side of the tube hole. The anchors for strain gauges E1 and E2 (see Fig. 3.13) were not included in Fig. 4.36 because they did not have appreciable strains.

The truss members had a maximum strain of 120 μs as shown in Fig. 4.37, well below the yielding point (see Fig. 3.5 for strain gauge locations). The axial forces in the truss members (horizontal and diagonal braces) can be determined by applying the maximum strains into Eq. 4.9. Using the equilibrium relation between the truss and external forces (see Fig. 5.2), an external load of 67 kN (15 kips) resulted. This is the load the diaphragm was able to transfer to the truss. Based on the total actuator force, the diaphragm resisted 89 kN (20 kips) by transmitting load directly to the support frames. Visible damage was not observed for the sheathing boards, nails, joists or anchor connections.

FIG. 4.32 Uplifting of Diaphragm MAE-2A at 13 mm of Applied Displacement

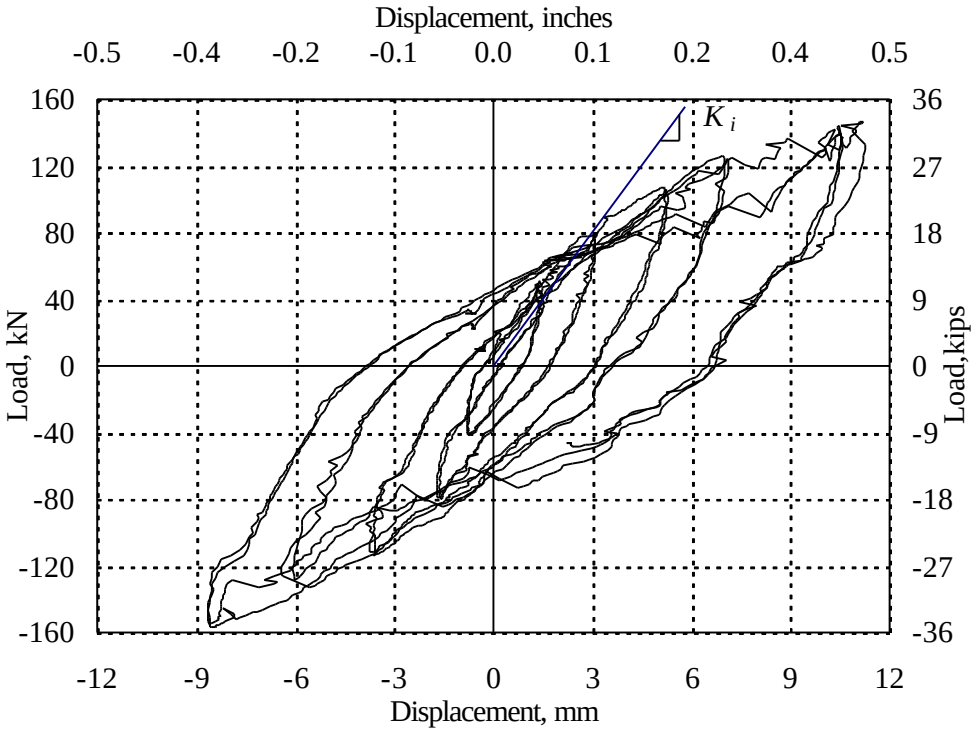

FIG. 4.33 Diaphragm MAE-2A. Load-Displacement at Loading Points

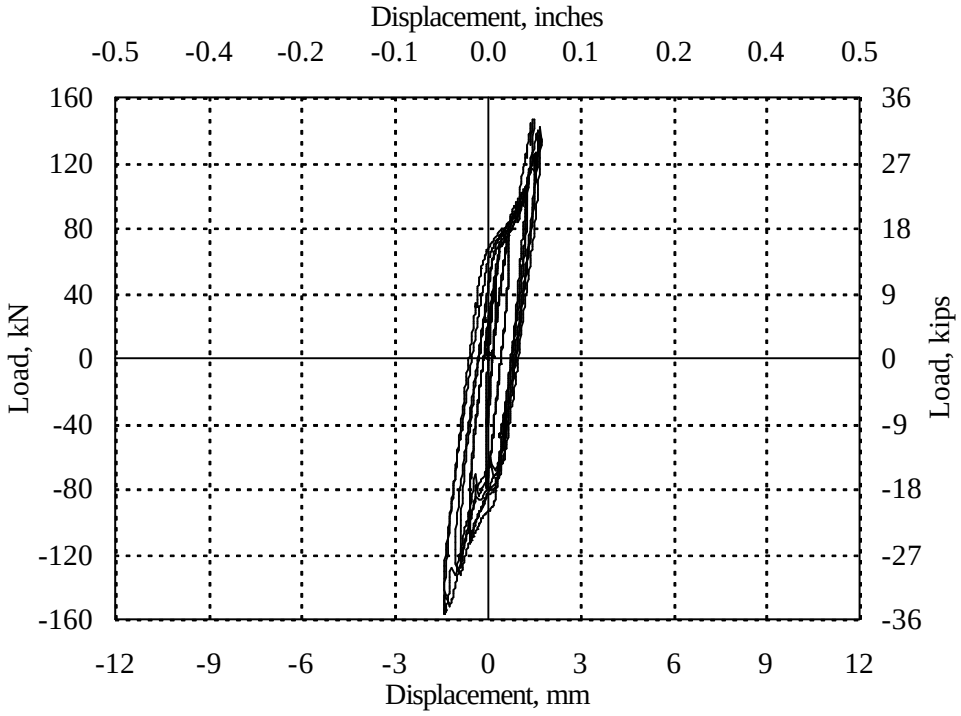

FIG. 4.34 Diaphragm MAE-2A. Load-Slip Displacement at Connection

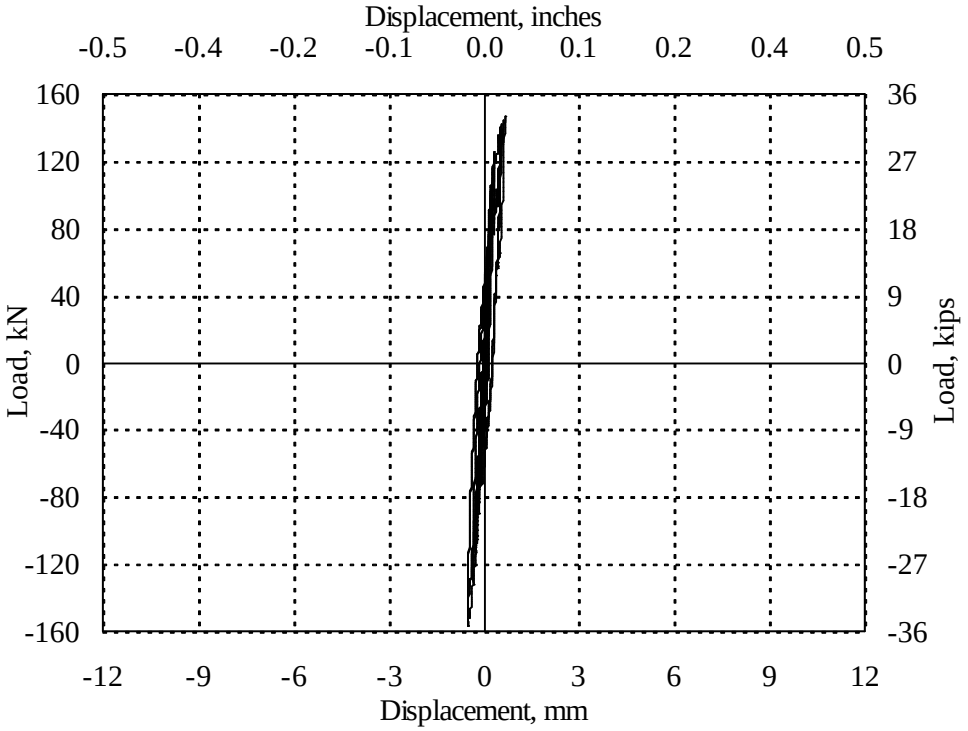

FIG. 4.35 Diaphragm MAE-2A. Load-Slip Displacement Between Boards

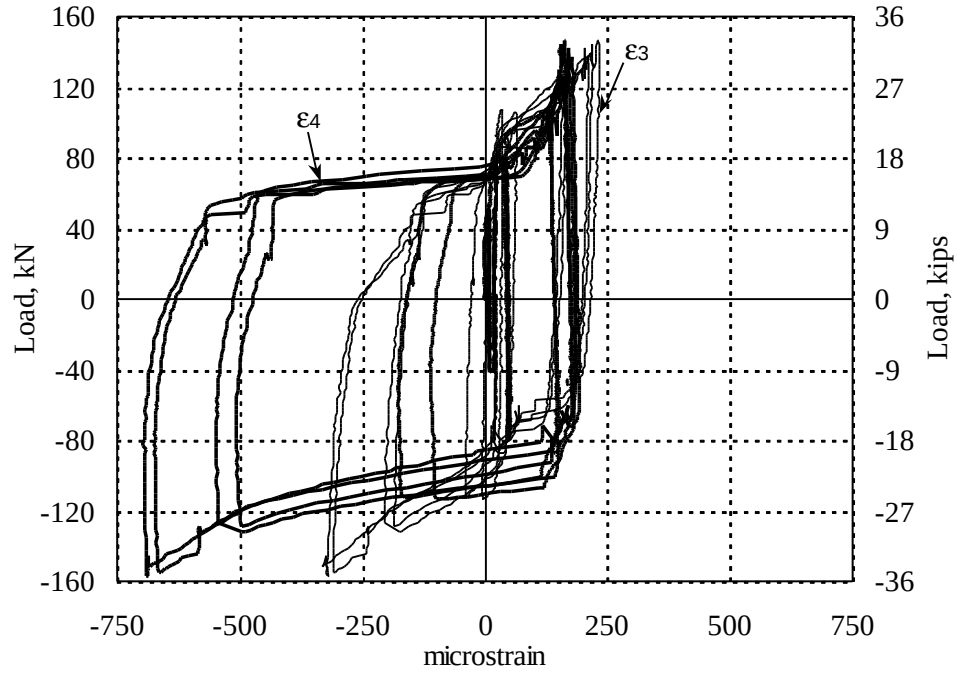

FIG. 4.36 Diaphragm MAE-2A. Load-Anchor Strain

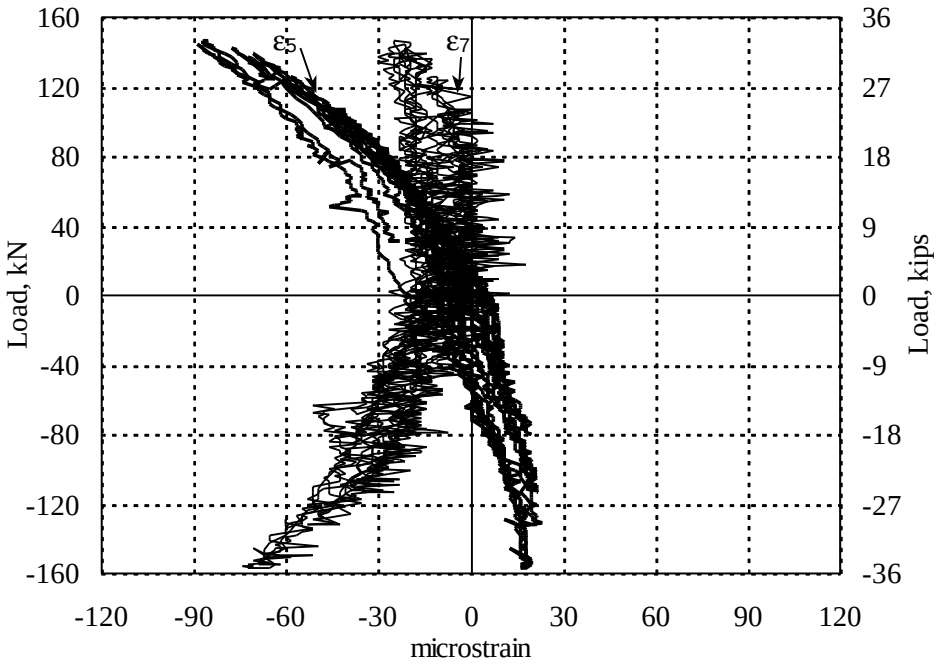

(a) Horizontal Braces

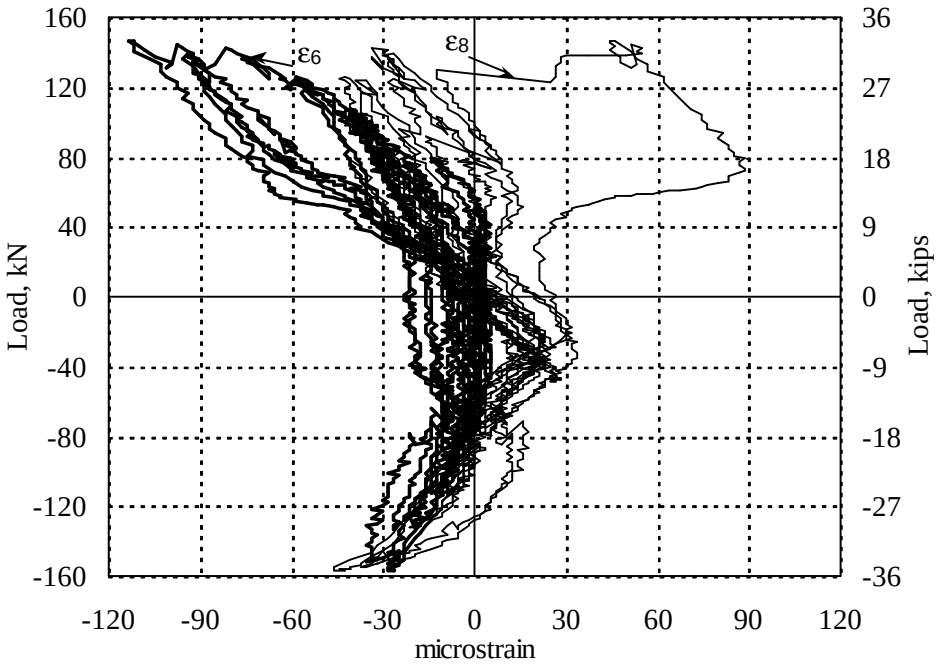

(b) Diagonal Braces

FIG. 4.37 Diaphragm MAE-2A. Load-Strain at Truss Braces

4.4.3 Unblocked Plywood Overlay Retrofit Diaphragm MAE-2B

The behavior of diaphragm MAE-2B during the quasi-static reversed cyclic loading test is shown in Figs. 4.38 to 4.41. The load versus average displacement at the loading points shown by the curve in Fig. 4.38 exhibits an initial tangent stiffness (K_i) of 104 kN/cm (59.5 kips/in.) and then declines in subsequent cycles to a tangent post-yield stiffness (K_2) of 18.2 kN/cm (10.4 kips/in.). The maximum force developed was 67.2 kN (15.1 kips) at a mid-point lateral displacement of 16.5 mm (0.65 in.). The maximum residual displacement was 8 mm (0.33 in.). Some pinching can be observed in the loops.

Fig. 4.39 shows that the maximum lateral displacement at the anchor connection was 2.3 mm (0.09 in.), which is 14% of the overall lateral displacement of the diaphragm. Pinching in the curves can be observed, indicating slack and possible local damage in the joists at the connections. Fig. 4.40 shows the load versus average slip displacement between panels. The maximum slip displacement was 2 mm (0.08 in.).

The anchor connections behaved similarly to the previous diaphragms (MAE-2 and MAE-2A), showing first low strains until 26.7 kN (6 kips) and then higher deformations occurred for higher loading. The unloading phase occurred with almost no reduction in the strains until a load of –9 kN (–2 kips) probably after the anchor bore on the opposite tube hole. The maximum anchor strain was 1,220 μs, on the limit of yielding, as shown in Fig. 4.41.

The test was terminated at a maximum applied displacement of 19 mm (0.75 in.). Only half of a cycle could be completed because one corner panel of the plywood overlay adjacent to the support frame began to pull out. The failure occurred at a relatively low level of load because the panel nails, at fairly wide spacing had been nailed such that the heads were too deep below the top of the plywood. The nailing was corrected for the next diaphragms. No signs of visible damage were observed in the joists, sheathing boards, or panels.

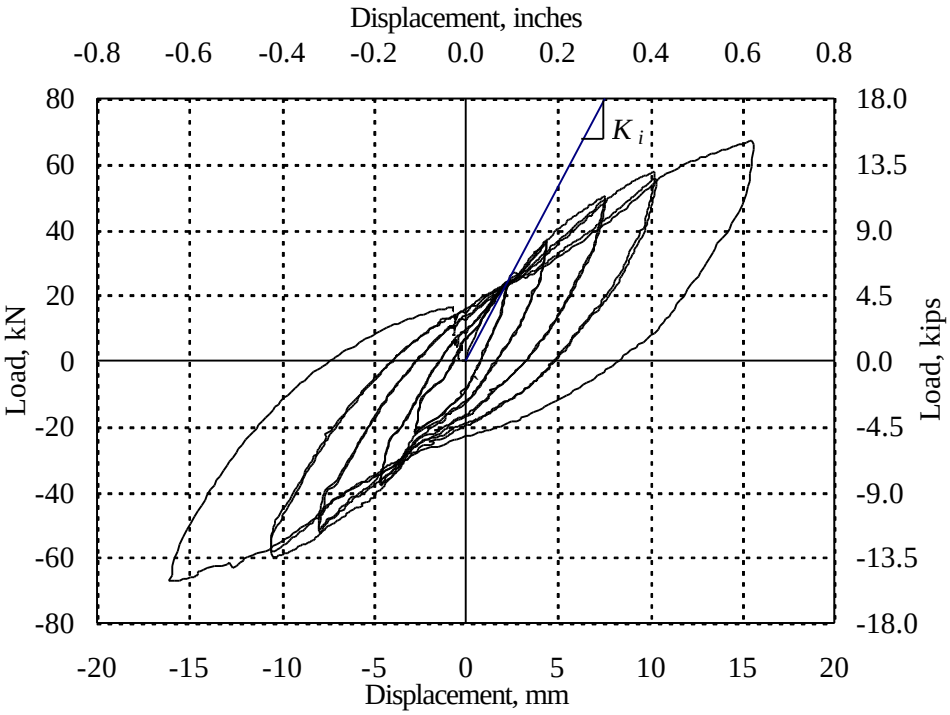

FIG. 4.38 MAE-2B. Load-Displacement at Loading Points

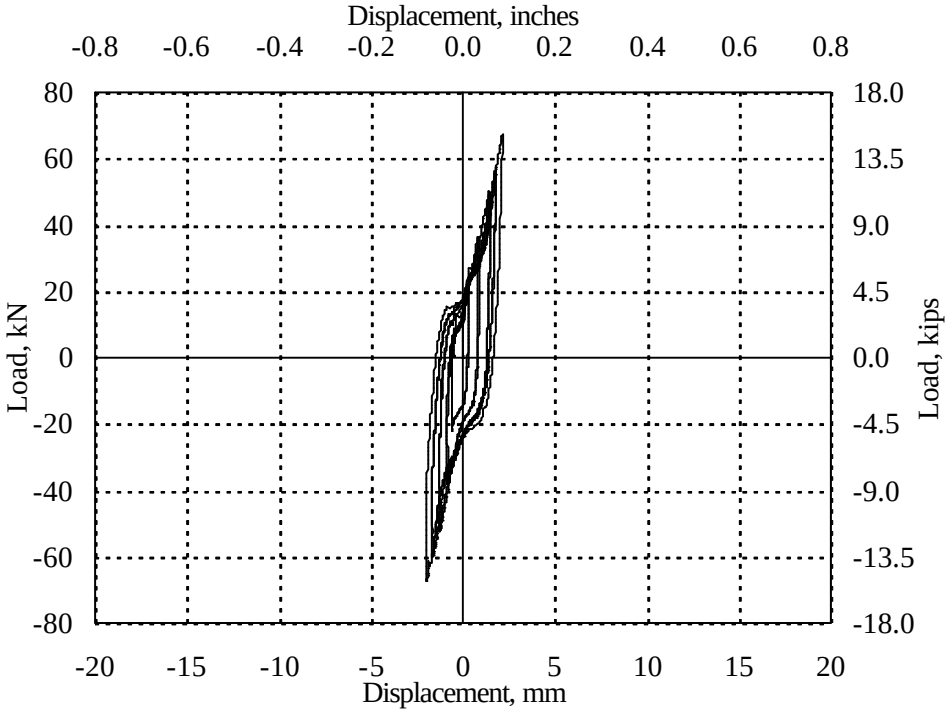

FIG. 4.39 MAE-2B. Load-Slip Displacement at Connection

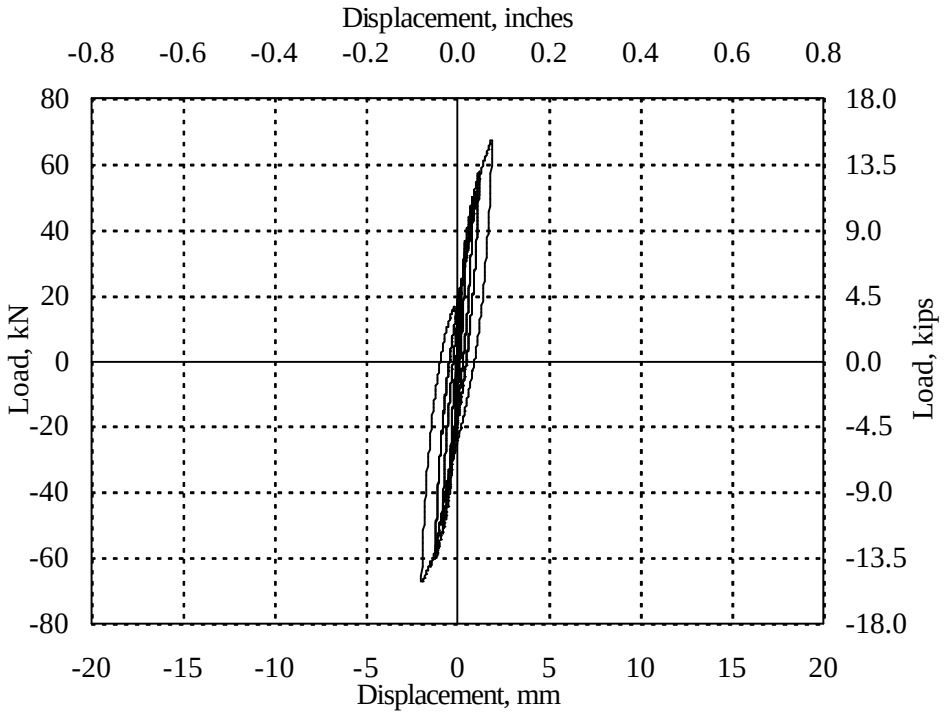

FIG. 4.40 MAE-2B. Load-Slip Displacement Between Panels

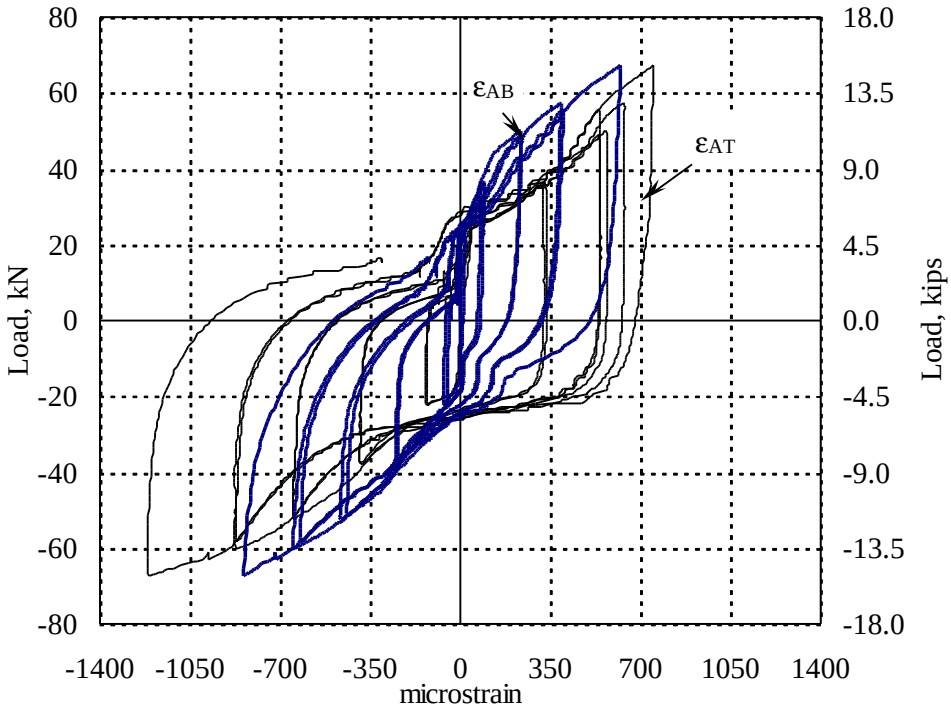

FIG. 4.41 MAE-2B. Load-Anchor Strain

4.4.4 Blocked Plywood Overlay Retrofit Diaphragm MAE-2C

Fig. 4.42 provides the load versus average displacement at the loading points of diaphragm MAE-2C, which shows an initial tangent stiffness (K_i) of 234 kN/cm (133.5 kips/in.) and a tangent post-yield stiffness of 55.2 kN/cm (31.5 kips/in.). The last cycle of the curve had a change in direction at 120 kN (27 kips), which was caused by uplifting of the diaphragm edge. The maximum actuator load was 153 kN (34.3 kips) at a mid-point displacement of 19.3 mm (0.76 in.). Pinching is observable in the loops of the curve. The maximum residual displacement was 10 mm (0.4 in.).

At 19 mm (0.75 in.) of applied displacement, large bearing cracks developed in the joist ends, at the hole made for the anchor connections. This might explain pinching observed in the load versus lateral displacement of the anchor connections curve (see Fig. 4.43). The maximum lateral displacement was 6.6 mm (0.26 in.) at the anchor connections, nearly 33% of the overall lateral displacement of the diaphragm. Fig. 4.44 shows the load versus average slip between panels with a maximum displacement of 2.3 mm (0.09 in.).

Fig. 4.45 shows that the anchor entered the post-yield range with a maximum deformation of 3,300 μs. The friction forces developed between the steel tubes and the joists were approximately 22 kN (5 kips). It was necessary to overcome these friction forces before bending the anchor. The unloading showed no loss of strain until the anchor bore on the tube hole at a load of 22.3 kN (5 kips).

At an applied displacement of 12.7 mm (0.5 in.) tiny cracks developed parallel to the grain of the plywood panels adjacent to the support frames. At 25 mm (1.0 in.) of applied displacement and 120 kN (27 kips) of actuator load, an overturning moment developed and lifted up one edge of the diaphragm approximately 25 mm (1.0 in). At the last level of applied displacement, 38 mm (1.5 in.), the diaphragm edge lifted up approximately 102 mm (4 in.), as shown in Fig. 4.46.

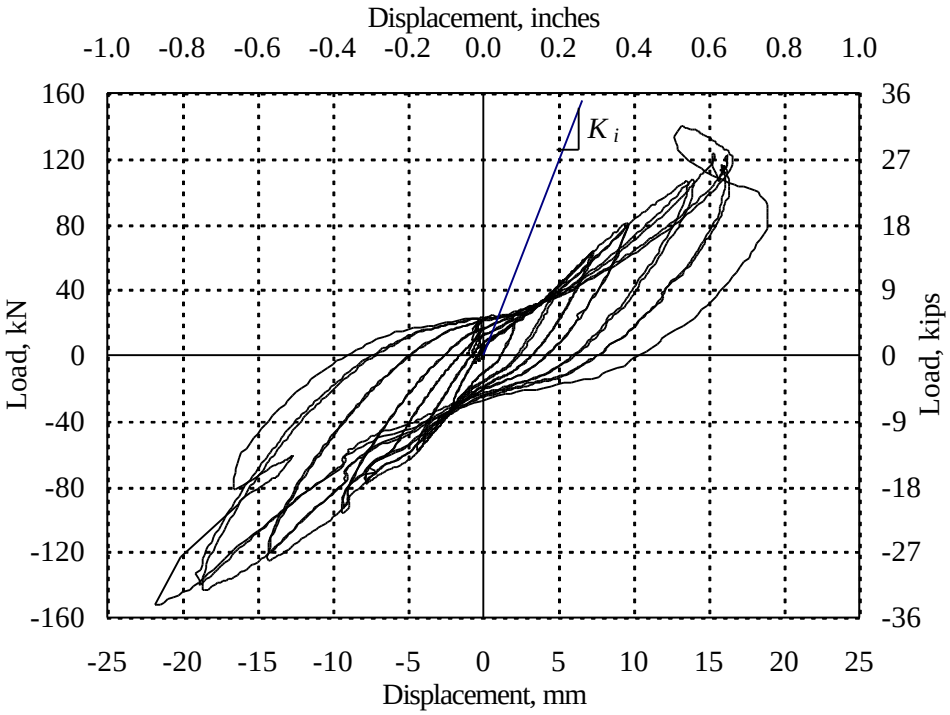

FIG. 4.42 MAE-2C. Load-Displacement at Loading Points

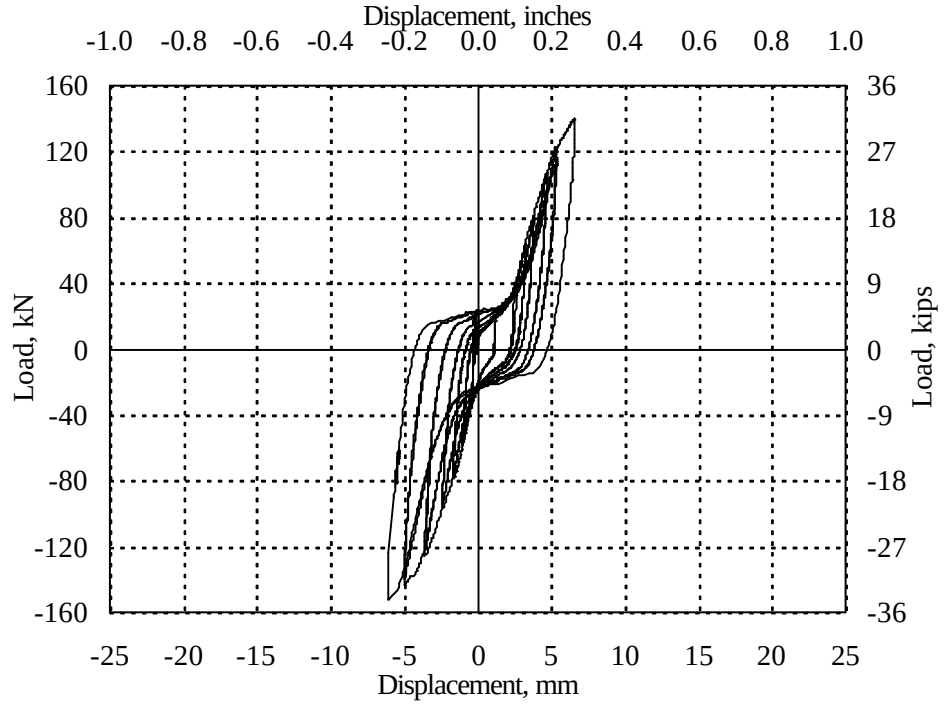

FIG. 4.43 MAE-2C. Load-Slip Displacement at Connection

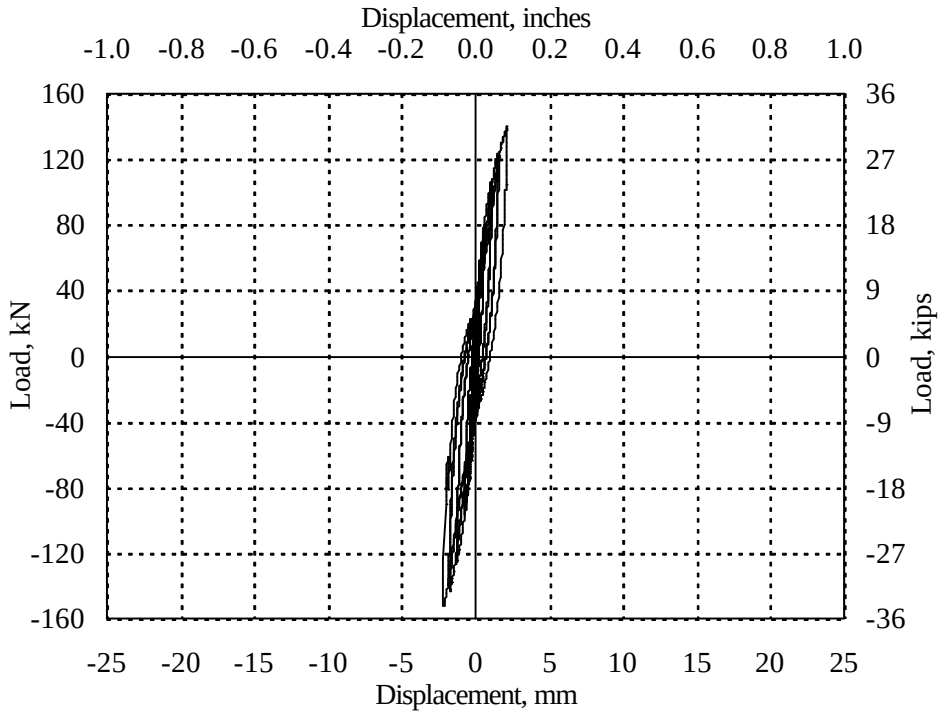

FIG. 4.44 MAE-2C. Load-Slip Displacement Between Panels

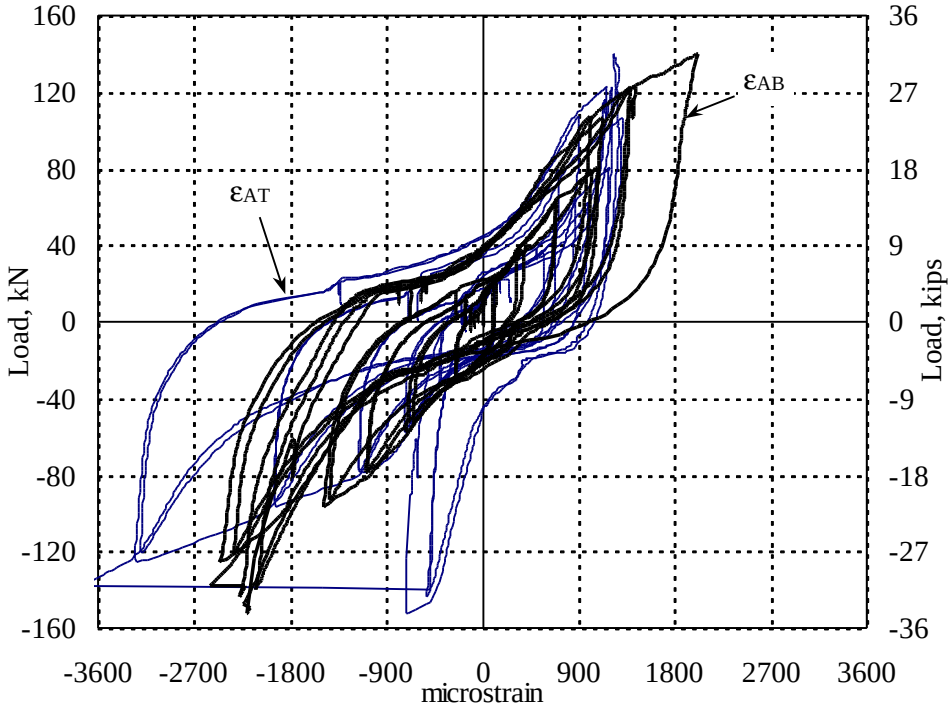

FIG. 4.45 MAE-2C. Load-Anchor Strain

FIG. 4.46 Uplifting of Diaphragm MAE-2C at 38 mm (1.5 in.) of Applied Displacement

4.4.5 Comparison of Responses

The backbone curves of diaphragm MAE-2 and retrofits, MAE-2A and MAE2B, shown in Figs. 4.47 through 4.49, were constructed based on the specifications from FEMA 273 for the overall lateral displacement at the diaphragm midpoint. For diaphragm MAE-2C, the values at the midpoint were distorted by the overturning moment and, therefore, the displacements at the loading points were used instead (see Fig. 4.50). Table 4.4 shows that the initial tangent stiffness (K_i) for diaphragms MAE-2A, MAE-2B and MAE-2C were 7.5, 2.9 and 6.5 times the stiffness of MAE-2, respectively.

Comparing the maximum actuator load on the diaphragms, the increase was 2.8, 1.2 and 2.7 times for diaphragms MAE-2A, MAE-2B and MAE-2C, respectively. As

observed in Fig. 4.51, all retrofits provided an increase in lateral load strength and stiffness.

Comparing the values and ratios of the bilinear curves given in Table 4.5, the yield force (V_y) increased 3.9, 1.6 and 2.3 times that in MAE-2, while the post-yield stiffness (K_2) increased by a factor of 3.5, 4.5 and 13.7 for diaphragms MAE-2A, MAE-2B and MAE-2C, respectively. The yield displacement (Δ_y) in the retrofitted diaphragms reduced to 30%, 40% and 40% of the MAE-2 value for MAE-2A, MAE-2B and MAE-2C, respectively.

The behavior of the anchor connections shown in Fig. 4.52 suggests that it was required to surpass friction forces between the joist and the connection tubes before appreciable lateral displacements could occur at the connections. This friction force was 22.3 kN (5 kips) in MAE-2 and only 8.9 kN (2 kips) in MAE-2C, probably because the connections were looser due to repetitive testing. Diaphragm MAE-2C had the highest lateral anchor displacement, nine times the lateral anchor displacement of MAE-2, followed by MAE-2B (3 times) and MAE-2A (2.3 times).

Comparing the slip between sheathing elements and the lateral deformation of the diaphragm (Δ_{MP} - Δ_{AC}) for diaphragms of similar type of sheathing, a relationship can be observed. Diaphragms MAE-2 and MAE-2A (sheathing boards) had a similar ratio $\Delta_{SB}/(\Delta_{MP} - \Delta_{AC})$ of 6% while in diaphragms MAE-2B and MAE-2C (plywood panel overlay) the ratio varied from 14% to 18%. This fact indicates that the panel overlay retrofit developed higher nail slip displacements, which is explained by the higher loads taken by this type of sheathing in the diaphragm.

TABLE 4.4 Response Parameters for Specimen 2 and Its Retrofits

Parameter	MAE-2	MAE-2A	MAE-2B	MAE-2C
Δ_{AMP}, mm (in.)	76 (3.0)	25 (1.0)	19 (0.8)	38 (1.5)
Δ_{MP}, mm (in.)	80 (3.2)	14 (0.6)	17 (0.7)	20 (0.8)
Δ_{LP}, mm (in.)	72 (2.9)	11 (0.4)	16 (0.6)	19 (0.8)
Δ_{AC}, mm (in.)	1 (0.05)	2 (0.07)	2 (0.09)	7 (0.26)
Δ_{SB}, mm (in.)	5 (0.19)	1 (0.03)	2 (0.08)	2 (0.09)
ε_{AC}, μs	640	695	1,218	3,300
F_{max}, kN (kips)	57 (12.7)	156 (35.0)	67 (15.1)	153 (34.3)
ε_T, μs	-	114	-	-
K_I, kN/cm (kips/in.)	36 (20.6)	269 (153.5)	104 (59.5)	234 (133.5)

Note: see Table 4.2 for definition of parameters

TABLE 4.5 Parameters from Bilinear Curves of Specimen 2 and Its Retrofits

Parameter	MAE-2	MAE-2A	MAE-2B	MAE-2C	2A/2	2B/2	2C/2
V_y, kN (kips)	29 (6.6)	115 (25.7)	48 (10.7)	68 (15.2)	3.9	1.6	2.3
Δ_y, mm (in.)	16 (0.6)	5 (0.2)	6 (0.2)	6 (0.2)	0.3	0.4	0.4
K, kN/cm (kips/in.)	18.4 (10.3)	233.0 (128.5)	83.6 (46.5)	113.0 (66.1)	12.5	4.5	6.4
K_2, kN/cm (kips/in.)	4.0 (2.3)	54.3 (31.0)	18.2 (10.4)	55.2 (31.5)	13.5	4.5	13.7

Note: see Table 4.3 for definitions of parameters

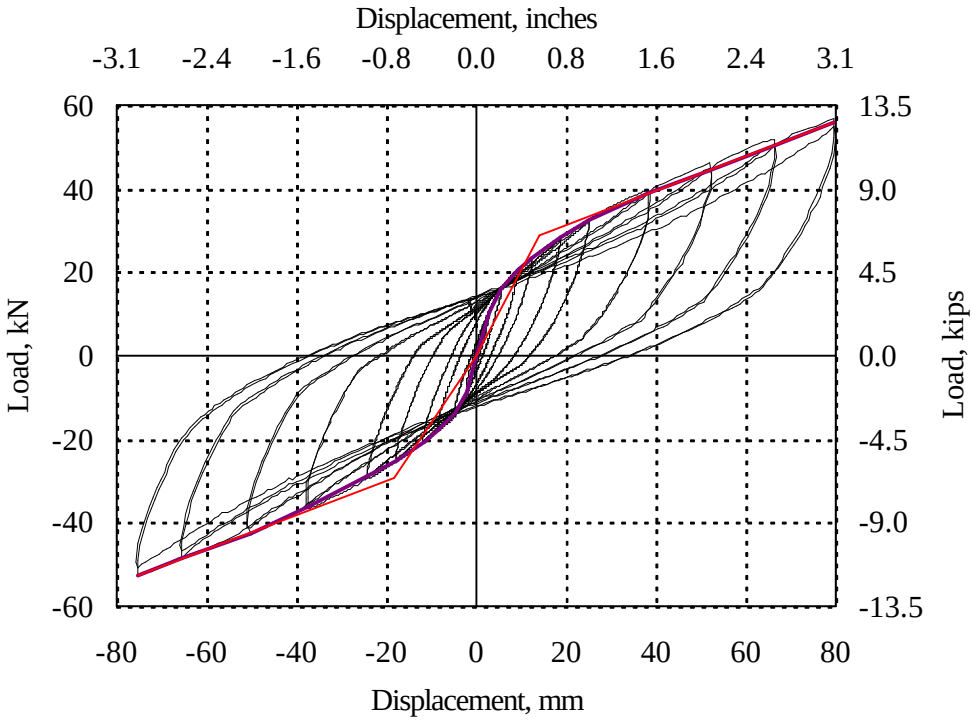

FIG. 4.47 Backbone Curve at Midpoint of Diaphragm MAE-2

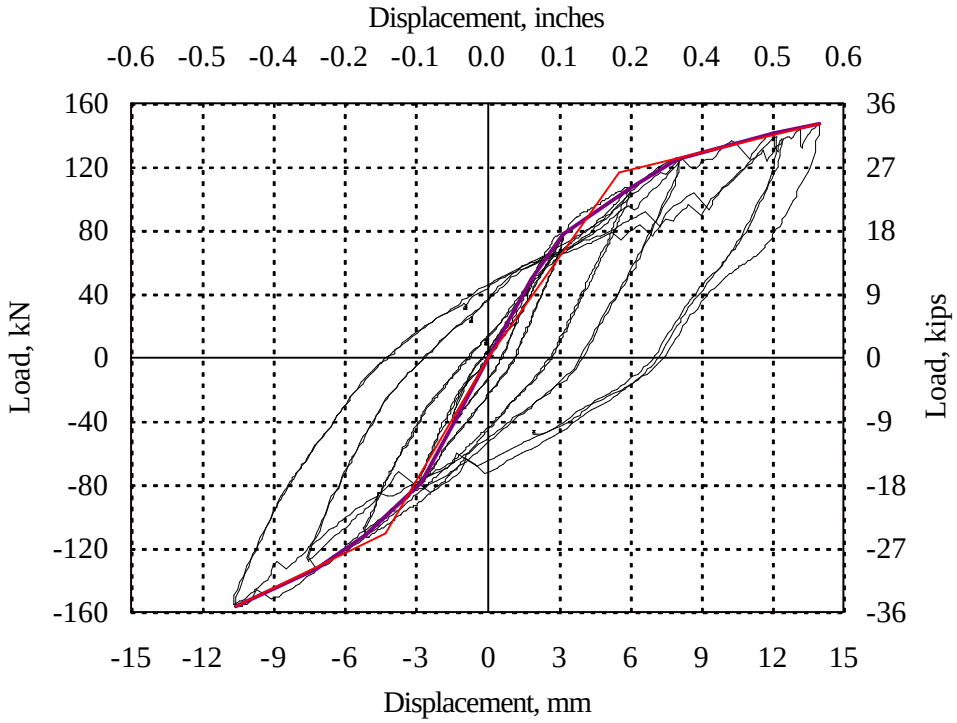

FIG. 4.48 Backbone Curve at Midpoint of Diaphragm MAE-2A

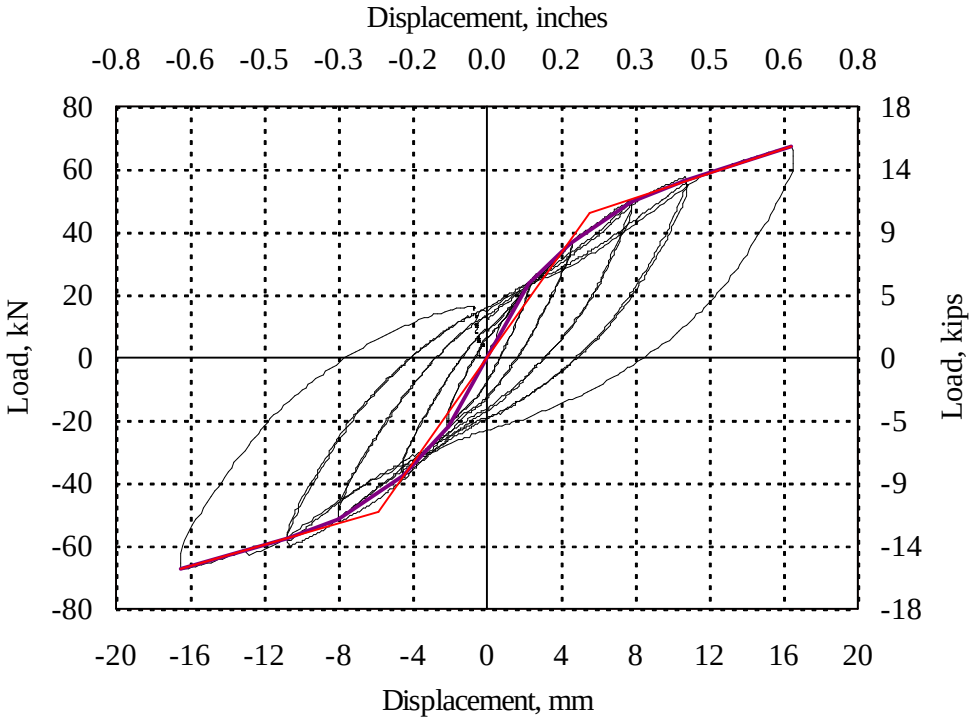

FIG. 4.49 Backbone Curve at Midpoint of Diaphragm MAE-2B

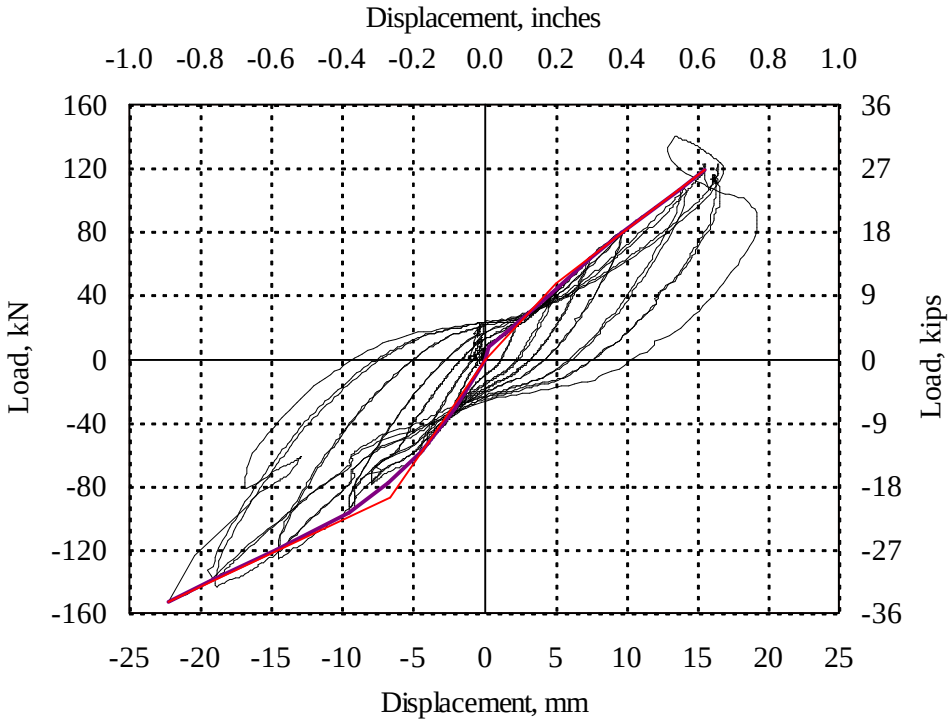

FIG. 4.50 Backbone Curve at Loading Points of Diaphragm MAE-2C

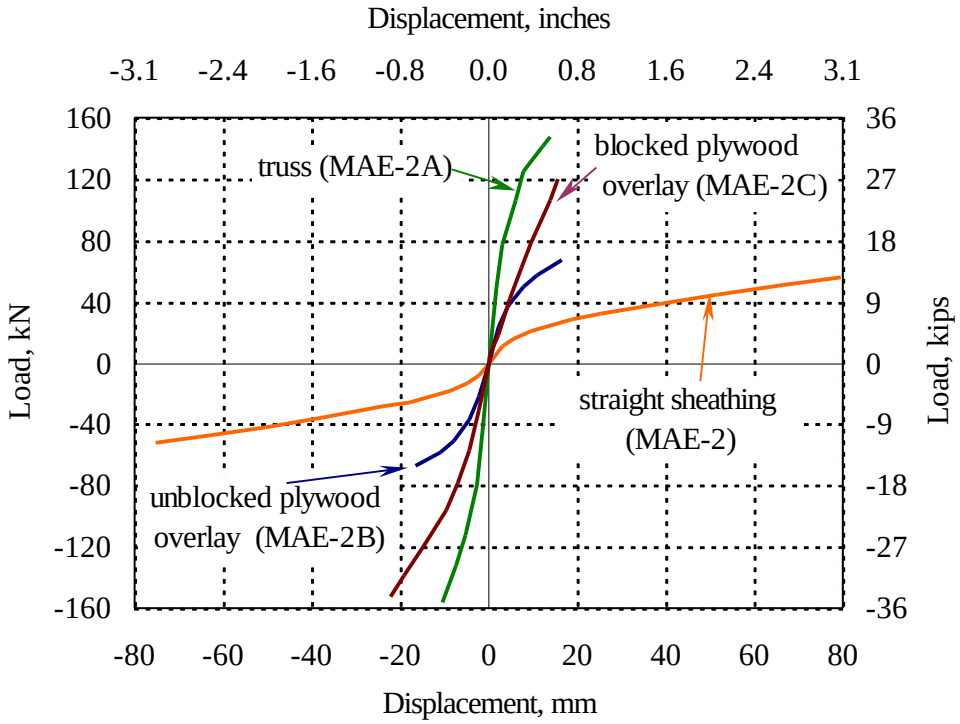

FIG. 4.51 Comparison of Backbone Curves at Midpoint of Diaphragm 2

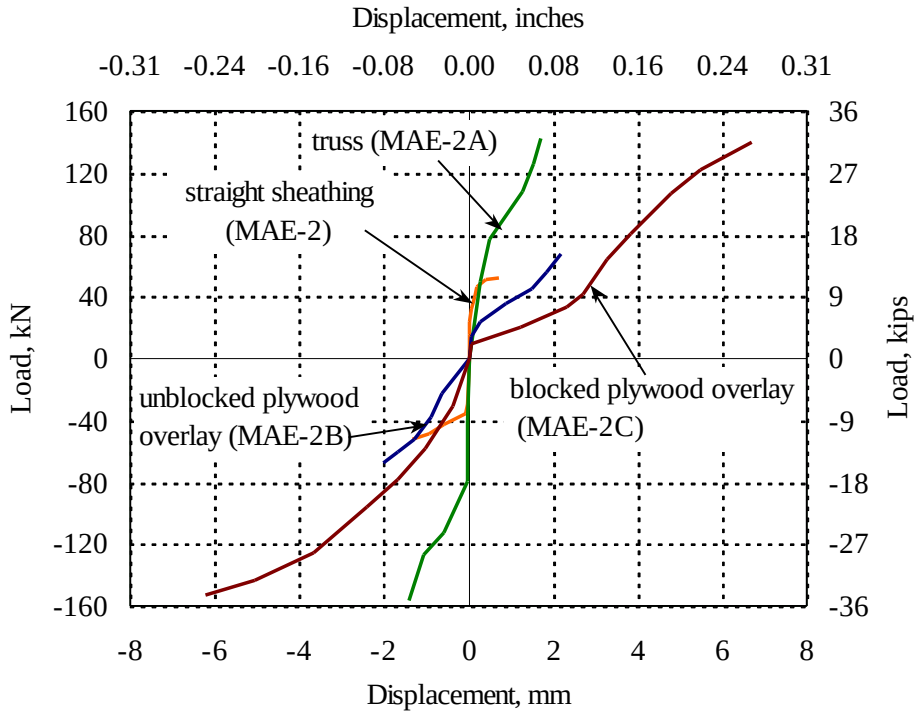

FIG. 4.52 Comparison of Backbone Curves at Connection of Diaphragm 2

4.5 SQUARE EDGED SINGLE STRAIGHT SHEATHED DIAPHRAGM WITH CORNER OPENING

4.5.1 Diaphragm MAE-3

Diaphragm MAE-3 was tested under quasi-static reversed cyclic loading for displacement amplitudes up to the maximum actuator stroke, 76 mm (3.0 in.). The elements surrounding the diaphragm opening did not show signs of permanent large deformation or failure, as can be seen in Fig. 4.53. The load versus average displacement curve at the loading points of the diaphragm in Fig. 4.54 shows the first cycles with an initial tangent stiffness (K_i) of 36 kN/cm (20.5 kips/in.) reducing on subsequent cycles to a tangent post-yield stiffness of 3.5 kN/cm (2 kips/in.). The maximum residual displacement was 30 mm (1.2 in.). The maximum actuator load was 47 kN (10.5 kips) and the diaphragm mid-point displacement was 80 mm (3.15 in.).

The maximum lateral displacement at the anchor connection was 2 mm (0.08 in.) which is 2.5% of the lateral displacement at the diaphragm midpoint, as shown in Fig. 4.55. Fig. 4.56 shows the load versus average slip displacement between sheathing boards of the diaphragm with a maximum slip of 6 mm (0.24 in.).

The average anchor strains shown in Fig. 4.57 exhibit a behavior similar to the anchors of diaphragm MAE-2. The first loops of the curve did not show strain gain until an average load of 22.3 kN (5 kips). From this load level the strains increased uniformly with loading. This behavior was attributed to the friction that had to be overcome before the anchor bore in the tube hole, deforming in bending and shear. The strains were higher for one load direction with a maximum strain of 862 μs.

The effect of the diaphragm opening can be observed by comparing the curves shown in Fig. 4.54 and Fig. 4.27 (diaphragm MAE-2). On average, the maximum actuator load reduced 16%. No visible damage was found in the joists, sheathing boards, nails or anchor connections.

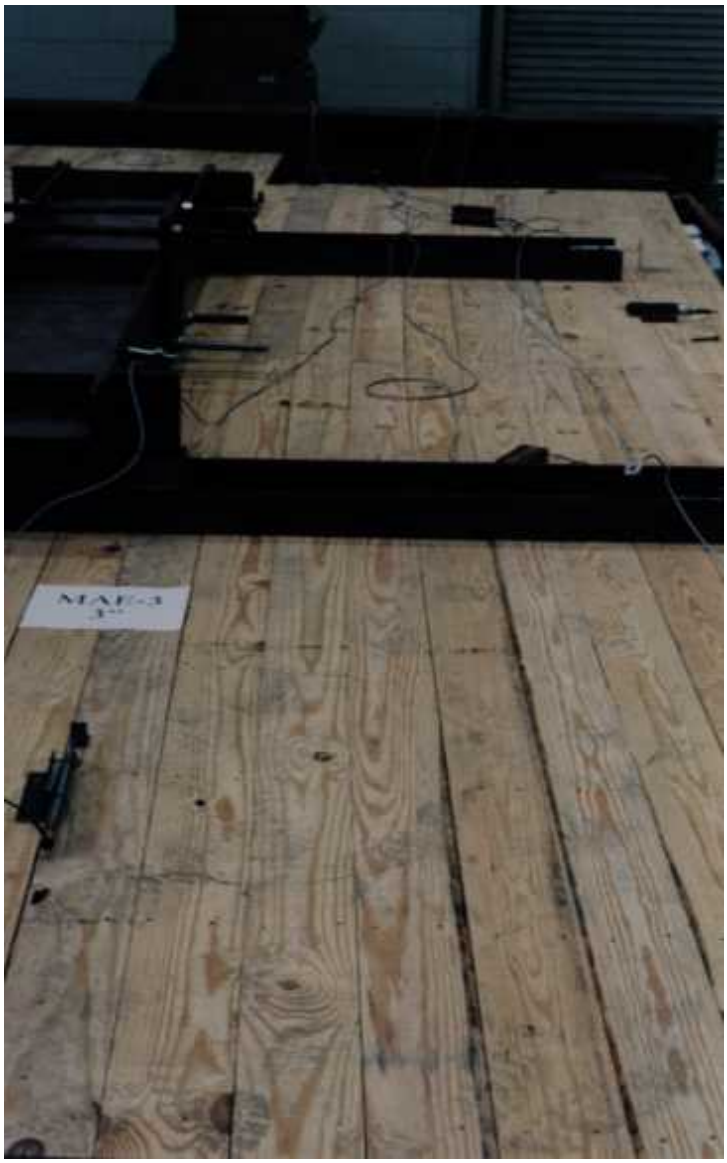

FIG. 4.53 Diaphragm MAE-3 at 76 mm (3 in.) of Applied Displacement

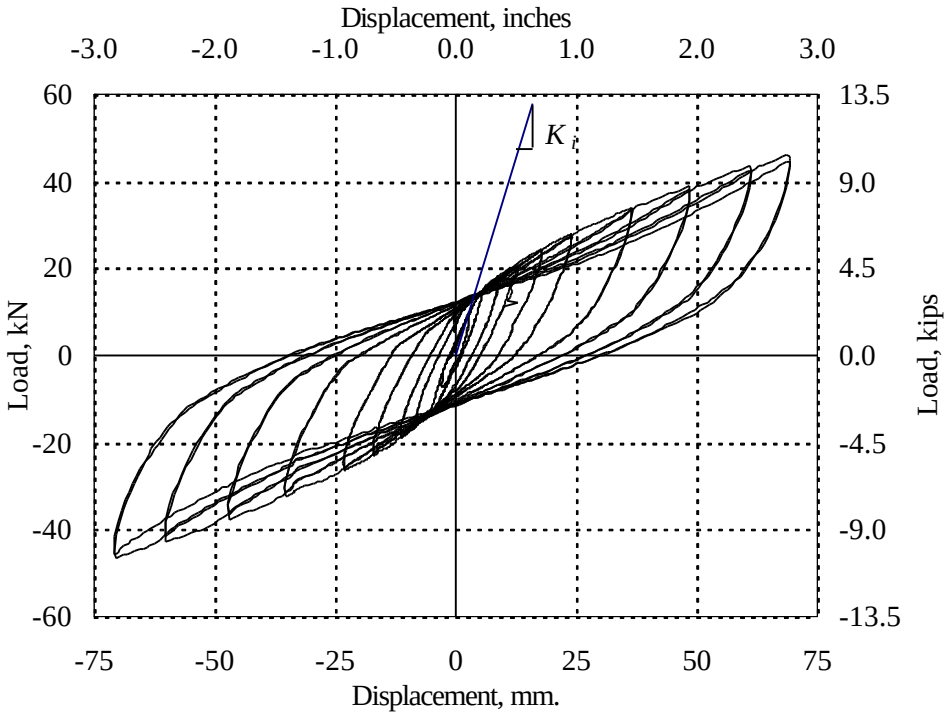

FIG. 4.54 MAE-3. Load-Displacement at Loading Points

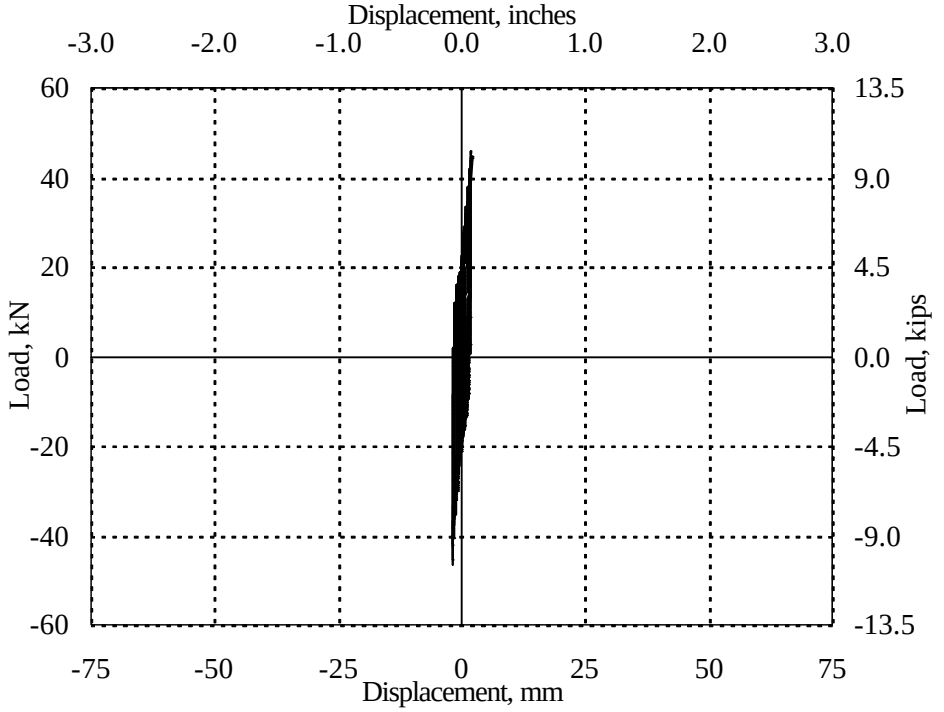

FIG. 4.55 MAE-3. Load-Slip Displacement at Connection

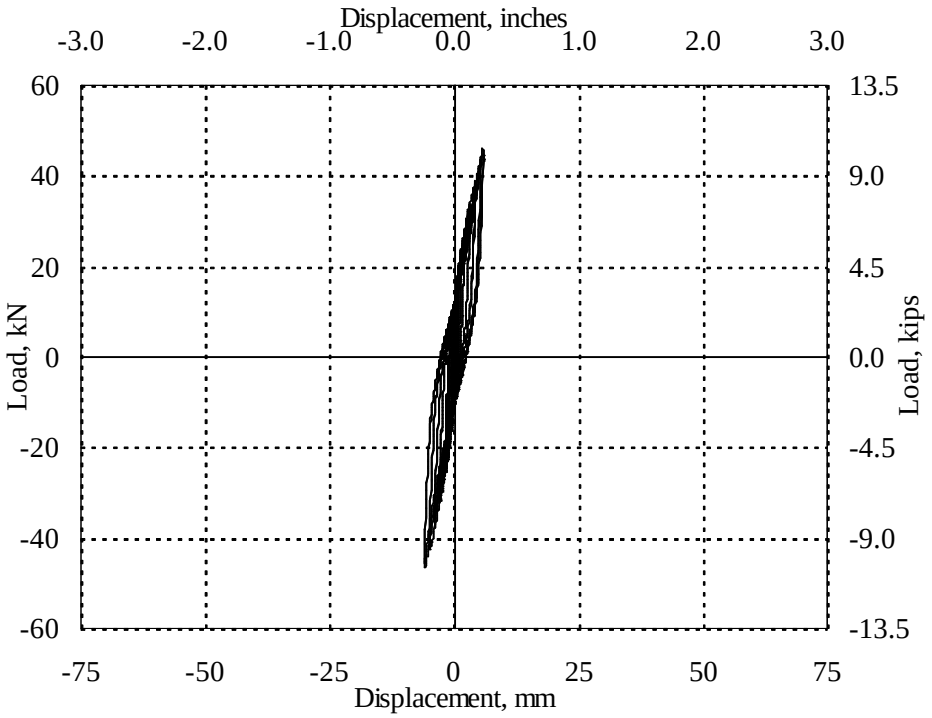

FIG. 4.56 MAE-3. Load-Slip Between Boards

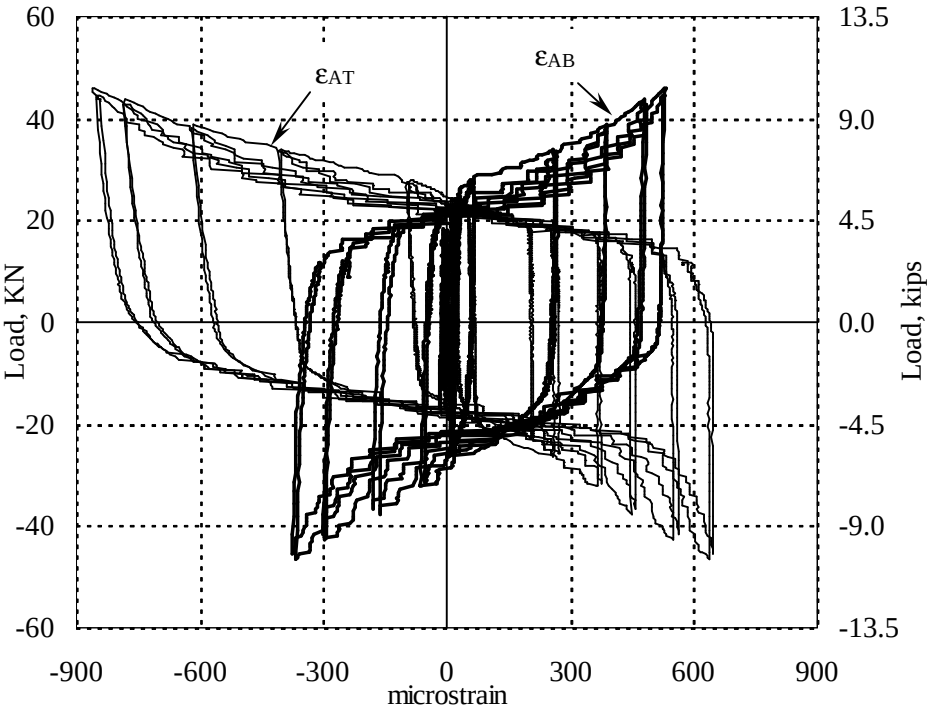

FIG. 4.57 MAE-3. Load-Anchor Strain

4.5.2 Unblocked Plywood Overlay Retrofit Diaphragm MAE-3A

Fig. 4.58 shows a plot of actuator load versus average displacement at the loading points of diaphragm MAE-3A. The diaphragm had a nonlinear force-displacement curve, characterized by two different stiffnesses, first an initial tangent stiffness (K_i) of 165 kN/cm (94 kips/in.), which degraded on each cycle until a tangent post-yield stiffness of 6.7 kN/cm (3.8 kips/in.). The loops of the curve show pinching and a maximum residual displacement of 25 mm (1 in.). The shear strength was controlled by the panel nails, which resisted a maximum load of 100 kN (22.5 kips). The maximum displacement at the diaphragm midpoint (Δ_{MP}) was 49 mm (1.9 in.).

The lateral displacement at the anchor connections (Δ_{AC}) was 5 mm (0.2 in.), which is 10% of the total lateral displacement of the diaphragm (see Fig. 4.59). Pinching can also be observed in the loops of the curve can be observed. As can be seen in Fig. 4.60, the slip displacement between sheathing boards reached a maximum of 14 mm (0.5 in.).

The behavior of the anchor connection is shown in Fig. 4.61. During loading no strain developed in the anchor connection until a load of 11 kN (2.5 kips). During unloading, a small strain loss occurred until a certain load, which was higher in each cycle and for the last cycle occurred at 38 kN (8.5 kips). After that strains developed in the other direction with a similar behavior. The strain was higher for one loading direction, developing a maximum strain of 2,150 μs, well beyond the yielding point.

The maximum amplitude displacement applied to diaphragm MAE-3A was 51 mm (2.0 in.). The test was terminated when nails from panels adjacent to the support frames of the diaphragm popped out such that they projected 40 to 50 mm (1.5 to 2 in.) from the top of the plywood. Besides the panel failure, the diaphragm did not show other signs of damage in the other wood or metal components. Overturning of the diaphragm did not occur in the test.

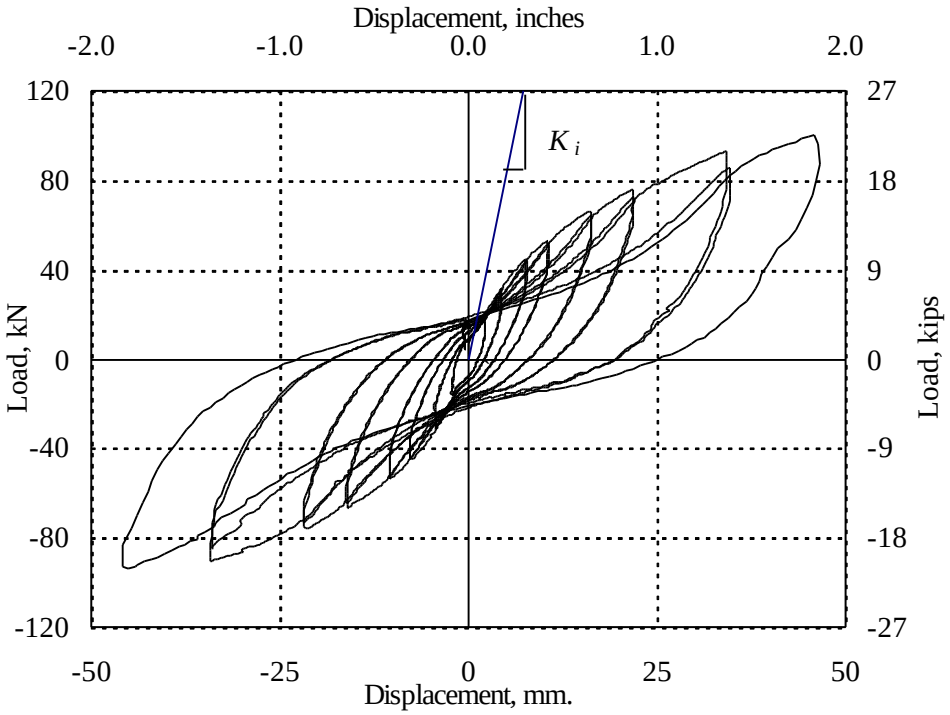

FIG. 4.58 MAE-3A. Load-Displacement at Loading Points

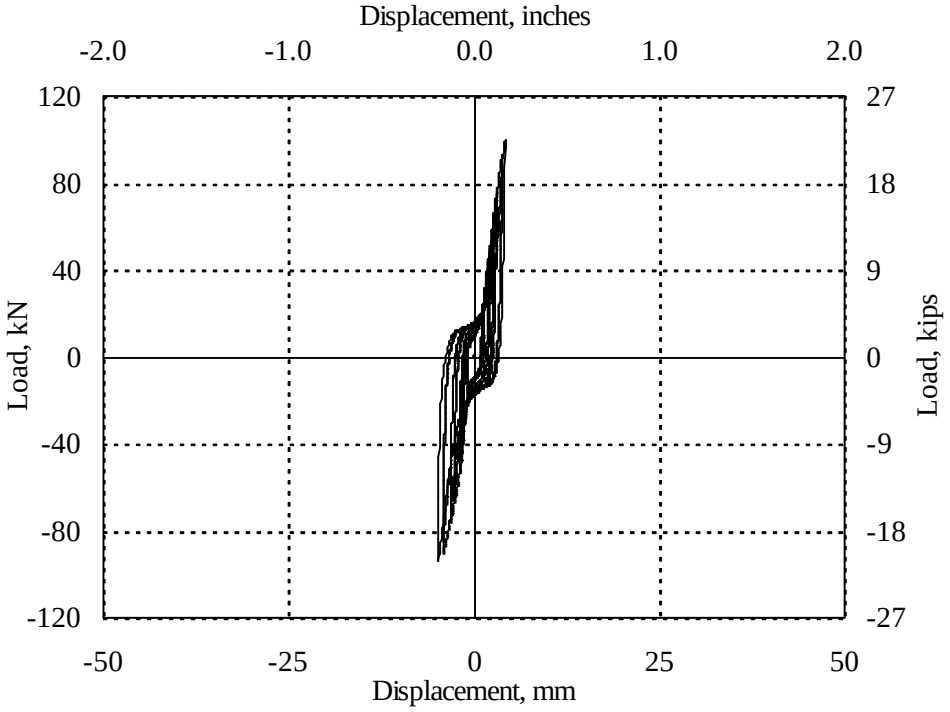

FIG. 4.59 MAE-3A. Load-Slip Displacement at Connection

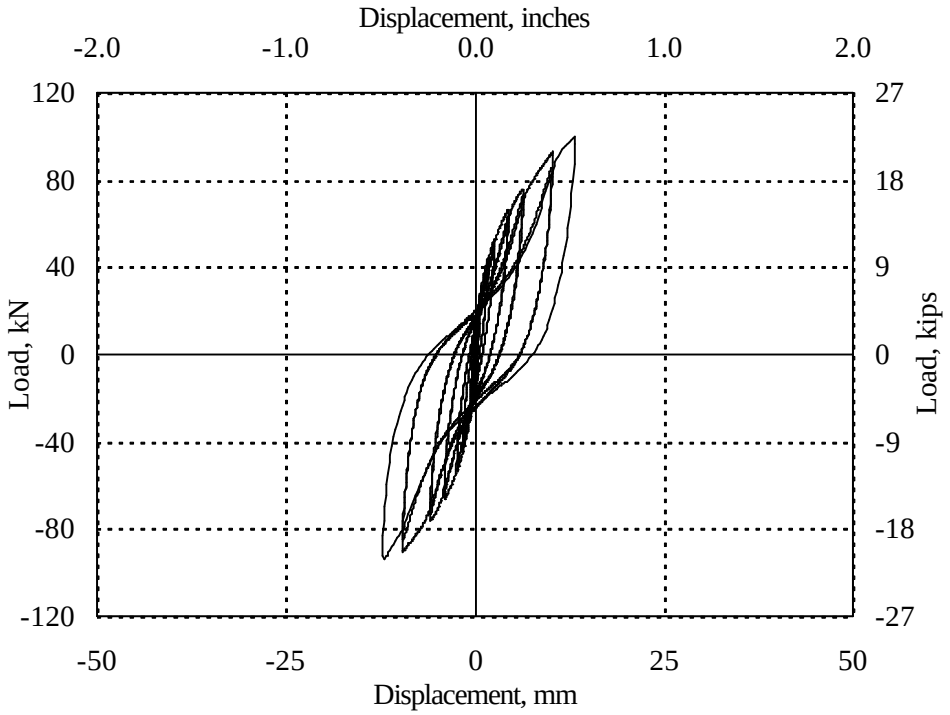

FIG. 4.60 MAE-3A. Load-Slip Displacement Between Panels

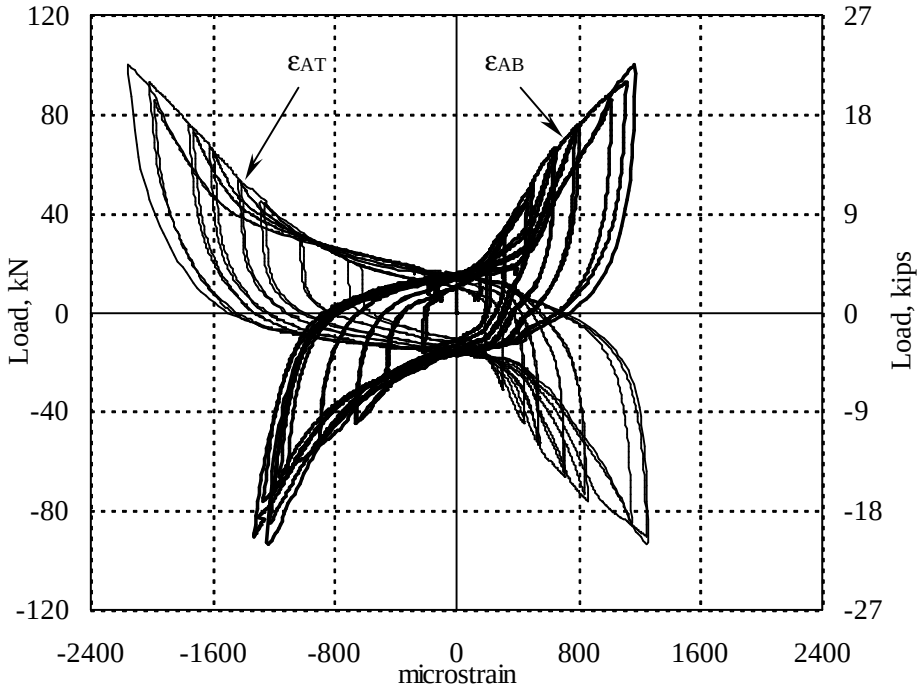

FIG. 4.61 MAE-3A. Load-Anchor Strain

4.5.3 Blocked Plywood Overlay Retrofit Diaphragm MAE-3B

The behavior of diaphragm MAE-3B is shown in Fig. 4.62. The initial tangent stiffness (K_i) was 120 kN/cm (68.5 kips/in.) and degraded on each cycle to a tangent post-yield stiffness of 29.1 kN/cm (16.6 kips/in.). The loops of the curve exhibited a maximum residual displacement of 13 mm (0.5 in.) and pinching phenomenon can also be observed. The actuator load was resisted by the nails on the panel overlays, until a maximum load of 138 kN (31 kips). Fig. 4.63 shows the average lateral displacement of the anchor connections (Δ_{AC}). The loops of the curve exhibit pinching and a maximum displacement of 13.2 mm (0.5 in.), 40% of the overall lateral displacement of the diaphragm. The average slip displacement between panels was 7 mm (0.3 in.) as can be observed in Fig. 4.64.

The behavior of the anchor is shown in Fig. 4.65. During the initial loading, no strains occurred until a load of 18 kN (4 kips). At this point, strains developed possibly after the anchors bore on the tube holes and then shear and bending actions occurred in the anchors. During unloading, strain loss occurred until a certain load, which for the last cycle was 36 kN (8 kips), possibly when the anchor bent in the opposite direction. In the latter cycles, the anchor strains went beyond the yield point (1,200 μs) following the same pattern of behavior. The maximum anchor strain was 2,440 μs.

The test was terminated after overturning moment developed in the diaphragm lifting up the diaphragm edge opposite to the actuator. At 25 mm (1 in.) of actuator displacement, existing bearing cracks (from the previous test for MAE-2A) in the joists at the anchor connection extended up to 762 mm (30 in.) long and a width of 3 mm (0.125 in.). No nails popped out from the top of the diaphragm. The maximum displacement applied on the diaphragm was 40 mm (1.5 in.) and the maximum measured displacement at the diaphragm midpoint (Δ_{MP}) was 33 mm (1.3 in.) with a maximum vertical uplift of 100 mm (4 in.) as shown in Fig. 4.66. No visible damage was observed around the opening, panel overlay, or nails.

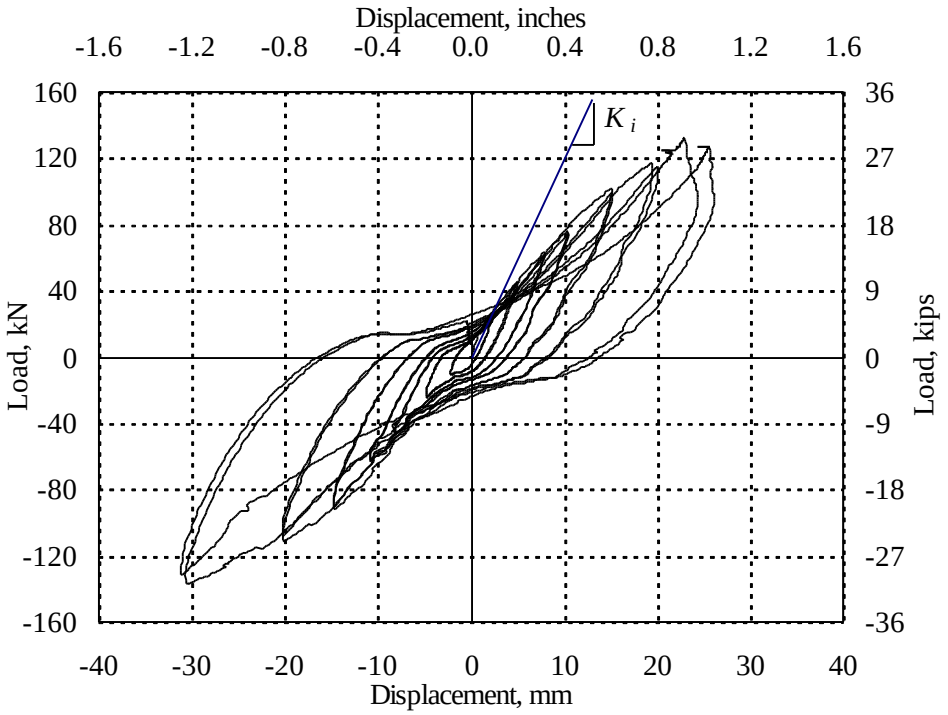

FIG. 4.62 MAE-3B. Load-Displacement at Loading Points

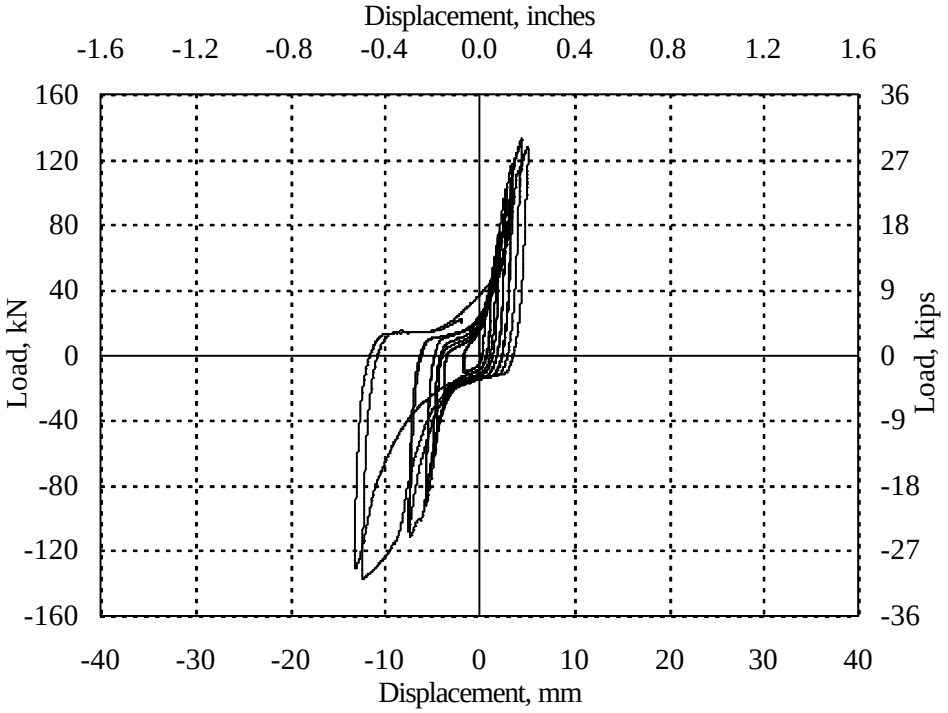

FIG. 4.63 MAE-3B. Load-Slip Displacement at Connection

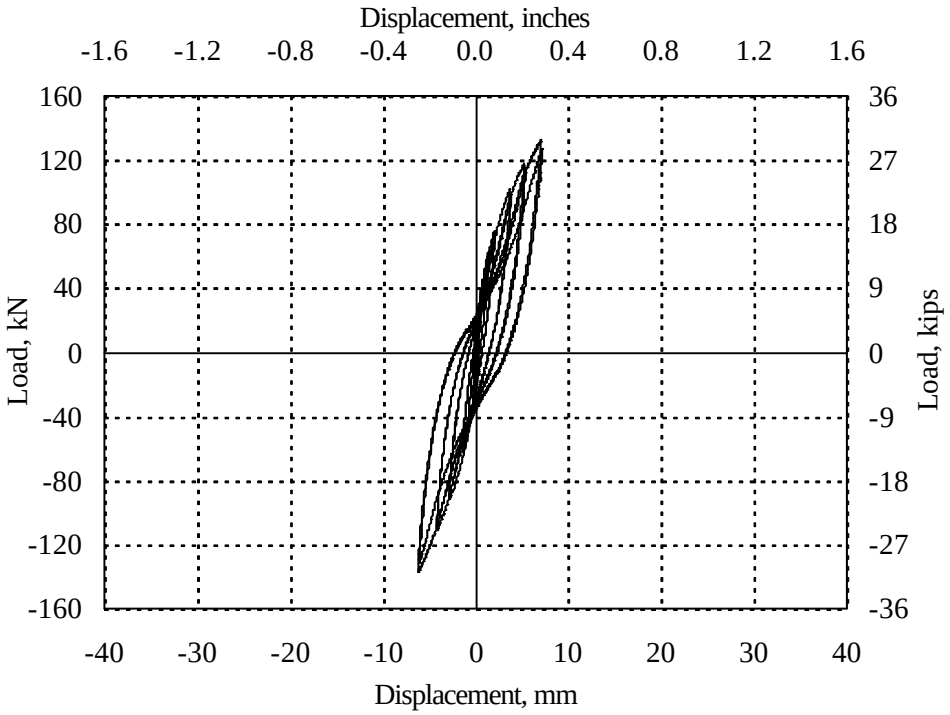

FIG. 4.64 MAE-3B. Load-Slip Displacement Between Panels

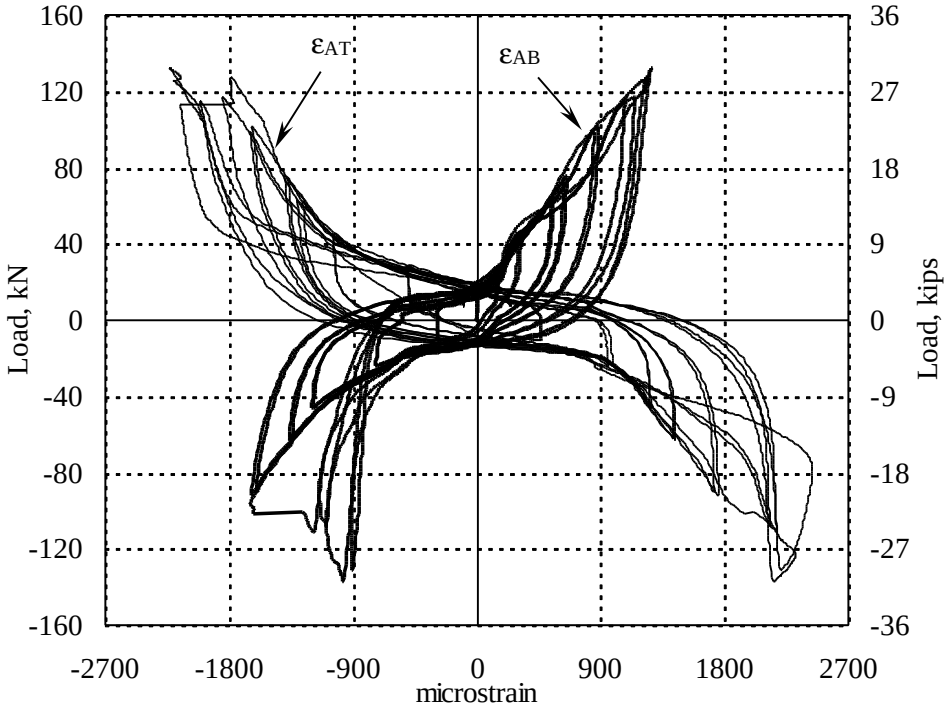

FIG. 4.65 MAE-3B. Load-Anchor Strain

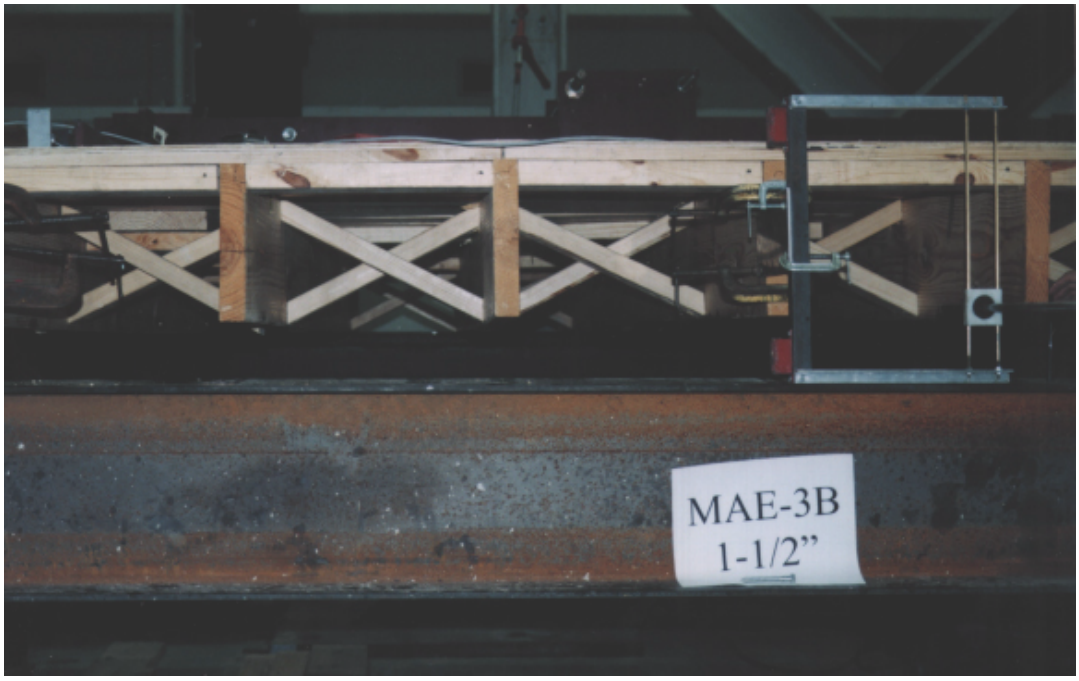

FIG. 4.66 Uplifting of Diaphragm MAE-3B at 38 mm

4.5.4 Comparison of Responses

Backbone curves for diaphragm MAE-3 and retrofits MAE-3A and MAE-3B are depicted in Figs. 4.67, 4.68 and 4.69 according to the procedure described in FEMA 273 (ATC, 1997a). The lateral displacement at the diaphragm mid-point was used to generate the backbone curves. The initial stiffness (K_i) given in Table 4.6 showed an increase over MAE-3 of 4.5 and 3.3 times K_i for MAE-3 for retrofits MAE-3A and MAE-3B, respectively. Comparing the maximum actuator load, the retrofitted diaphragms MAE-3A and MAE-3B sustained two and three times the load of MAE-3, respectively. A comparison between the backbone curves is shown in Fig. 4.70, which shows that the retrofits provide higher lateral load strength and stiffness.

Observing the values of the bilinear parameters in Table 4.7, diaphragm MAE-3B shows the largest shear strength and stiffness. The yield displacement remained unchanged for the three diaphragms.

Fig. 4.71 compares the backbone curves at the anchor connections. At the beginning of loading, no lateral displacement occurred until the load overcame friction forces between the end joist and the tube connections at approximately 13.4 kN (3 kips). Then bending, shear and possibly axial deformations occurred in the anchors. It is also observed that when the maximum shear force in the diaphragm increased, the maximum anchor lateral displacement also increased. The maximum lateral anchor displacements of the retrofitted diaphragms MAE-3A and MAE-3B were 2.5 and 6.5 times higher than that of MAE-3, respectively.

Comparing the slip between sheathing boards for MAE-3 and panel overlays for MAE-3A and MAE-3B (Δ_{SB}) over the diaphragm deformation ($\Delta_{MP} - \Delta_{AC}$), the sheathing slip over diaphragm deformation ratio was 8% (MAE-3), 30% (MAE-3A) and 36% (MAE-3B). The percentage increases correspond to the higher shear forces applied to the diaphragm.

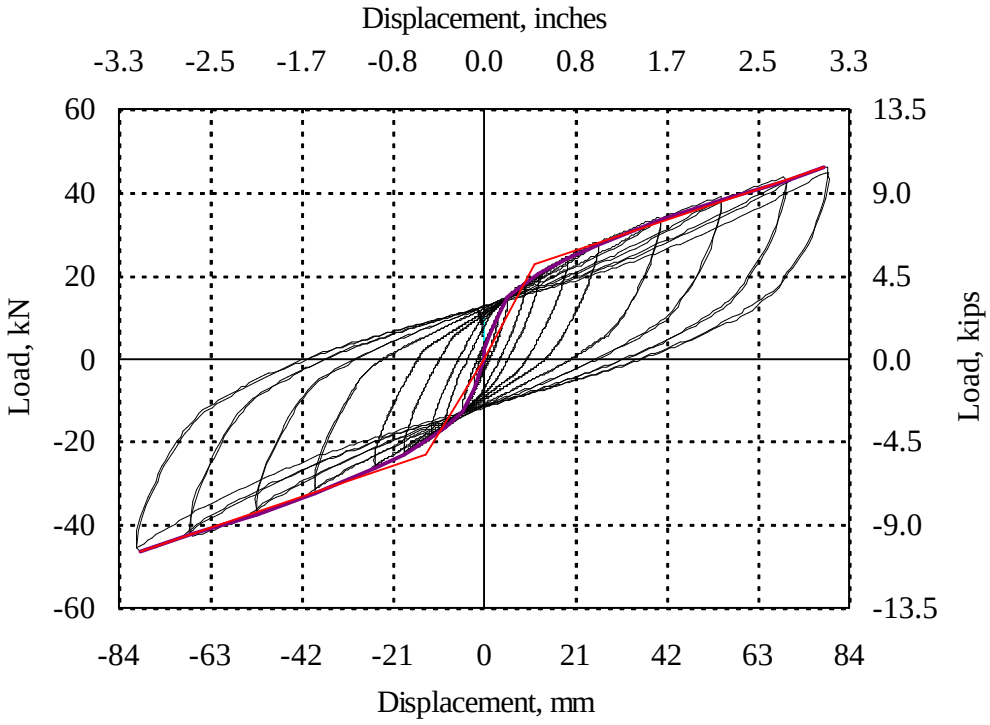

FIG. 4.67 Backbone Curve at Midpoint of Diaphragm MAE-3

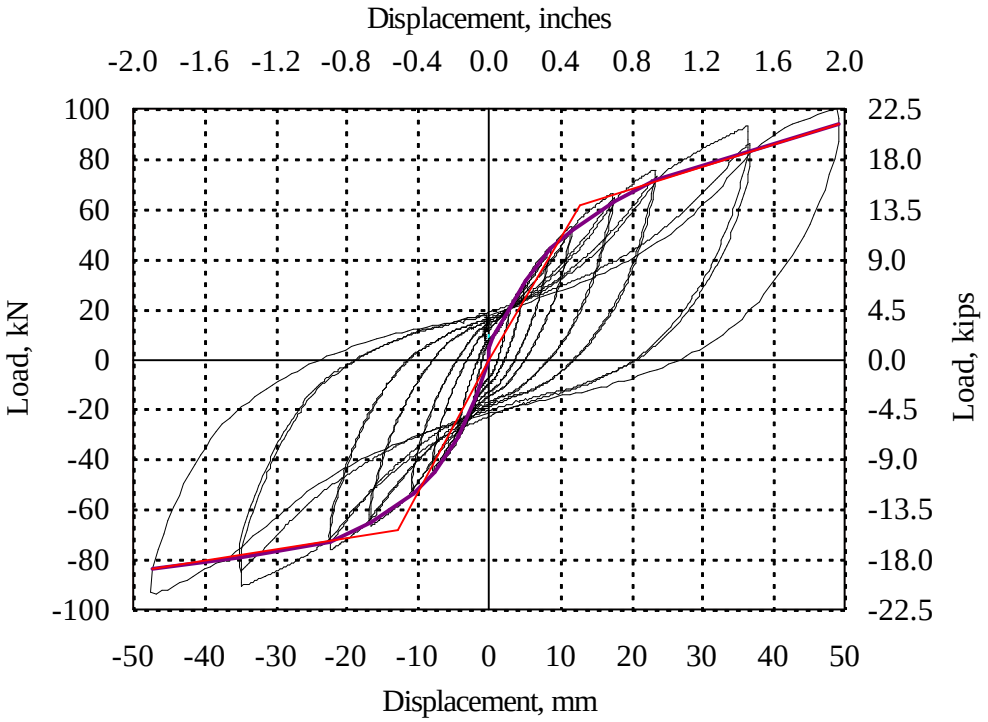

Fig. 4.68 Backbone Curve at Midpoint of Diaphragm MAE-3A

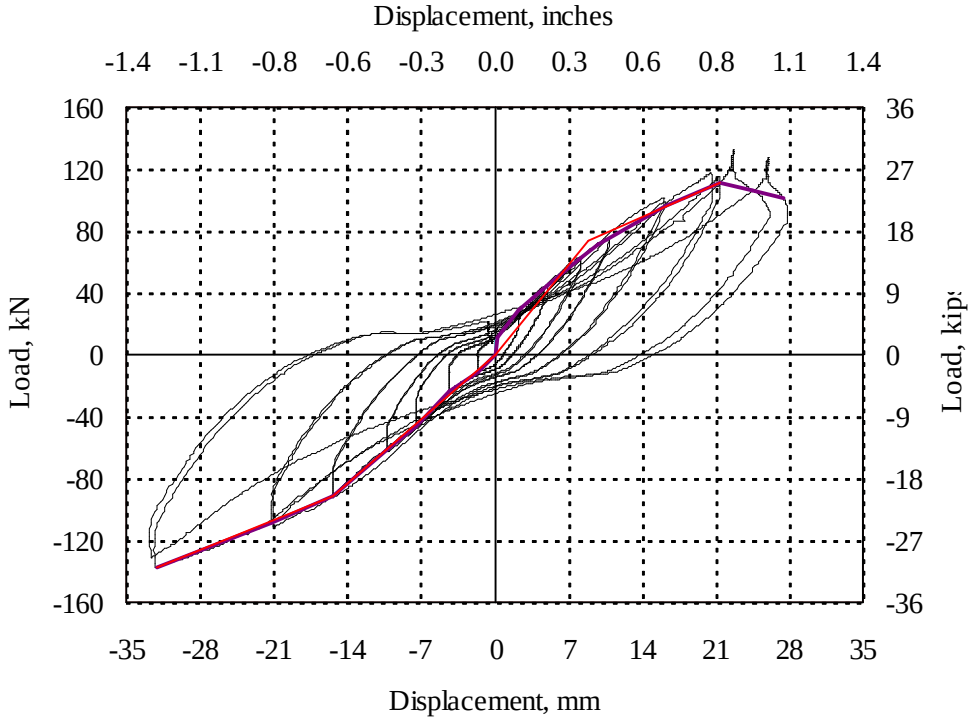

FIG. 4.69 Backbone Curve at Midpoint of Diaphragm MAE-3B

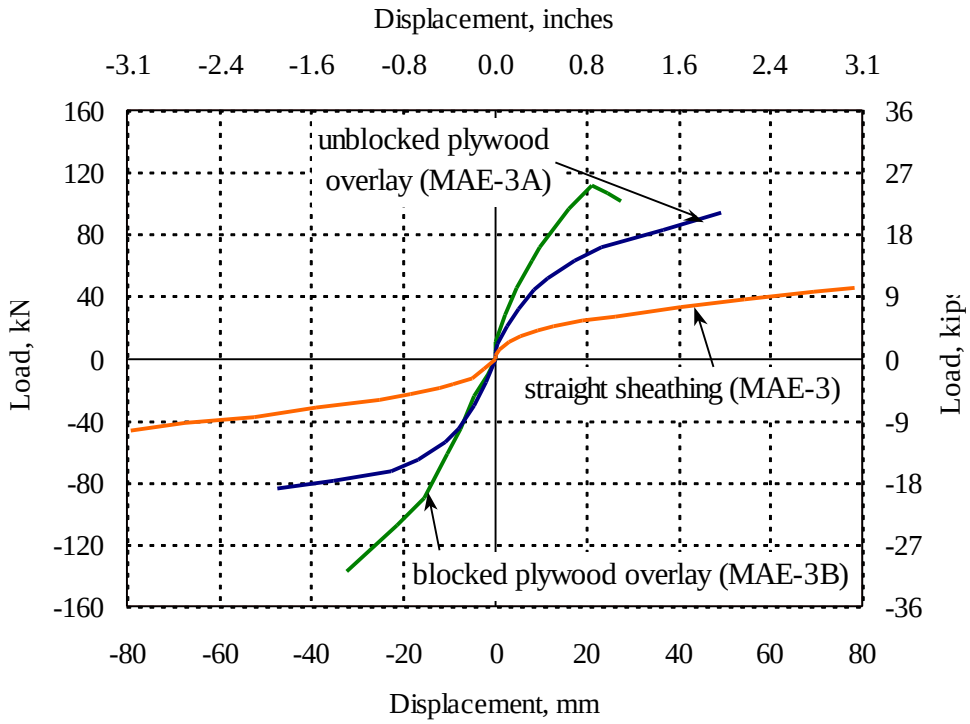

FIG. 4.70 Comparison of Backbone Curves at Midpoint of Diaphragm 3

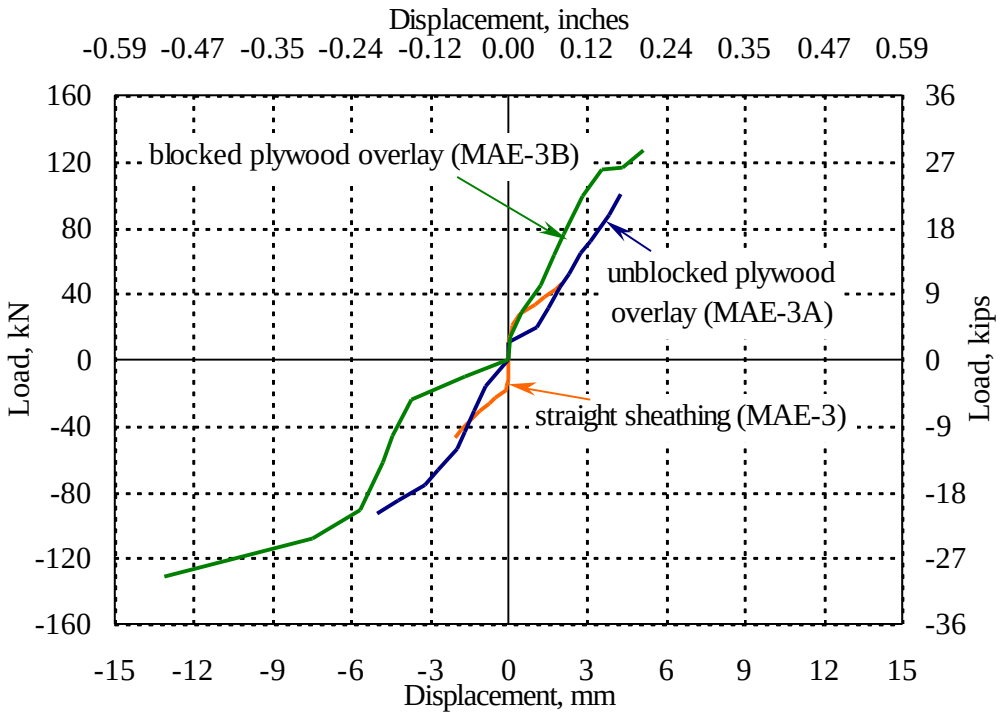

FIG. 4.71 Comparison of Backbone Curves at Connection of Diaphragm 3

TABLE 4.6 Response Parameters for Diaphragm MAE-3 and Its Retrofits

Parameter	MAE-3	MAE-3A	MAE-3B
Δ_{AMP}, mm (in.)	76 (3.0)	51 (2.0)	38 (1.5)
Δ_{MP}, mm (in.)	80 (3.2)	49 (1.9)	33 (1.3)
Δ_{LP}, mm (in.)	71 (2.8)	47 (1.9)	26 (1.0)
Δ_{AC}, mm (in.)	2 (0.08)	5 (0.20)	13 (0.52)
Δ_{SB}, mm (in.)	6 (0.24)	14 (0.53)	7 (0.28)
ε_{AC}, μs	862	2,150	2,440
F_{max}, kN (kips)	47 (10.5)	100 (22.5)	138 (31)
K_I, kN/cm (kips/in.)	36 (20.5)	165 (94.0)	120 (68.5)

Note: see Table 4.2 for definitions of parameters

TABLE 4.7 Parameters from Bilinear Curves of Specimen 3 and Its Retrofits

Parameter	MAE-3	MAE-3A	MAE-3B	3A/3	3B/3
V_y kN (kips)	23 (5.2)	65 (14.6)	82 (18.5)	2.8	3.6
Δ_y mm (in.)	12 (0.5)	13 (0.50)	12 (0.5)	1.0	1.0
K kN/cm (kips/in.)	18.6 (10.6)	51.2 (29.2)	71.2 (38.5)	2.8	3.6
K_2 kN/cm (kips/in.)	3.5 (2.0)	6.7 (3.8)	29.1 (16.6)	1.9	8.3

Note: see Table 4.3 for definitions of parameters

5. COMPARISON OF EXPERIMENTAL RESULTS WITH PREDICTIONS

The values determined in the FEMA Guidelines for seismic rehabilitation of buildings: FEMA 273 (ATC, 1997a) and FEMA 356 (ASCE, 2000) of the in-plane lateral yield shear strength, stiffness, backbone curves and failure modes for each diaphragm specimen are provided in this section and compared with the experimental results from the previous section.

5.1 PREDICTED DIAPHRAGM IN-PLANE ELASTIC LATERAL STIFFNESS AND YIELD SHEAR STRENGTH

The calculation procedures for the effective stiffness (K) and in-plane yield shear strength (v_y) of the diaphragm specimens and their retrofits are presented here based upon the FEMA guidelines. The guidelines used are for: (1) single straight-sheathed diaphragms; (2) plywood panel overlays on unblocked, unchorded straight sheathed diaphragms; and (3) plywood panel overlays on blocked, unchorded straight sheathed diaphragms. The FEMA Guidelines do not provide recommendations for tongue & groove (T&G) sheathed diaphragms, as in the case of diaphragm specimen MAE-1. For this reason, the specifications for straight-sheathed diaphragms were used for comparison. The steel truss used for retrofit of diaphragms MAE-1B and MAE-2A was designed using the AISC-LRFD (AISC, 1995) manual. In the case of straight-sheathed diaphragm with a corner opening (MAE-3, MAE-3A and MAE-3B), a reduction of stiffness and yield shear strength of the diaphragm was expected, due to the discontinuity and the reduced width of the diaphragm. To account for this discontinuity, an average diaphragm width of 2.9 m (9.5 ft.) was used as an approximation and the specifications for regular straight-sheathed diaphragms were followed.

5.1.1 Diaphragm In-Plane Effective Lateral Stiffness

5.1.1.1 FEMA 273 Procedure

The in-plane effective lateral stiffness of straight-sheathed diaphragms with or without plywood panel overlays can be approximated from the deflection equation for horizontal diaphragms provided in FEMA 273 (ATC, 1997a):

$$\Delta = \frac{vL^4}{G_d b^3} \tag{5.1}$$

where:

Δ = Calculated diaphragm lateral deflection, in m
v = Shear force per unit diaphragm dimension in the direction under consideration, in kN/m = $V/2b$
L = Diaphragm span between shear walls or collectors, 7.32 m (24 ft.)
b = Diaphragm width, 3.66 m (12 ft.)
V = Total force in the diaphragm, in kN
G_d = Diaphragm shear stiffness from FEMA 273, in kN/m

The effective stiffness (K) can be obtained from this expression as follows:

$$K = \frac{V}{\Delta} = 2G_d\left(\frac{b}{L}\right)^4 \tag{5.2}$$

5.1.1.2 FEMA 356 Procedure

FEMA 356 (ASCE, 2000) uses equation 5.3 to determine the in-plane effective lateral stiffness of straight-sheathed diaphragms with or without plywood panel overlays:

$$\Delta_y = \frac{v_y L}{2G_d} \tag{5.3}$$

where:

Δ_y = Calculated diaphragm deflection at yield, in m

v_y = Shear at yield in force per unit diaphragm dimension in the direction under consideration, in kN/m = $V_y/2b$
L = Diaphragm span between shear walls or collectors, 7.32 m (24 ft.)
G_d = Diaphragm shear stiffness from FEMA 356, in kN/m

Similarly to the previous case the effective stiffness can be obtained from Eq. 5.3 as follows:

$$K = \frac{4bG_d}{L} \tag{5.4}$$

Table 5.1 lists the shear stiffnesses (G_d) from FEMA 273 and FEMA 356 for the diaphragm specimens and retrofits tested and the calculated in-plane effective stiffness (K) from Eq. 5.2 and Eq. 5.4, respectively. The effective stiffness of the T&G sheathed diaphragms MAE-1 and MAE-1A were calculated based on the effective stiffness of a straight-sheathed diaphragm, similar to MAE-2. In order to estimate the effective stiffness for the diaphragms retrofitted with the steel truss, MAE-1B and MAE-2A, it was assumed that the loading and truss were in the same plane and that the wood diaphragm did not contribute to the stiffness. An effective stiffness (K) of 933 kN/m (532 kips/in.) was estimated from Eq. 5.5, based on the axial deformations of the truss members.

$$K = \frac{4EA}{\frac{L_d}{\sin^2(a)} + \frac{L_t}{2\tan^2(a)}} \tag{5.5}$$

where:

E = Modulus of elasticity of steel, 20,020 kN/cm^2 (29,000 ksi)
A = Area of truss member, 12.4 cm^2 (1.92 in^2) for a WT4x6.5 section (designed in Section 5.1.2)
L_d = Length of diagonal brace member, 305 cm (120 in.)
L_t = Length of horizontal brace member, 244 cm (96 in.)
a = Orientation angle of diagonal brace member, 37• (see Fig. 5.2)

Eq. 5.5 was derived from the equilibrium of forces, compatibility of displacements of the brace members and Hooke's law. The effective stiffness (*K*) of the diaphragm with a corner opening, MAE-3 and its retrofits MAE-3A and MAE-3B, was approximated using Eq. 5.2 with an average diaphragm width of 2.9 m (9.5 ft.).

TABLE 5.1 Predicted In-plane Effective Lateral Stiffness of Diaphragms

Diaphragm	Type of Diaphragm	Shear Stiffness (G_d) kN/cm (kips/in.)		Effective Stiffness (*K*) kN/cm (kips/in.)	
		FEMA 273	FEMA 356	FEMA 273	FEMA 356
MAE-1	T&G sheathed	351 (200)[1]	3.5 (2)	44 (25)	7 (4)
MAE-1A	Shear Connection & Strapping R.	351 (200)[1]	3.5 (2)	44 (25)	7 (4)
MAE-1B	Steel Truss R.	--	--	933 (532)[2]	
MAE-2	Straight Sheathed	351 (200)	3.5 (2)	44 (25)	7 (4)
MAE-2A	Steel Truss R.	--	--	933 (532)[2]	
MAE-2B	Unblocked Panel Overlay R.	877 (500)	8.8 (5)	110 (62.5)	17.5 (10)
MAE-2C	Blocked Panel Overlay R.	1,227 (700)	12.3 (7)	153 (87.5)	24.5 (14)
MAE-3	Straight Sheathed w/ Opening	351 (200)	3.5 (2)	17 (9.8)	5.6 (3.2)
MAE-3A	Unblocked Panel Overlay R.	877 (500)	8.8 (5)	43 (24.6)	13.8 (7.9)
MAE-3B	Blocked Panel Overlay R.	1,227 (700)	12.3 (7)	60 (34.4)	19.4 (11.1)

[1] For straight sheathed diaphragm
[2] From Eq. 5.5

5.1.2 Diaphragm In-Plane Lateral Yield Shear Strength

The in-plane lateral yield shear strength (v_y) of straight-sheathed diaphragms can be calculated depending on the direction of the lateral loads with respect to the sheathing boards. Shear forces parallel to the direction of the sheathing are transferred through the

nails in the supporting joists, as in the case of diaphragm MAE-1 and its retrofits. Shear forces perpendicular to the direction of the sheathing are resisted by the moment capacities of the nail couples in each sheathing board to joist connection (see Fig. 5.1), as in the case of diaphragms MAE-2, MAE-3 and their retrofits. The FEMA Guidelines are used to determine the yield shear strength for the case of straight-sheathed and plywood overlay on straight-sheathed diaphragms. For the case of T&G diaphragm and the steel strap retrofit, the National Design Specification for Wood Construction (NDS) and the FEMA Guidelines were used to determine the yield shear strength. For the case of the steel truss retrofits, AISC was used to determine the shear strength.

5.1.2.1 FEMA 273 Procedure

5.1.2.1.1 Tongue & Groove Single Straight Sheathed Diaphragms

Because T&G sheathed diaphragms are not addressed in FEMA 273, the in-plane lateral allowable shear force of diaphragm MAE-1 was estimated by summing the allowable shear of the nails connecting the sheathing board to the framing across the diaphragm width. The yielding shear force was then obtained by multiplying the allowable shear by a factor of 2.8 given in FEMA 274 (ATC, 1997b) for single straight-sheathed diaphragms.

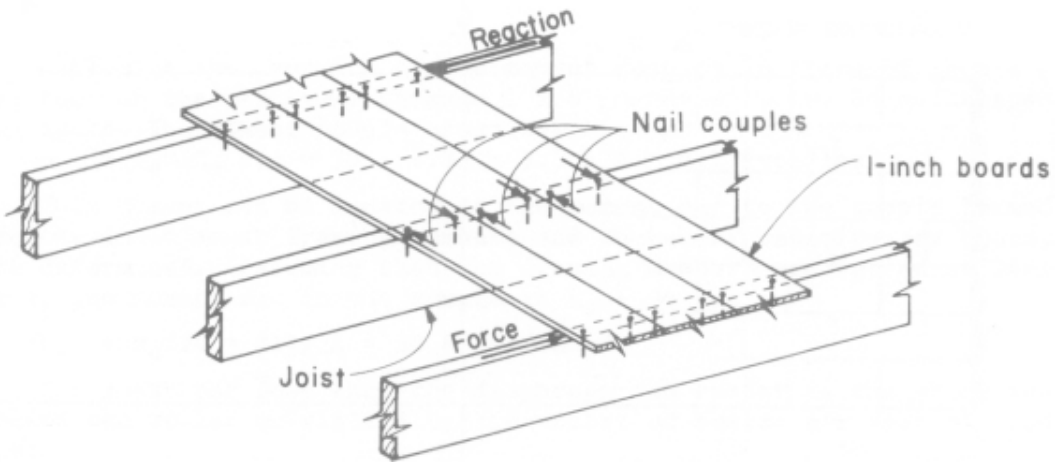

FIG. 5.1 Straight Sheathed Diaphragm – Moment Couples (ATC-7, 1981)

The National Design Specification for Wood Construction (NDS) (AF&PA, 1997) was used to calculate the allowable shear strength for a nail (*Z'*) in a single shear wood-to-wood connection (two members):

$$Z' = Z\, C_D\, C_M\, C_t\, C_d\, C_{eg}\, C_{di}\, C_{tn} \tag{5.6}$$

where:

Z = Nominal design value for single shear, in N (see Eq. 5.7)
C_D = Duration factor, taken as 1.6 for earthquake loading
C_M = Wet service factor, taken as 1.0 for a moisture content less than 19%
C_t = Temperature factor, taken as 1.0 for a temperature less than 100• F
C_d = Penetration depth factor, taken as 1.0 for nail penetration (p) more than 12 times 10d finishing nail diameter (D) (p = 1.75 in. > 12D = 0.75 in.)
C_{eg} = End grain factor, taken as 0.67 for nail axis parallel to the wood fibers
C_{di} = Diaphragm factor, taken as 1.1 for nails used in diaphragms
C_{tn} = Toe nail factor, taken as 0.83 for toe-nail connections.

The design value for single shear (*Z)* can be determined from the lesser value of the following:

$$Z \le \begin{cases} \dfrac{Dt_s F_{es}}{K_D} & \text{Mode } I_s \text{ (bearing of side member)} \\ \dfrac{k_1 DpF_{em}}{K_D(1+2R_e)} & \text{Mode } III_m \text{ (nail bending at one plastic hinge in the main member)} \\ \dfrac{k_2 Dt_s F_{em}}{K_D(2+R_e)} & \text{Mode } III_s \text{ (nail bending at one plastic hinge in the side member)} \\ \dfrac{D^2}{K_D}\sqrt{\dfrac{2F_{em}F_{yb}}{3(1+R_e)}} & \text{Mode IV (nail bending at two plastic hinges)} \end{cases} \tag{5.7}$$

where:

$$k_1 = -1 + \sqrt{2(1+R_e) + \frac{2F_{yb}(1+2R_e)D^2}{3F_{em}p^2}}$$

$$k_2 = -1 + \sqrt{\frac{2(1+R_e)}{R_e} + \frac{2F_{yb}(2+R_e)D^2}{3F_{em}t_s^2}}$$

$R_e = F_{em}/F_{es}$, taken as 1.0 for Southern Pine lumber

p = Penetration of nail in joist, taken as 4.45 cm (1.75 in.)

t_s = Actual thickness of the sheathing board, taken as 1.90 cm (0.75 in.) for 1x4 T&G lumber
F_{em} = Dowel bearing strength of joist, taken as 3,800 N/cm^2 (5,550 psi) for Southern Pine grade II lumber
F_{es} = Dowel bearing strength of sheathing board, taken as 3,800 N/cm^2 (5,550 psi) for Southern Pine grade II lumber
F_{yb} = Bending yield strength of nail, taken as 69,000 N/cm^2 (100,000 psi) from NDS
D = Nail diameter, taken as 0.16 cm (0.0625 in.) for 10d finishing nail
K_D = 2.2 for nails with diameter D less than 0.43 cm (0.17 in.)

Table 5.2 shows the calculated nominal design values for shear for the T&G diaphragm used in the experimental study. The lowest value of *Z*, which corresponds to yield mode IV, was selected and then used to find *Z*' with Eq. 5.6. Multiplying this value of *Z*', 108 N (24 lb.) by the number of nails per unit diaphragm width, an allowable in-plane shear strength (v_a) of 259 N/m (18 lb./ft.) was determined for the diaphragm specimen. Using the same factor (2.8) from FEMA-274 to achieve yield shear strength (v_y) for straight-sheathed diaphragms, a value of 725 N/m (50 lb./ft.) was computed.

TABLE 5.2 Nominal Shear of 10d Finishing Nail in T&G Sheathed Diaphragms

Yield Mode	Design Shear Z N (lb.)
I_s	263 (59)
III_m	414 (93)
III_s	109 (24)
IV	108 (24)

The steel strap and enhanced connections retrofit in diaphragm MAE-1A was based from rehabilitation projects developed in California. The design was adapted for the dimensions of the diaphragm specimen (see Fig. 3.4). To determine the shear strength of the T&G diaphragm retrofitted with steel strap and bolted connections (MAE-1A), the additional shear strength of 6 mm ϕ x 76 mm (0.25 in. ϕ x 3 in.) lag

screws that attached the straps to the framing was calculated (see Fig. 3.4). The tabulated nominal shear design value (Z) given by NDS for one lag screw was 624 N (140 lb.). According to the NDS, the expression for allowable shear strength (Z') for a lag screw is:

$$Z' = Z\, C_D\, C_M\, C_t\, C_g\, C_D\, C_d\, C_{eg} \tag{5.8}$$

where:

C_g = Group action factor, taken as 1.0 for a single lag screw
C_D = Geometry factor, taken as the ratio end distance/4D equal to 0.75
C_d = Penetration depth factor, taken as 1.0, for p/8D greater than 1.0

The other factors have the same definitions and values as for the 8d finishing nail calculated using Eq. 5.6. From Eq. 5.8, an allowable shear strength (Z') of 503 N (113 lb.) resulted for one lag screw. Considering two lag screws per sheathing board width (one lag screw per board along each of the two long edges of the diaphragm) and dividing by the diaphragm width, an allowable shear force of 278 N/m (19 lb./ft.) resulted from the additional shear strength of the lag screws. Therefore, a total allowable shear strength (v_a) of 541 N/m (37 lb./ft.) for diaphragm MAE-1A was computed. Again using the factor of 2.8 from FEMA 274 to determine in-plane yield strength (v_y), a value of 1,520 N/m (104 lb./ft.) resulted. This implies a shear strength increase of about 100% of MAE-1 due to the addition of the steel strapping and bolted connections in MAE-1A.

5.1.2.1.2 Square Edged Single Straight Sheathed Diaphragms

For straight sheathed diaphragms with two or more nails at each sheathing board to joist connection (diaphragms MAE-2 and MAE-3), the FEMA 273 guidelines provide an approximate in-plane diaphragm yield shear strength (v_y) of 1,753 N/m (120 lb./ft.) without further explanation, regardless of the load direction. Alternatively, because the shear forces during lateral loading act perpendicular to the direction of the sheathing, for

MAE-2 and MAE-3, resistance is provided by the nail couple at the sheathing board to joist connections. Therefore, the nail-couple method was also used to calculate the allowable in-plane shear strength (v_a) of the diaphragm. A discussion of the nail-couple method for calculating the shear capacity of straight-sheathed diaphragms is given in ATC-7 (ATC, 1981). In summary, the allowable shear strength (v_a) per unit diaphragm width can be determined as follows:

$$v_a = \frac{Z' s_n}{s_f h} \tag{5.9}$$

where:

Z' = Allowable shear per nail, N (see Eqs. 5.6 and 5.7)
s_n = Spacing between nails, taken as 0.114 m (4.5 in.) for 1x6 sheathing
s_f = Spacing between framing members, taken as 0.406 m (16 in.)
h = Actual width of sheathing board, taken as 0.14 m (5.5 in.) for 1x6 sheathing

The allowable shear per nail (Z') was calculated using Eqs. 5.6 and 5.7 considering an 8d common nail and all the adjustment factors used in the previous case except the toe-nail factor. Table 5.3 shows the nominal design shear (Z) based on the four yield modes with a governing value of 463 N (104 lb.). A corresponding allowable shear (Z') of 548 N (123 lb.) was computed.

TABLE 5.3 Nominal Shear of 8d Common Nail in Straight Sheathed Diaphragms

Yield Mode	Design Shear (Z) N (lb.)
I_s	1,100 (248)
III_m	900 (202)
III_s	463 (104)
IV	472 (106)

Using Eq. 5.9, an allowable in-plane shear strength (v_a) of 1,100 N/m (75 lb./ft.) was obtained. Again using the allowable to yield shear factor (2.8) from FEMA 274 for straight-sheathed diaphragms, the in-plane yield shear strength of straight-sheathed diaphragms was determined to be 3,070 N/m (210 lb./ft.). It can be observed that the nail-couple method predicts about a 75% larger yield shear strength value as compared to FEMA 273.

5.1.2.1.3 Plywood Panel Overlays on Straight-Sheathed Diaphragms

For the case of unblocked, unchorded plywood panel overlays on straight-sheathed diaphragms (MAE-2B and MAE-3A), FEMA 273 provides a typical in-plane yield shear strength of 4,384 N/m (300 lb./ft.). Alternatively, the allowable shear strength of comparable wood structural panel diaphragms without the existing sheathing below can be used. APA - the Engineered Wood Association (until 1994 the American Plywood Association) developed a design shear table for plywood diaphragms under wind or seismic loading that is recognized in major model building codes. The design shear table is based on the lesser of the shear strength of plywood (v_{cp}) from the Plywood Design Specification (APA, 1986) and the shear strength of the nails (v_{np}) (from NDS) at the boundary of the diaphragm parallel to the load direction:

$$v_{cp} = F_v \, C_D \, t_s \tag{5.10}$$

$$v_{np} = Z \, C_{di} \, C_D \, n \tag{5.11}$$

where:

F_v = Allowable shear strength through the thickness (t_s) of the plywood, taken as 131 N/cm^2 (190 psi) for S-1 grade stress level and dry conditions
C_D= Loading duration factor, taken as 1.33 for plywood and 1.6 for nails
C_{di}= Diaphragm factor, taken as 1.1 for diaphragms
n = Number of fasteners per unit length, taken as 6.6/m (2/ft.)

Table 5.4 gives the design values Z for the different possible yield modes of the nails based on Eq. 5.7 with a limiting value of 347 N (78 lb.). The shear strength of

plywood (v_{cp}) results in 16,700 N/m (1,140 lb./ft.) and the shear strength of the nails (v_{np}) results in 4,010 N/m (275 lb./ft.).

TABLE 5.4 Nominal Shear of 8d Common Nail in Plywood Overlay Diaphragms

Yield Mode	Design Shear (*Z*) N (lb.)
I_s	552 (124)
III_m	900 (202)
III_s	347 (78)
IV	472 (106)

FEMA 273 recommends a factor of 1.5 to obtain the in-plane lateral yield shear of blocked plywood overlay diaphragm from the allowable shear strength of a comparable blocked plywood diaphragm. This same factor of 1.5 was used to determine the in-plane lateral yield shear of the unblocked plywood overlay diaphragm from the allowable shear of a comparable unblocked plywood diaphragm. The yield shear strength of plywood and the yield shear strength of the nails result in 25,000 N/m (1,710 lb./ft.) and 6,010 N/m (412 lb./ft.), respectively.

In the case of the blocked, unchorded plywood panel overlays on straight sheathed diaphragms (MAE-2C and MAE-3B) FEMA 273 suggests an in-plane yield shear capacity (v_y) approximately equal to half the ultimate shear capacity (v_u) or 1.5 times the allowable shear capacity (v_a) of a comparable plywood structural panel diaphragm without existing sheathing. The latter was used to determine the yield shear capacity (v_y) of the diaphragm specimens. The allowable in-plane shear of plywood remains the same as the unblocked case, 16,700 N/m (1,140 lb./ft.), and the allowable shear strength based on nails triples to 12,020 N/m (824 lb./ft.). This increase is because additional nails were used in the blocked diaphragms to reduce spacing to 0.05 m (2 in.) center-to-center. Also, an allowable shear of 6,640 N/m (454 lb./ft.) obtained from the APA design table for horizontal plywood diaphragms with framing of Southern Pine for

seismic loading with reduction factors was considered. The in-plane yield shear strength (v_y) was determined from these three results using the 1.5 factor provided by FEMA 273 and are listed in Table 5.5. It can be observed that the yield shear given by APA predicts the lowest value.

5.1.2.2 FEMA 356 Procedure

The procedure that FEMA 356 follows is based on design resistance values associated with the "Standard for Load and Resistance Factor Design (LRFD) for Engineered Wood Construction" (AF&PA/ASCE 16-95). All adjustment factors shall be considered, except for the load duration factor. Instead, the time-effect factor should be included, which is applicable in accordance with ASCE 16-95. The time-effect factor, λ, specified for LRFD is 1.0 for load combinations that include earthquake loads. The resistance factor, ϕ, shall be taken as unity. The design lateral resistance is calculated as the product of the adjusted lateral resistance Z', the resistance factor ϕ, and the time effect factor λ. Being both factors equal to 1.0, the design lateral resistance has the same value of the adjusted lateral resistance. The same values of the allowable design lateral values (Z') used for the FEMA 273 procedure are used here, multiplied by a format conversion factor, K_E, equal to 3.32 and divided by the load duration factor (C_D) equal to 1.6 for nails, resulting in a factor of 2.08. The following equation gives the final conversion factor:

$$Z'_{\text{FEMA 356}} = 2.08\, Z'_{\text{FEMA 273}} \tag{5.12}$$

5.1.2.2.1 Tongue & Groove Single Straight Sheathed Diaphragms

FEMA 356 does not provide specifications for T&G diaphragms. The same procedure followed in FEMA 273 was used here. Using the allowable shear determined for FEMA 273, 259 N/m (18 lb./ft.) in Eq. 5.12, a design lateral resistance of 540 N/m (37 lb./ft.) was determined.

Similar procedure was followed to determine the design lateral resistance for the steel strap retrofit of the T&G diaphragm. A design lateral resistance of 1,125 N/m (77 lb./ft.) was found from Eq. 5.12 and an allowable shear of 540 N/m (37 lb./ft.).

5.1.2.2.2 Square Edged Single Straight Sheathed Diaphragms

FEMA 356 provides a default in-plane diaphragm yield shear capacity of 1,750 N/m (120 lb./ft.). The shear capacity of straight-sheathed diaphragms can be calculated using the nail-couple method. The allowable shear force from the FEMA 273 procedure is 1,100 N/m (75 lb./ft.) From Eq. 5.12, a yield shear capacity of 2290 N/m (156 lb./ft.) is obtained.

5.1.2.2.3 Plywood Panel Overlays on Straight-Sheathed Diaphragms

For the case of unblocked, unchorded plywood panel overlays on straight-sheathed diaphragms FEMA 356 provides a typical in-plane yield shear capacity of 4,380 N/m (300 lb./ft.). Tissell and Elliott (1997) provide an alternative method based on the lesser of the yield shear of plywood and the yield shear of nails. From the calculations done for FEMA 273, the allowable shear of plywood was 16,700 N/m (1,140 lb./ft.) and the allowable shear of nails was 4,020 N/m (275 lb./ft.). Because the load duration factor used for plywood was 1.33, a new conversion factor was determined to be 3.32/1.33 = 2.5. Therefore the yield shear of plywood resulted equal to 41,750 N/m (2,850 lb./ft.). Applying Eq. 5.2, the yield shear of nails resulted equal to 8,360 N/m (572 lb./ft.)

The yield shear capacity for blocked plywood panel overlay on straight-sheathed diaphragms can be calculated without the contribution of the straight sheathing. Similarly as the unblocked case, the yield shear based on plywood and on nails is calculated here. The yield shear based on plywood remains the same as the unblocked case, 41,750 N/m (2,850 lb./ft.), and the yield shear based on nails triples to 25,080 N/m (1715 lb./ft.). The “LRFD Manual for Engineered Wood Construction” (AF&PA,

1996), which is to be used in conjunction with AF&PA/ASCE 16-95, provides a table of factored shear resistance for structural-use panel horizontal diaphragms with framing of southern pine for seismic loading. A factored yield shear capacity of 11,383 N/m (780 lb./ft.) was found from the table. Reduction factors of 0.89x0.85 should be applied to consider the use of 2 in. nominal width of framing and 2 in. nail spacing o.c. at the boundary. Additionally, is required to divide by the resistance factor ϕ equal to 0.65 (for connections). The yield shear capacity becomes 13,250 N/m (908 lb./ft.).

5.1.2.3 Steel Truss Retrofits

The steel truss retrofits used in diaphragms MAE-1B and MAE-2A were designed to limit the lateral displacements of the diaphragm. Structural WT rolled shapes were selected for the truss for ease of installation. A WT4x6.5 shape was selected based on the flange width required to attach sufficient lag screws to transfer the loading from the diaphragm to the truss. For the analysis, the loads applied by the loading frame on the diaphragm were considered to be in the same plane as the truss and distributed as shown in Fig. 5.2. The resulting internal forces showed that the highest compression force occurred in the diagonal braces. Using an effective length of 2.44 m (8 ft.), AISC-LRFD gives design compression strength of 125 kN (28 kips) for the diagonal brace. Dividing the strength by the compression reduction factor taken as 0.85 and using the relationship of forces acting in the diagonal brace and the total external load, based on equilibrium of forces in the truss, (shown in Fig. 5.2), a required total force (V) in the truss of 352 kN (79 kips) was computed. The maximum capacity of the actuator was 500 kN (110 kips), so it seemed possible to load the diaphragm to failure with the selected truss configuration and member sizes. Dividing the total external load (V) by two and by the diaphragm width, a yield shear strength (v_y) of 48,220 N/m (3,300 lb./ft.) was obtained for the retrofitted diaphragm using an underside truss system. This value neglects the contribution of the wood diaphragm to the yield shear strength.

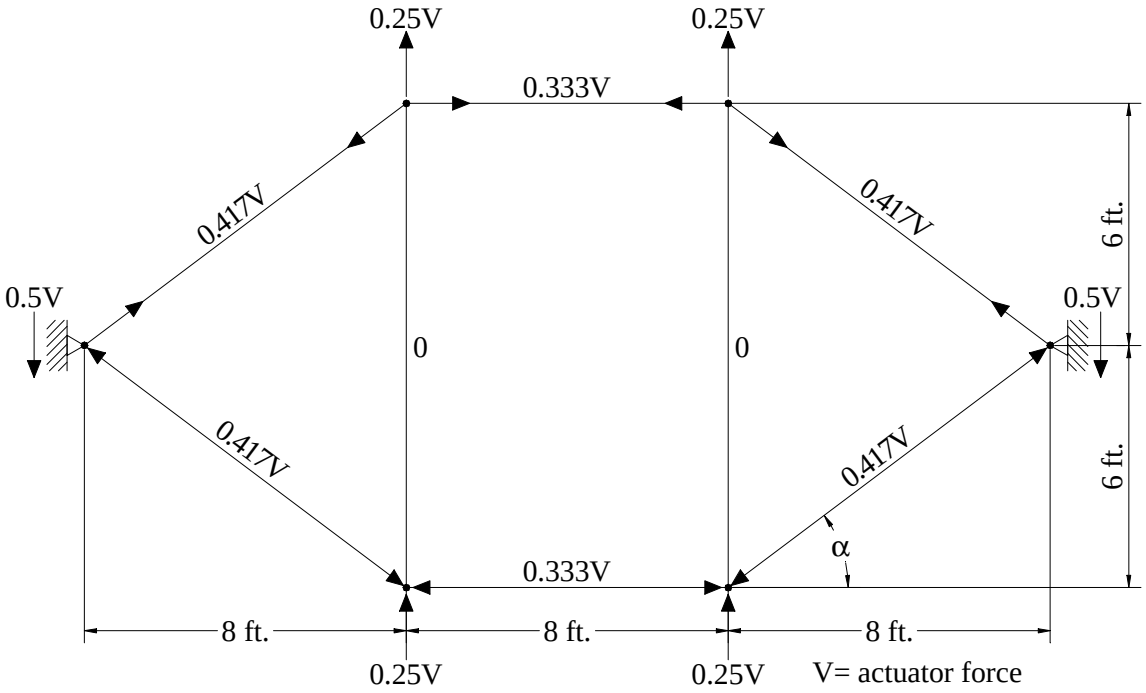

FIG. 5.2 Loads and Internal Forces of Steel Truss

Table 5.5 summarizes computed values and recommendations for the predicted in-plane lateral yield shear strength of the diaphragms. When there was more than one shear strength, the lowest value was chosen as the predicted strength.

TABLE 5.5 Predicted In-plane Lateral Yield Shear Strength of Diaphragms

ID	Diaphragm Type	Yield Shear v_y (N/m)		Failure Mechanism
		FEMA 273	FEMA 356	
MAE-1	T&G Sheathed	725	540	Nail Yielding
MAE-1A	Conn. & Strap Retrofit	1,500	1,125	Nail & Lag Screw Yielding
MAE-1B	Steel Truss Retrofit	48,200	-	Diagonal Brace Buckling.
MAE-2 & MAE-3	Straight Sheathed	1,750 3,070	1,750 2,290	Diaphragm Yield Shear Nail Couple Yielding
MAE-2A	Steel Truss Retrofit	48,200	-	Diagonal Brace Buckling
MAE-2B & MAE-3A	Unblocked Panel Overlay	4,380 6,010 25,000	4,380 8,360 41,750	Diaphragm Yield Shear Nail Yielding Plywood Panel Shear
MAE-2C & MAE-3B	Blocked Panel Overlay	9,950 18,030 25,000	13,250 25,080 41,750	APA Shear Nail Yielding Plywood Panel Shear

Note: 1 N/m = 0.0685 lb./ft.

5.2 COMPARISON OF EXPERIMENTAL AND PREDICTED DIAPHRAGM STRENGTH AND STIFFNESS

In this section, the in-plane lateral effective stiffness (K) and yield shear strength (v_y) from the measured experimental responses given in Section 4 are compared with the predictive methods defined in the previous sections. The predicted in-plane lateral yield shear strength (v_y) was used to obtain a total yield force (V_y) developed in the diaphragm, defined in Eq. 5.13, which was then directly compared with the experimental results obtained as explained in Section 4.2.

$$V_y = 2\, v_y\, b \tag{5.13}$$

Table 5.6 shows the predicted and experimental values for effective stiffness (*K*) and total yield force for all diaphragm specimens. As expected, the predicted in-plane effective stiffness of the T&G sheathed diaphragms (MAE-1 and MAE-1A) using the effective stiffness for straight sheathing is considerably overestimated and does not provide a good approximation of the stiffness measured during experimental testing. The yield shear forces of the T&G sheathed diaphragms were also overestimated by 52% and 13% in average, from FEMA 273 and FEMA 356, respectively. In the case of the steel truss retrofit of the T&G diaphragm (MAE-1B), the predicted yield force and effective stiffness of the diaphragm were three and 15 times of the experimental values, respectively. The discrepancy is explained by the assumption made for the predicted case in that the load was transferred directly to the truss. The loading apparatus had a significant eccentricity with respect to the truss plane (0.41 m, 18 in.) that caused an overturning moment. As a result, the joists rotated about their longitudinal axes causing the sheathing to displace laterally with respect to the truss. Consequently, the lateral stiffness of the diaphragm diminished because of the additional lateral displacement caused by the rotating joists.

For the straight-sheathed diaphragm MAE-2 and retrofitted diaphragm MAE-2B, the predicted total yield force was the same from both procedures, 44% and 68% of the experimental values, respectively. For retrofitted diaphragm MAE-2C the yield force was overpredicted by 108% and 143% of the experimental values, respectively. The predicted effective stiffness of diaphragms MAE-2, MAE-2B and MAE-2C using FEMA 273 was 2.4, 1.3 and 1.4 times the experimental values, respectively. Using FEMA 356 the predicted values were 0.4, 0.2 and 0.2 times the experimental responses. In the case

of the steel truss retrofit diaphragm MAE-2A, the predicted total yield force and effective stiffness were 3.1 and 4.0 times the experimental values, respectively. An overturning moment due to the eccentricity of the loading apparatus caused one side of the diaphragm to lift up during the larger applied load levels, controlling the limiting actuator load during testing. The effective stiffness was less than expected because of the additional lateral displacement of the diaphragm due to the eccentricity of loading.

The comparison of predicted effective stiffness (*K*) using FEMA 273 of the straight sheathed diaphragm with corner opening (MAE-3) and its retrofits (MAE-3A and MAE-3B) showed that, on average, the predictive methods underestimated the experimental effective stiffness by 17%. An average width of 2.9 m (9.5 ft.) was used in Eq. 5.13 to calculate the total yield force. The predicted yield forces underestimated the experimental values and were 44% (MAE-3), 40% (MAE-3A) and 70% (MAE-3B) of the experimental results. The predictions of stiffness based on FEMA 356 resulted in just 30% in average, of the experimental values. Yield forces remained the same as in FEMA 273, except for the shear force in diaphragm MAE 3B, which was 93% of the experimental value.

TABLE 5.6 Experimental and Predicted Effective Stiffness and Shear Strength of Diaphragms

	Effective Stiffness, kN/cm			Yield Shear Strength, kN		
Diaphragm	**FEMA 273**	**FEMA 356**	**Experi-mental**	**FEMA 273**	**FEMA 356**	**Experi-mental**
MAE-1	43.8	7.0	1.4	5.3	4.0	3.6
MAE-1A	43.8	7.0	5.1	11.1	8.2	7.1
MAE-1B	933[1]	-	59.3	352	-	116
MAE-2	43.8	7.0	18.4	12.9	12.9	29.4
MAE-2A	933[1]	-	233.0	352[2]	-	115
MAE-2B	110	17.5	83.6	32.0	32.0	47.7
MAE-2C	153	24.5	113.0	72.8	96.9	67.7
MAE-3	17.2	5.60	18.6	10.2	10.2	23.2
MAE-3A	43.0	13.9	51.2	25.4	25.4	65.0
MAE-3B	60.2	19.4	71.2	57.6	76.7	82.4

Note: 1 kN/cm = 0.5703 kips/in.; 1 kN = 0.2245 kips
[1] From Eq. 5.3
[2] From Section 5.1.2.3

5.3 COMPARISON OF PREDICTED AND EXPERIMENTAL *m* FACTORS

The FEMA guidelines (FEMA 273 and FEMA 356) provide equivalent linear-elastic design criteria for buildings that respond nonlinearly. This procedure uses a ductility factor called the *m* factor. The FEMA guidelines provide tables for primary and secondary components of various materials to determine the *m* factors at different structural performance levels. The length-to-width ratio of the diaphragm is required to select the value of the *m* factor. The listed values in the guidelines indicate that the higher the length-to-width ratio, the lower the *m* factor value. Table 5.7 lists the predicted *m* factors, which are the same in both guidelines, for primary components considering collapse prevention performance level (CP). These values are compared

TABLE 5.7 Experimental *m* Factors and Comparison with Predicted Values

Diaphragm	K[1] kN/cm	D_u[1] cm	F_u[1] kN	m_i[2]	Experimental m[3]	Predicted m[4]
MAE-1	1.8	6.6	9.4	1.3	1.2	2.0
	1.2	6.9	7.1	1.1		
MAE-1A	5.4	7.9	16.0	2.6	2.5	2.5
	4.6	7.6	14.7	2.4		
MAE-1B	65.4	3.3	153.7	1.4	1.3	-
	55.6	3.8	168.8	1.2		
MAE-2	16.1	7.6	52.6	2.3	2.6	2.0
	20.7	7.9	56.1	2.9		
MAE-2A	257.9	1.0	157.2	1.8	1.9	-
	209.5	1.5	147.4	2.0		
MAE-2B	84.7	1.8	67.3	2.1	2.0	2.5
	82.4	1.8	67.3	2.0		
MAE-2C	132.9	2.3	152.8	1.9	1.5	2.5
	92.9	1.5	119.8	1.2		
MAE-3	17.2	7.9	46.8	2.9	3.1	2.0
	19.8	7.9	46.3	3.4		
MAE-3A	54.0	4.8	83.7	3.1	2.8	2.5
	48.4	4.8	94.0	2.5		
MAE-3B	59.6	3.3	137.6	1.4	1.5	2.5
	82.6	2.0	111.3	1.6		

Note: 1 kN/cm = 0.5703 kips/in.; 1 cm = 0.3937 in. 1 kN = 0.2245 kips

[1] Experimental values for two loading directions per specimen

[2] Each m_i calculated from Eq. 5.14

[3] Average of two directions

[4] From the FEMA Guidelines (same values in FEMA 273 and FEMA 274)

with the experimental values calculated from the measured data using the following expression derived from FEMA 274 (ATC, 1997b):

$$m = \frac{K\Delta_u}{F_u} \tag{5.14}$$

where:

K = Effective stiffness, kN/cm (kips/in.)
Δ_u = Ultimate displacement of the diaphragm, cm (in.)
F_u = Ultimate force applied to the diaphragm, kN (kips)

Table 5.7 lists the response values as an average for both positive and negative loading directions used to determine the *m* factors of the diaphragm specimens. In general, the *m* factor has a similar value for the positive and negative loading directions for a given specimen. A comparison of the average experimental and predicted *m* factors shows some differences. Four specimen *m* factors lie on the non-conservative side (MAE-1, MAE-2B, MAE-2C and MAE-3B), where the predicted *m* factor is larger than the corresponding *m* factor based on the experimental measurements. For these cases, the experimental *m* factors were overpredicted by 25% to 67%.

An *m* factor close to one indicates linear elastic behavior, which is approximately the case for the experimental value of 1.2 for the tongue & groove diaphragm MAE-1. The predicted value of 2.0 overestimated the experimental *m* factor by 67%. The addition of the steel strapping added ductility to diaphragm MAE-1A, doubling the

resulting *m* factor to 2.5. The steel truss in diaphragm MAE-1B behaved almost linearly with an experimental *m* factor of 1.3.

The predicted *m* factor of the square edged single straight-sheathed diaphragm MAE-2 underestimated the experimental value by 23%. The addition of the steel truss (MAE-2A) resulted in an experimental *m* factor of 1.9. In retrofitted diaphragm MAE-2B, the predicted *m* factor was overestimated by 25%. The reason for this difference may be caused by the early failure of diaphragm MAE-2B, provoked by inadequate nailing of the plywood panels. A larger difference resulted for diaphragm MAE-2C, where the experimental *m* factor was overpredicted by 67%, even though the additional nailing was adequate. The difference is attributed to the uplifting of the diaphragm before the ultimate displacement was developed.

The square edged single straight-sheathed diaphragm with corner opening (MAE-3) had a relatively high experimental *m* factor and was underpredicted by 35%. The *m* factor for the unblocked plywood overlay retrofit (MAE-3A) was underpredicted by 11%. In the case of the blocked plywood overlay diaphragm (MAE-3B) the experimental *m* factor was overpredicted by 67%.

5.4 DIAPHRAGM FORCE VERSUS DEFORMATION CURVES

The FEMA guidelines provide simplified backbone curves to determine an idealized in-plane non-linear force versus deformation relationship for wood diaphragms. Fig. 5.3 shows samples of force versus deformation curves for both guidelines. Both curves are similar, except that FEMA 356 mandates a 50% increase of yield strength before the first loss occurs. The curves are defined by the predicted total yield force in the diaphragm (V_y), yield deformation (Δ_y) and non-dimensional parameters *c*, *d* and *e* given in the FEMA guidelines for each type of diaphragm. The yield deformation was calculated by dividing the yield force by the predicted effective stiffness (*K*) listed in Table 5.6. Distance *d* is considered to be the maximum deformation ratio of the diaphragm at the point of first loss of strength. Distance *e* is the maximum deformation ratio at a reduced shear strength ratio *c*. The points denoted by IO (immediate occupancy), LS (life safety) and CP (collapse prevention) shown in Fig. 5.3a, are the deformations limits that satisfy these performance levels, defined in the FEMA guidelines, for primary components. In FEMA 356, the deformation limits depend on the type of diaphragm.

The values of the non-dimensional parameters and the yield deformation for the diaphragms are listed in Table 5.8. The T&G diaphragms MAE-1 and MAE-1A were not defined in the FEMA guidelines and the parameters *c*, *d* and *e* for straight-sheathed diaphragms were used instead for comparison. Diaphragm MAE-1A was considered chorded. The effective stiffness and shear strength of diaphragms MAE-1B and MAE-2A were based on the behavior of the steel truss alone. Parameters for the square edged single straight-sheathed diaphragms MAE-2 and MAE-3 were taken directly from the FEMA guidelines. For the panel overlay diaphragms (MAE-2B, MAE-2C, MAE-3A and MAE-3B), the FEMA guidelines provide the same values for unchorded diaphragms regardless of whether they are blocked or unblocked.

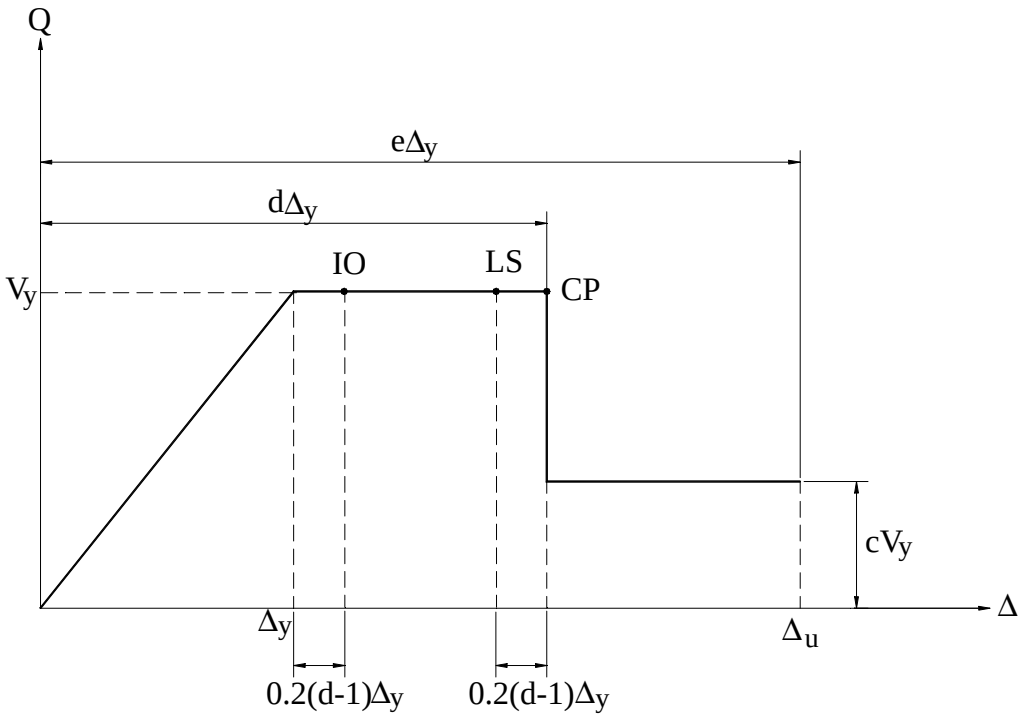

(a) FEMA 273

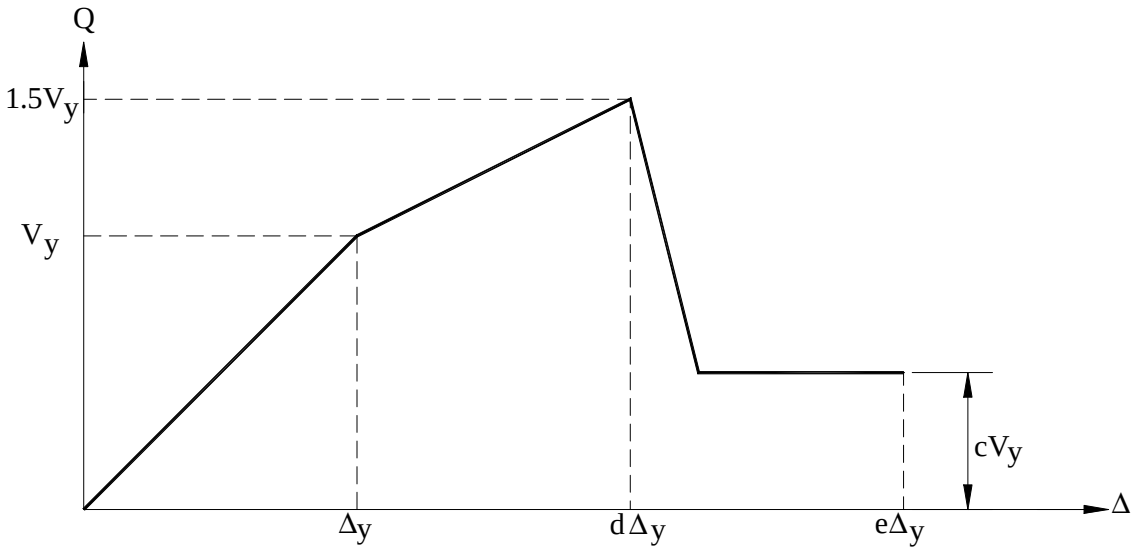

(b) FEMA 356

FIG. 5.3 Simplified Backbone Curve for Wood Diaphragms (adapted from FEMA 273 and FEMA 356)

TABLE 5.8 Parameters of Predicted Backbone Curves of Diaphragm Specimens

Diaphragm	Diaphragm Type	D_y mm (in.)		c^3	d^3	e^3
		FEMA 273[1]	FEMA 356[2]			
MAE-1	T&G sheathed	1.3 (0.05)	5.6 (0.22)	0.3	2.0	3.0
MAE-1A	Conn. & Strap Retrofit	2.5 (0.10)	11.7 (0.46)	0.2	2.5	3.5
MAE-1B	Steel Truss Retrofit	3.8 (0.15)	-	-	-	-
MAE-2	Straight Sheathed	3.0 (0.12)	18.3 (0.72)	0.3	2.0	3.0
MAE-2A	Steel Truss Retrofit	3.8 (0.15)	-	-	-	-
MAE-2B	Unblocked. Panel Overlay	3.0 (0.12)	18.3 (0.72)	0.4	2.5	3.5
MAE-2C	Blocked. Panel Overlay	4.8 (0.19)	39.6 (1.56)	0.4	2.5	3.5
MAE-3	Straight Sheathed w/ Opening	5.8 (0.23)	18.3 (0.72)	0.3	2.0	3.0
MAE-3A	Unblocked. Panel Overlay	5.8 (0.23)	18.3 (0.72)	0.4	2.5	3.5
MAE-3B	Blocked. Panel Overlay	9.6 (0.38)	39.6 (1.56)	0.4	2.5	3.5

[1] Using Eq. 5.1
[2] Using Eq. 5.3
[3] From the FEMA Guidelines (same for both)

5.5 COMPARISON OF EXPERIMENTAL AND PREDICTED FORCE VERSUS DEFORMATION CURVES

From the predicted yield shear listed in Table 5.6 and the values listed in Table 5.8, plots of the predicted backbone curves were developed in Figs. 5.4 through 5.6. The predicted backbone curves were superimposed with the bilinear force versus displacement curves determined from the experimental backbone curves, described in Section 4.2 (see Figs. 5.4 through 5.6). The curves may be compared using the effective stiffness (K), yield shear strength force (V_y), yield displacement (Δ_y) and ultimate displacement (Δ_u) as parameters.

Fig. 5.4 shows the predicted backbone curves and a portion of the experimental bilinear curves for diaphragms MAE-1 (T&G) and MAE-1A (steel strapping & bolted connection retrofit) for both procedures, FEMA 273 and FEMA 356. Also shown in the figures is part of the bilinear curve for diaphragm MAE-1B, which was retrofitted with the steel truss. The FEMA Guidelines did not provide a backbone curve for a T&G diaphragm. The predicted yield displacements (Δ_y), calculated from Eq. 5.1 for FEMA 273, were 20 and six times smaller than the experimental yield displacements for MAE-1 and MAE-1A, respectively (see Table 5.9). The ultimate displacements (Δ_u) also differ considerably, with predicted values of only 6% (MAE-1) and 12% (MAE-1A) of the experimental values. It can be observed that the predicted backbone curves provide a poor estimate of the experimental bilinear curves for diaphragms MAE-1 and MAE-1A. FEMA 356 provides Eq. 5.3 to predict the yield displacement. The values found were 22% and 81% of the experimental value for MAE-1 and MAE-1A, respectively. The ultimate displacement values were 25% and 53%, respectively. The FEMA 356 predicted backbone curves showed a better approximation to the experimental curves compared to the curves from FEMA 273, but still is not considered a good approximation.

Fig. 5.5 shows the predicted backbone and experimental bilinear curves for the square edged single straight sheathed diaphragm (MAE-2), unblocked plywood overlay retrofit (MAE-2B) and blocked plywood overlay retrofit (MAE-2C), for both procedures, FEMA 273 and FEMA 356. Also shown is the experimental bilinear curve for diaphragm MAE-2A (steel truss retrofit). The measured yield displacements obtained from FEMA 273, were underestimated by 81% (MAE-2), 48% (MAE-2B) and 17% (MAE-2C), see Table 5.9. The ultimate displacements were also underestimated considerably in one case. The predicted values were 11% (MAE-2), 60% (MAE-2B) and 88% (MAE-2C) of the experimental values. In general, the behavior of plywood overlay retrofitted diaphragms MAE-2B and MAE-2C were better predicted by the FEMA 273 parameters than the unretrofitted diaphragm MAE-2. FEMA 356 predicts

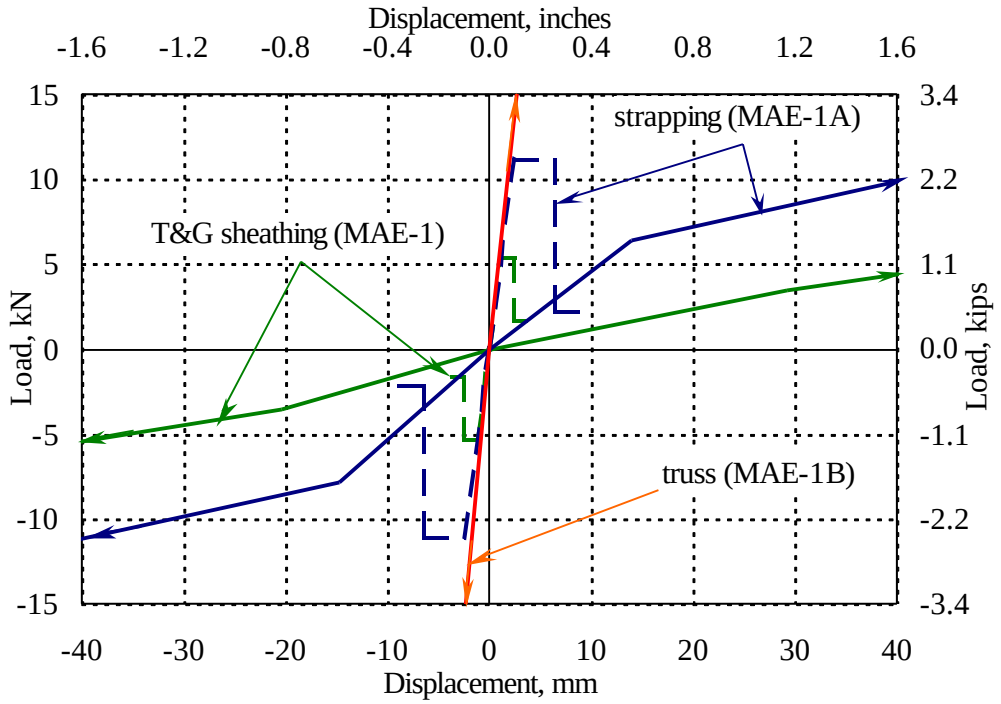

a) FEMA 273

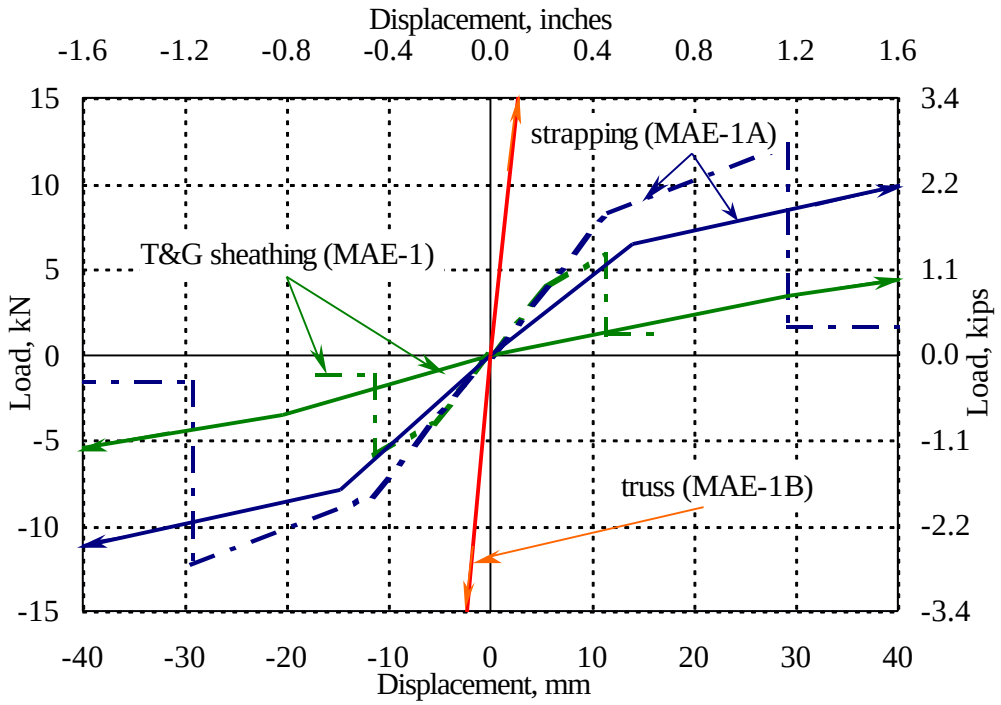

b) FEMA 356

FIG. 5.4 Comparison of Backbone Curves with Bilinear Curves for Diaphragm 1 (Bilinear Curves ——— FEMA 273 – – – – FEMA 356– · – · –)

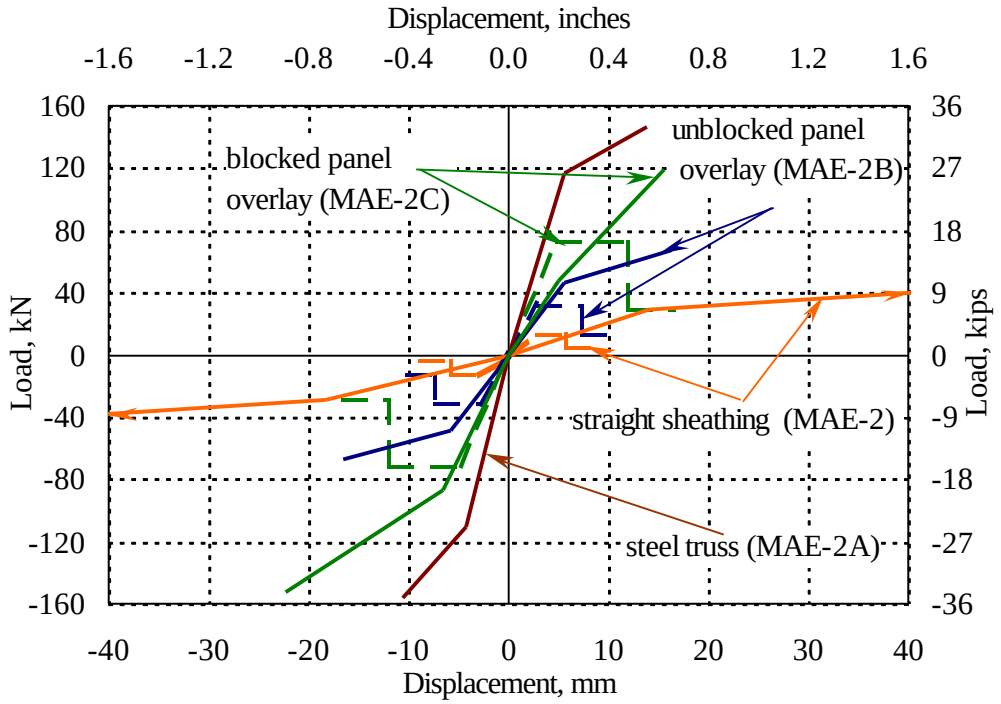

a) FEMA 273

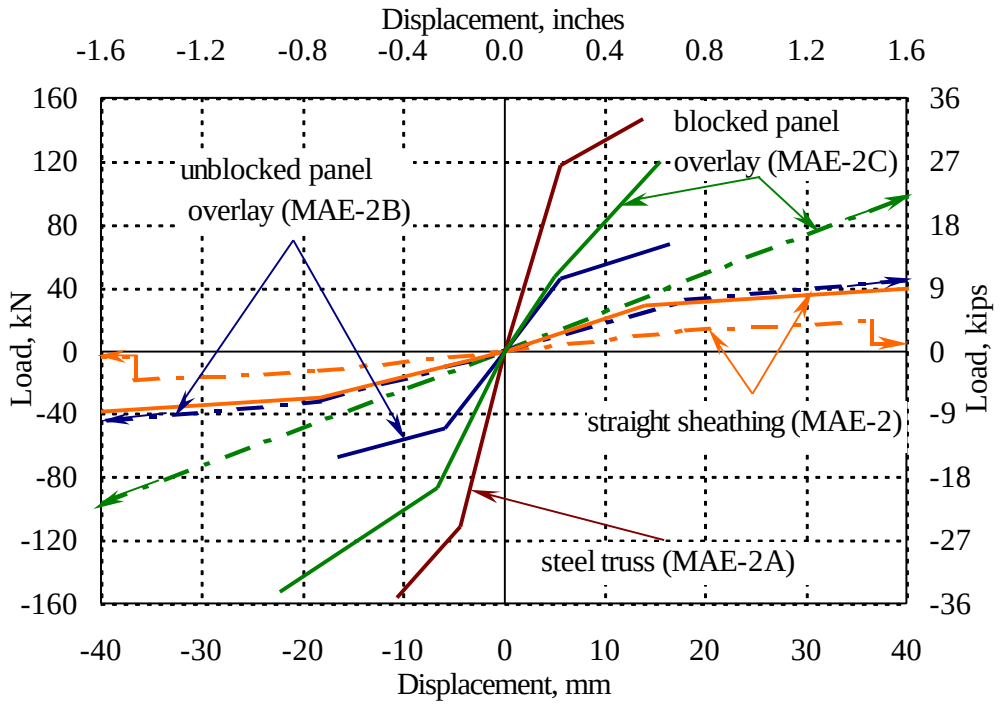

b) FEMA 356

FIG. 5.5 Comparison of Backbone Curves with Bilinear Curves for Diaphragm 2 (Bilinear Curves ——— FEMA 273 – – – – FEMA 356 – · – · –)

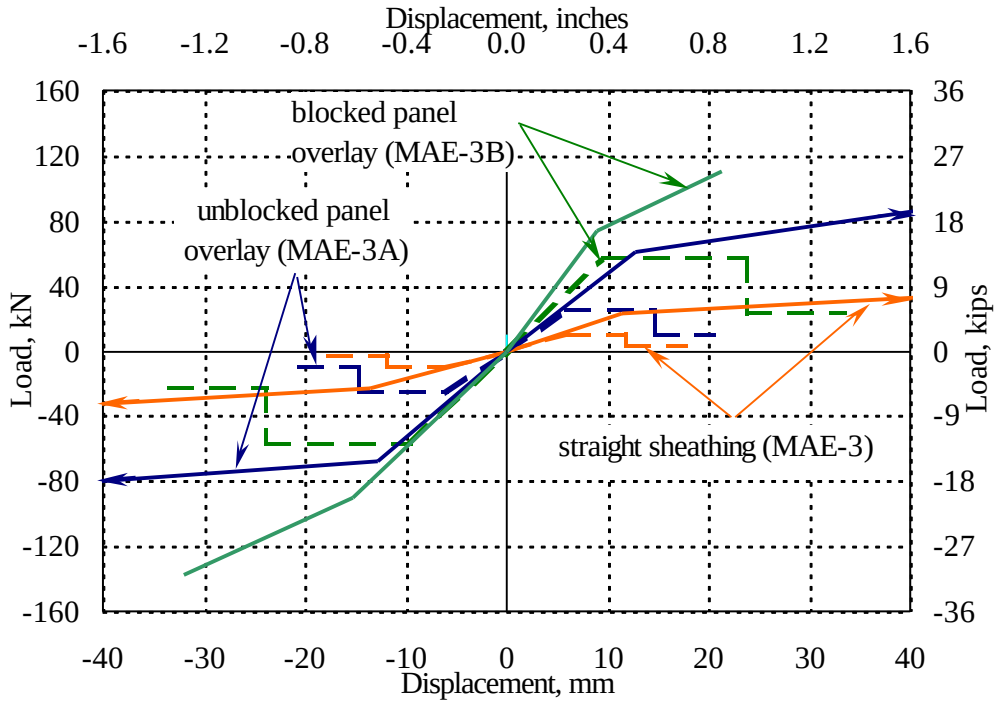

a) FEMA 273

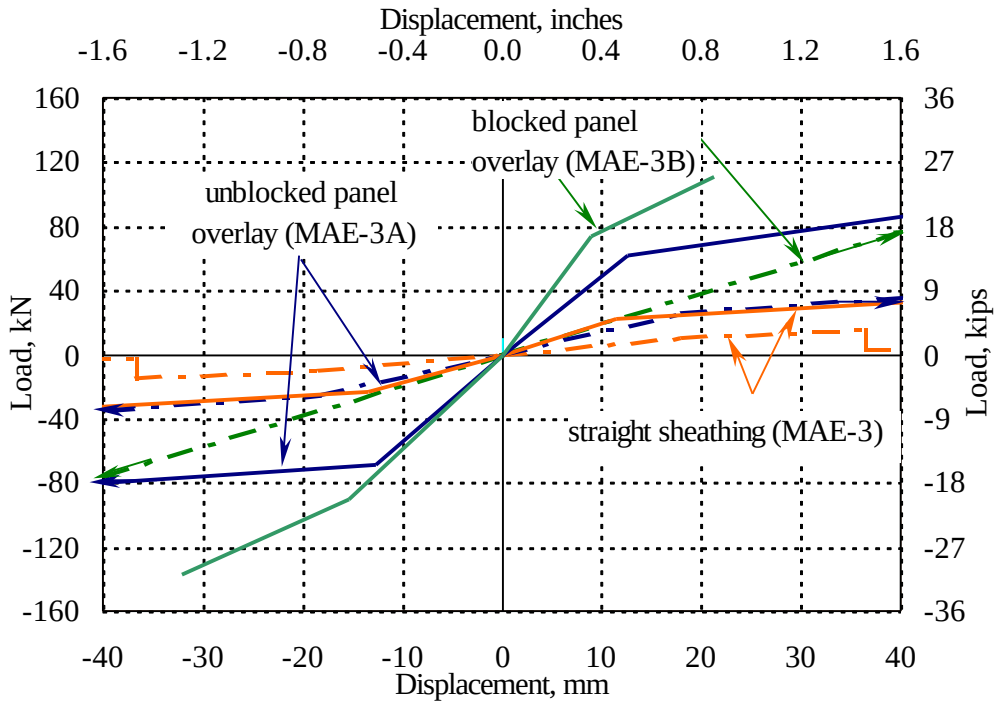

b) FEMA 356

FIG. 5.6 Comparison of Backbone Curves with Bilinear Curves for Diaphragm 3 (Bilinear Curves ——— FEMA 273 – – – – FEMA 356 – · – · –)

yield displacements that are 112% (MAE 2), 316% (MAE 2B) and 683% (MAE –2C) of the experimental values. The predicted values of ultimate displacement were 71% (MAE-2), 360% (MAE-2B) and 726% (MAE-2C) of the experimental values. In this case the prediction of behavior of the unretrofitted diaphragm MAE-2 was better compared to the predictions for the retrofitted diaphragms.

Fig. 5.6 shows the curves for the square edged single straight-sheathed diaphragm with corner opening (MAE-3), unblocked plywood overlay retrofit diaphragm (MAE-3A) and blocked plywood overlay diaphragm (MAE-3B), for both procedures, FEMA 273 and FEMA 356. The yield displacements obtained by FEMA 273 were underestimated by 53% (MAE-3), 54% (MAE-3A) and 21% (MAE-3B), as shown in Table 5.9. The predicted ultimate displacements were 22% (MAE-3), 42% (MAE-3A) and 127% (MAE-3B) of the measured values. FEMA 273 better predicted the results for the retrofitted diaphragms compared to the values of the unretrofitted case. FEMA 356 overpredicted the yield displacement values by 48% (MAE-3), 44% (MAE-3A) and 225% (MAE-3B). The predicted ultimate displacement values were 70% (MAE-3), 133% (MAE-3A) and 519% (MAE-3B) of the experimental values. FEMA 356 gave better values for the unretrofitted diaphragm compared to the values of the retrofitted diaphragms.

The yield (Δ_y) and maximum lateral displacements (Δ_u) predicted by FEMA 273 are, in general, smaller than the experimental maximum lateral displacements. This was not the case for the blocked plywood overlay diaphragm MAE-3B, because diaphragm overturning made it necessary to terminate the tests at a lower lateral displacement than ultimate. The values predicted by FEMA 356 are always much higher than the values of FEMA 273. For FEMA 356 the yield displacements are higher than the experimental values, except for diaphragm MAE-1 and MAE-1A. The ultimate displacements were

lower than the experimental values for the unretrofitted diaphragms and higher for the retrofitted diaphragms.

An additional difference between the predicted and experimental curves is the strength at the final stage of the diaphragm lateral displacement. In the predicted curves, the final strength is only a fraction of the yield strength (average of 35%). However the experimental response shows that the strength continued increasing for higher lateral displacements. Is possible that a loss of strength would eventually occur but after applying a much higher deformation to the diaphragm specimens. The guidelines do not give an explanation for the adoption of such a backbone curve shape for wood diaphragms. FEMA 356 improves the predicted curves of FEMA 273 by recognizing the gain of strength after yielding, as found in the specimen tests.

The experimental bilinear curves represent only the behavior determined from the diaphragm tests, without considering any limitation on the lateral displacements from other attached components. Therefore the ultimate measured displacements may exceed the allowable deformation of other structural building components, such as the out of plane URM walls that are laterally supported by the diaphragm.

TABLE 5.9 Predicted and Experimental Displacements of Diaphragms

ID	D_y mm			D_u mm		
	FEMA 273[1]	**FEMA 356[1]**	**Exper.[2]**	**FEMA 273[3]**	**FEMA 356[3]**	**Exper.[4]**
MAE-1	1.3	5.6	24.9	3.8	16.8	67.3
MAE-1A	2.5	11.7	14.5	8.9	41.0	77.5
MAE-1B	3.8	-	19.6	-	-	35.6
MAE-2	3.0	18.3	16.3	9.1	54.9	77.5
MAE-2A	3.8	-	5.1	-		12.7
MAE-2B	3.0	18.3	5.8	10.7	64.1	17.8
MAE-2C	4.8	39.6	5.8	16.9	138.6	19.1
MAE-3	5.8	18.3	12.4	17.5	54.9	78.7
MAE-3A	5.8	18.3	12.7	20.5	64.1	48.3
MAE-3B	9.6	39.6	12.2	33.8	138.6	26.7

1 mm = 0.03937 in.
[1] From Table 5.8
[2] From Tables 4.3, 4.5, 4.7
[3] From Table 5.8, $\Delta_u = e\Delta_y$
[4] Average value, from Table 5.7

6. ANALYTICAL MODELING OF WOOD DIAPHRAGMS

6.1 INTRODUCTION

The diaphragm specimens tested in the experimental phase of the research program were modeled using a computer program based on the finite element method. The objective of the analytical models is to determine appropriate modeling parameters to post-calculate the measured diaphragm response.

Detailed finite element (FE) models of the specimens in the experimental program were developed using ABAQUS (Hibbitt, Karlsson & Sorensen. 2000). ABAQUS is a general-purpose FE program, capable of performing inelastic pushover analyses, inelastic quasi-static cyclic stress analyses, and inelastic dynamic time history analyses. Each component of the diaphragm, including the sheathing, framing, bridging, blocking and nailed connections, was modeled using the different element types available in the program and is discussed below.

6.2 MODELING ASSUMPTIONS AND MATERIAL PROPERTIES

The basic assumptions for modeling the wood diaphragms in this study are as follows:

1. Fasteners are the only source of material nonlinearity in the system. Sheathing, framing, and bridging materials are linear elastic. This assumption is primarily consistent with the results from the experimental program and those in the literature.
2. Mechanical contact interaction between contiguous sheathing boards or panels is neglected.
3. Friction forces between diaphragm components are not considered.

Reference axes are defined as x-axis along the diaphragm length (span), y-axis along the diaphragm width (depth), and z-axis in the vertical direction (see Fig. 6.1).

The material properties of the wood diaphragm specimens were determined from AF&PA (1997) and APA (1986) and are listed in Table 6.1. Southern pine lumber was used for the solid wood elements.

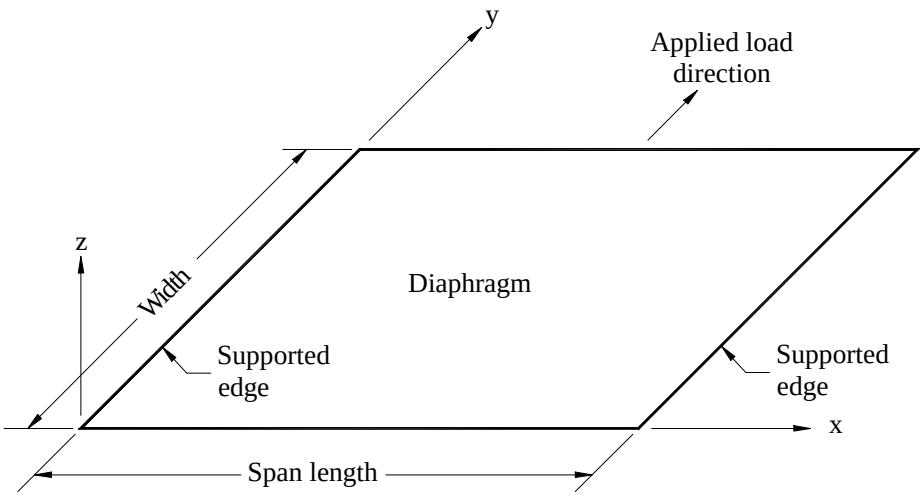

FIG. 6.1 Orientation of Cartesian Coordinates in the FE Diaphragm Model

TABLE 6.1 Material Properties

Property	Solid Wood	Plywood
Young Modulus, MPa (ksi)	12400 (1800)	1490 (216)
Poisson's Ratio	0.20	0.20
Specific Gravity	0.55	-

6.3 ELEMENT TYPES

The wood diaphragm specimens are idealized as an assemblage of elastic beams and plane stress elements connected by nonlinear spring elements. The main characteristics of the detailed FE models are given as:

1. Framing members (beam joists) were modeled using 2-node linear Timoshenko beam elements with one point of integration (element B21). Three degrees of freedom were assigned to each of these nodes: two for translation (x,y) and one for rotation (z).
2. Sheathing boards and panels were modeled using 8-node rectangular plane-stress elements (element CPS8R). In this manner, a second order (quadratic) interpolation was used for higher geometric accuracy. The element also uses a reduced integration scheme (four integration points) that generally provides higher accuracy for second order elements and reduces CPU time. Two translational degrees of freedom were assigned to each node (x,y).
3. Each nail was idealized by two perpendicular nonlinear springs in the x and y directions (element JOINTC for monotonic loading and USER element for cyclic loading). The springs connect a plane-stress element, representing a sheathing board or panel, to a beam element (joist) to form a joint. The lateral load-nail slip relationship was investigated in detail by various researchers and is defined in the next section.
4. Blocking boards used in the rehabilitated diaphragms were modeled to account for differences in axial stiffness in compression and tension. Nonlinear spring elements were used to model the blocking boards (element JOINTC). An axial force-displacement model is defined for this element in Section 6.4.3.

6.4 FORCE-DISPLACEMENT MODELS

6.4.1 General

From previous tests of wood shear walls and diaphragms reported in the literature, Foliente (1995) observed that the hysteresis trace of a wood subsystem or subassembly is governed by the hysteretic characteristics of its primary connection. Thus, the characterization of the hysteretic behavior of wood connections is only needed to characterize the behavior of wood structures. This section describes force–displacement models of various types of nailed connections and blocking members used in the diaphragms. Because tests on nailed joints were not performed in this study, existing models found in the literature were adopted.

6.4.2 Backbone Curves for Shear Force - Slip Behavior of Nailed Connections

Fundamental for a proper characterization of the diaphragm behavior is the selection of appropriate models for shear force–slip behavior of nailed joints. Fig. 6.2 shows a typical single nailed connection of a wood diaphragm. The nailed connection under study here has the nail driven into the side grain (perpendicular to the grain) of the main member (joist) and the load V_n is applied perpendicular to the length of the nail. Slip (e_n) between the main and side member occurs as shown in Fig. 6.2. Past research has led to the development of several models to characterize the behavior of nailed connections under lateral loading. Models were selected for this study to represent V_n-e_n behavior of nailed connections for the case when a tongue & groove (T&G) or square edged board is the side member (sheathing). A second model was selected for the case when a plywood panel is the side member. For all models, the monotonic load versus interlayer slip (V_n-e_n) relationship is curvilinear from the beginning of loading.

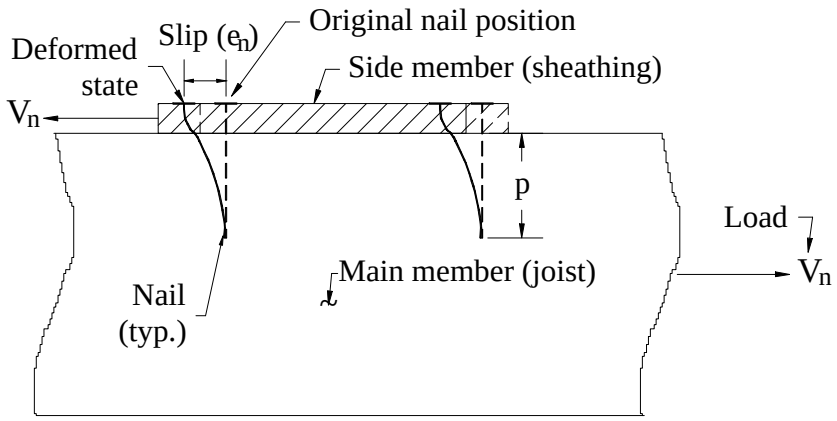

FIG. 6.2 Slip in a Nailed Connection

One important parameter to estimate in the nailed connection is the maximum nail slip that can sustain lateral loads. This parameter is necessary to define failure of the nailed connection, and therefore the initiation of diaphragm damage. The only information related to this subject is given in NDS (AF&PA, 1997) and ASCE 16 (AF&PA/ASCE, 1995). The documents define the penetration depth (p) of the nail as the length of the nail into the member holding the point in a single or double shear connection. Fig. 6.2 shows p for a single shear connection. According to the specifications, the minimum penetration of the shank shall be 6D, where D is the nail diameter. Therefore, the maximum slip of the nail before it can no longer take lateral loads can be calculated as:

$$e = p - 6D \tag{6.1}$$

If the actual penetration depth of the nail is less than 6D, it is assumed that the nailed connection cannot take lateral loads. For an 8d common nail, D is 3.3 mm (0.131 in.) so the minimum penetration 6D is 20 mm (0.786 in.). Fig. 6.3 shows the penetration depths for the two types of nailed connections used in the diaphragm specimens.

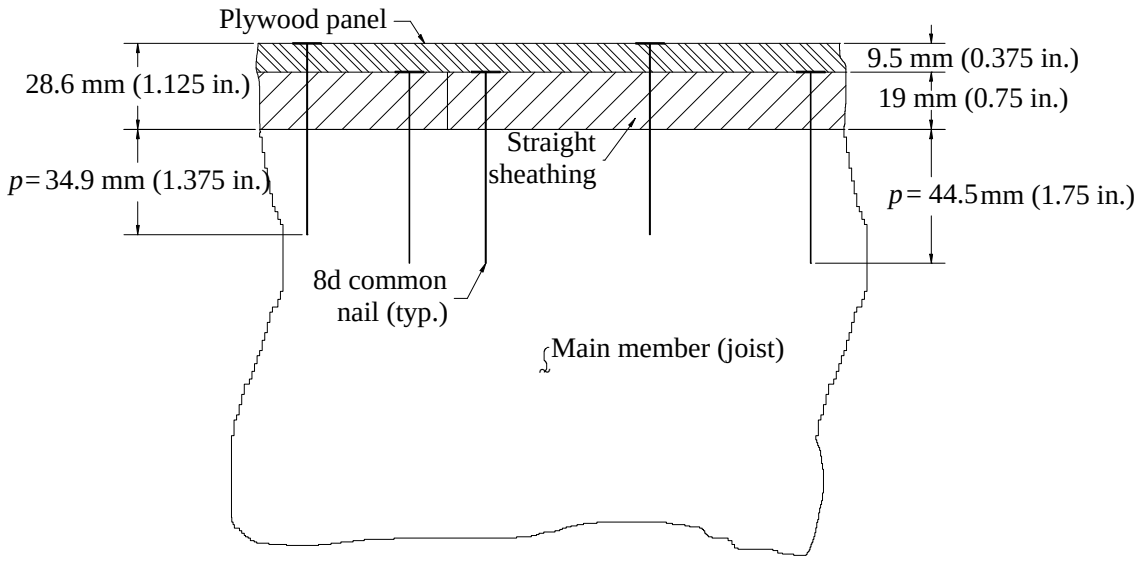

FIG. 6.3 Penetration Depth for Nailed Connections

For a nailed connection with a straight sheathing board as side member of the unretrofitted diaphragm specimens, the penetration depth is p = 44.5 mm (1.75 in.). From Eq. 6.1, the maximum slip is 24.5 mm (0.964 in.). For a nailed connection with plywood panel as side member of the retrofitted diaphragm specimens, the penetration depth is p = 34.9 mm (1.375 in.). Eq. 6.1 gives a maximum slip of 14.9 mm (0.589 in.). The lesser of the two maximum slip values has been adopted as the limiting value and rounded down to a slip of 12.7 mm (0.5 in.).

6.4.2.1 T&G or Square Edged Sheathing Board as Side Member

The basic model used for the nailed connection of T&G or square edge sheathing to a joist is based on investigations made by McLain (1975). McLain developed an empirical equation to predict the lateral force-displacement behavior of nailed joints as shown below:

$$V_n = A \log_{10}(1 + B\, e_n) \tag{6.2}$$

where:

V_n = Lateral load, kN
A, B = Empirically-derived constants, kN and mm^{-1}, respectively
e_n = Interlayer slip, mm (relative displacement of joint members)

The McLain model was developed based on experimental tests for a single-shear joint consisting of a solid-wood main member and a 19 mm (0.75 in.) thick side member connected with one 8d common wire nail. Friction between the main and side members was eliminated by placing a 0.38 mm (0.015 in.) thick metal shim between the two elements during joint construction. The shim was removed prior to testing. Forty static load-slip curves were selected from the tests to fit a curve, which is described by Eq. 6.2. This relationship is limited to a maximum of 2.54 mm (0.1 in.) of slip displacement. This value was chosen as a practical limit for curve fitting since an inflection point occurs in the experimental curve at some distance after this slip, precluding the use of a simple function. The function curve is a conservative estimation of the experimental curve since the function curve lies below the experimental curve.

Fundamental to the success of Eq. 6.2 was a method to determine the empirical parameters A and B. McLain found that parameter A could best be predicted as a function of the specific gravities (SG) of the main and side members (SG model). The equation recommended for joints with only solid wood members is:

$$A = I\left[0.2053 + \frac{0.232}{SGS} - 0.0324\, SGS * SGM\right] \tag{6.3}$$

where:

I = 4.448 for A in kN (1.0 for A in kips)
SGS = Specific gravity of side member
SGM = Specific gravity of main member

McLain reported that it was not possible to determine an expression for parameter B with a sufficient degree of accuracy. An alternate approach to determining parameter B involved rearranging Eq. 6.2 into the form:

$$B = \frac{10^{V_n / A} - 1}{e_n} \tag{6.4}$$

Eq 6.4 requires a known point on the V_n-e_n curve. An approach followed by Pellicane et al. (1991) to predict a point was to use a technique developed by Wilkinson (1971) based in the work of Kuenzi (1955), who developed an equation of the theory of beams on elastic foundations that enables the prediction of the load associated with a joint slip of 0.38 mm (0.015 in.). Appendix A contains the details of Kuenzi's work and the calculations to determine the parameters used here. Table 6.2 lists in the first row the values of parameters *A* and *B*, using Eqs. 6.3 and 6.4.

McLain also reports parameters *A* and *B* based on static and cyclic tests for different types of wood specific gravities. The parameter values corresponding to the main and side members with similar specific gravity (SG = 0.556) to the members used in this study (Southern Pine, SG = 0.55) were selected. Parameter *A* is based upon the SG model (Eq. 6.3) and parameter *B* is obtained from the experimentally determined load corresponding to a slip of 0.38 mm (0.015 in.). These values from McLain's static and cyclic tests are listed in Table 6.2.

Because coefficients A and B were calculated for an 8d common nail (3.3 mm, 0.131 in. diameter), modifications were made to consider the smaller finishing nail diameter of 1.6 mm (0.0625 in.) used in the T&G sheathing nailed joints. This is the approach followed by Pellicane et al. (1991) based on a series of experimental tests with the main goal of predicting the shear force–slip relationship for a wide range of nailed joint configurations. For this purpose, Pellicane developed a procedure to predict

parameters A and B, including the effects of nail size, side member thickness, interlayer gap, and specific gravities of side and main members. Correction coefficients were developed for each type of effect. The correction coefficients for nail diameter effects reported by Pellicane et al. (1991) are:

$$C_{Ad} = -2.21 + 39.3 \cdot f \cdot d - 113.0 \cdot f^2 \cdot d^2 \quad (6.5a)$$

$$C_{Bd} = 2.83 - 14.6 \cdot f \cdot d \quad (6.5b)$$

where:

f = 0.03937 when d is in mm (1.0 when d is in in.)
d = Nail diameter, mm (in.)

The corrected coefficients A and B are then calculated as:

$$A = C_{Ad}\, A' \quad (6.6a)$$

$$B = C_{Bd}\, B' \quad (6.6b)$$

where A' and B' are reference values for A and B calculated with Eqs. 6.3 and 6.4.

The tested diameter range was limited from 6d to 10d common nails (2.9 mm to 3.8 mm). Because the 10d finishing head nail diameter (1.6 mm) used in the T&G connection was out of this range, Eq. 6.5a was not used and C_{Ad} was taken as 0.788, the minimum value of the range (6d nail). The resulting value for C_{Bd} is 2.773. Parameters *A* and *B* for T&G sheathing nailed joints are also listed in Table 6.2.

Fig. 6.4 shows a plot of the lateral load-slip equations for nailed joints using an 8d common nail and a square edged or T&G sheathing board as the side member for the sets of nail parameters given in Table 6.2. There is an increasing difference between the curves after a slip value of 0.381 mm (0.015 in.). The lower and upper curves (1 and 3) were used for the analysis of the diaphragm models with square edged sheathing to determine lower and upper bound limits of the diaphragm response.

TABLE 6.2 Parameters *A* and *B* in McLain's Nail Slip Equation

No.	Side member	*A* kN (kips)	*B* mm^{-1} ($in.^{-1}$)	Description
1	Sq. edged	2.746 (0.617)	2.54 (64.6)	Eqs. 6.3, 6.4* (upper bound)
2	Sq. edged	0.958 (0.215)	15.84 (402.3)	McLain's static test
3	Sq. edged	0.914 (0.206)	14.97 (380.2)	McLain's cyclic test (lower bound)
4	T&G	2.161 (0.486)	1.53 (38.9)	Eqs. 6.3, 6.4, 6.6

* Calculations in Appendix A

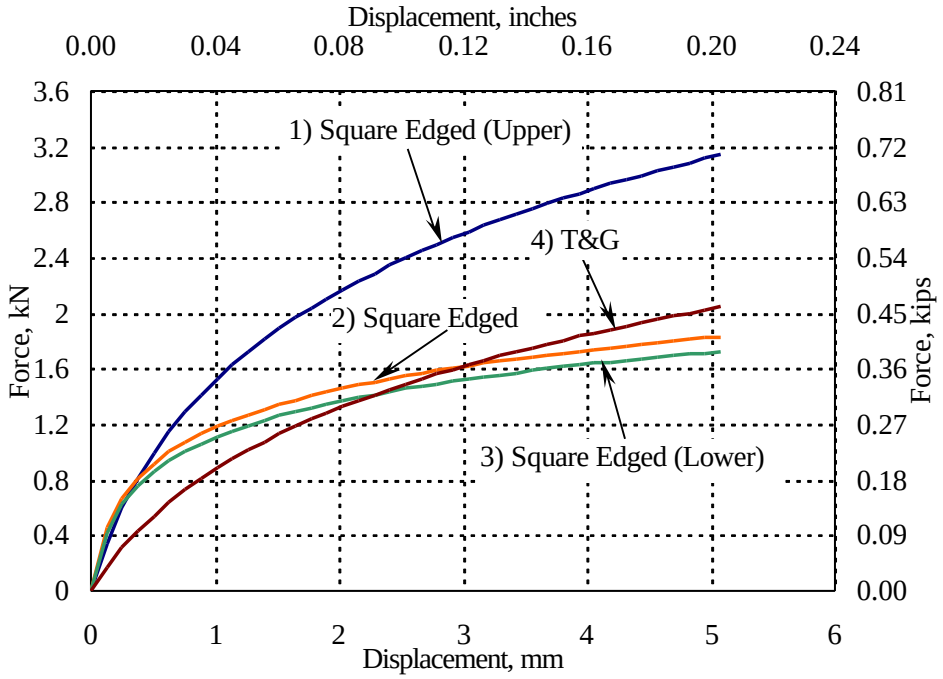

FIG. 6.4 Lateral Load - Slip Backbone Curves of Nailed Connections: T&G and Square Edged Sheathing Boards as Side Member

6.4.2.2 Plywood Panel as Side Member

Three expressions were found in the literature that represent the lateral load - slip behavior of plywood nailed connections using 8d common nails based on lateral load tests: (1) Eq. 6.7a, from West Virginia University (Zagajeski et al., 1984); (2) Eq. 6.7b from Washington State University (Cheung, 1984); and (3) Eq. 6.7c from the Engineered Wood Association - APA (Countryman, 1952).

$$e_n = \frac{V_n}{10}\left[1 + 2.2\left(\frac{V_n}{10}\right)^5 10^9\right] \tag{6.7a}$$

$$V_n = 0.578 e_n^{0.387} \tag{6.7b}$$

$$V_n = 0.616 e_n^{0.3313} \tag{6.7c}$$

where:

V_n = Fastener load, kips
e_n = Slip, in.

Fig. 6.5 shows the lateral load - slip curves of a nailed connection when the side member is a plywood panel. The APA relationship (Eq. 6.7c) was selected to represent the plywood connection for this study, because of the numerous tests conducted by APA and because it is adopted by most codes. Countryman (1952) reports a minimum nail penetration of 36.6 mm (1.44 in.) into the main member for maximum loads up to 0.979 kN (0.220 kips). This nailed connection model was included in the FE models of the diaphragm specimens retrofitted with plywood overlay (MAE-2B, MAE-2C, MAE-3A and MAE-3B) to represent the behavior of the nails added to secure the plywood panels in place.

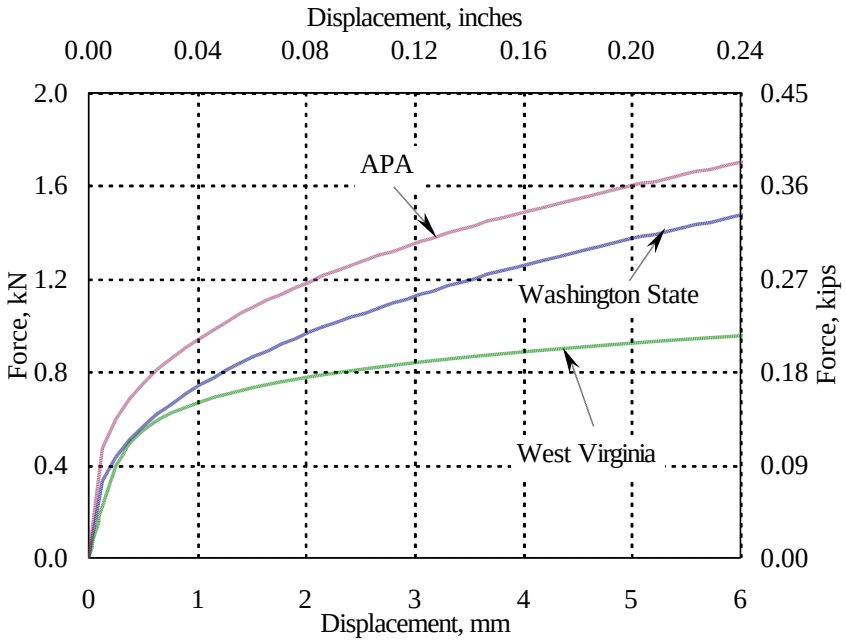

FIG. 6.5 Lateral Load - Slip Backbone Curves of Nailed Connections: Plywood Panel as Side Member

6.4.3 Hysteretic Model for Lateral Load - Slip Behavior of Nailed Connections

The three-parameter model by Park et al. (1987) was used to model the hysteretic behavior of the nailed connections. This model was originally developed for reinforced concrete members under cyclic loading using a non-symmetric tri-linear backbone curve with the points corresponding to the first cracking and yielding of the member. The nailed connections were modeled as one-dimensional axial springs having a symmetric backbone curve with respect to the origin of coordinates, in which the elongation is the nail slip. The backbone curves defined for each type of nailed connection in the previous section were used to determine the tri-linear backbone curves required by the three-parameter model. The parameters that define the tri-linear backbone curve (see Fig. 6.6 and Table 6.3) were selected by matching the energy absorption of the continuous backbone curve. Fig. 6.7 shows the backbone and tri-linear curves for each type of nailed connection.

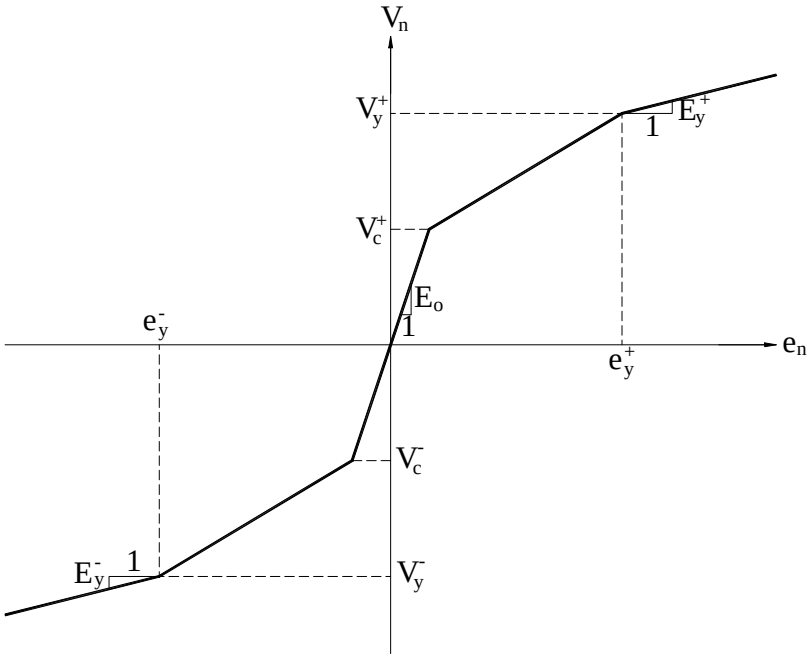

FIG. 6.6 Tri-Linear Backbone Curve

TABLE 6.3 Three-Parameter Model Properties

Parameter	Sq. Edged Board Lower Bound	Sq. Edged Board Upper Bound	Plywood Panel
Elastic Shear Stiffness E_o, kN/cm (kips/in.)	36.1 (20.62)	21.2 (12.11)	37.3 (21.30)
Post-Yield Stiffness E_y, kN/cm (kips/in.)	1.3 (0.76)	3.7 (2.12)	1.5 (0.85)
Cracking Shear Load V_c, kN (kips)	0.45 (0.10)	0.80 (0.18)	0.45 (0.11)
Yield Shear Load V_y, kN (kips)	1.4 (0.31)	1.9 (0.42)	1.1 (0.24)
Yield Displacement e_y, mm (in.)	1.1 (0.045)	1.3 (0.050)	1.0 (0.040)

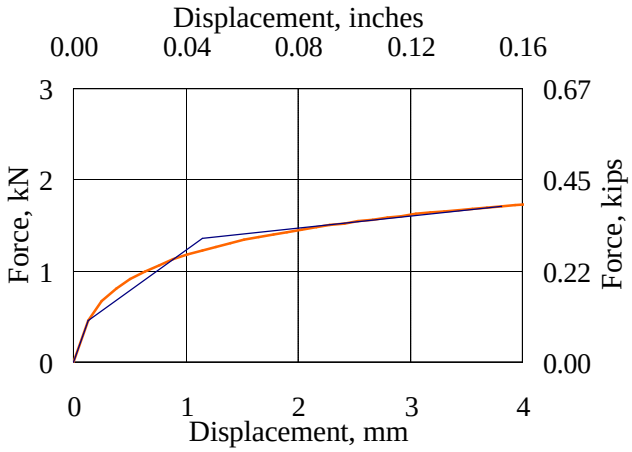

(a) Square Edged Sheathing - Lower Bound Model

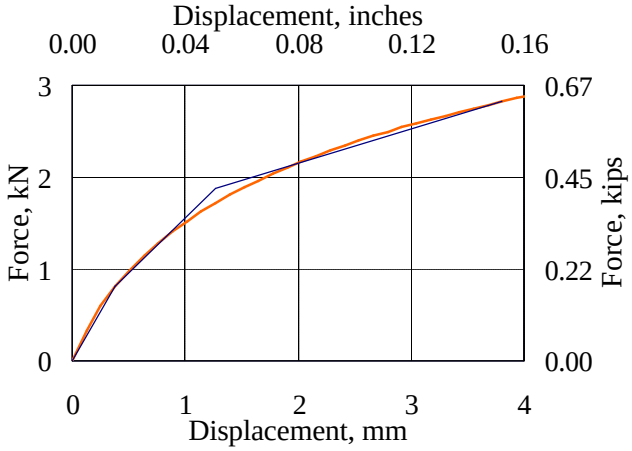

(b) Square Edged Sheathing - Upper Bound Model

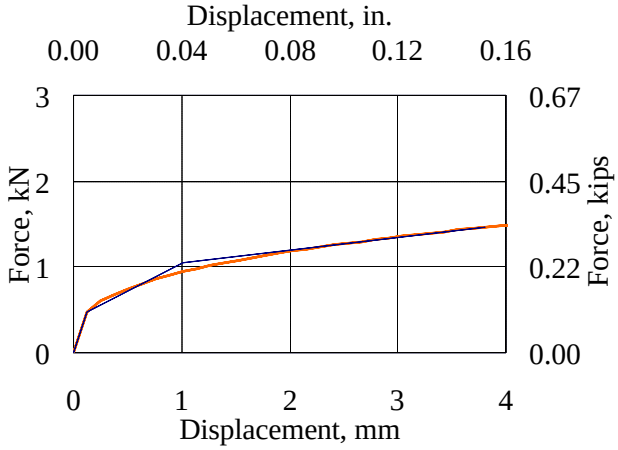

(c) APA Plywood Model

FIG. 6.7 Backbone and Tri-Linear Curves for Nailed Connection Models

Three significant characteristics of the hysteretic loops are included in the model: stiffness degradation, α; strength deterioration, β; and pinching behavior, γ. These characteristics can be observed for the specimens tested in this study (see Section 4) and elsewhere. Stiffness degradation (unloading stiffness) is introduced by aiming at a point based on the yield point of the initial backbone curve line until zero displacement is reached (see Fig. 6.8a). The stiffness degradation factor α is the ratio of the force corresponding to this point and the yielding force, V_y. Slip or pinching behavior occurring at the start of a reverse loading cycle is attributed to the slack in nailed joints associated with local damage caused by the previous loading cycle. The pinching factor γ lowers the target maximum point (point A in Fig. 6.8b) to a level γV_y (point B) along the previous unloading line. Reloading branches aim toward point B until the slack is gradually recovered (u_s). After this, the branch aims toward the previous target point A. Strength deterioration (see Fig. 6.8c) is provided in the model by defining parameter β as the ratio of maximum response over ultimate deformation under monotonic loading and the normalized incremental hysteretic energy:

$$b = \frac{ddmV_y}{dE} \tag{6.8}$$

where:

ddm = Increase of the maximum response
V_y = Yield strength
dE = Incremental hysteretic energy

A FORTRAN subroutine was required to define a single-degree of freedom hysteretic connector element for ABAQUS to perform the quasi-static reversed cyclic analysis. The subroutine was originally written for the computer program IDARC, (Inelastic Damage Analysis of Reinforced Concrete Frame-Shear-Wall Structures) (Park et al., 1987) and was adapted for ABAQUS (White and Kim, 2000).

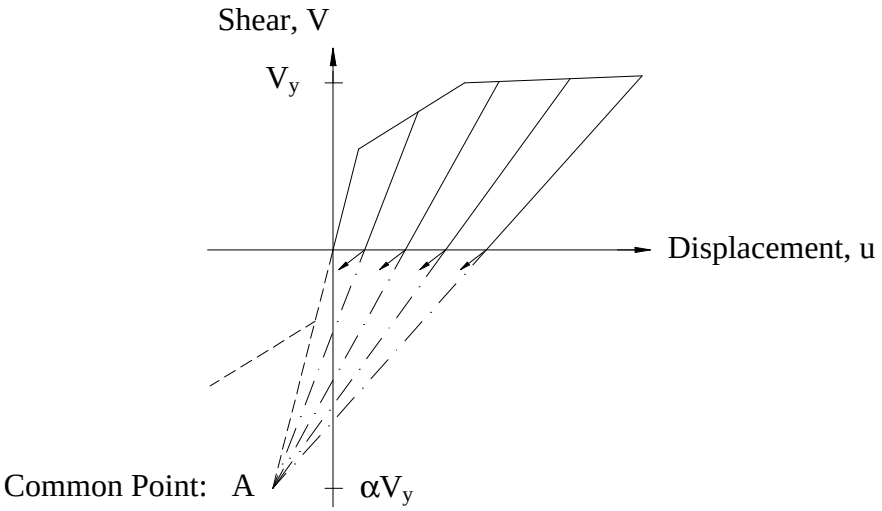

(a) Stiffness Degradation (a**)**

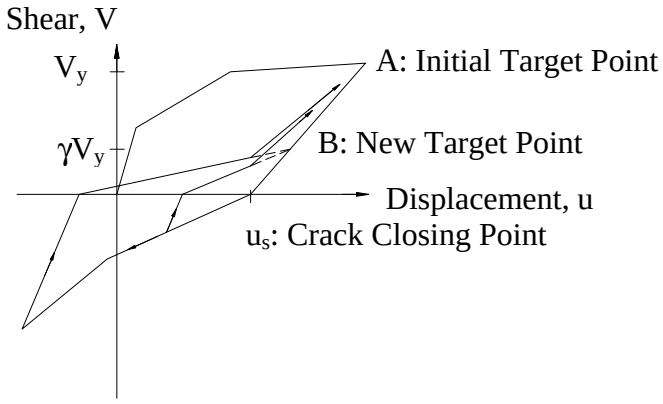

(b) Pinching Behavior (b**)**

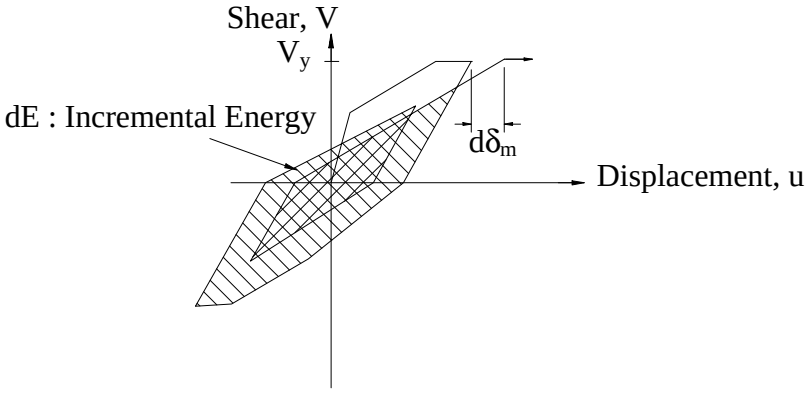

(c) Strength Deterioration (g**)**

FIG. 6.8 Hysteretic Parameters in Park's Model (adapted from Park et al., 1987)

The values of the hysteretic parameters were determined using a trial-and-error process. The first stage of the calibration procedure was to develop FE models of the diaphragm specimens. The force-displacement output obtained from ABAQUS was calibrated to correlate with the experimentally obtained force-displacement data for the selected diaphragm specimens. After the trials, the hysteretic parameters α, β, and γ were selected to have relatively low stiffness, strength degradation and pinching effects in the diaphragm models, because this gave the closest approximation to the experimental results. The numerical values of the hysteretic parameters are listed in Table 6.4. A plot of the hysteretic and the backbone curves for each nailed connection type is shown in Fig. 6.9. Each of the ten loops of the curves shown corresponds to an amplitude increment of 0.4 mm (0.015 in.) displacement. The equation of the backbone curves shown in each graph is in U.S. units.

TABLE 6.4 Three-Parameter Model Hysteretic Parameters

Parameter	Sq. Edged Board Lower Bound	Sq. Edged Board Upper Bound	Plywood Panel
Stiffness Degradation Factor α	100,000	100,000	100,000
Strength Degradation Factor β	0.02	0.02	0.02
Pinching Factor γ	0.9	0.9	0.9

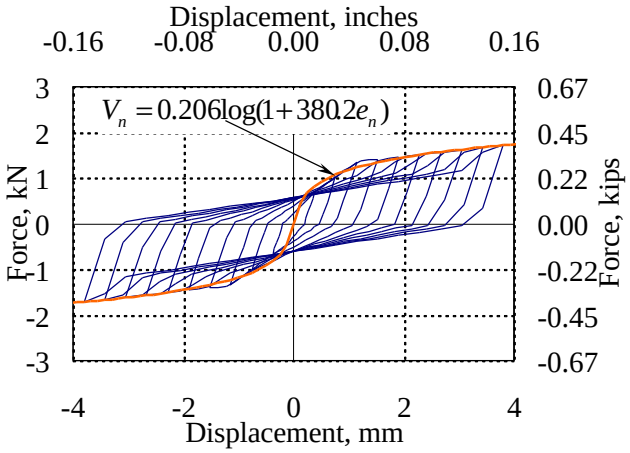

(a) Square Edged Sheathing - Lower Bound Model

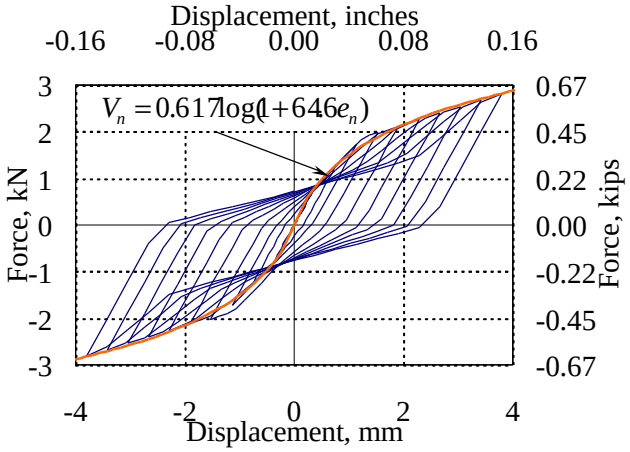

(b) Square Edged Sheathing – Upper Bound Model

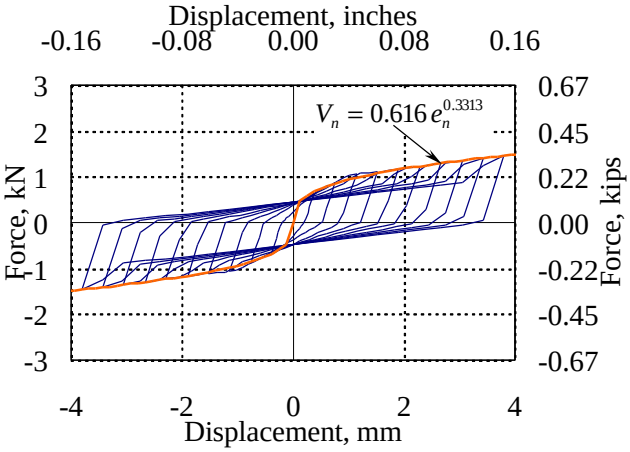

(c) APA Plywood Model

FIG. 6.9 Hysteretic Models for Nailed Connections

6.4.4 Model for Axial Stiffness of Blocking

Blocking members were present in diaphragm specimens that were rehabilitated with a plywood panel overlay. The blocking members undergo axial deformation when lateral forces are applied to the diaphragm. The basic idea of the model is to assign different constant stiffness values to define the response of the blocking members to tension and to compression. In compression, the full section of the wood blocking participates by bearing against a joist. In tension, the nails that attach the blocking to the joists can pull out. Withdrawal test results of nailed connections made by Winistorfer and Soltis (1994) were used to select the stiffness of the blocking boards in tension. The materials and dimensions used in Winistorfer's specimens were similar to the materials used in this research. Compression stiffness K_c is determined from the following expression:

$$K_c = \frac{EA}{L} \tag{6.9}$$

where,

E = Young's modulus of wood (See Table 6.1)
A = Cross sectional area of 2x4 blocking, 31.6 cm^2 (4.9 $in.^2$)
L = Length of blocking member, 36.8 cm (14.5 in.)

Tension and compression stiffness values of 10.5 kN/cm (6 kips/in.) and 1,030 kN/cm (590 kips/in.), respectively, are used for this study.

6.5 FINITE ELEMENT MODELS OF DIAPHRAGMS

6.5.1 General

The FE models for the unretrofitted diaphragm specimens and the plywood panel overlay retrofits of the testing program are described here. The FE models were focused on the more typical retrofits using plywood panel overlays, therefore diaphragms retrofitted with steel strapping and steel truss were not modeled. The anchor connections were not included in the models, because of a lack of information needed to model this type of connection. Instead, pinned supports were defined at the anchor

locations. Displacement-controlled quasi-static monotonic and cyclic analyses were performed for the diaphragm models. The displacements were applied at the third points of the diaphragm span length along the diaphragm width, at the same locations where the loading frame applied displacements to the diaphragm specimens (see Section 3.3.1). The measured anchor lateral displacements were subtracted from the total measured diaphragm displacements at the loading points (both shown in Section 4) and the resulting displacement histories were applied in the FE analyses. Similarly, the measured anchor lateral displacements were subtracted from the measured total diaphragm midspan displacements and the resulting measured response was compared with computed diaphragm midspan displacements from the FE analysis.

The models for diaphragm specimens MAE-2 and MAE-3 had the following common characteristics: the square edged sheathing boards had two nails per connection at joist intersections and three nails at the board ends. To ease the model construction, the nonlinear spring elements representing the nails of the connection were placed at the boundary of the boards, thus the actual spacing between the nails in the connection was increased by approximately 38 mm (1.5 in.). Fig. 6.10a shows the location of the undeformed springs and Fig. 6.10b shows the springs elongations amplified several times, where the solid points represent the ends of each spring. The sheathing boards are overlapped, because contact forces were not considered in the model. The McLain model was used to define the lateral load-slip of the nailed connections using both the lower and upper bound load-slip curves. To simplify the mesh generation, it was assumed that the length of each sheathing board was 7.32 m (24 ft.). The actual sheathing was composed of alternating lines of two 3.53 m (11 ft. 7 in.) pieces and a line of a 1.91 m, 3.66 m and 1.50 m (6 ft. 3 in., 12 ft., and 4 ft. 11 in.) pieces (see Fig. 3.6).

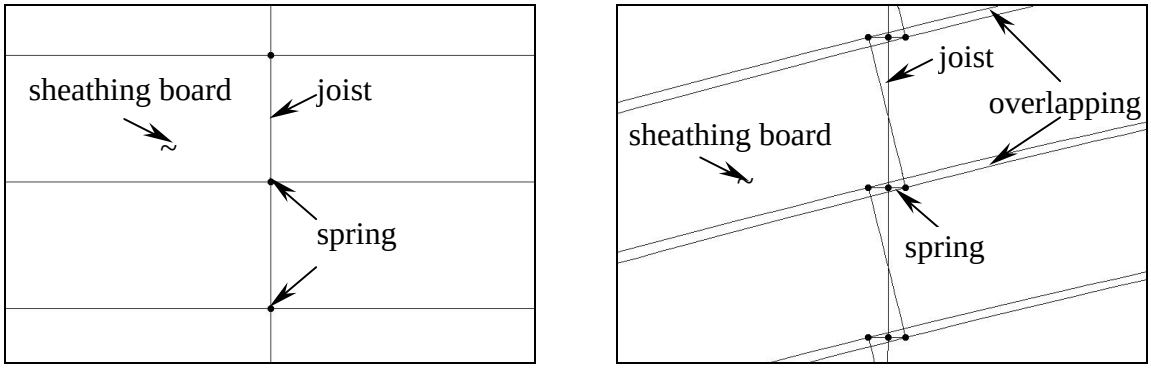

(a) Undeformed **(b) Deformed**

FIG. 6.10 Detail of Nonlinear Spring Elements

To simplify the development of the model for the diaphragms retrofitted with plywood panel overlay, a FE mesh was developed for the panels, their nailed connections and framing and analyzed separately from the unretrofitted diaphragm. Because the displacements were applied in the joist direction, the only function of the joists was to hold one end of the springs in place. The analytical responses were obtained for the diaphragm midspan of both unretrofitted diaphragm and panel FE meshes and superimposed together assuming they are connected in parallel. Therefore, for the same midspan displacement, the corresponding forces of both responses were added. The presence of joists in both sub-models was not considered to change the behavior of the retrofitted diaphragms. The deformed shapes of the two sub-models are not the same, and a different displacement can exist at any point of the diaphragm except for the loading points. However, because the forces of the unretrofitted diaphragm response are significantly lower when compared to the panel response, the error introduced in superimposing the forces is quite small.

For comparison of the model and experimental cyclic responses, the total dissipated energy and stiffness at the last cycle of loading are reported. The total dissipated energy was determined by summing the enclosed area of each cycle of the hysteretic response. The area was calculated from points of the cyclic curves, assuming

straight lines between points. Since imposed experimental loading consisted of two cycles at each incremental displacement level, and the FEM had only one cycle per peak displacement, the reported experimental dissipated energy values were halved. The stiffness at the last cycle of loading was defined as the absolute sum of the maximum forces in the positive and negative directions of loading at the last cycle divided by the absolute sum of the maximum displacements in the two directions at the last cycle.

6.5.2 Diaphragm MAE-1

The MAE-1 diaphragm test specimen had a framing structure with an arrangement of 2x10 by 7.32 m (24 ft.) long beam joists spaced at 406 mm (16 in.) centers. Sheathing was composed of 1x4 by 3.66 m (12 ft.) long T&G boards oriented at right angles to the joists and nailed at every intersection with one 10d finishing head nail. Three rows of bridging composed of 2x4 angled boards were placed between the joists in rows every 2.43 m (8 ft.). Refer to Fig. 3.3 for a detailed view of the specimen.

The FE model consisted of an assemblage of 810 beam elements for the joists, 738 beam elements for the T&G sheathing, 700 nonlinear spring elements for the nails that connected the sheathing and joists, and 18 bar elements for the bridging members. Fig. 6.11a shows the beam elements for the joists and T&G sheathing as the straight lines. Springs used for the nails are shown as circles. Fig. 6.11b shows the deformed diaphragm for a maximum midspan displacement of 76 mm (3 in.) with the displacements factored five times. The lateral load-slip model used for the nailed connections was based on a procedure developed by Pellicane et al. (1991) using the equation given by McLain (1975) with some modifications to consider the smaller nail diameter (see Section 6.4.1.1). Because only one nail per sheathing connection was used in the construction of the T&G diaphragm sheathing, which runs parallel to the applied load, it was determined that beam elements would be sufficient for modeling the sheathing boards. In the case of the bridging boards, bar elements (2 nodes per element)

were used because they provide connectivity between joists for force transfer, with no increase in the lateral stiffness of the diaphragm.

A monotonic displacement-controlled static analysis was performed for the MAE-1 FE model, as described in Section 6.5.1. Displacement was applied at the third points of the diaphragm span, as indicated by the arrows in Fig. 6.11a, to match the experimental setup. Fig. 6.12 shows the response for several types of analyses made with the model. The response obtained from a geometrically linear analysis resulted in a significantly low lateral stiffness and strength compared to the measured lateral stiffness of the diaphragm specimen.

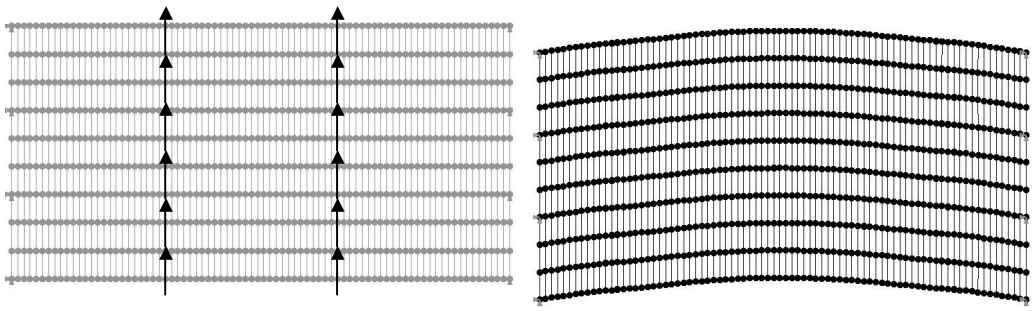

(a) Finite Element Mesh **(b) Deformed Shape**

FIG. 6.11 Diaphragm MAE-1

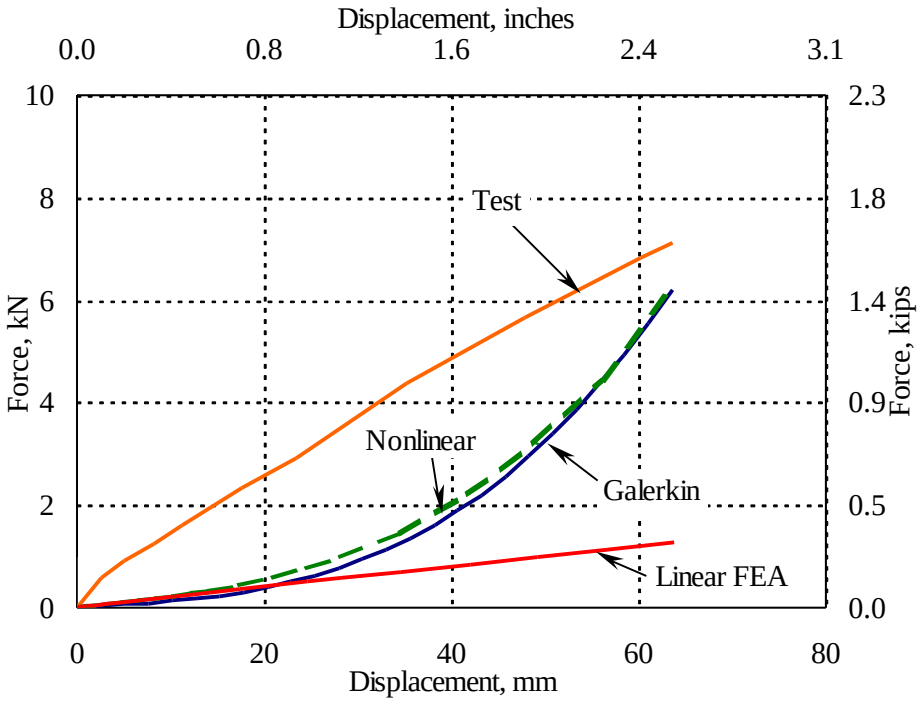

FIG. 6.12 Comparison of Static Responses of Diaphragm MAE-1 at Midspan

A second type of analysis was made, considering now the stretching of the joist beams (assuming that the supports are pinned), resulting in a relationship between strain and displacement that is nonlinear. Two more responses were then determined, one was obtained from a geometrically nonlinear FE analysis and the second from the governing nonlinear equation of a beam hinged at both immovable ends under distributed load as given by Sathyamoorthy (1997):

$$EI\frac{d^4w}{dx^4} - \frac{EA}{2L}\int_0^L\left(\frac{dw}{dx}\right)^2 dx\frac{d^2w}{dx^2} = q(x) \tag{6.10}$$

where:

w = Beam deflection

E = Modulus of elasticity
I = Moment of inertia of the beam cross-section about the principal axis
A = Area of the cross-section
L = Length of the beam joist
$q(x)$ = Applied external load

Sathyamoorthy provides an approximate solution for the case of uniformly distributed loading. Using the Galerkin method, a sinusoidal shape function was chosen, and the following solution is found:

$$\frac{A_1}{L} + 3\left(\frac{L}{h}\right)^2\left(\frac{A_1}{L}\right)^3 = \frac{4}{p^5}\frac{q_o L^3}{EI} \tag{6.11}$$

where:

A_1 = Amplitude of the deflection
h = Beam depth
q_o = Load per unit length of the beam

An equivalent uniform load q_o was calculated in order to apply this solution to the diaphragm model. A plot of the deflection A_1 multiplied by the number of joist beams attached to the anchor connections (four total) is shown in Fig. 6.12. The two geometric nonlinear solutions are very close; this suggests that the nonlinear springs of the nails in the FE analysis did not contribute to the response. Another conclusion is that the T&G diaphragm does not behave as a unit, but rather as a group of joist beams having the same lateral displacement. The bridging and T&G sheathing boards provide a mechanism to transfer the applied loads to all the joists.

The shape of the nonlinear response shows that the lateral stiffness of the diaphragm increases with increasing load. The discrepancy in shape of the curve with the test response can be attributed to the assumption of unmovable end supports used in the model. Another factor that can be considered to explain the greater loads in the

experimental response compared to the analytical response is the presence of friction forces acting between the surfaces of the sheathing and joists. Friction is not included in either the nailed connection model or the beam elements. Since T&G sheathing is used, significant friction forces may have developed. Additional analyses (linear and geometrically nonlinear) performed for diaphragm FE model MAE-1 using cyclic quasi-static loading indicates that the spring elements representing the nails remained in the elastic range and no degradation of stiffness, strength or energy dissipation occurred under load reversals. Therefore, this diaphragm was not used in the calibration process of the hysteretic parameters.

6.5.3 Diaphragm MAE-2

Diaphragm test specimen MAE-2 was composed of 2x10 by 3.66 m (12 ft.) long beam joists spaced at 406 mm (16 in.). Sheathing was 1x6 square edge straight boards, staggered with a maximum length of 3.66 m (12 ft.). Three 8d common nails were used at the ends and two at the interior joints of each sheathing board. Two rows of bridging members spaced at 2.44 m (8 ft.) connected the joists, as shown in Fig. 3.6.

The FE model consisted of 546 linear beam elements to model the joists, 468 8-node 2D solid elements were used to model the sheathing boards, and 990 nonlinear spring elements were used to model the nails (see Fig. 6.13a). The size of the solid elements and number of nodes per element were defined based on the locations of the nailed connections along the sheathing length in the actual diaphragm specimen.

A monotonic displacement-controlled static analysis was performed for diaphragm MAE-2. Fig. 6.13b show the deformed shape for diaphragm MAE-2 (displacement factored 5 times) at a maximum displacement of 76 mm (3 in.) and is similar to that observed for the specimen during the experimental testing. The analytical model and experimental monotonic responses at the diaphragm midspan are shown in Fig. 6.14. The response based on the lower bound model of the nailed connection lies

underneath the experimental curve, and the upper bound response shows greater forces than the experimental values after 40 mm (1.57 in.) of lateral deflection. Friction forces were not considered in the analytical model, which may explain the differences.

A comparison of the nail spring elongations in both directions showed that the elongation in the sheathing direction (perpendicular to the applied lateral load) was much higher than the elongation in the joist direction. It was also observed that the two spring elements representing the nails on each nailed connections slipped in opposite directions relative to the joist, following the extension or contraction of the fibers of the sheathing boards. Fig. 6.10b shows the elongation of the deformed springs used to model the nailed connections.

Cyclic quasi-static analyses were performed for diaphragms MAE-2. The cyclic quasi-static responses using the lower (Fig. 6.15a) and upper (Fig. 6.15b) bound model of the nailed connection are shown and compared to the experimental response (Fig. 6.15c). Table 6.5 compares the dissipated energy and stiffness (as defined in Section 6.5.1) calculated for the models and test responses. The dissipated energy is predicted to be 83% and 58% of the test value, for the lower and upper bound model, respectively. The stiffness is estimated to 83% and 107% of the experimental value for the lower and upper bound model, respectively.

TABLE 6.5 Comparison of Cyclic Responses for Diaphragm MAE-2

From	Dissipated Energy kN-cm (kip-in.)	Stiffness (last cycle) kN/cm (kips/in.)
Lower Bound Model	1105 (97.8)	6.0 (3.4)
Upper Bound Model	774 (68.5)	7.7 (4.4)
Experimental	1337 (118.3)	7.2 (4.1)

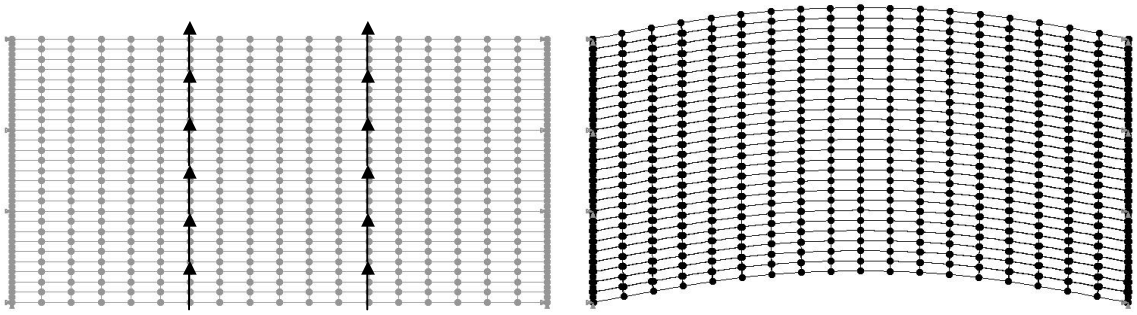

(a) Finite Element Mesh **(b) Deformed Shape**

FIG. 6.13 Diaphragm MAE-2

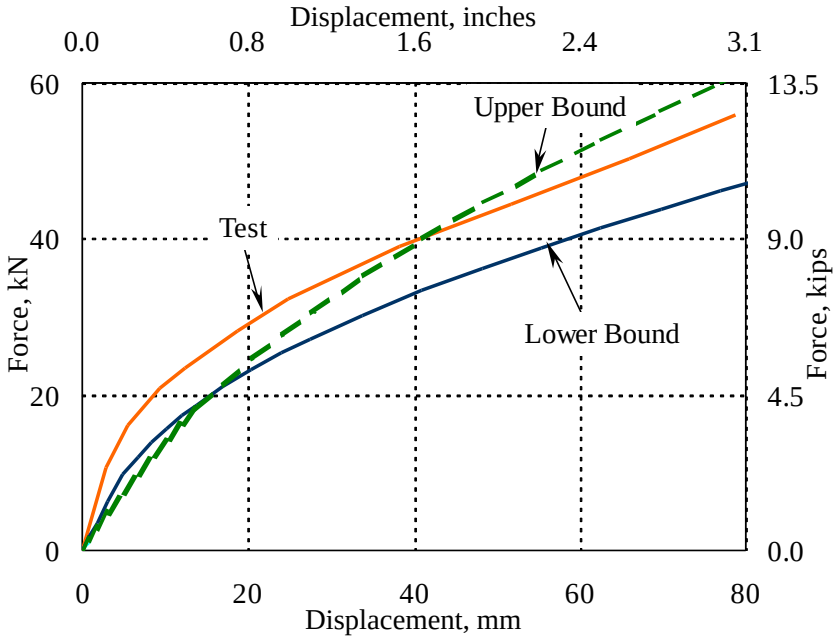

FIG. 6.14 Comparison of Static Responses of Diaphragm MAE-2 at Midspan

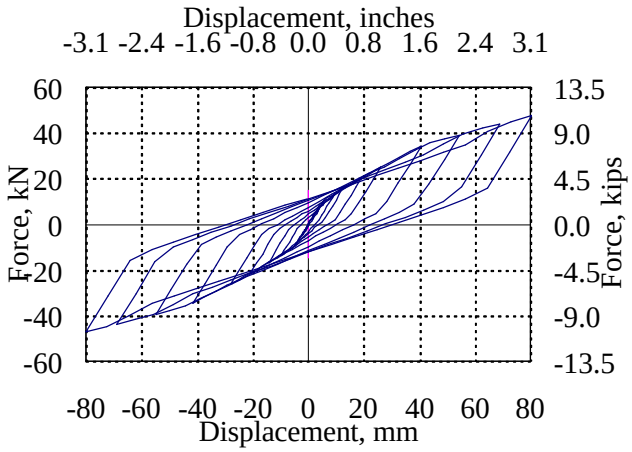

(a) Lower Bound Nailed Connection Model

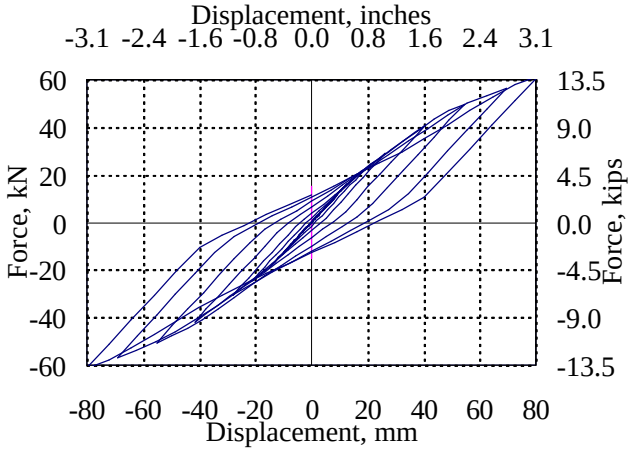

(b) Upper Bound Nailed Connection Model

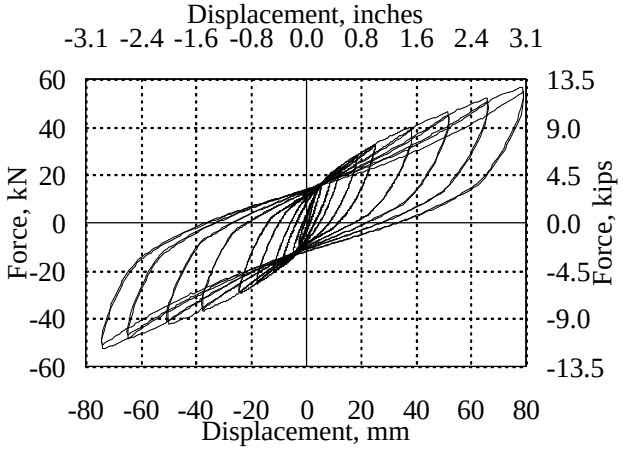

(c) Experimental

FIG. 6.15 Cyclic Quasi-Static Responses of Diaphragm Model MAE-2

6.5.4 Retrofitted Diaphragm MAE-2B

Diaphragm specimen MAE-2 was retrofitted with an unblocked plywood panel overlay nailed with 8d common nails spaced at 152 mm (6 in.) at the supported edges and 305 mm (1 ft.) along interior supporting joists. The thickness of the plywood panels was 9.5 mm (0.375 in.) and the panels were arranged as shown in Fig. 3.8.

The FE model of the panel overlay, shown in Fig. 6.16a, was composed of 280 linear beam elements for the joists, 216 8-node 2-D solid elements for the panels (24 elements per panel), and 342 nonlinear springs for the nailed connections. The elements of the FE mesh for the panels were 406 mm by 305 mm (16 in. by 12 in.) based on the location of the springs that attach the panels to the joists. To simplify the FE mesh construction, the spring elements representing the nails next to the supported panel edges were located at the edges, as shown in Fig. 6.16c.

Separate monotonic displacement-controlled static analyses were performed for the sheathed model and the panel overlay model for diaphragm MAE-2B. The responses were added together to determine the analytical response for the retrofitted diaphragm (see Section 6.5.1). Fig. 6.16b shows the deformed shape of the panel model for the maximum applied displacement during testing, 19 mm (0.75 in.), scaled five times. A detail of the deformed spring elements is shown in Fig. 6.16c. The monotonic responses are shown in Fig. 6.17. The response based on the lower bound nailed connection models lies barely over the upper bound model response for the deformation range shown. Beyond that range the situation is reversed, but this region is not shown in the figure. The responses are similar because of the similar behavior of both models in the unretrofitted diaphragm for the displacement range analyzed. Therefore the differences in response of both models are hidden by the higher response of the panel overlay. Both model responses lie below the experimental response by as much as 17.8 kN (4 kips) or 26%. This difference in the response can be attributed to friction forces present in the

test specimen that were not included in the analytical model. Another reason may be the use of an approximate model for the nailed connection behavior.

Cyclic quasi-static analyses were performed for diaphragm MAE-2B. The cyclic responses of the diaphragm based on the upper and lower bound load slip curve of the nailed connection are shown in Figs. 6.18a and 6.18b. Table 6.6 provides values of the dissipated energy and stiffness (as defined in Section 6.5.1) from the models and test results. The dissipated energy is significantly underpredicted as 53% and 37% of the experimental value by the lower and upper bound models, respectively. Both models underpredict the stiffness as 72% and 74% of the experimental value.

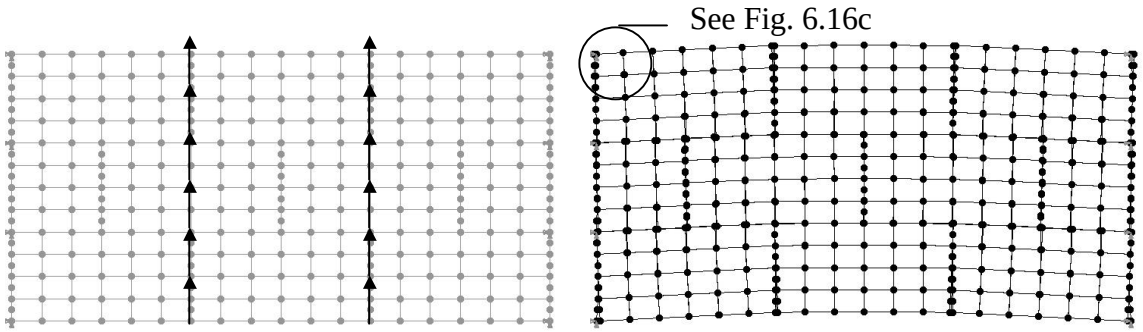

(a) Finite Element Mesh **(b) Deformed Shape**

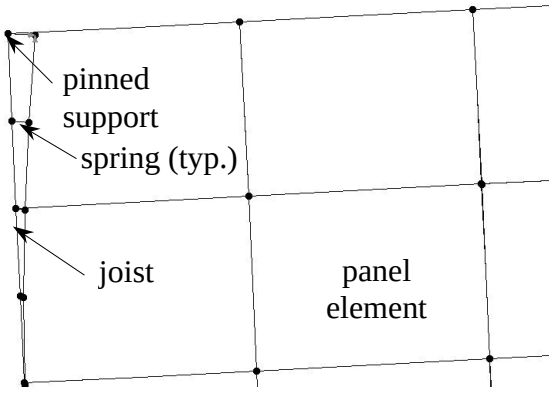

c) Detail of Deformed Spring Elements

FIG. 6.16 Diaphragm MAE-2B (Unblocked Panel Overlay)

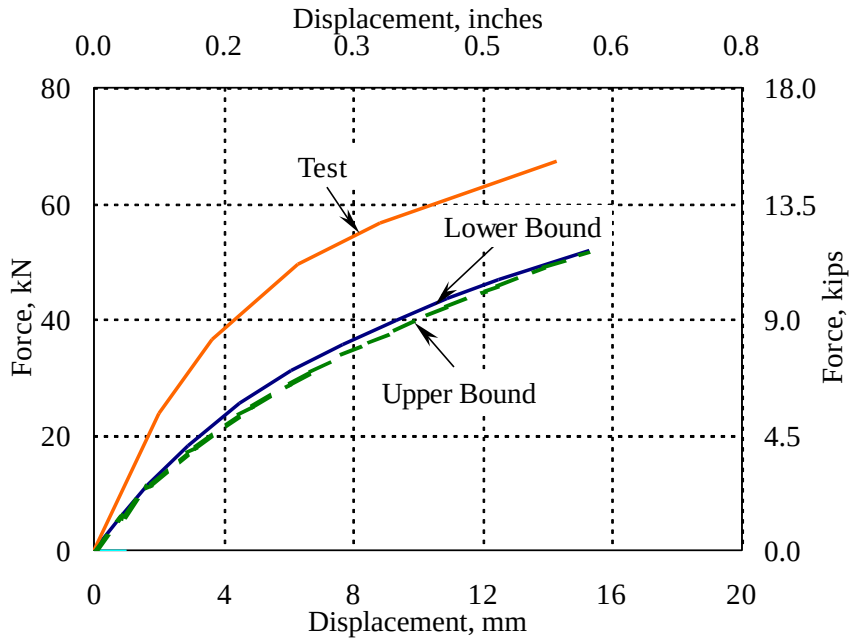

FIG. 6.17 Comparison of Static Responses of Diaphragm MAE-2B at Midspan

TABLE 6.6 Comparison of Cyclic Responses for Diaphragm MAE-2B

From	Dissipated Energy kN-cm (kip-in.)	Stiffness (last cycle) kN/cm (kips/in.)
Lower Bound Model	99.4 (8.8)	34.1 (19.5)
Upper Bound Model	68.9 (6.1)	34.9 (19.9)
Experimental	186 (16.5)	47.1 (26.9)

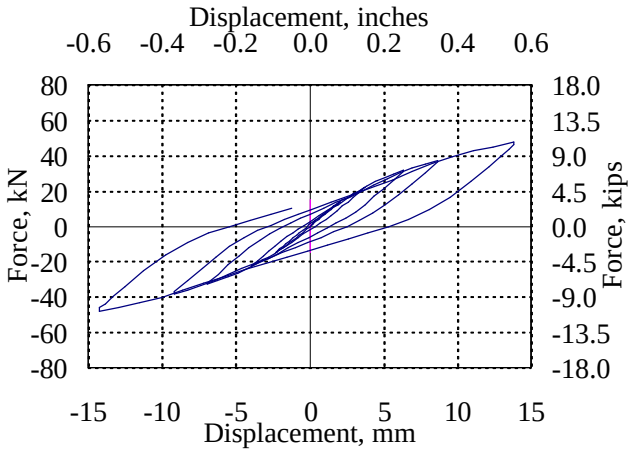

(a) Lower Bound Nailed Connection Model

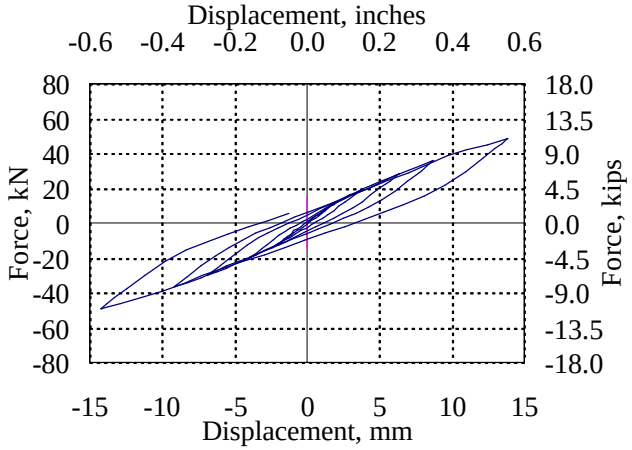

(b) Upper Bound Nailed Connection Model

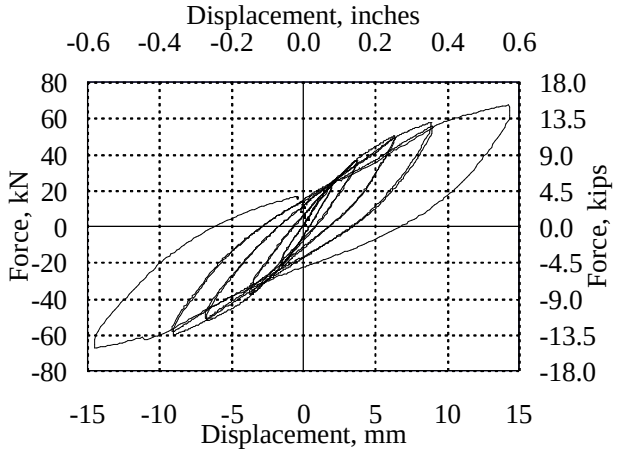

(c) Experimental

FIG. 6.18 Cyclic Quasi-Static Responses of Diaphragm Model MAE-2B

6.5.5 Retrofitted Diaphragm MAE-2C

Blocking was added to diaphragm MAE-2B using 2x4 by 368 mm (14.5 in.) long boards placed underneath the unsupported edges of the plywood panels. In addition, nails were added to reduce the spacing to 51 mm (2 in.) at diaphragm boundaries and 76 mm (3 in.) at the other panel edges (both directions). This retrofit was designated as diaphragm MAE-2C.

The FE model of the panel overlay, shown in Fig. 6.19a, was composed of 280 linear beam elements for the joists, 216 8-node 2D solid elements for the panels, 450 nonlinear springs for the nailed connections and 144 nonlinear spring elements for the blocking boards. Because the same mesh developed for the diaphragm MAE-2B panel overlay was also used for the panel overlay for MAE-2C, the nodes were spaced 152 to 203 mm (6 to 8 in.) apart. Therefore, 3 to 4 nails were lumped together at each node to consider the higher density of the nails used for the blocked diaphragm (MAE-2C). The load-slip model for plywood connections (Eq. 6.5c) was increased accordingly, multiplying the force component of the curve by the number of nails at each node.

Monotonic displacement-controlled static analyses were performed separately for the straight-sheathed mesh and panel overlay mesh for diaphragm MAE-2C and added together to determine the response of the retrofitted diaphragm (see Section 6.5.1). The deformed shape of the panel model for a maximum displacement of 19 mm (0.75 in.) is shown in Fig. 6.19b (displacement factored 5 times). The monotonic responses are shown in Fig. 6.20. The upper and lower bound models gave nearly the same response. The responses are similar because of the relatively similar behavior of both models in the unretrofitted diaphragm for the displacement range analyzed (within +/- 15 mm, at midspan). In addition, the panel overlay provides the significant contribution to the in-plane strength of the retrofitted diaphragm. A good approximation of the computed responses to the experimental response is observed, with a maximum difference of 13.3

kN (3 kips) or 14%. The difference is attributed to friction not modeled and approximations in the nailed connection model.

Cyclic quasi-static analyses were performed for diaphragm MAE-2C. The cyclic responses of diaphragm model MAE-2C are shown in Figs. 6.21a and 6.21b, using the lower and upper bound nailed connection model, respectively. The measured response is shown in Fig. 6.21c for comparison with the model results. Table 6.7 shows the calculated values of dissipated energy and stiffness (as defined in Section 6.5.1) of the models and test results. Both models significantly underpredict the dissipated energy as 46% and 36% of the experimental response for the lower and upper bound models, respectively. Both models estimated the stiffness to be 87% of the experimental stiffness.

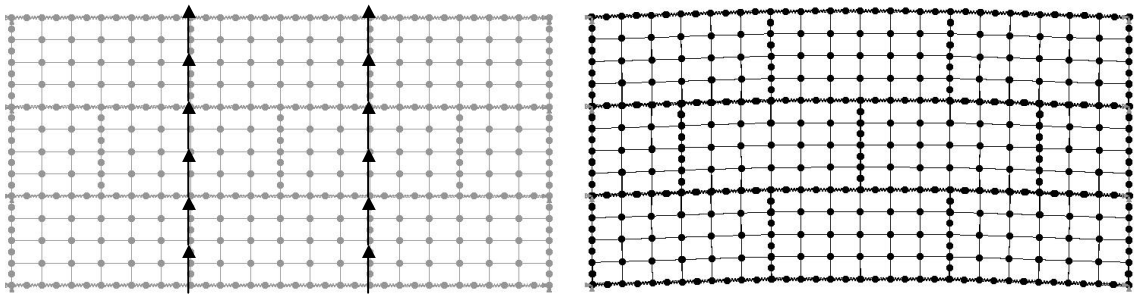

(a) Finite Element Mesh **(b) Deformed Shape**

FIG. 6.19 Diaphragm MAE-2C (Blocked Panel Overlay)

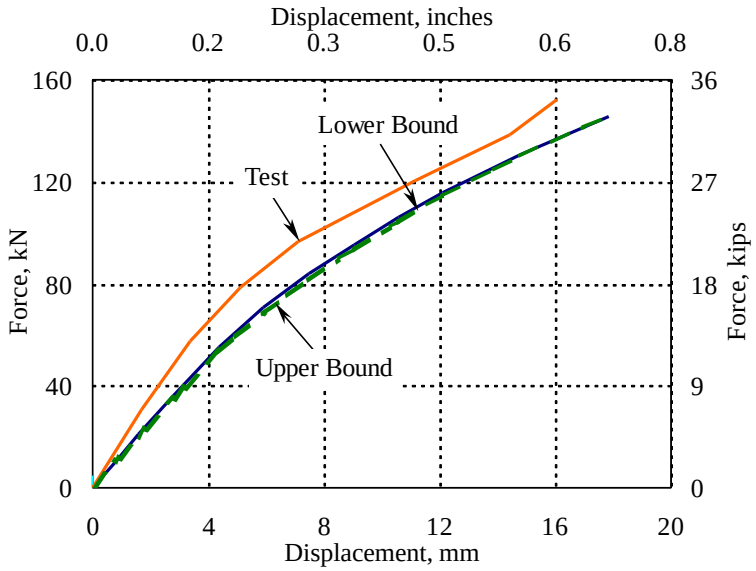

FIG. 6.20 Comparison of Static Responses of Diaphragm MAE-2C at Midspan

TABLE 6.7 Comparison of Cyclic Responses for Diaphragm MAE-2C

From	Dissipated Energy kN-cm (kip-in.)	Stiffness (last cycle) kN/cm (kips/in.)
Lower Bound Model	61.0 (5.40)	99.8 (57.0)
Upper Bound Model	46.3 (4.10)	99.5 (56.8)
Experimental	121 (10.7)	115 (65.4)

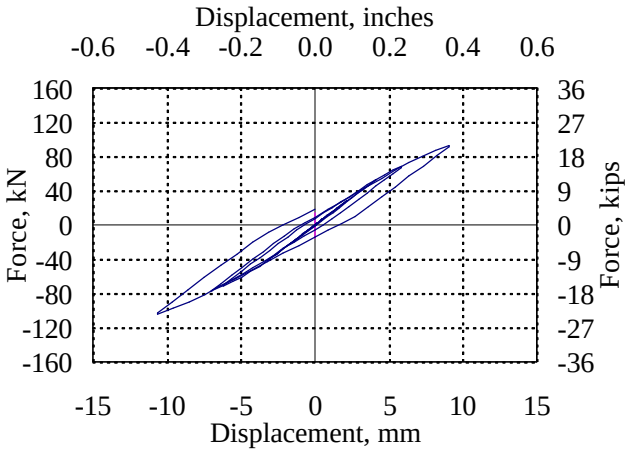

(a) Lower Bound Nailed Connection Model

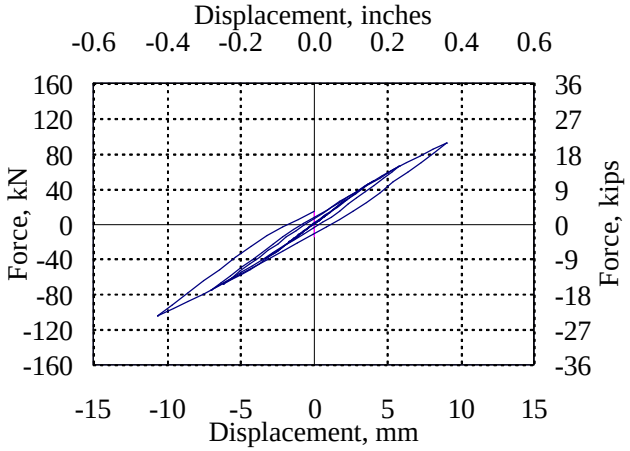

(b) Upper Bound Nailed Connection Model

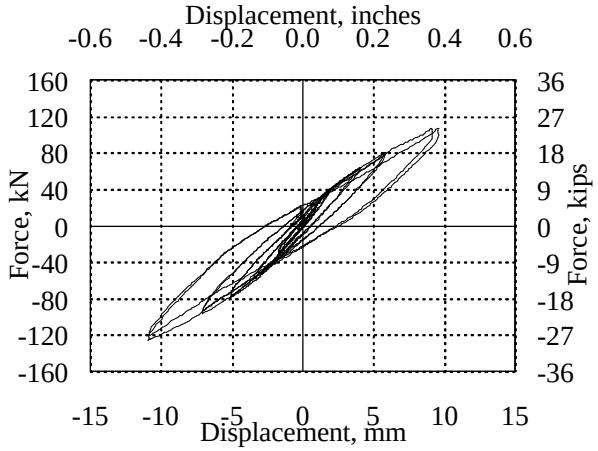

(c) Experimental

FIG. 6.21 Cyclic Quasi-Static Responses of Diaphragm Model MAE-2C

6.5.6 Diaphragm MAE-3

Diaphragm specimen MAE-3 was similar to diaphragm MAE-2 with the addition of a 0.81 m x 1.57 m (2 ft. 8 in. x 5 ft. 2 in.) opening located at one corner, as shown in Fig. 3.10. The FE model developed for diaphragm MAE-3 is shown in Fig. 6.22a. A total of 524 linear beam elements were used to model the joists, 446 quadratic 2D solid elements were used to model the sheathing boards, and 968 nonlinear spring elements were used to model the nails.

Monotonic displacement-controlled static analyses were performed for diaphragm model MAE-3. The deformed diaphragm is shown in Fig. 6.22b for a midspan lateral displacement of 76 mm (3 in.), scaled five times. The results from the analyses are shown in Fig. 6.23. The response based on the lower bound curve of the nailed connection model gives a closer approximation to the experimental response. The maximum force difference when comparing the lower bound response to the measured response is 5.8 kN (1.3 kips). The difference with the test results can be attributed to friction forces, which were not considered in the models. Another factor to be considered is the nail slip model adopted, which is only an approximation to the behavior of the actual nailed connection.

Cyclic quasi-static analyses were performed for diaphragm MAE-3. Figs. 6.24a and 6.23b show the cyclic responses based on the lower and upper bound models of the nailed connections, respectively. The measured response of diaphragm MAE-3 is shown in Fig. 6.24c. Table 6.8 shows values of the dissipated energy and stiffness (as defined in Section 6.5.1) calculated from the models and test results. The dissipated energy was underpredicted as 75% and 53% of the experimental value for the lower and upper bound models, respectively. The stiffness was predicted to 94% and 120% of the test value for the lower and upper bound models, respectively. The lower bound model provides a closer prediction of the static and cyclic response of diaphragm MAE-3.

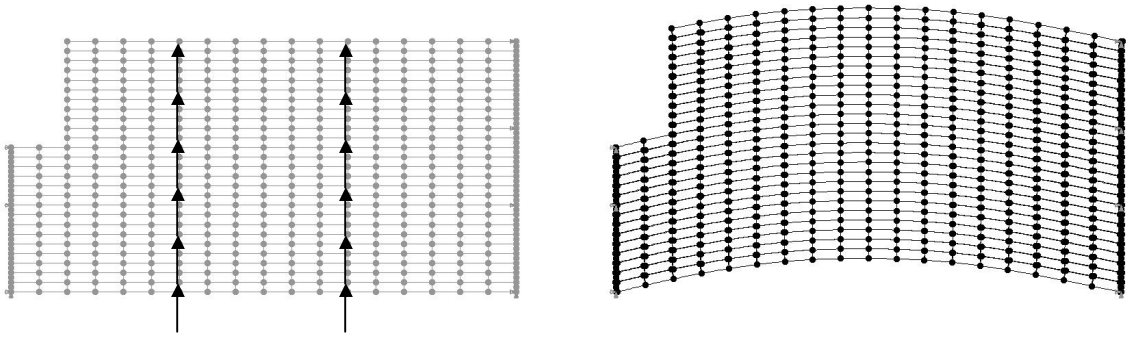

(a) Finite Element Mesh **(b) Deformed Shape**

FIG. 6.22 Diaphragm MAE-3

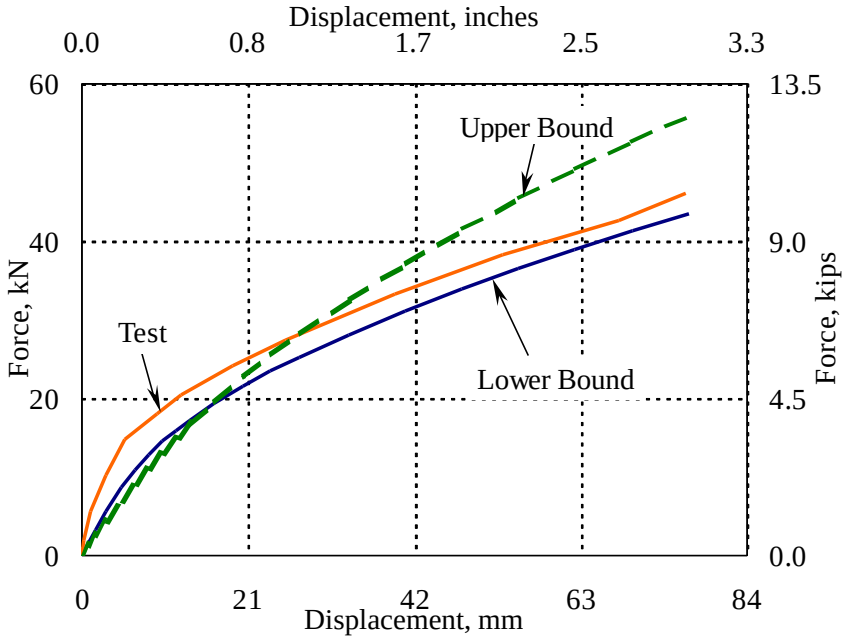

FIG. 6.23 Comparison of Static Responses of Diaphragm MAE-3 at Midspan

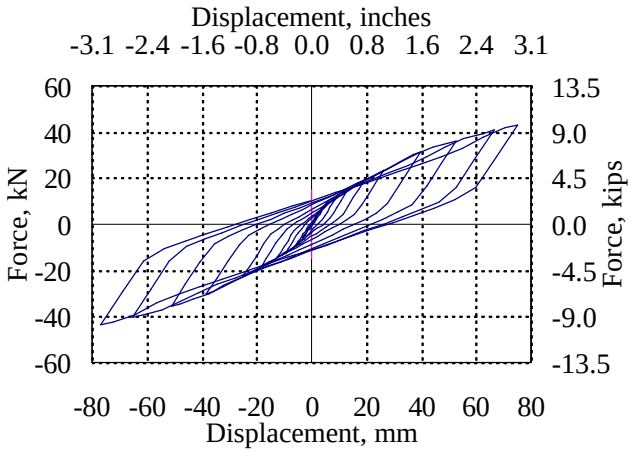

(a) Lower Bound Nailed Connection Model

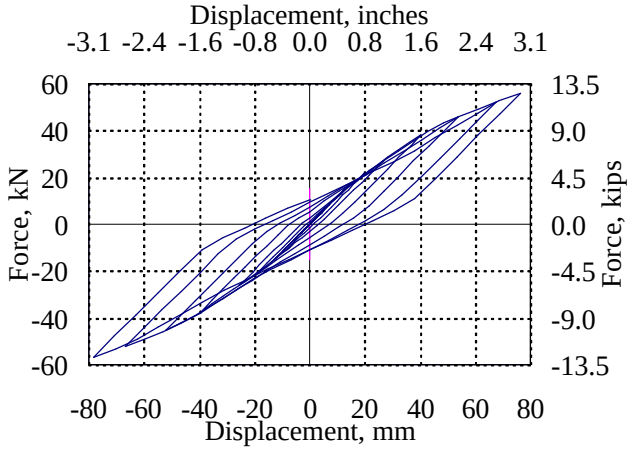

(b) Upper Bound Nailed Connection Model

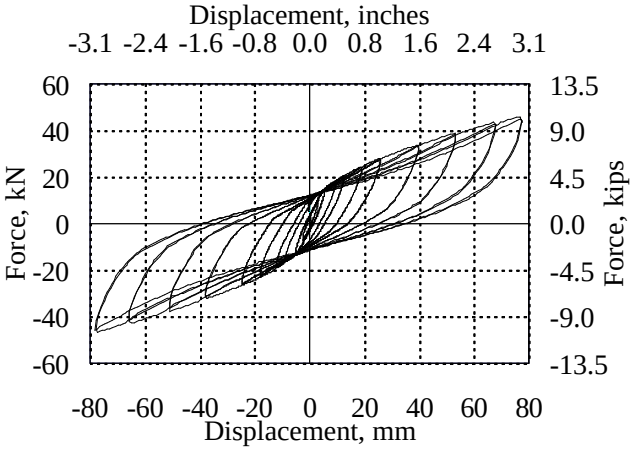

(c) Experimental

FIG. 6.24 Cyclic Quasi-Static Responses of Diaphragm Model MAE-3

TABLE 6.8 Comparison of Cyclic Responses for Diaphragm MAE-3

From	Dissipated Energy kN-cm (kip-in.)	Stiffness (last cycle) kN/cm (kips/in.)
Lower Bound Model	925 (81.9)	5.8 (3.3)
Upper Bound Model	650 (57.5)	7.4 (4.2)
Experimental	1250 (110)	6.1 (3.5)

6.5.7 Retrofitted Diaphragm MAE-3A

Retrofitted diaphragm test specimen MAE-3A included an unblocked plywood overlay, similar to diaphragm MAE-2B (see Fig. 3.11). Fig. 6.25a shows the FE model of the panel overlay. A total of 272 linear beam elements were used to model the joists, 206 quadratic 2D solid elements were used to model the plywood panels and 385 nonlinear spring elements were used to model the nails.

Separate monotonic displacement-controlled static analyses were performed for the sheathed diaphragm and the plywood panel overlay models. The responses for each model were added together to determine the response of the retrofitted diaphragm (see Section 6.5.1). Fig. 6.25b shows the deformed shape of the FE mesh magnified five times, for an applied maximum displacement of 51 mm (2 in.). The responses of model diaphragm MAE-3A are shown in Fig. 6.26. Upper and lower bound curves were used for the nailed connection model. Both responses lie below the experimental response following a path almost parallel to the test response. The model responses are similar up to 20 mm (0.8 in.), but diverge above that displacement. The similarity is attributed to the dominance of the panel overlay in the behavior of the retrofitted diaphragm. The maximum discrepancy in force is 15.6 kN (3.5 kips). The difference can be attributed to friction forces present in the test, but not included in the models. In addition, the approximation of the adopted nail slip model could contribute to this difference.

Cyclic quasi-static analyses were performed for diaphragm MAE-3A. The cyclic responses of the diaphragm shown in Figs. 6.27a and 6.27b were based on the lower and upper bound models of the nailed connection used for the square-edged sheathing boards. Table 6.9 provides values of the dissipated energy and stiffness (as defined in Section 6.5.1) of the models and experimental results. The dissipated energy values for both models were well below the experimental value, 68% and 52% of the experimental value for the lower and upper bound models, respectively. The stiffness values were underpredicted as 85% and 92% of the experimental stiffness for the lower and upper bound models, respectively, a good approximation to the experimental value.

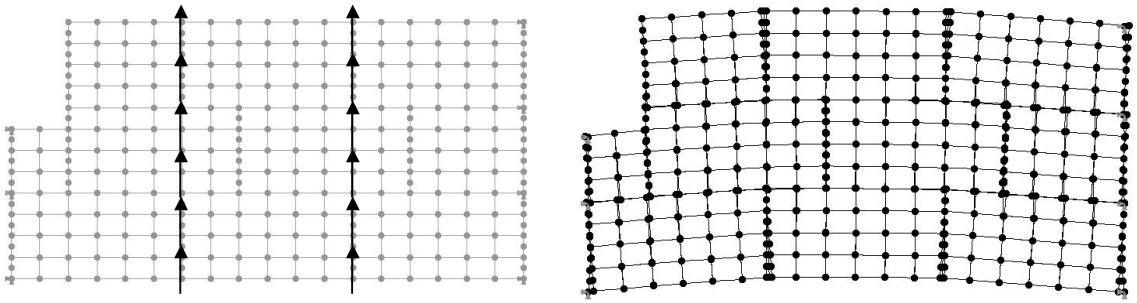

(a) Finite Element Mesh (b) Deformed Shape

FIG. 6.25 Diaphragm MAE-3A (Unblocked Panel Overlay)

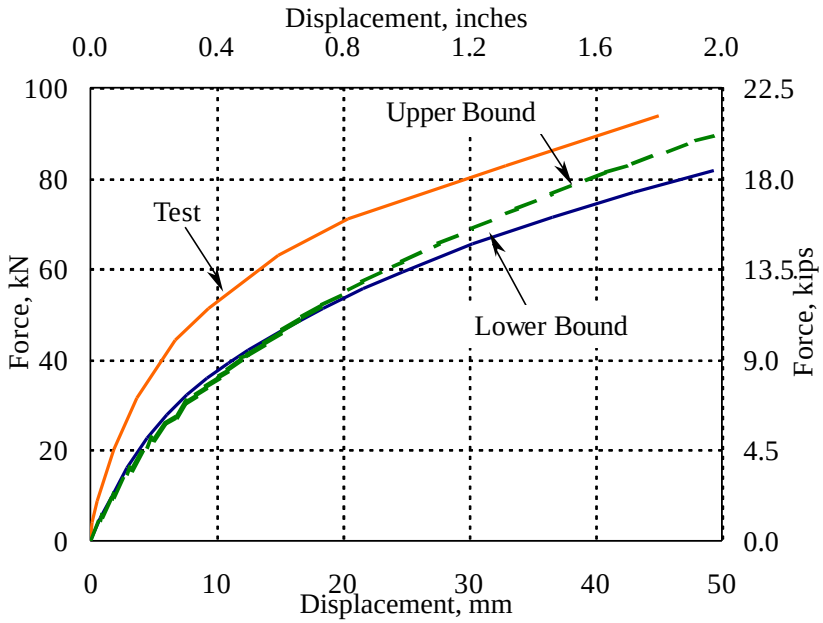

FIG. 6.26 Comparison of Static Responses of Diaphragm MAE-3A at Midspan

TABLE 6.9 Comparison of Cyclic Responses for Diaphragm MAE-3A

From	Dissipated Energy kN-cm (kip-in.)	Stiffness (last cycle) kN/cm (kips/in.)
Lower Bound Model	667 (59.0)	19.1 (10.9)
Upper Bound Model	508 (45.0)	20.7 (11.8)
Experimental	985 (87.2)	22.4 (12.8)

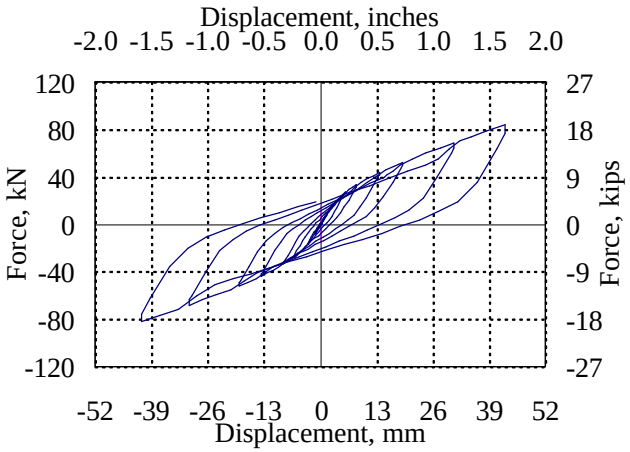

(a) Lower Bound Nailed Connection Model

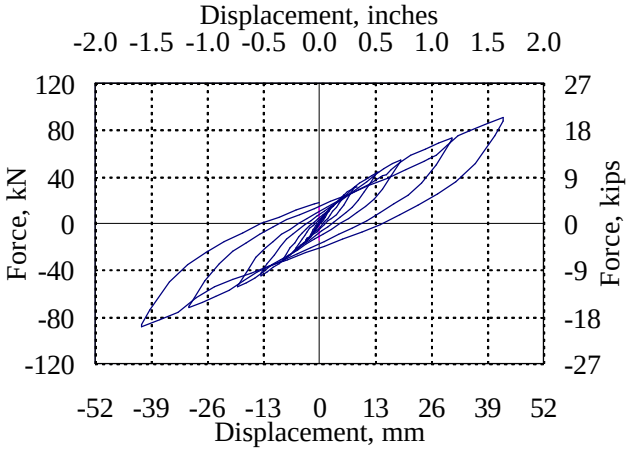

(b) Upper Bound Nailed Connection Model

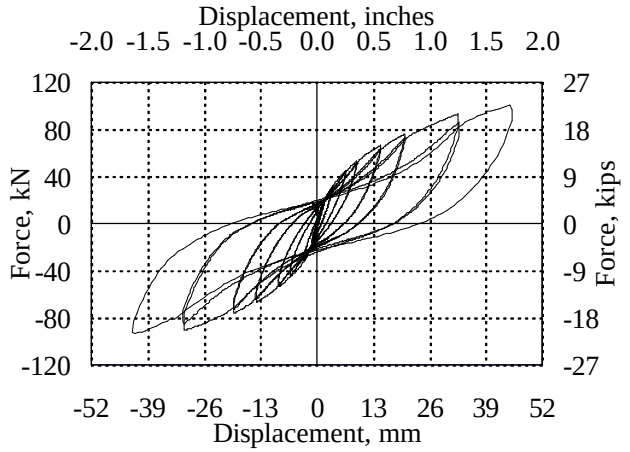

(c) Experimental

FIG. 6.27 Cyclic Quasi-Static Responses of Diaphragm Model MAE-3A

6.5.8 Retrofitted Diaphragm MAE-3B

Retrofitted diaphragm specimen MAE-3B included the addition of 2x4 blocking boards for a blocked plywood panel overlay, similar to diaphragm MAE-2C. A steel strap was attached along the short side of the opening with 8 mm diameter x 76 mm (0.3125 in. diameter x 3 in.) lag screws spaced at 51 mm (2 in.) centers.

The FE model of the panel overlay is shown in Fig. 6.28a. The model had 272 linear beam elements to model the joists, 206 quadratic 2D solid elements to model the plywood panels, 489 nonlinear spring elements to model the nailed connections and 140 nonlinear springs to model the blocking boards. Each spring element used for the nailed connections represented the response of several nails (3 to 4) in parallel. This allowed the use of the same mesh developed for the unblocked panel diaphragm (MAE-3A).

Separate monotonic displacement-controlled static analyses were performed for each layer of diaphragm model MAE-3B and added together to determine the response (see Section 6.5.1). A plot of the deformed shape of the diaphragm for the maximum applied lateral displacement 38 mm (1.5 in.) is shown in Fig. 6.28b. The displacements are factored five times. The monotonic responses of model MAE-3B are compared with the measured response in Fig. 6.29. The retrofitted diaphragm responses using the upper and lower bound nailed connection model have almost the same values and slightly overestimated the test results, with a maximum difference of 17.8 kN (4 kips). The responses are similar because of the similar behavior of both models in the unretrofitted diaphragm for the displacement range analyzed.

Cyclic quasi-static analyses were performed for diaphragm MAE-3B. The cyclic responses of the diaphragm based on the lower and upper bound nailed connection models are shown in Figs. 6.30a and 6.30b. The measured response, shown in Fig. 6.30c, includes only the unperturbed loops, for comparison with the model results. Table 6.10 compares the dissipated energy and stiffness for the models and test results.

The dissipated energy was significantly underpredicted as 44% and 37% of the experimental value for the lower and upper bound models, respectively. The stiffness values were overpredicted as 112% of the experimental stiffness for both nailed connection models.

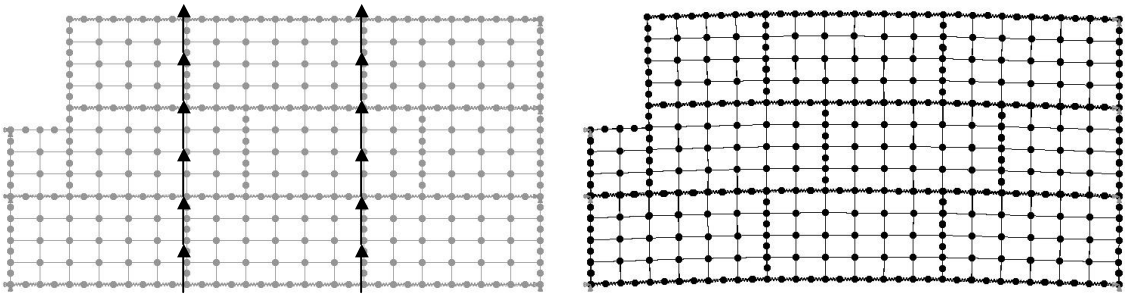

(a) Finite Element Mesh **(b) Deformed Shape**

FIG. 6.28 Diaphragm MAE-3B (Blocked Panel Overlay)

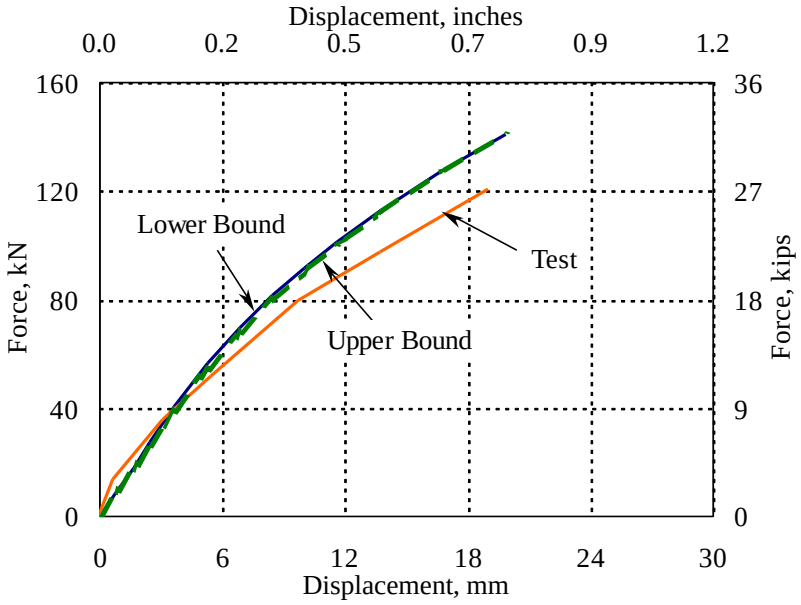

FIG. 6.29 Comparison of Static Responses of Diaphragm MAE-3B at Midspan

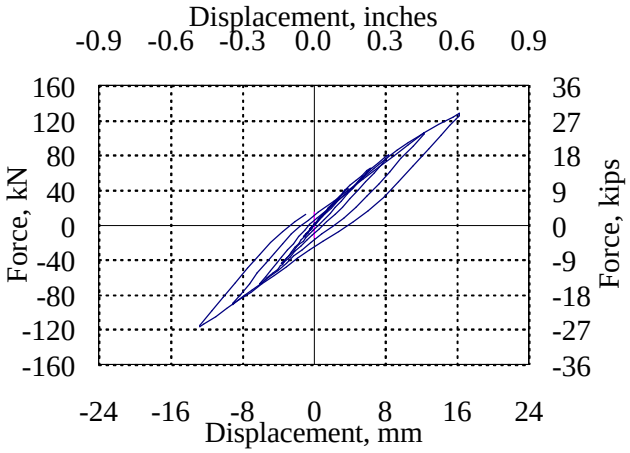

(a) Lower Bound Nailed Connection Model

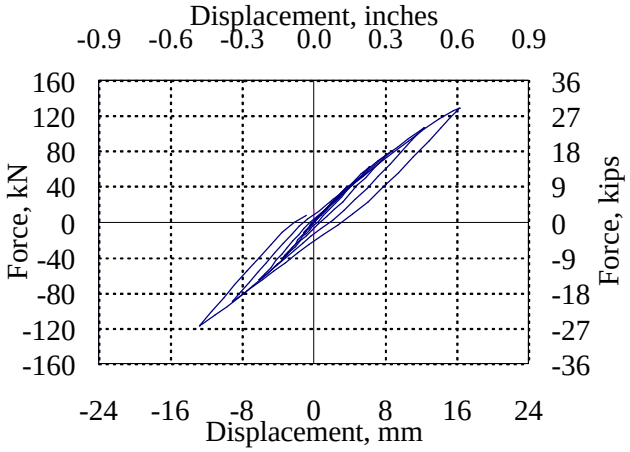

(b) Upper Bound Nailed Connection Model

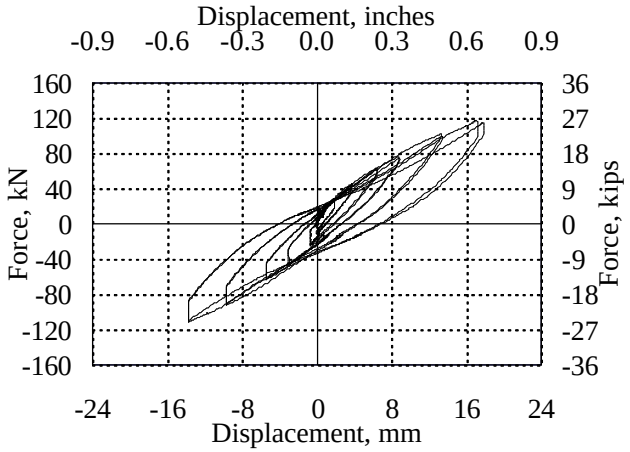

(c) Experimental

FIG. 6.30 Cyclic Quasi-Static Responses of Diaphragm Model MAE-3B

TABLE 6.10 Comparison of Cyclic Responses for Diaphragm MAE-3B

From	Dissipated Energy kN-cm (kip-in.)	Stiffness (last cycle) kN/cm (kips/in.)
Lower Bound Model	140 (12.4)	83.4 (47.6)
Upper Bound Model	107 (9.50)	84.1 (48.0)
Experimental	301 (26.6)	74.6 (42.6)

6.5.9 Nailed Connection Behavior

Is important to describe the behavior of the nailed connection for lateral loads because the behavior of the diaphragm is governed by the characteristics of its primary connections and because failure of the diaphragm starts at the most deformed nailed joint. The behavior of the nailed connections that have the most deformation in the diaphragm models under cyclic loading is shown in Fig. 6.31. The hysteretic responses shown in the figure were determined in the following sequence:

(1) The most deformed spring element was identified after observation of the deformed shape of the diaphragm FE models when subjected to static loads.
(2) A cyclic quasi-static analysis was performed on the diaphragm FE model to determine the history of displacements at both ends of the spring element.
(3) Because the spring was defined in ABAQUS as a user element, the spring force could not be determined in this analysis. A single spring element of the diaphragm model was analyzed separately applying the history of elongations found for the most deformed spring element to determine the corresponding force.

The cyclic responses of the joints shown in Fig. 6.31 are from diaphragms MAE-2 and MAE-2B, which were selected for the square-edged straight sheathing and plywood panel overlay connection, respectively. It can be observed that the maximum elongation of the square edged straight sheathing connections (lower and upper bound)

is below 4 mm (0.15 in.). For the case of the plywood panel overlay connection, the maximum elongation is 5 mm (0.20 in.). These results can help explain the better accuracy obtained in the unretrofitted diaphragm models compared to the retrofitted diaphragm models. As mentioned in Section 6.4.1.1, the accuracy of the straight sheathing nailed connection model is limited to a maximum displacement of 2.5 mm (0.10 in.). Beyond this value the model forces tend to have lower values than the actual forces developed in the nailed connection. The APA model for the plywood panel type of nailed connection does not have a limiting displacement for its accuracy, but it reports a maximum load of 979 N (220 lbs.). Although the slip values reached in the unretrofitted and retrofitted diaphragms were below the maximum slip of 12.7 mm (0.5 in.) adopted in Section 6.4.1 to control failure of the nailed connection for lateral loads, withdrawal of the nailed connections might occur as was reported in the tests of the diaphragm specimens. At the corner of diaphragm specimen MAE-3B, retrofitted with unblocked plywood panel overlay, the nails attaching the panels popped out suggesting axial forces (withdrawal) occurred in the nails during lateral loading of the diaphragm.

To determine quantitatively the influence of the nailed connections on the behavior of straight-sheathed diaphragms, an example calculation was done for specimen MAE-2. To determine the contribution of the diaphragm sheathing only, one board of the sheathing was idealized as a simply supported beam with the same span length of the diaphragm, and loaded at the third points of the beam. Then the sheathing midspan displacement can be determined for this type of loading. Or, for a given displacement the loading force on the sheathing can be obtained as:

$$F_{sheathing} = \frac{1296EI\Delta}{23L^3} \tag{6.12}$$

where:

$F_{sheathing}$ = Sheathing force
E = Young modulus of wood, see Table 6.1
I = Moment of inertia of a 1x6 sheathing board, bending about strong axis

Δ = Midspan displacement
L = Diaphragm span

The diaphragm force is determined by multiplying the sheathing force by the number of rows of sheathing boards, *n*. From Eq. 6.12 and the number of sheathing rows (26), the total force that corresponds for a midspan displacement of 76 mm (3 in.) is 15.3 kN (3.44 kips).

The diaphragm force was calculated using a modified FE model of specimen MAE-2, which had only 5% of the original force that defines the force-displacement relationship for the non-linear spring model. Having a reduced contribution of the springs, the diaphragm response can be attributed to the sheathing only. The sheathing force at 76 mm (3 in.) of displacement results in a similar value as obtained with Eq. 6.12 and is approximately one third of the force considering the full nail slip model (Lower Bound curve in Fig. 6.14). Therefore, the nailing controls the lateral response of straight-sheathed diaphragms, providing approximately two thirds of the total in-plane force. Table 6.11 compares the forces obtained for the sheathing and nailing components.

TABLE 6.11 Contribution to the Response of Sheathing and Nailed Connections. Force at 76 mm of Midspan Displacement for Diaphragm MAE-2

Component	Force, kN (kips)
Sheathing + Nailing	43 (10.5)
Sheathing	15.3 (3.44)
Nailing	27.7 (7.06)

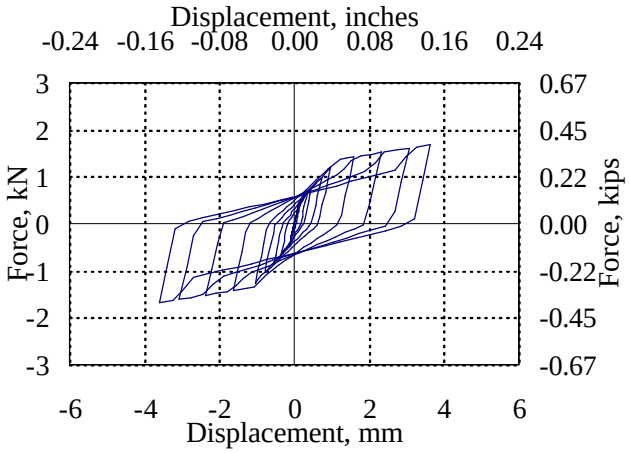

(a) Square Edged Sheathing - Lower Bound Nailed Connection Model

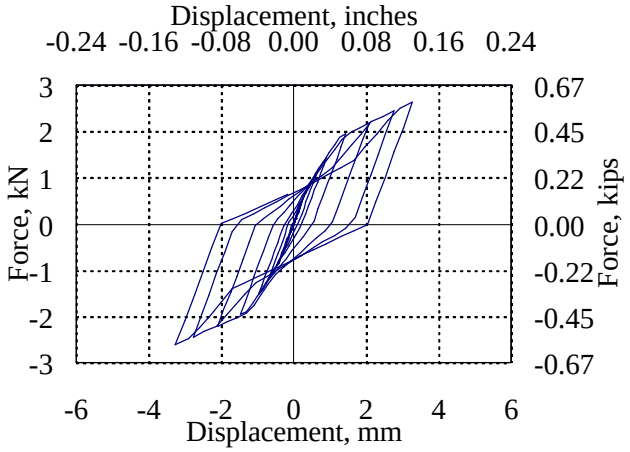

(b) Square Edged Sheathing - Upper Bound Nailed Connection Model

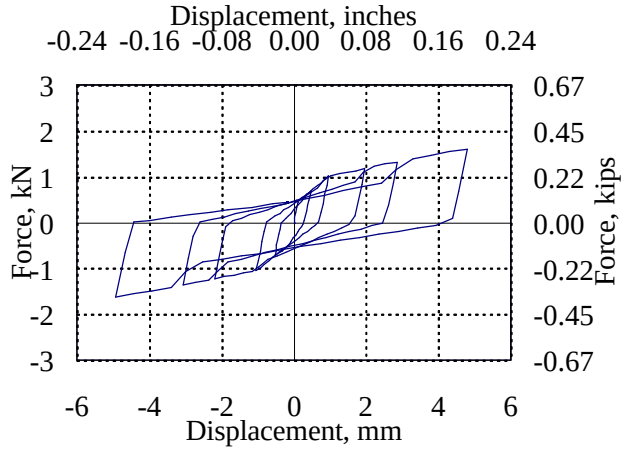

(c) APA Plywood Nailed Connection Model

FIG. 6.31 Hysteretic Curves of the Most Deformed Nailed Connections

6.6 SUMMARY

This section described the details of the finite element models and analyses of the diaphragm specimens with a comparison to the experimentally measured behavior. Linear finite elements were used to model the wood members and nonlinear springs were used for the nailed connections. The nonlinear springs adopted existing models for the shear force–slip backbone curves of two types of nailed connections: T&G and square edged sheathing board as side member (McLain, 1975); and plywood as side member (Countryman, 1952). Hysteretic behavior, based on the three-parameter model (Park et al., 1987), was also modeled for the nailed connections for the cyclic quasi-static cases. Diaphragm responses were computed for monotonic and cyclic loading.

The linear elastic FE analysis of diaphragm MAE-1 (T&G sheathing) significantly underpredicted the stiffness and strength of the diaphragm. A geometrically nonlinear analysis which considers stretching of the joists was then performed which resulted in a higher strength but showing a different behavior when compared to the experimental response. The difference in the response can be attributed to the presence of friction forces acting among the surfaces of the sheathing (between the interlocking tongue & groove) and between sheathing and joists in the actual diaphragm specimen. The FE model developed requires improvement beyond the scope of the study to be able to predict the behavior of this type of diaphragms under lateral loads. The T&G diaphragm was more flexible when compared to straight-sheathed diaphragms because only one nail is used for each sheathing-to-joist connection and therefore, a moment couple could not be developed in the connection. Additionally, the direction of loading applied was such that the T&G diaphragm framing provided lower in-plane flexural stiffness through weak axis bending of the joists, as compared to the in-plane flexural stiffness of the straight-sheathed diaphragms through strong axis bending of the sheathing boards.

In general, the monotonic and cyclic responses of the square edged straight-sheathed diaphragm models MAE-2, MAE-3 and their retrofits exhibited slightly lower stiffness (as defined in Section 6.5.1) when compared to the test results. The analyses of the unretrofitted diaphragms, gave on average, a stiffness of 89% and 114% of the measured response for the lower and upper bound nailed connection models, respectively. For the panel overlay diaphragms, the stiffness was 82% and 84% of the measured value for the lower and upper bound nailed connection models, respectively; except for MAE-3B, which overpredicted the stiffness as 112% of the experimental value. The dissipated energy values from the models were always significantly lower than the experimental values, especially for the panel overlay diaphragms, with was on average as low as 41% and 55% of the measured response for the upper and lower bound nailed connection models, respectively. The analysis of the unretrofitted diaphragms gave dissipated energy values of 55% and 79% of the measured response for the upper and lower bound nailed connection models, respectively. The reasons for the differences are attributed to the friction forces that were present during testing but not included in the models. The other factor considered is inaccuracies that may be present for the adopted nailed connection model, which greatly impacts the diaphragm response.

The hysteretic parameters of the three-parameter model were calibrated for low stiffness and strength degradation and pinching effects in the diaphragm models (see Table 6.4). The best comparisons were obtained for the unretrofitted diaphragms. The good performance is attributed to the low nail slip displacement that occurred on the straight-sheathed diaphragm, so the nailed connections deformed within the range of accuracy. For the case of the retrofitted models (plywood panel overlay), the analytical results did not show sufficient dissipated energy (the loops were not wide enough).

This is attributed to the high slip displacements on the panel overlay nailed connections, which were beyond the range of accuracy of the APA nailed connection model.

Based on the values of stiffness and dissipated energy, the analysis based on the lower bound nailed connection model gave, in general, better results than the response based on the upper bound nailed connection model, for both unretrofitted and retrofitted diaphragms. Both nailed connection models perform better for the unretrofitted diaphragms, which is attributed to the lower nail slip values with respect to the nail slip values for the retrofitted diaphragms. Therefore, the use of the lower bound nailed connection model for analysis provides a good approximation of the actual behavior of nailed connections of straight-sheathed diaphragms. For retrofitted diaphragms with a plywood panel overlay, the analysis using both types of nailed connections provides a low estimation of the dissipated energy. This is attributed to the APA nail slip equation, which is not suitable for the higher values of nail slip that occurred in the retrofitted diaphragm specimens. This drawback can be changed by improving the APA nail slip equations for higher nail slip values. The required experimental testing is beyond the scope of this study.

7. RESPONSE PREDICTIONS

7.1 INTRODUCTION

To extend the scope of the experimental study of straight-sheathed wood diaphragms to similar diaphragms with varying width-to-length aspect ratios, several finite element (FE) models have been developed to predict the force-displacement static response for unretrofitted and retrofitted square edge straight-sheathed diaphragms. The retrofit selected for the analytical models is a blocked plywood panel overlay. The response predictions have been conducted for both main directions of lateral loading. The response characteristics for several aspect ratios provide information to derive a simple relationship that describes the lateral force - deflection behavior of wood diaphragms.

7.2 DESCRIPTION OF DIAPHRAGMS AND FINITE ELEMENT MODELS

Five straight-sheathed diaphragms with different geometries or framing orientation and retrofitted with blocked plywood panel overlays were modeled with the FE method to predict their behavior under in-plane lateral loads for both main directions of loading. The diaphragm models have the same characteristics as the diaphragm specimens tested experimentally, as described in Section 3. One difference is the absence of the anchor bolt connections to support the diaphragm laterally. Because no model for the anchor bolt connections was found in the literature review, it was decided to replace it with an ideal pinned connection as was done for the models discussed in Section 6. The common characteristics of the straight-sheathed diaphragms are: framing composed of 2x10 beam joists spaced 406 mm (16 in.) o.c.; sheathing composed of 1x6 square edge straight sheathing boards; nailed joints composed of two 8d common nails at interior joist support locations and three 8d common nails at the supports ends for each sheathing board. For more details about straight-sheathed diaphragms, see Section 3.2.

The common characteristics of the blocked plywood panel overlay retrofits are: a 9.5 mm (0.375 in.) thick plywood panel, arranged as shown in Fig 7.1; each plywood panel was nailed with 8d common nails spaced at 51 mm (2 in.) at the diaphragm boundaries and 76 mm (3 in.) at the other panel edges (both directions); 2x4 blocking boards were added at the unsupported edges of the panels for this purpose; and a nail spacing of 305 mm (1 ft.) was used along the intermediate joists. For more details of this type of diaphragm retrofit, see the description of the test specimens in Section 3.2. Fig. 7.1 shows the straight-sheathed diaphragms and their retrofitted diaphragms. To identify the diaphragms, the following labels were developed:

N#

where: N = diaphragm number
= indicates type of diaphragm, unretrofitted (U) or retrofitted (R)

The unretrofitted diaphragms are shown with the straight sheathing partially removed to show the joist orientation. The retrofitted diaphragms are presented with the panel overlay partially removed to show the sheathing and joist orientation. Locations of the pinned supports are shown for one direction of loading only. For the case of loading applied in the second main horizontal direction, the supports were located equally spaced along the other two horizontal edges of the diaphragms (not shown in the figure).

Diaphragms 1, 2 and 3 have the same width, while the length was one, two and three times the width dimension respectively. These three diaphragms cover a range of length-to-width aspect ratios from 1:1 to 3:1 and allow study of the variation of the diaphragm lateral response for this range of aspect ratios. Diaphragm 4 has similar overall dimensions as Diaphragm 2 but the joist framing is oriented in the long direction of the diaphragm and the sheathing is oriented accordingly in the short direction, allowing a comparison between both diaphragm types. Diaphragm 5 has a square shape with similar geometry and characteristics to the wood diaphragms of a full-scale two-

story URM building specimen that is scheduled for testing under quasi-static loads at Georgia Institute of Technology in 2002 (Yi et al., 2002).

Table 7.1 summarizes the length-to-width aspect ratio, plan dimensions, joist orientation (parallel to "short" or "long" dimensions of diaphragm) and a description of each diaphragm model. Fig. 7.1 shows the geometry of the diaphragm models. Diaphragms 1U and its retrofitted case 1R have a square shape. Diaphragms 2U and its retrofitted case 2R are similar to diaphragm specimens MAE-2 and MAE-2C, which are described in Section 3. The joists were oriented in the short direction. Diaphragms 3U and its retrofitted case 3R have the joists oriented in the short direction. Diaphragm 4U and its retrofitted case 4R have dimensions similar to diaphragms 2U and 2R, but with the joists oriented in the long direction of the diaphragm. Diaphragm 5U and its retrofitted case 5R have a square shape.

TABLE 7.1 Diaphragm Description

Diaphragm	Aspect Ratio	Dimensions m x m (ft. x ft.)	Joist orientation	Description
1U	1:1	3.66x3.66 (12x12)	short	1x6 straight sheathing
1R	1:1	3.66x3.66 (12x12)	short	1x6 straight sheathing with blocked plywood overlay
2U	2:1	7.32x3.66 (24x12)	short	1x6 straight sheathing
2R	2:1	7.32x3.66 (24x12)	short	1x6 straight sheathing with blocked plywood overlay
3U	3:1	10.97x3.66 (36x12)	short	1x6 straight sheathing
3R	3:1	10.97x3.66 (36x12)	short	1x6 straight sheathing with blocked plywood overlay
4U	2:1	7.32x3.66 (24x12)	long	1x6 straight sheathing
4R	2:1	7.32x3.66 (24x12)	long	1x6 straight sheathing with blocked plywood overlay
5U	1:1	7.32x7.32 (24x24)	short	1x6 straight sheathing
5R	1:1	7.32x7.32 (24x24)	short	1x6 straight sheathing with blocked plywood overlay

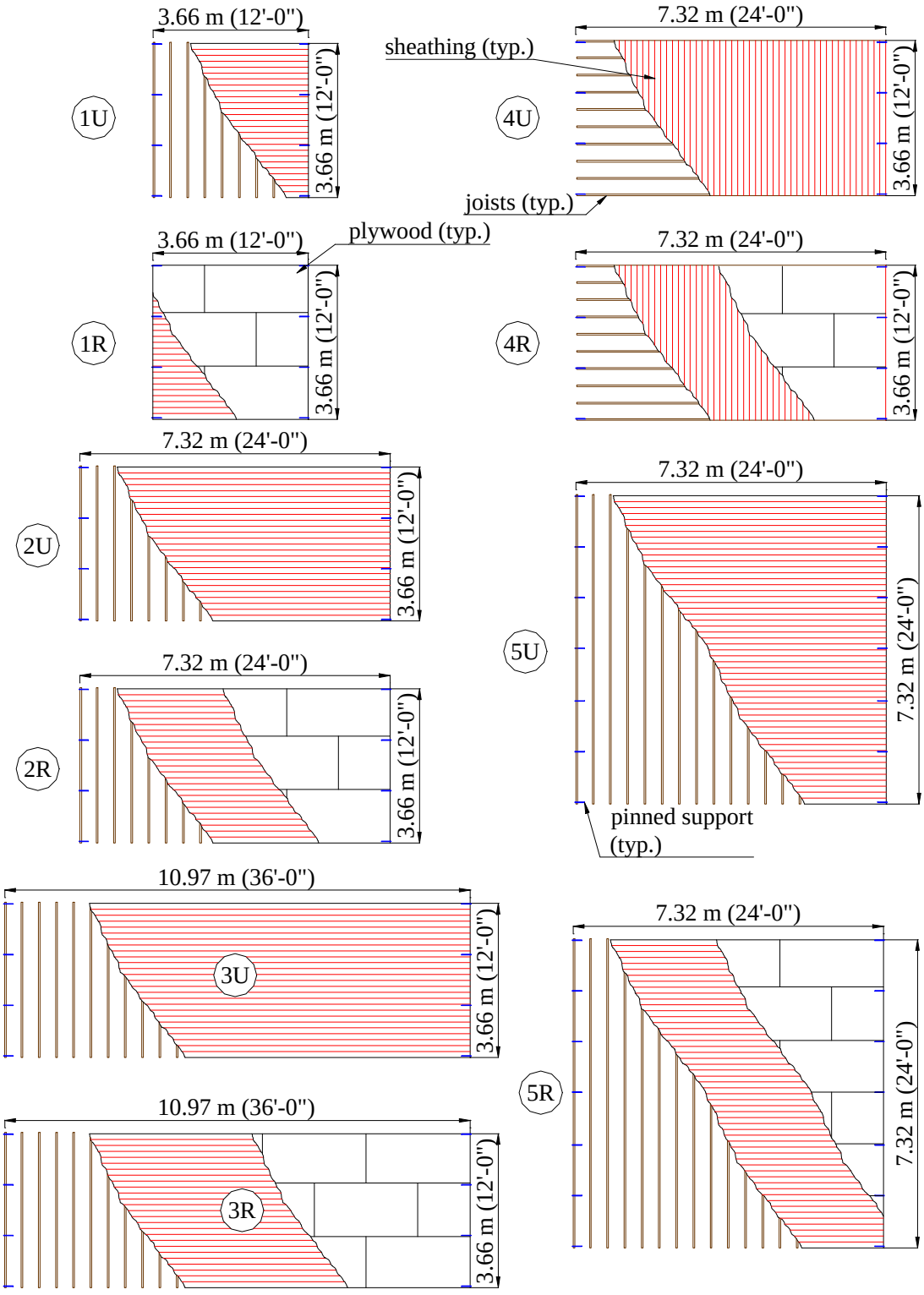

FIG. 7.1 Layout of Diaphragms

The diaphragms described previously were modeled for analysis under lateral monotonic loads using the FE program, ABAQUS. The common features of the diaphragm FE assemblages are described here. The nailed connections of the diaphragm were idealized by two perpendicular nonlinear springs. Two types of nonlinear spring elements were required. The first one models the nailed connection that has a straight-sheathed board as side member, and a second one models the nailed connection when the side member is a plywood panel. The lower bound nailed connection model based on McLain (1975) was used for the straight-sheathed connection, since it gave a better fit with the experimental data. A second model developed by APA was used for the plywood panel connection. For more details on these models refer to Section 6.4. As for the models described in Section 6, the beam joists were idealized using 2-node linear beam elements. The sheathing boards and plywood panels were idealized with 8-node rectangular plane-stress elements. Blocking boards were modeled with nonlinear spring elements to account for different axial stiffness in compression and tension.

Figs. 7.2a through 7.6a show the FE meshes for the unretrofitted diaphragms. The circles indicate the location of the spring elements, while the lines indicate the boundaries of the sheathing boards. The beam elements, which lie perpendicular to the sheathing, lie along the same lines as the spring elements. Figs. 7.2b through 7.6b show the FE meshes for blocked plywood panel overlay retrofits. The straight sheathing underneath is not included in these models. However, the combined response from the sheathing and plywood overlay is determined by superposition, as described in Section 6.5.1. The circles represent the spring elements and the horizontal and vertical lines indicate the boundaries of the solid elements used to model the plywood panels. The springs are denser along the boundaries of the plywood panels. Three to four spring elements were lumped together at the nodes as described for the blocked plywood overlay models in Section 6.5.5

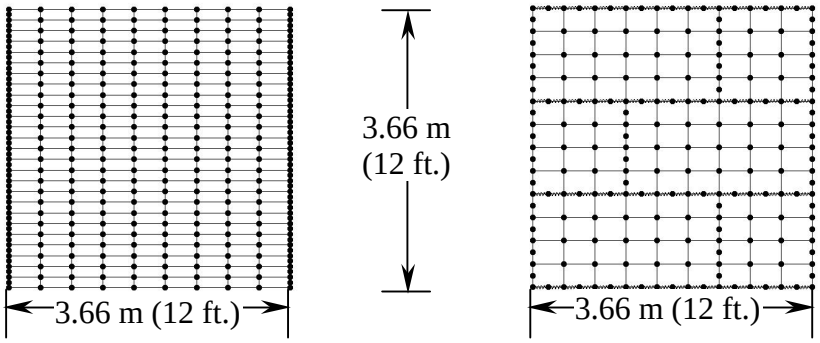

(a) Straight Sheathing – Unretrofitted **(b) Panel Overlay - Retrofitted**

FIG. 7.2 FE Meshes of Diaphragms 1U and 1R (aspect ratio 1:1)

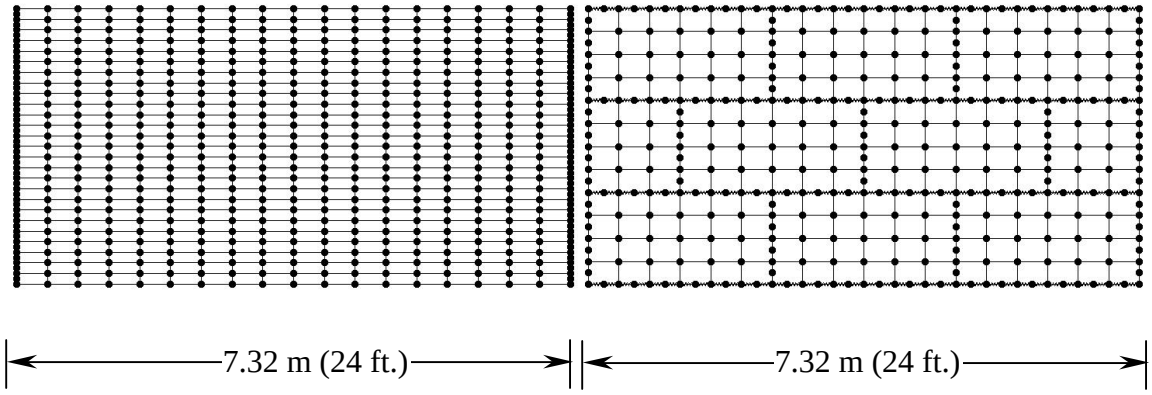

(a) Straight Sheathing - Unretrofitted **(b) Panel Overlay - Retrofitted**

FIG. 7.3 FE Meshes of Diaphragms 2U and 2R (aspect ratio 2:1)

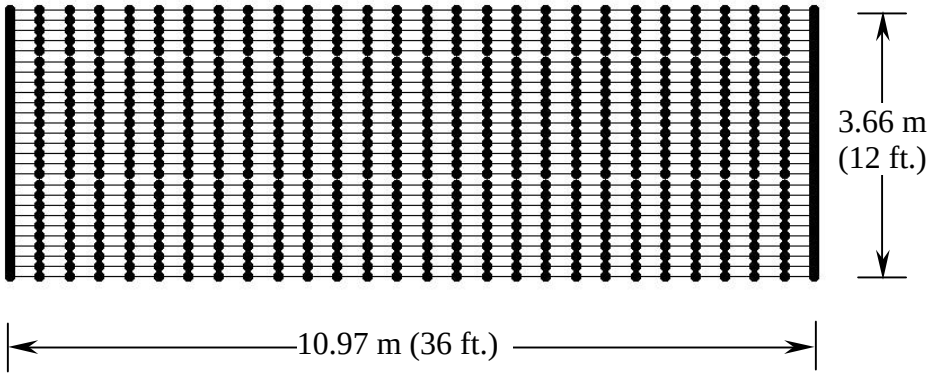

(a) Straight Sheathing - Unretrofitted

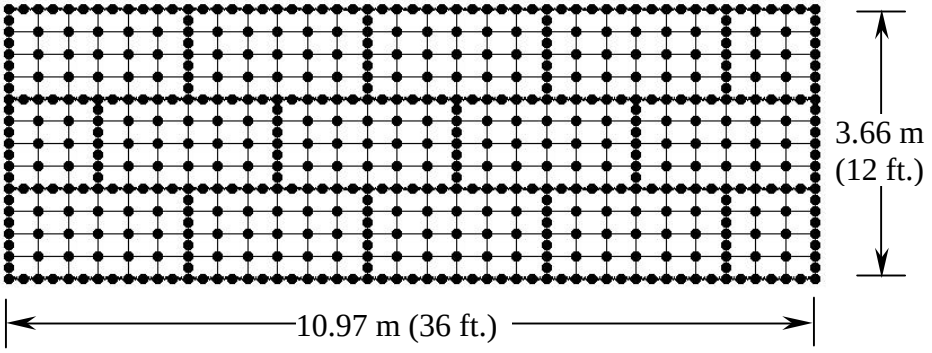

(b) Panel Overlay - Retrofitted

FIG. 7.4 FE Mesh of Diaphragms 3U and 3R (aspect ratio 3:1)

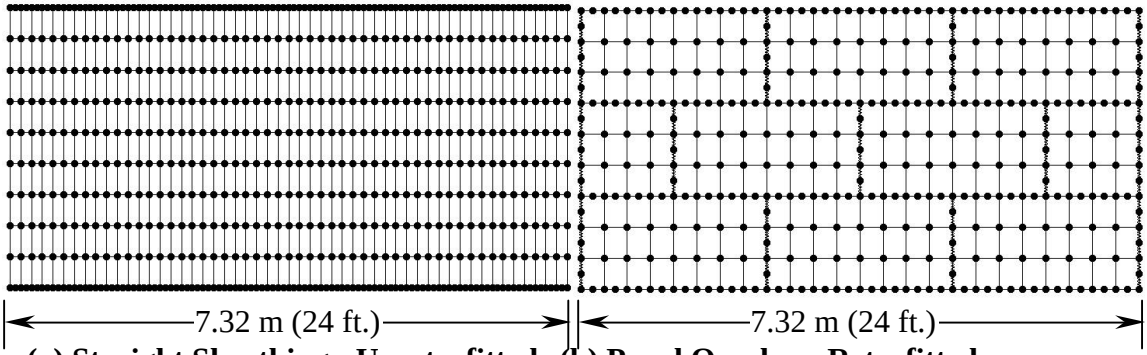

(a) Straight Sheathing - Unretrofitted (b) Panel Overlay - Retrofitted

FIG. 7.5 FE Mesh of Diaphragms 4U and 4R (aspect ratio 2:1)

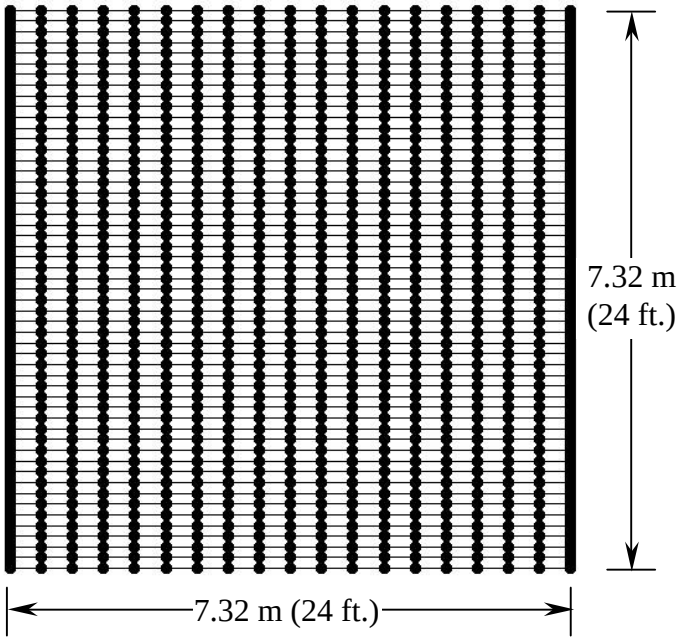

(a) Straight Sheathing – Unretrofitted

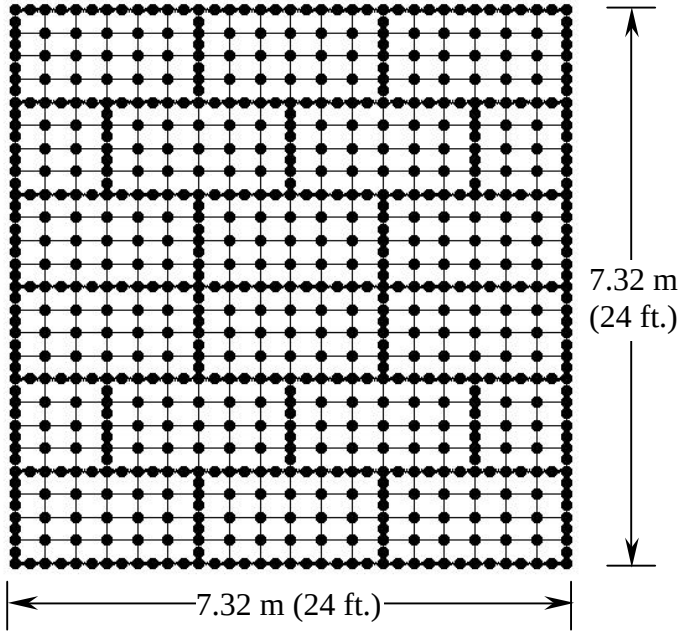

(b) Panel Overlay - Retrofitted

FIG. 7.6 FE Mesh of Diaphragms 5U and 5R (aspect ratio 1:1)

Each diaphragm model was analyzed under load in both directions, i.e. parallel and perpendicular to the joist span direction. Prescribed displacements were applied at the third points of the diaphragm length dimension perpendicular to the direction of interest. The displacements were applied monotonically from zero up to a maximum displacement of 76 mm (3 in.), similarly to the magnitude of displacements applied to the test specimens. For the purpose of developing a simple model for the lateral response, it was decided that the application of monotonic loading would provide sufficient information, instead of using cyclic loading. Fig. 7.7 shows the FE responses for monotonic and cyclic loading of the unretrofitted straight-sheathed diaphragm MAE-2 and retrofitted diaphragm MAE-2C. The monotonic response is indicated with a thick line. The superposition of both responses indicates that the monotonic response provides an accurate estimate of the envelope of the cyclic response.

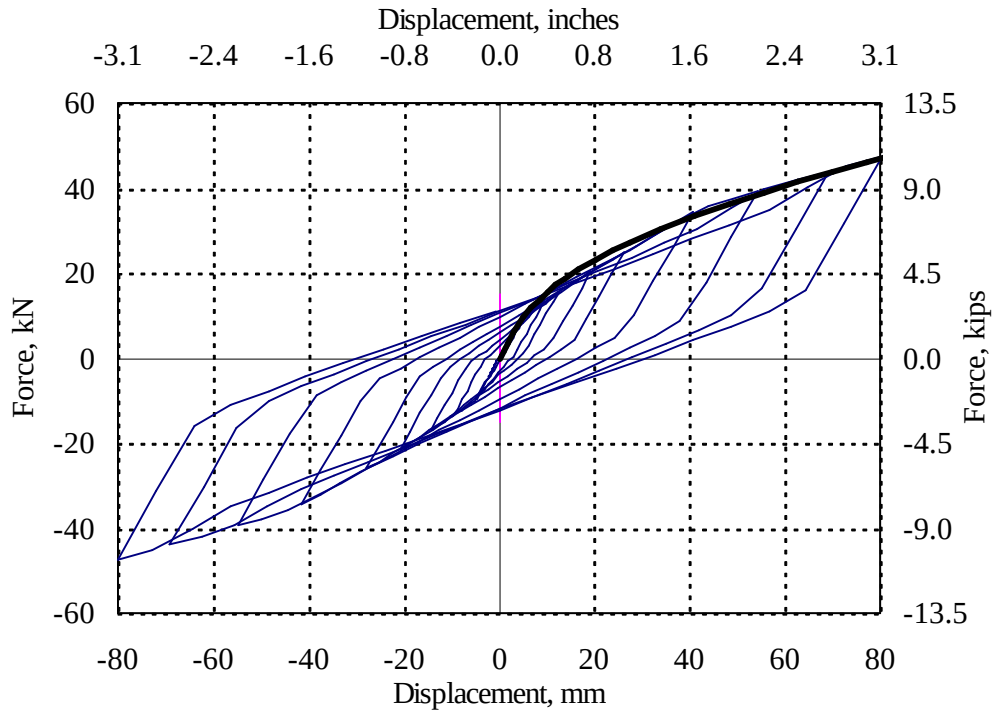

a) Unretrofitted Diaphragm MAE-2

FIG. 7.7 Superposition of Monotonic and Cyclic Responses

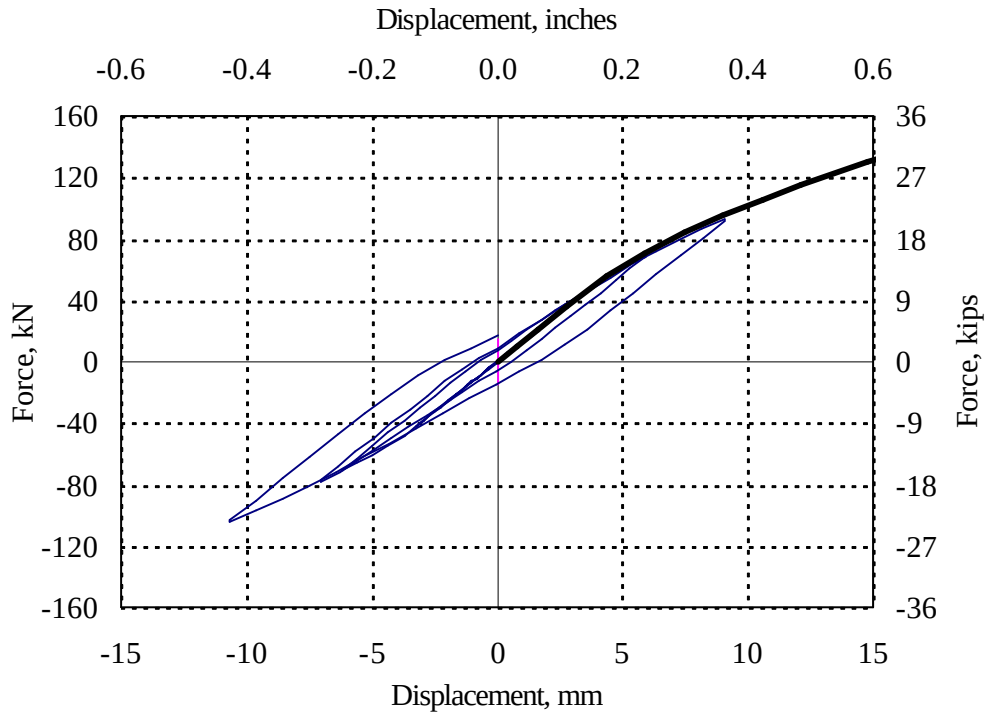

b) Retrofitted Diaphragm MAE-2C

FIG. 7.7 Continued

7.3 RESULTS AND DISCUSSION

7.3.1 General

The diaphragm response is reported in the following sections using the total reaction force per unit dimension parallel to the loading versus midspan diaphragm displacement. For some diaphragms, the analysis was terminated before reaching a midspan displacement of 76.2 mm (3 in.), because a nailed joint reached the maximum nail slip of 12.7 mm (0.5 in.) for the nailed connection models (see Section 6.4.1.). The following notation has been used to label the response curves in the figures, based on the diaphragm type and direction of the response:

NU¦ : Straight sheathed unretrofitted diaphragm, load parallel to joist span direction.

NU- : Straight sheathed unretrofitted diaphragm, load perpendicular to joist span direction.

NR¦ : Straight sheathed diaphragm retrofitted with blocked plywood panel overlay, load parallel to joist span direction.

NR- : Straight sheathed diaphragm retrofitted with blocked plywood panel overlay, load perpendicular to joist span direction.

N varies from 1 through 5 identifying the diaphragm number (see Fig. 7.1).

7.3.2 Response of Straight Sheathed Diaphragms

For comparison purposes, the response of the diaphragms with loading parallel to the joists, shown in Fig. 7.8, is divided into two groups. One group is composed of diaphragms 1U, 2U and 3U, and the second group consists of diaphragms 4U and 5U. In each group the diaphragms have the same joist span length . In the first group of diaphragms, diaphragm 1U, which has the smallest aspect ratio and the shortest sheathing boards, has the largest stiffness and strength response (1U¦). On the other hand, diaphragm 3U, having the largest aspect ratio and longest sheathing boards has the most flexible response of the three (3U¦). Similarly as in the first group of diaphragms, in the second group the response of the shorter diaphragm span (4U¦) is stronger and stiffer compared with response of the longer diaphragm span (5U¦). Also, response 4U¦ is the same of 1U¦ , when the force is normalized by the diaphragm dimension parallel to the load direction. Similarly, response 5U¦ is the same as response 2U¦ . Notice that in both pairs of diaphragms the diaphragm span, when the load is applied parallel to joists, is the same (3.66 m and 7.32 m, respectively). This similarity in the response can be explained because each sheathing board in the diaphragm contributes equally to the response. Therefore, the response per unit width (depth parallel to the load) of diaphragms with the same sheathing board lengths is the same, regardless of the number of rows of sheathing boards in the diaphragm. This suggests that it may be

adequate to model only one row of sheathing boards and then multiply the resulting response of this model by the number of rows to get the total response of the diaphragm. This approach would work only when the loading is parallel to the joists.

Following the same groups of diaphragms as before to make the comparison for the case of loading perpendicular to the joists, it was found that diaphragm 1U has the stiffest and strongest response (1U-), followed closely by responses 2U- and 3U- , as Fig. 7.9 shows. A similar tendency is found in responses 4U- and 5U- . Both groups of diaphragms show that the shorter the diaphragm span is, the stiffer its response.

The symbols in Figs. 7.8 and 7.9 indicate the first occurrence of certain nailed connection slip values within the diaphragms. The results of the analyses show that the largest nail slip values within the diaphragms occurred at the ends of the sheathing boards. In Fig. 7.8, the marks in the responses for loading parallel to the joists and the maximum slip values reported in Table 7.2 indicate that a larger maximum nailed connection slip developed in response 1U¦ followed by the nail slips of responses 2U¦ and 3U¦ . Similar tendency occurred comparing responses 4U¦ and 5U¦ . This finding suggests that the shorter the diaphragm span, the larger the nail slip. The opposite is true when the diaphragms are loaded perpendicular to the joists. As the marks in Fig. 7.9 indicate, for the same midspan displacement, the nail slip is largest in the longest diaphragm (response 3U-) and smallest in the shortest diaphragm (response 1U-), in the first group of diaphragms. Similar tendency occurred in responses 4U- and 5U- . The analysis was terminated when the nail slip reached 12.7 mm (0.5 in.) or when the total applied displacement was 76.2 mm (3 in.), whichever occurred first. Because of the constraint of limiting nail slip, the maximum midspan displacement was larger on response 1U- followed by responses 2U- and 3U- . This did not occur in responses 4U- and 5U- . The maximum nail slip reached for each analysis is reported in Table 7.2. Greater nailed connection slips are observed for loading perpendicular to the joists compared to slips for loading parallel to the joists.

TABLE 7.2 Maximum Nailed Connection Slip for Straight Sheathed Diaphragms

Diaphragm ID	Nail Slip, mm (in.) for Loading	
	Parallel to Joists	Perpendicular to Joists
1U	5.18 (0.204)	11.9 (0.468)
2U	2.87 (0.113)	12.7 (0.5)
3U	2.29 (0.090)	12.7 (0.5)
4U	5.18 (0.204)	6.07 (0.239)
5U	2.87 (0.113)	10.3 (0.407)

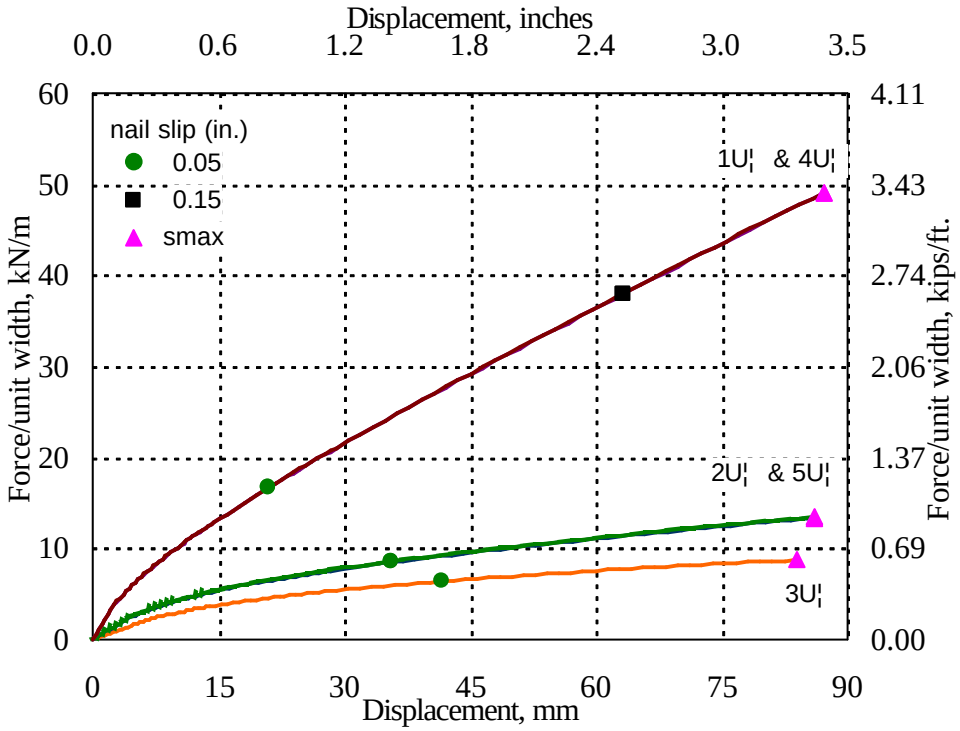

FIG. 7.8 Response of Straight Sheathed Diaphragms - Loading Parallel to Joists

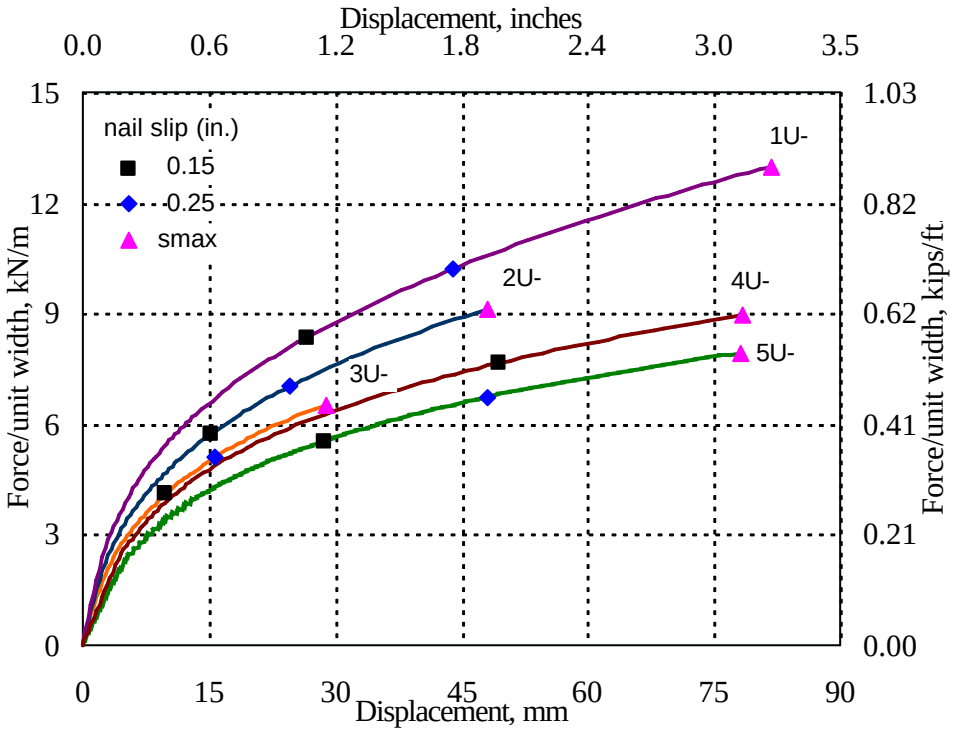

FIG. 7.9 Response of Straight Sheathed Diaphragms Loading Perpendicular to Joists

7.3.3 Response of Retrofitted Diaphragms

As expected, the response of the diaphragms retrofitted with a blocked plywood panel overlay is much stiffer and stronger than the unretrofitted diaphragms in both directions of loading. Fig. 7.10 shows the response of the blocked plywood panel overlay diaphragms for loading parallel to the joists. Comparing the response of diaphragms 1R, 2R and 3R first, response 1R¦ has the largest strength and stiffness, followed by responses 2R¦ and 3R¦ . This was expected because of the shorter span and smaller aspect ratio of diaphragm 1R, followed by diaphragms 2R and 3R. It was found that the response of diaphragms 1R and 4R are very similar, this also true for diaphragms 2R and 5R. This was expected because each pair of diaphragms has similar framing, sheathing, panel overlay arrangement and the same span. As occurred for the unretroffited diaphragms, larger nailed connection slips for the same midspan

displacement occurred in the shorter diaphragms. Compare nail slip in responses 1R¦ , 2R¦ and 3R¦ , or 4R¦ and 5R¦ shown by the marks in Fig. 7.10. Table 7.3 lists the values of maximum nailed connection slip for each diaphragm and direction of loading. The values are generally larger for loading perpendicular to the joists, compared to the other direction.

Fig. 7.11 shows the response of the retrofitted diaphragms loaded perpendicular to the joist span direction. First, diaphragms 1R, 2R and 3R are compared to each other. The responses for these three diaphragms are similar, which is reasonable because the diaphragm span length is the same for all three models. The greatest strength and stiffness response is observed in response 1R- and the smallest in response 3R- , indicating that the shorter the diaphragm width, the larger the strength and stiffness of the response. The three diaphragms develop the 0.5 in. nail slip at an average midspan displacement of 33 mm (1.3 in.). Diaphragm 4R and 5R, which have the same diaphragm span length, show similar responses and a significantly lower strength and stiffness response compared to the first group of diaphragms because they have two times the length of the other diaphragms. Similarly as occurred in the unretrofitted diaphragms, for the same midspan displacement, the nail slip was larger in the longer diaphragms (3R- followed by 2R- and 1R- , or 5R- and 4R-).

TABLE 7.3 Maximum Nailed Connection Slip for Retrofitted Diaphragms

Diaphragm ID	Nail Slip, mm (in.) for Loading	
	Parallel to Joists	Perpendicular to Joists
1R	12.7 (0.500)	12.7 (0.500)
2R	9.14 (0.360)	12.7 (0.500)
3R	6.35 (0.250)	12.7 (0.500)
4R	12.7 (0.500)	8.89 (0.350)
5R	11.4 (0.450)	12.7 (0.500)

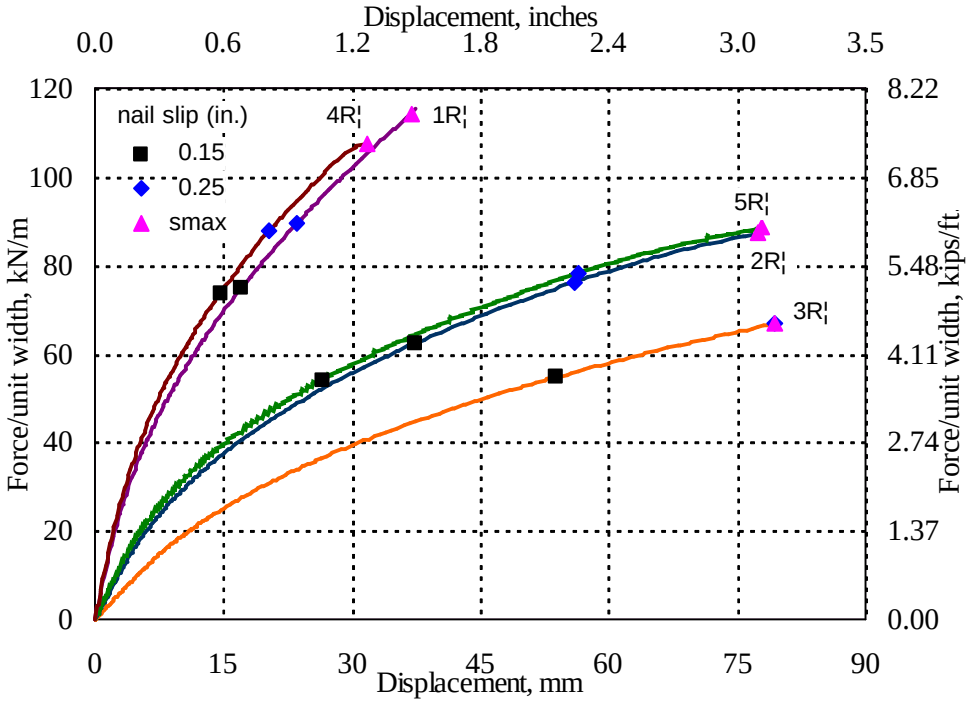

FIG. 7.10 Response of Retrofitted Diaphragms – Loading Parallel to Joists

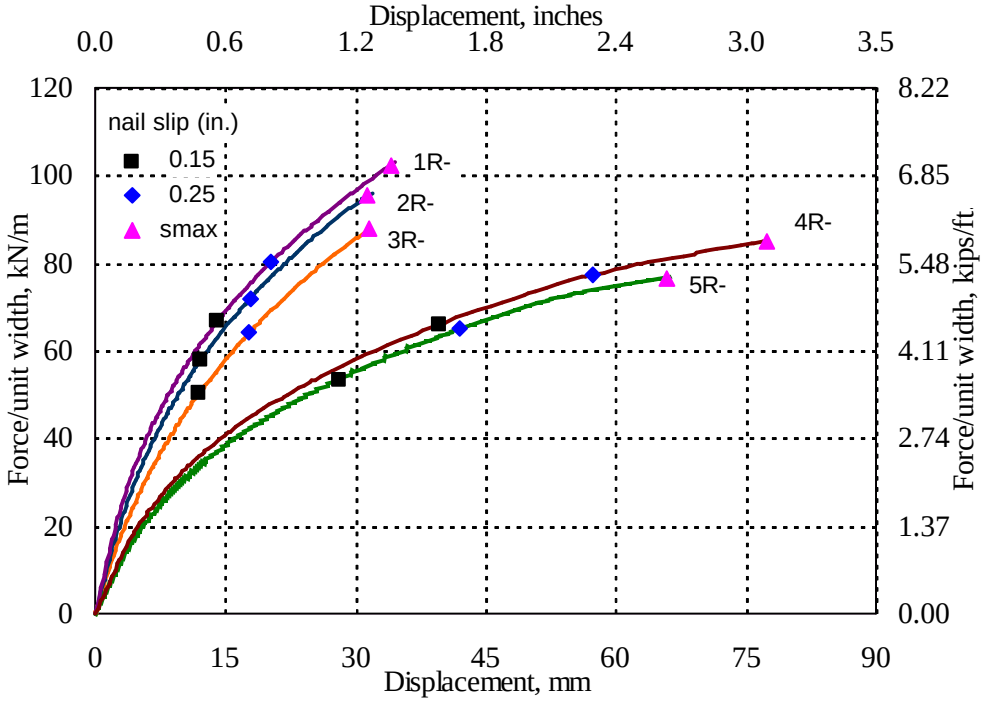

FIG. 7.11 Response of Retrofitted Diaphragms – Loading Perpendicular to Joists

7.3.4 Comparison of Diaphragm Responses

7.3.4.1 General

This section compares the four responses obtained for each diaphragm; unretrofitted and retrofitted, and for loading parallel and perpendicular to the joist span direction.

7.3.4.2 Diaphragm 1

The four types of responses for diaphragms 1U and 1R are compared in Fig. 7.12. A significant difference was observed in the responses found in each direction for the unretrofitted case (labeled as 1U¦ and 1U-). The response of diaphragm 1U¦ exhibits increasingly greater stiffness and strength than response 1U- . The different behavior is attributed to the larger flexural stiffness of the sheathing boards compared to the flexural stiffness of the joists. In the case of the retrofitted diaphragms, it was found that the blocked plywood panel overlay increases the response several times and the diaphragm response is similar in both directions. The similarity can be attributed to the square aspect ratio of the diaphragm. A small difference in the response is observed at greater displacements, which can be attributed to the difference in the sheathing response observed for the unretrofitted case.

Slip of the nailed joints of the unretrofitted diaphragm for loading perpendicular to the joists (1U-) is almost two times of the slip for loading parallel to the joists (1U¦), for the same applied displacement, as Fig. 7.12 indicate. This indicates a more significant contribution of the nailed joints to the response for loading perpendicular to the joists. In the retrofitted diaphragms, the nailed joint slip has similar values in both directions. It is observed that for the same applied displacement, the nail joint slip of the retrofitted diaphragms is two to three times larger than the nailed joint slip of the unretrofitted diaphragms. Table 7.4 lists the maximum nailed joint slip values for diaphragm 1.

TABLE 7.4 Maximum Nailed Connection Slip for Diaphragm 1

Diaphragm ID	Nail Slip, mm (in.) for Loading	
	Parallel to Joists	Perpendicular to Joists
1U	5.18 (0.204)	11.9 (0.468)
1R	12.7 (0.500)	12.7 (0.500)

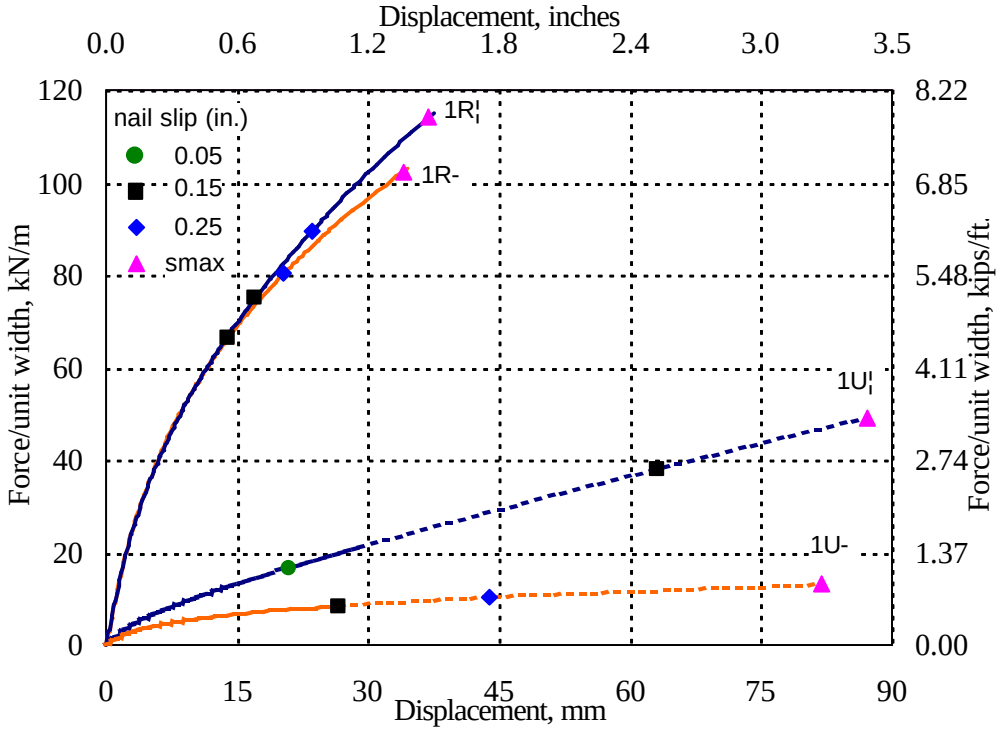

FIG. 7.12 Responses of Diaphragms 1U and 1R – Both Directions

7.3.4.3 Diaphragm 2

The normalized force versus midspan displacement responses for diaphragms 2U and 2R are shown in Fig. 7.13. It was found that the responses for the unretrofitted diaphragm are similar in both directions. For the retrofitted diaphragm 2R, the strength and stiffness for loading perpendicular to the joists (2R-) is greater than the strength and

stiffness for 2R¦ . For the same applied displacement, the total force for perpendicular loading is about 1.5 times the force corresponding to loading in the joist direction. Greater strength and stiffness was expected for loading perpendicular to the joists because the shorter span of the diaphragm gave a greater stiffness for the plywood panel overlay.

With regard to the behavior of the nailed connections, the slip for loading perpendicular to the joists in the unretrofitted diaphragm is about seven times larger than the slip for loading parallel to the joists for the same applied displacement. This indicates a more significant contribution of the nailed connections to the response for loading perpendicular to the joists. In the case of the retrofitted diaphragm and referring to the panel-to-joist nailed connections, the nailed connection slip for loading perpendicular to the joists is approximately 2.5 times larger than the slip for loading parallel to the joists, for the same applied displacement. Table 7.5 lists values of the maximum nailed connection slips for diaphragm 2.

TABLE 7.5 Maximum Nailed Connection Slip for Diaphragm 2

Diaphragm ID	Nail Slip, mm (in.) for Loading	
	Parallel to Joists	Perpendicular to Joists
2U	2.87 (0.113)	12.7 (0.500)
2R	9.14 (0.360)	12.7 (0.500)

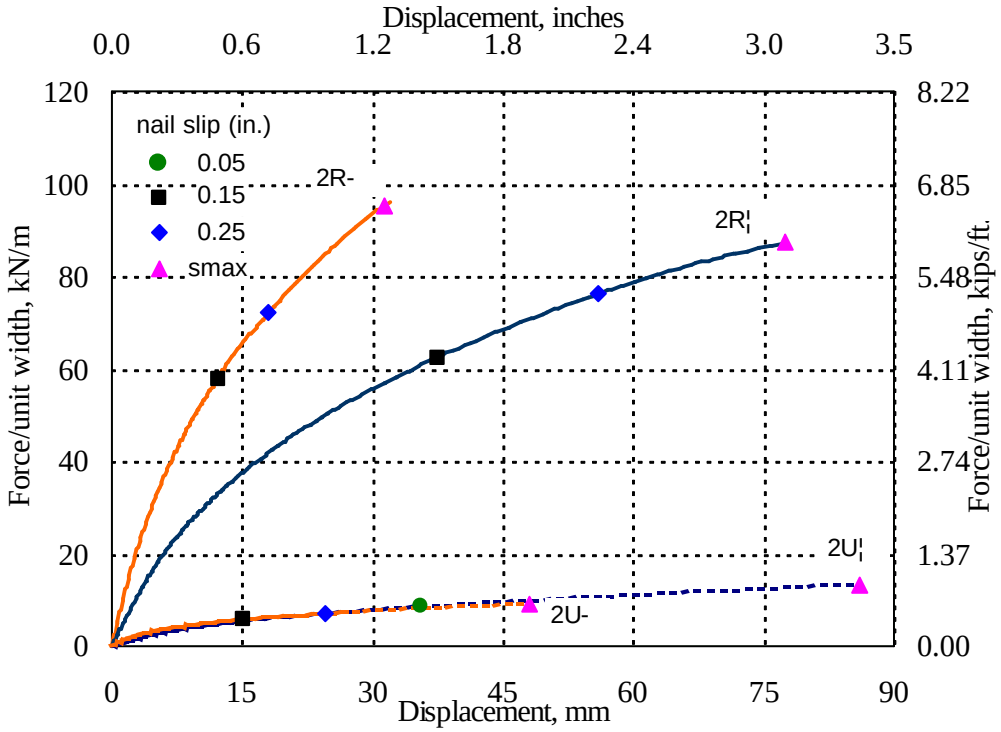

FIG. 7.13 Responses of Diaphragms 2U and 2R – Both Directions

7.3.4.4 Diaphragm 3

Fig. 7.14 illustrates the four types of responses obtained for diaphragms 3U and 3R. The unretrofitted diaphragm models show a similar response in both directions of loading. In the retrofitted diaphragm, the strength and stiffness for loading perpendicular to the joists are greater than the corresponding values for loading parallel to the joists. For the same applied displacement the total force for response 3R- is at least two times that of response 3R¦ . Response 3R- was expected to be stiffer because the shorter span of the diaphragm results in a larger in-plane stiffness of the plywood panel overlay.

It is observed that the nailed joint slip in the unretrofitted diaphragm 3U is at least ten times larger for loading perpendicular to the joists compared to the nailed joint slip for loading parallel to the joists, for the same applied displacement. This fact

indicates a more significant contribution of the nailed connections to the response for loading perpendicular to the joists. In the case of the retrofitted diaphragm 3R, nail slip of the panel-to-joist nailed connections in response 3R- is about five times greater than nail slip in response 3R¦ , for the same applied displacement. Table 7.6 lists values of the maximum nailed connection slips for diaphragm 3.

TABLE 7.6 Maximum Nailed Connection Slip for Diaphragm 3

Diaphragm ID	Nail Slip, mm (in.) for Loading	
	Parallel to Joists	Perpendicular to Joists
3U	2.3 (0.090)	12.7 (0.500)
3R	6.4 (0.250)	12.7 (0.500)

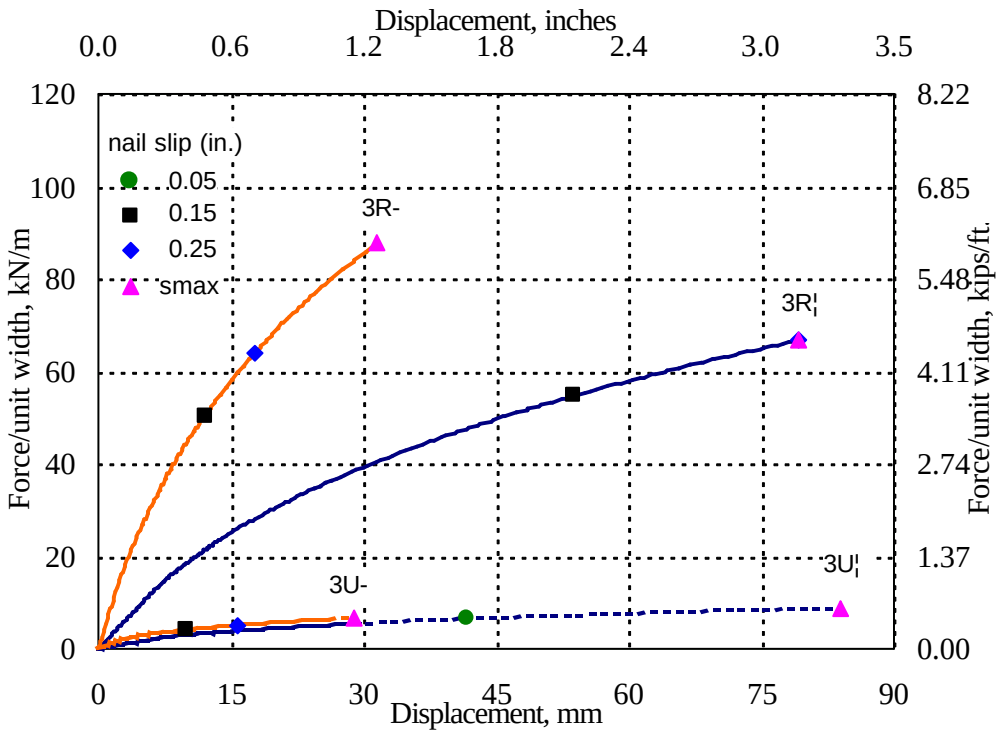

FIG. 7.14 Responses of Diaphragms 3U and 3R – Both Directions

7.3.4.5 Diaphragm 4

The responses obtained for diaphragms 4U and 4R (2:1 aspect ratio, 7.32x3.66 m) are shown in Fig. 7.15. It is observed that the response of the unretrofitted diaphragm is different in each direction of loading. The strength response for loading parallel to the joists (4U$_{\|}$) is increasingly greater than the response for loading perpendicular to the joists (4U-). A greater strength was expected because of the larger flexural stiffness provided by the sheathing boards for loading parallel to the joists, compared to the stiffness of the joists in minor axis bending for loading perpendicular to the joists. A similar behavior occurs in the retrofitted case, in which the response for loading parallel to the joists is stronger and stiffer to the response for loading perpendicular to the joists. This was expected because the additional stiffness of the assemblage of panels is larger in the shorter direction and because of the stronger and stiffer response of the unretrofitted diaphragm for this direction of loading.

It is observed that the nail slip in the unretrofitted diaphragm 4U for loading perpendicular to the joists is about 1.5 times the slip for loading parallel to the joists, for the same applied displacement. This fact indicates a more significant contribution of the nailed connections to the response for loading perpendicular to the joists. Nailed connection slip in the retrofitted diaphragm for loading parallel to the joists is about four times larger of the nailed connection slip for loading perpendicular to the joists. Table 7.7 lists values of the maximum nailed joint slips in diaphragm 4.

TABLE 7.7 Maximum Nailed Connection Slip for Diaphragm 4

Diaphragm ID	Nail Slip, mm (in.) for Loading	
	Parallel to Joists	Perpendicular to Joists
4U	5.2 (0.204)	6.1 (0.239)
4R	12.7 (0.500)	8.9 (0.350)

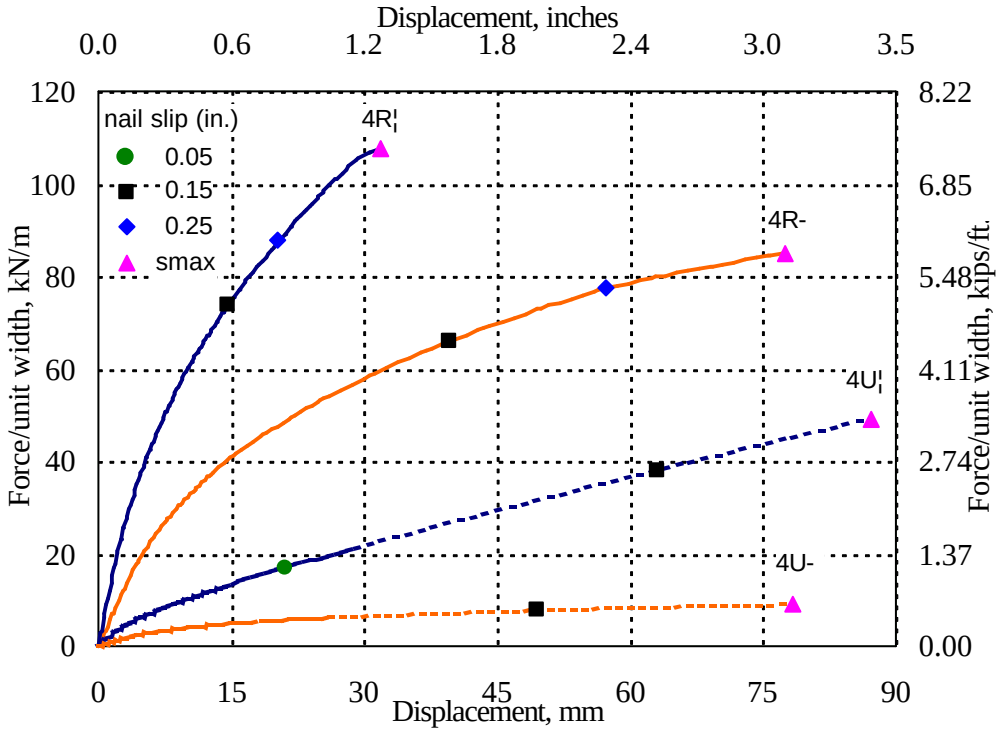

FIG. 7.15 Responses of Diaphragms 4U and 4R – Both Directions

7.3.4.6 Diaphragm 5

Fig. 7.16 shows the responses for diaphragms 5U and 5R (1:1 aspect ratio, 7.32x7.32 m). In the unretrofitted diaphragm, the response for loading parallel to the joists (5U¦) is slightly stiffer compared to the response for loading perpendicular to the joists (5U-). This result was expected because of the larger flexural stiffness of the sheathing boards compared to the stiffness of the joists. In the case of the retrofitted diaphragm 5R, the contribution of the blocked panel overlay gives a significant increase in the strength and stiffness in both directions, as observed in Fig. 7.16. A similar response is observed in both directions of loading because of the square shape of the

diaphragm. At larger displacements a small difference in the response is observed, which can be attributed to the difference in response for each direction of loading of the unretrofitted diaphragm.

Nailed connection slip in the unretrofitted diaphragm 5U for loading perpendicular to the joists is at least three times larger than the slip for loading parallel to the joists. This indicates a more significant contribution of the nailed connections to the response for loading perpendicular to the joists (parallel to the sheathing). In the nailed connections of the panel overlay, the slip is similar in either direction until a slip of 3.8 mm (0.15 in.) but after that, the slip becomes 1.5 times larger for loading perpendicular to the joists. Table 7.8 lists values of the maximum nailed connection slips in diaphragm 5.

TABLE 7.8 Maximum Nailed Connection Slip for Diaphragm 5

Diaphragm ID	Nail Slip, mm (in.) for Loading	
	Parallel to Joists	Perpendicular to Joists
5U	2.9 (0.113)	10.3 (0.407)
5R	11.4 (0.450)	12.7 (0.500)

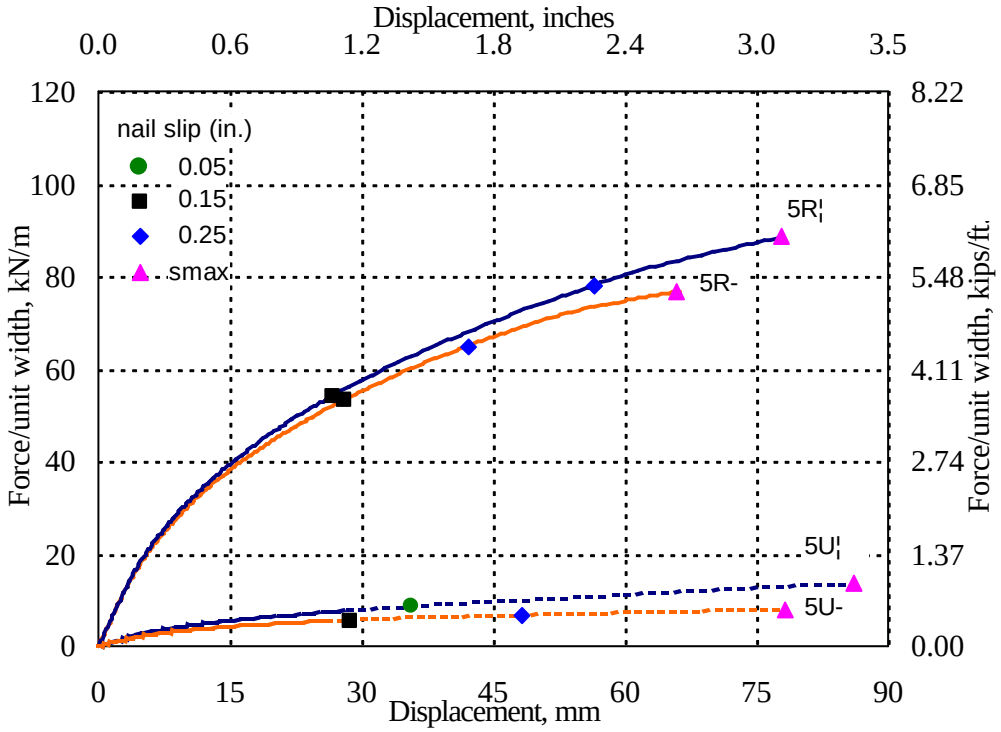

FIG. 7.16 Responses of Diaphragms 5U and 5R – Both Directions

7.3.5 Comparison of Diaphragms 2 and 4

Both diaphragms 2 and 4 have the same length-to-width aspect ratio of 2:1 with plan dimension of 7.32x3.66 m (24x12 ft.), but with the sheathing and joists oriented in the opposite direction. The comparison of their responses provides information on the level of influence of the joist and sheathing orientation in the diaphragm behavior under lateral in-plane loads. Fig. 7.17 compares the responses of the unretrofitted diaphragms 2U and 4U. The response of diaphragm 2U in the short direction is about 40% stiffer and stronger than diaphragm 4U in the same direction. But the response of diaphragm 4U in the long direction compared to the response of diaphragm 2U in the same direction of loading is at least three times stiffer and stronger.

The comparison of responses of the retrofitted diaphragms 2R and 4R are shown in Fig. 7.18. In this case the differences of the responses, for the same direction of loading, are very small. This is because the contribution of the retrofit panels to the response is much larger than the unretrofitted diaphragm response.

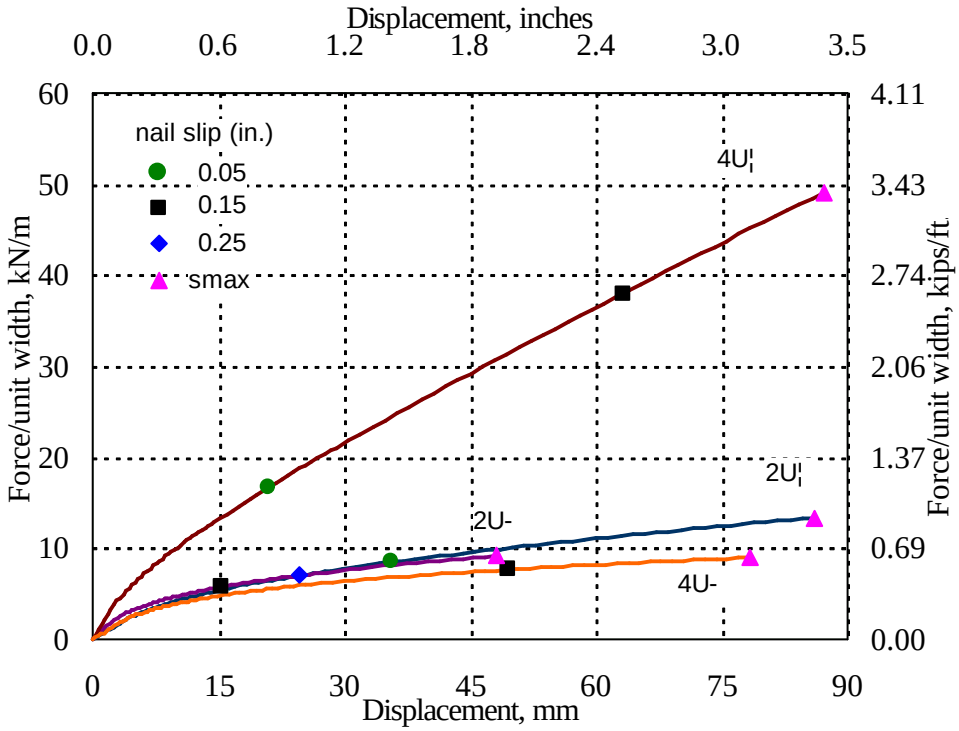

FIG. 7.17 Comparison of Responses of Diaphragms 2U and 4U

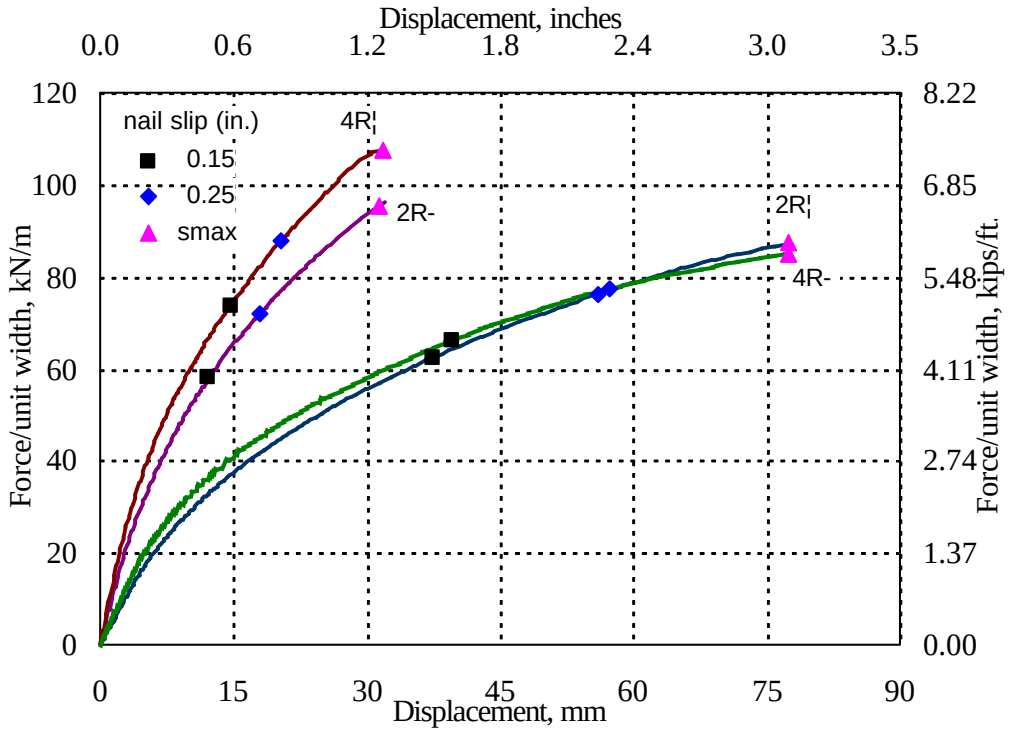

FIG. 7.18 Comparison of Responses of Diaphragms 2R and 4R

7.3.6 Comparison of Diaphragm Responses with FEMA 356 Backbone Curves

7.3.6.1 General

FEMA 273 and FEMA 356 backbone curves were constructed and compared with the FE responses of the diaphragms developed in this section. In general, the FEMA 273 curves showed very small displacement levels for most of the diaphragm length-to-width span ratios and it was decided not to continue with the comparison. Fig. 7.19 shows the FE responses and the FEMA 273 backbone curves for diaphragm 2. The backbone curves for loading perpendicular to the joists have displacement levels that are too small to be appreciated. The comparison was continued only with the results from FEMA 356.

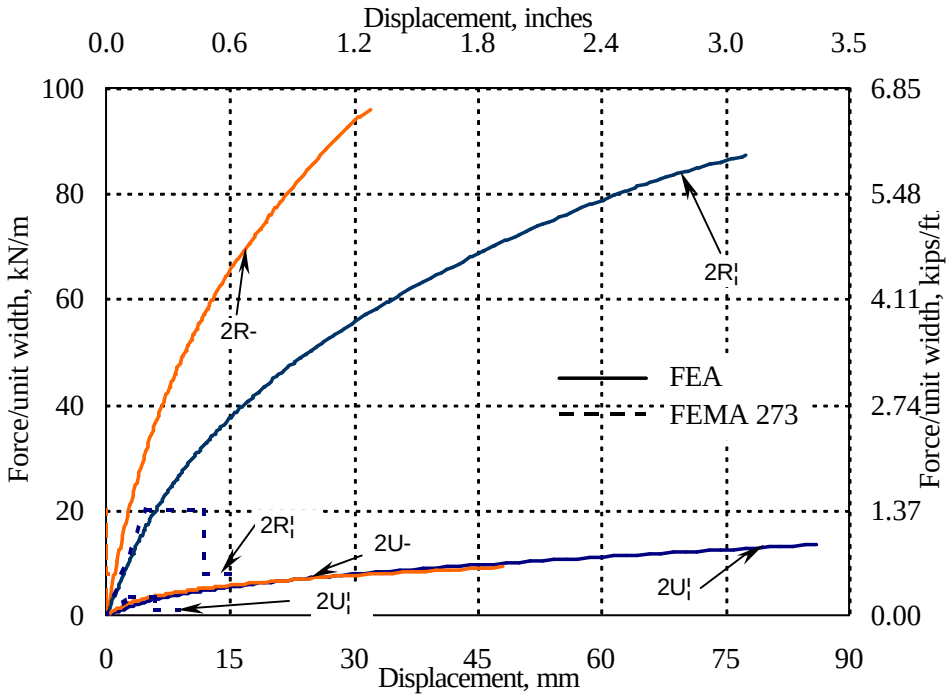

FIG. 7.19 Comparison of FE Responses and FEMA 273 Backbone Curves – Diaphragm 2

7.3.6.2 Unretrofitted Diaphragms

The backbone curves were constructed in terms of total force per unit width versus midspan displacement for both main directions of loading using the FEMA 356 guidelines. The procedure for constructing these backbone curves is given in Section 4.2. Comparison of the backbone curves based on FEMA 356 and the predicted FE responses for the unretrofitted straight-sheathed diaphragms, shown in Figs. 7.20 to 7.24, gave the following similarities and differences:

- For most cases, the strength from the FE models and FEMA 356 is at similar levels in both main directions of loading, especially for load perpendicular to joists, but only until the loss of strength occurs on the FEMA 356 backbone curves.

- Large discrepancies in strength were found for diaphragms having a short (3.66 m) span and loaded parallel to the joists ($1U_{\dagger}^{\dagger}$ and $4U_{\dagger}^{\dagger}$). For these cases, the yield shear strength has been underestimated significantly.
- In all cases, the displacement at the point of first loss of strength has been underestimated by the FEMA 356 backbone curves. In other words, parameter *d* of the FEMA backbone curve has been underestimated. (See Fig. 5.3)

From the differences found for the unretrofitted straight-sheathed diaphragms above, it is concluded that the equation that FEMA 356 uses to model the lateral deflection of unretrofitted straight-sheathed diaphragms can be made suitable after some modifications. The yield shear strength values should be extended to consider the direction of loading with respect to the diaphragm joist span. Parameter *d*, which defines the displacement at the point of first loss of strength (see Section 5.4), should be increased.

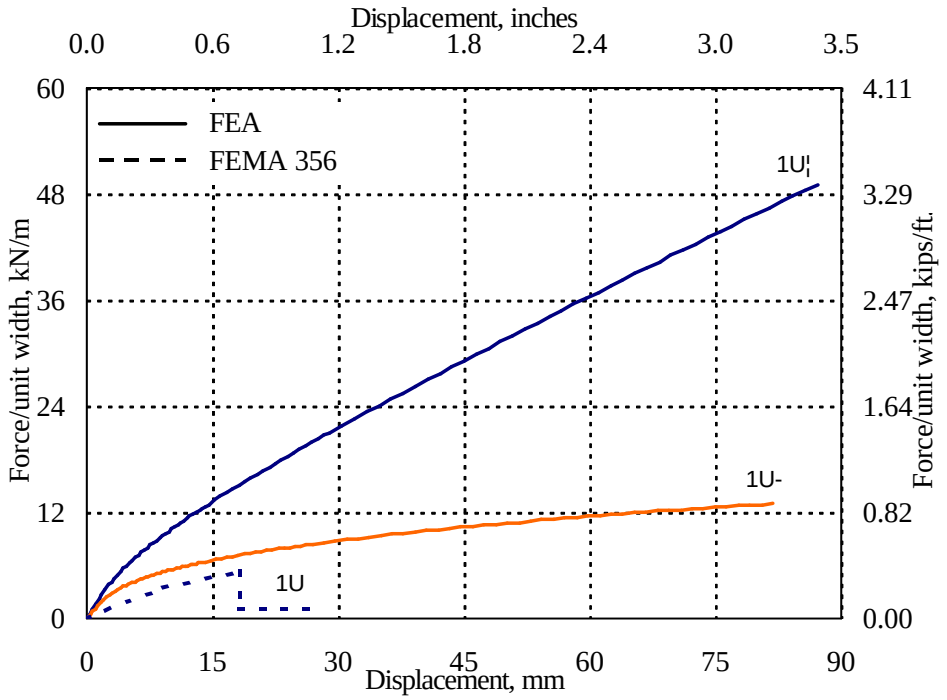

FIG. 7.20 FE Response vs. FEMA Backbone Curve – Unretrofitted Diaphragm 1

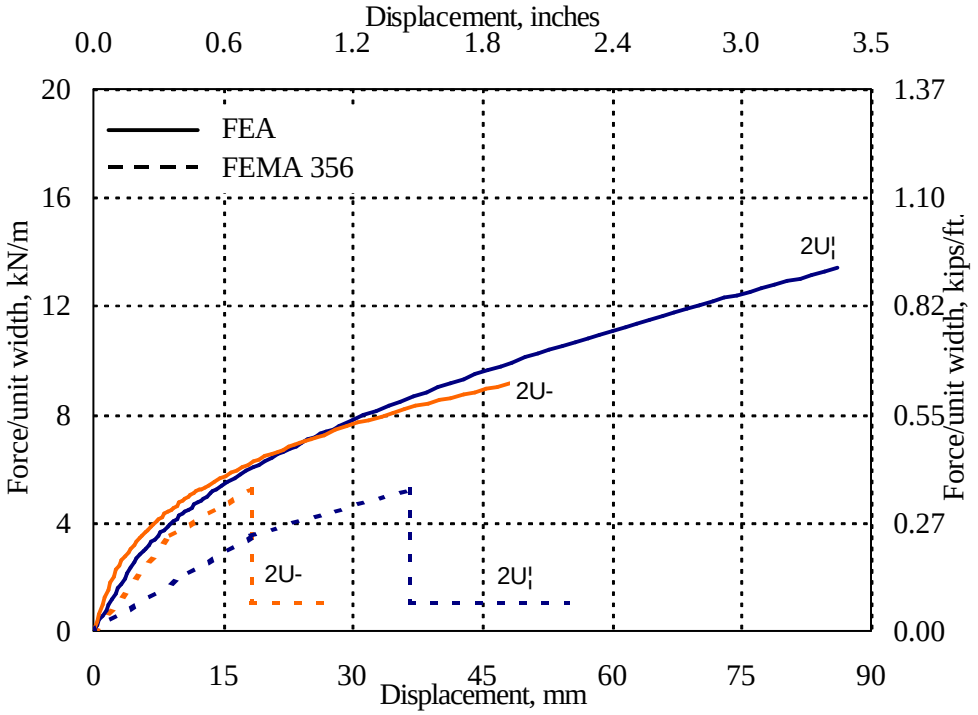

FIG. 7.21 FE Response vs. FEMA Backbone Curve – Unretrofitted Diaphragm 2

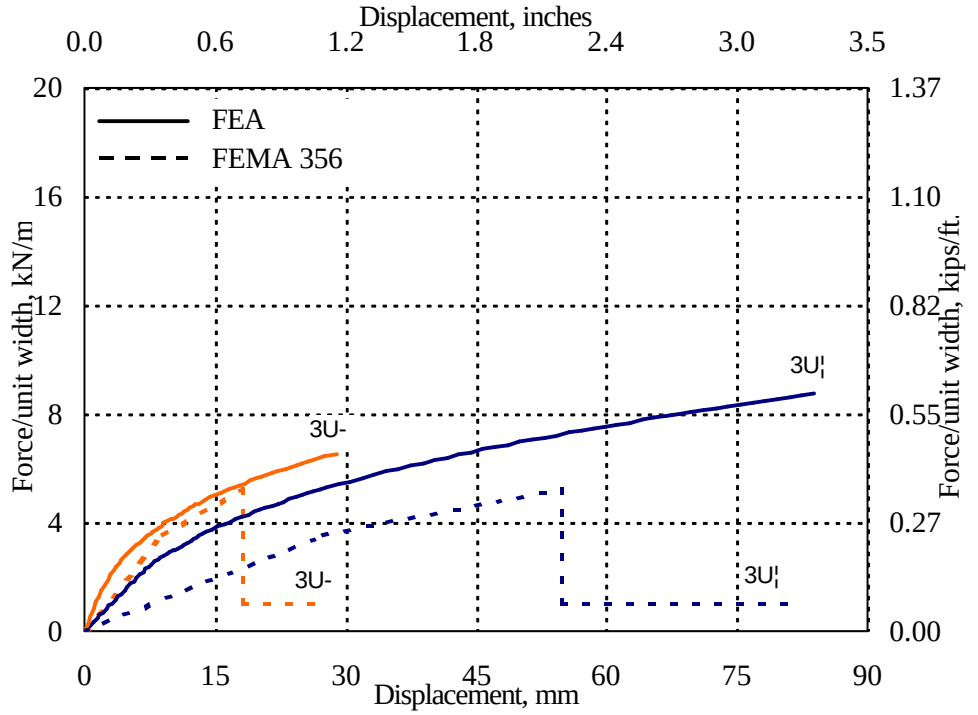

FIG. 7.22 FE Response vs. FEMA Backbone Curve – Unretrofitted Diaphragm 3

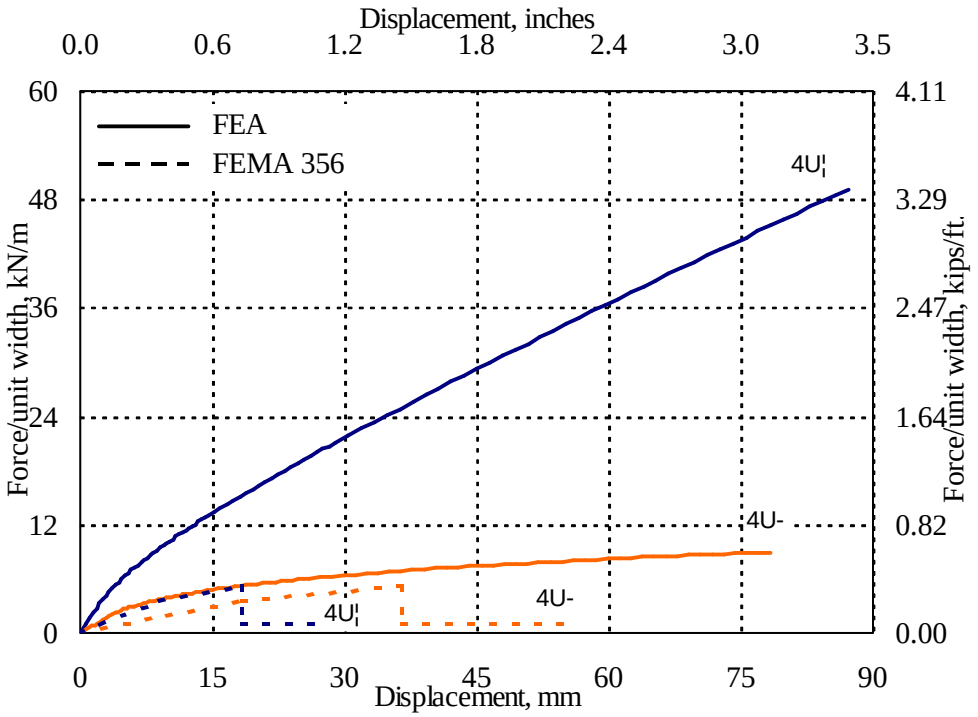

FIG. 7.23 FE Response vs. FEMA Backbone Curve – Unretrofitted Diaphragm 4

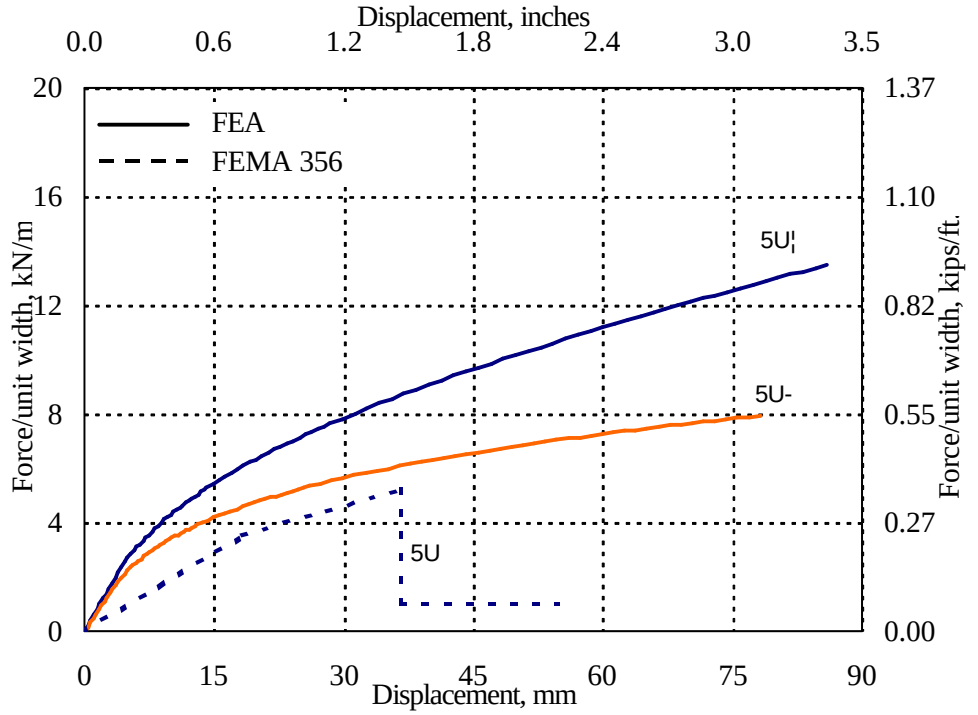

FIG. 7.24 FE Response vs. FEMA Backbone Curve – Unretrofitted Diaphragm 5

7.3.6.3 Retrofitted Diaphragms

From Figs. 7.25 to 7.29 the following similarities and differences have been found for the retrofitted diaphragms, based on comparisons between the FEMA 356 backbone curves and the predicted FE responses (the bilinear curves are for the next section):

- Strength levels have been underpredicted by FEMA 356 curves in all cases.
- Displacement levels have been overpredicted by FEMA 356 in all cases.

7.3.6.4 Proposed Modifications to FEMA 356

To account for the differences found in the shear strength and displacement for the retrofitted diaphragms described above, bilinear curves were constructed from the FE responses for each diaphragm and in both directions of loading (except for square diaphragms 1 and 5), following the criteria established in Section 4.2, to compare them with the FEMA backbone curves. After comparison of the yield shear and shear at first loss of strength and corresponding displacements of both type of curves (see Figs. 7.25 to 7.29), new values are proposed for the yield shear strength, v_y, shear stiffness, G_d, (by means of a factor determined for each parameter) and for the displacement ratio at first loss of strength, d. The strength ratio at the point of first loss of strength (α) resulted in the same value as the ratio given in FEMA 356. In the following, the values were determined for each diaphragm and in both directions of loading.

The factor for the yield shear (f_{vy}) was determined by dividing the yield shear of the bilinear curve by the yield shear from FEMA 356 (minimum value from blocked panel overlay retrofit in Table 5.5):

$$f_{ny} = \frac{n_{yFE}}{n_{yFEMA}} \tag{7.1}$$

A factor was also determined for the shear stiffness (f_{Gd}) dividing the shear stiffness based on the yield shear and displacement values of the bilinear curve (See Eq. 5.3 of FEMA 356) by the shear stiffness from FEMA 356 (value from blocked panel overlay retrofit in Table 5.1):

$$f_{Gd} = \frac{G_{dFE}}{G_{dFEMA}} \tag{7.2}$$

The displacement ratio at first loss of strength, *d*, was determined from the bilinear curve by dividing the maximum displacement (Δ_U) by the displacement at yield (Δ_Y).

$$d = \frac{\Delta_U}{\Delta_Y} \tag{7.3}$$

The strength ratio α, was calculated from the bilinear curve by dividing the strength at maximum displacement by the yield strength:

$$a = \frac{n_U}{n_Y} \tag{7.4}$$

Table 7.9 lists the parameter values determined with Eqs. 7.1 to 7.4 for each diaphragm and direction of loading (for square diaphragms 1 and 5 the parameters were assumed the same in either direction). Averages, standard deviations and coefficients of variations were computed from the list of parameter values, and rounded values are proposed as final values of the parameter factors. In general the values for each parameter are similar. For the case of the shear stiffness, the value corresponding to diaphragm 4R¦ was not used to compute the average. The proposed factors and values were used to construct a modified version of the FEMA 356 backbone curves, which are shown in Figs. 7.30 to 7.34. In general the proposed curves lie close to the predicted FE response of the diaphragms.

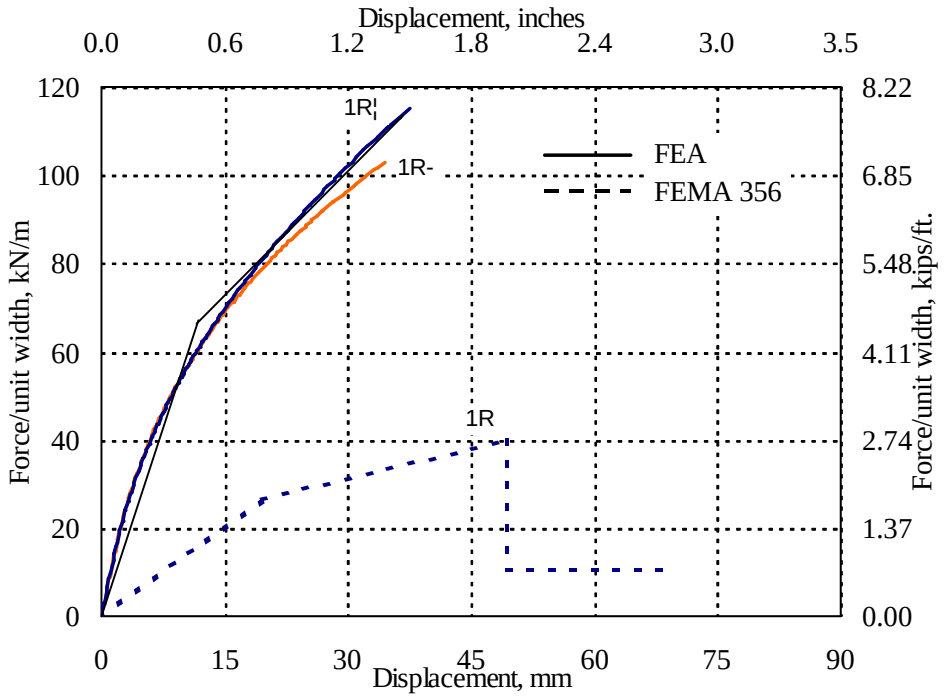

FIG. 7.25 Comparison of Responses for Diaphragm 1

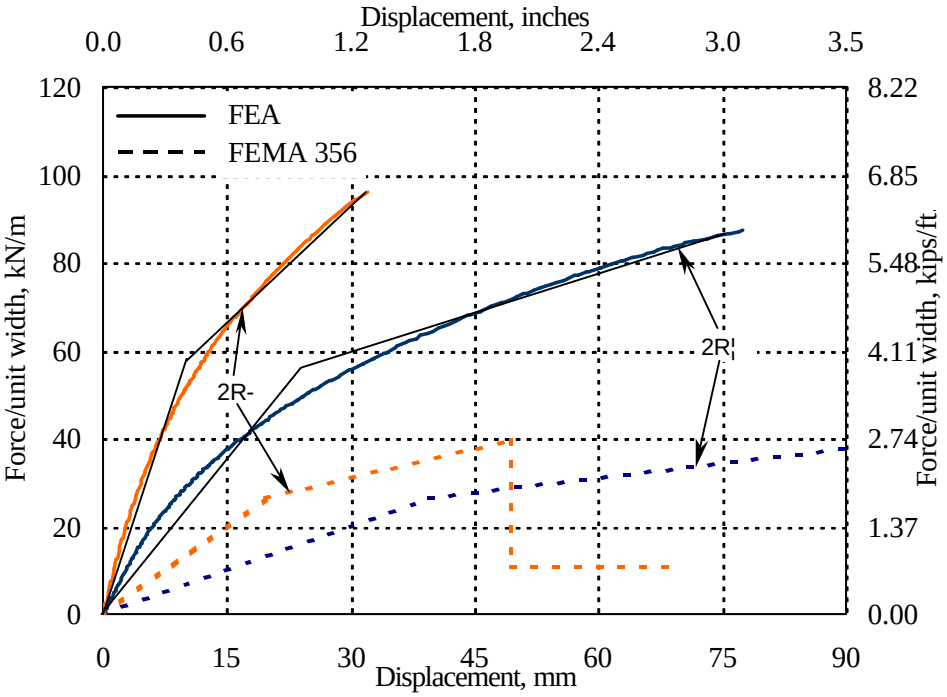

FIG. 7.26 Comparison of Responses for Diaphragm 2

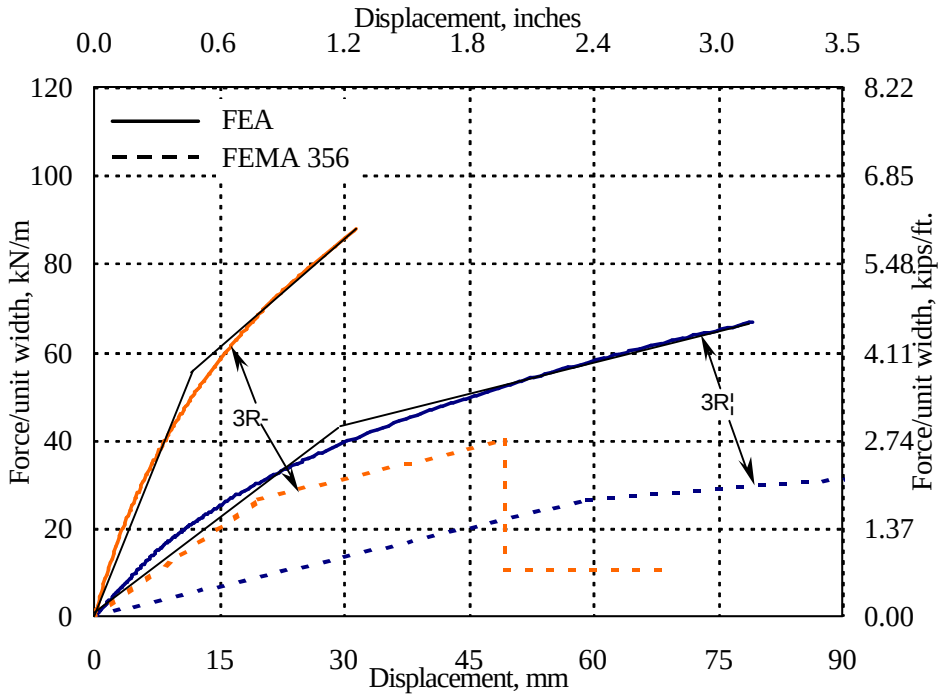

FIG. 7.27 Comparison of Responses for Diaphragm 3

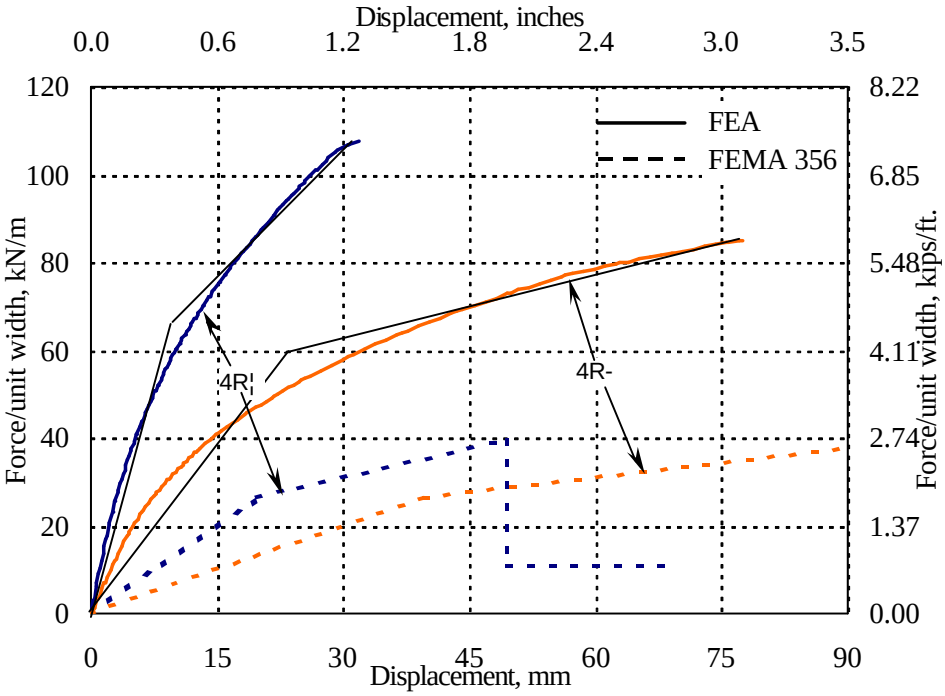

FIG. 7.28 Comparison of Responses for Diaphragm 4

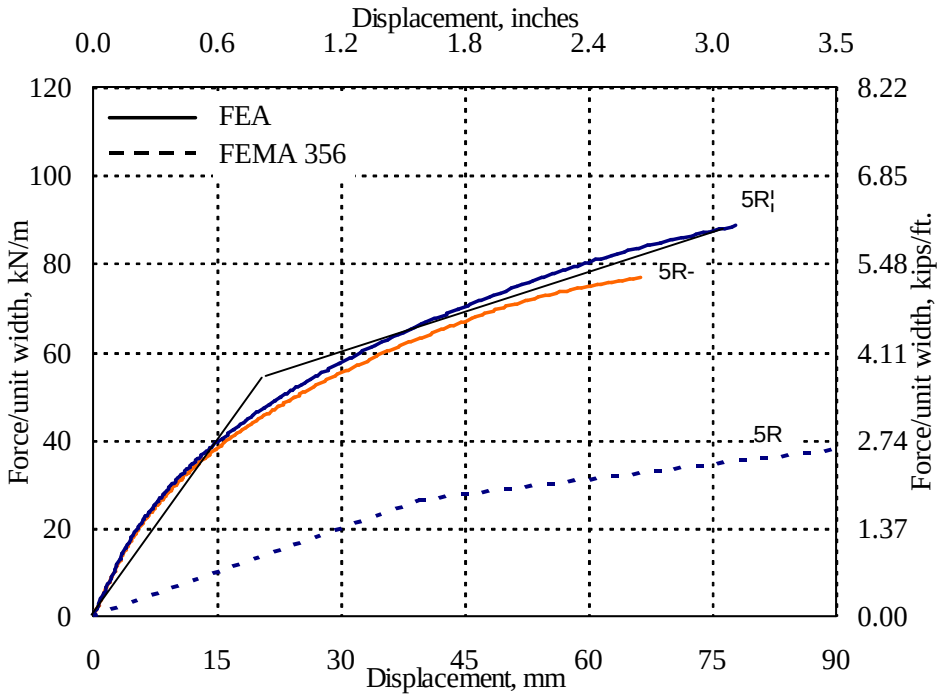

FIG. 7.29 Comparison of Responses for Diaphragm 5

Table 7.9 Proposed Modifying Values of FEMA Backbone Curve Parameters

ID	f_{Gd}	f_{vy}	*d*	a
1R	4.69	2.59	3.44	1.68
2R¦	3.59	2.17	3.24	1.52
3R¦	3.44	1.70	2.72	1.49
4R¦	6.19	2.54	3.91	1.60
5R	3.80	2.03	3.69	1.65
2R-	3.77	2.18	2.80	1.66
3R-	3.84	2.12	2.89	1.56
4R-	3.87	2.26	3.35	1.42
Average	3.86	2.20	3.25	1.57
Std. Dev.	0.37	0.27	0.40	0.09
Coeff. of Var.	9.6 %	12 %	12 %	5.7 %
Rounded	3.5	2.0	3.0	1.5

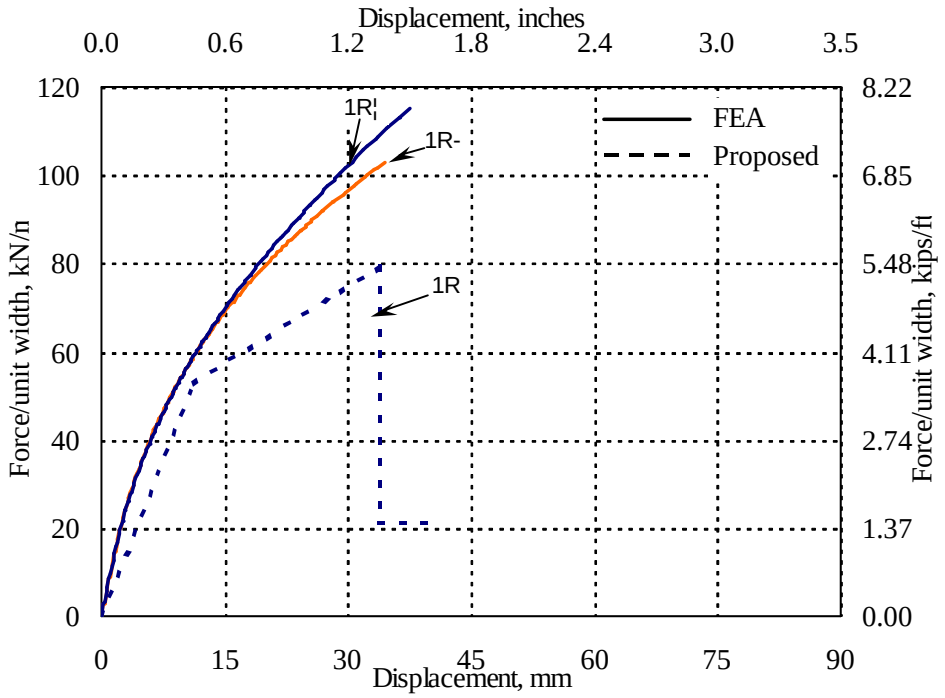

FIG. 7.30 Proposed Modification of FEMA 356 Backbone Curve – Diaphragm 1

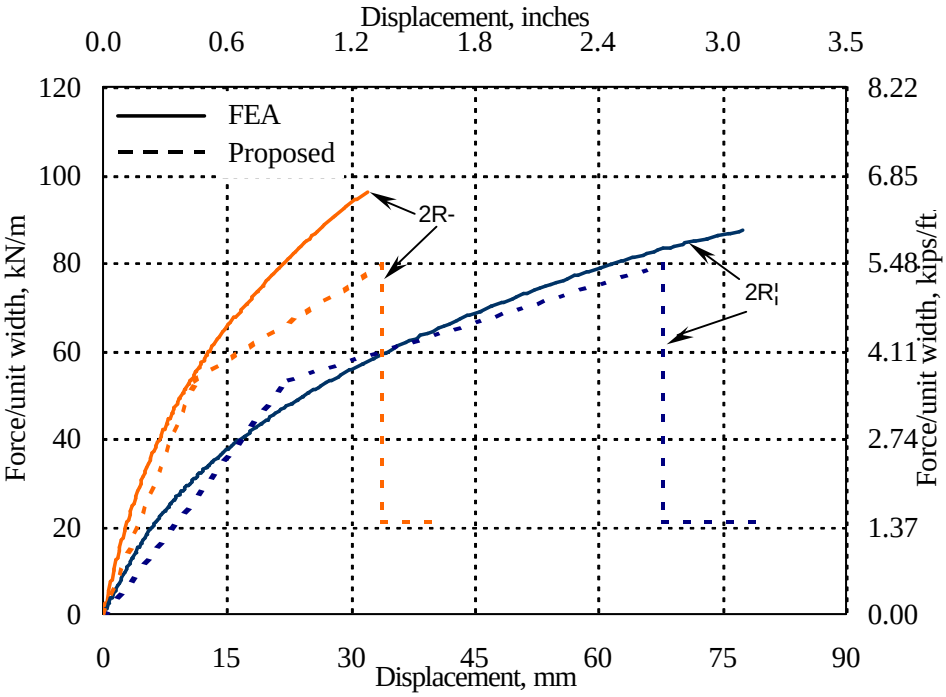

FIG. 7.31 Proposed Modification of FEMA 356 Backbone Curve – Diaphragm 2

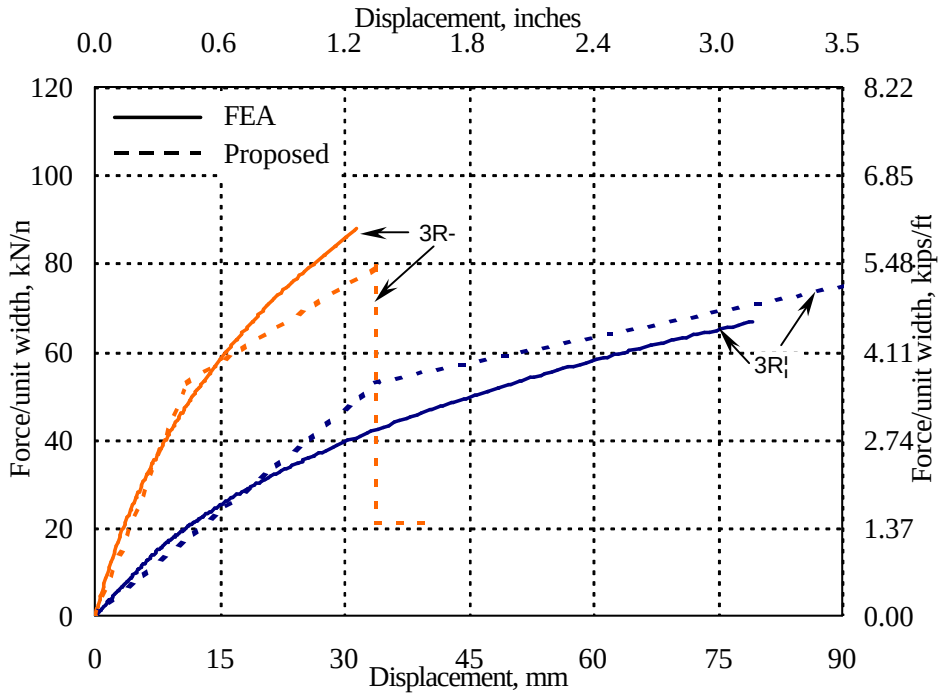

FIG. 7.32 Proposed Modification of FEMA 356 Backbone Curve – Diaphragm 3

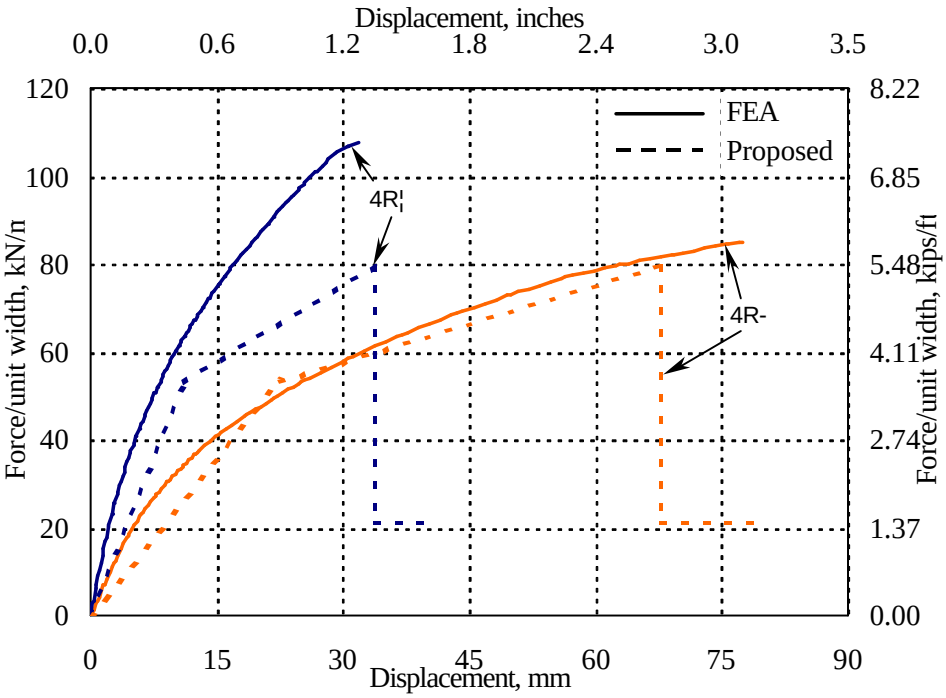

FIG. 7.33 Proposed Modification of FEMA 356 Backbone Curve – Diaphragm 4

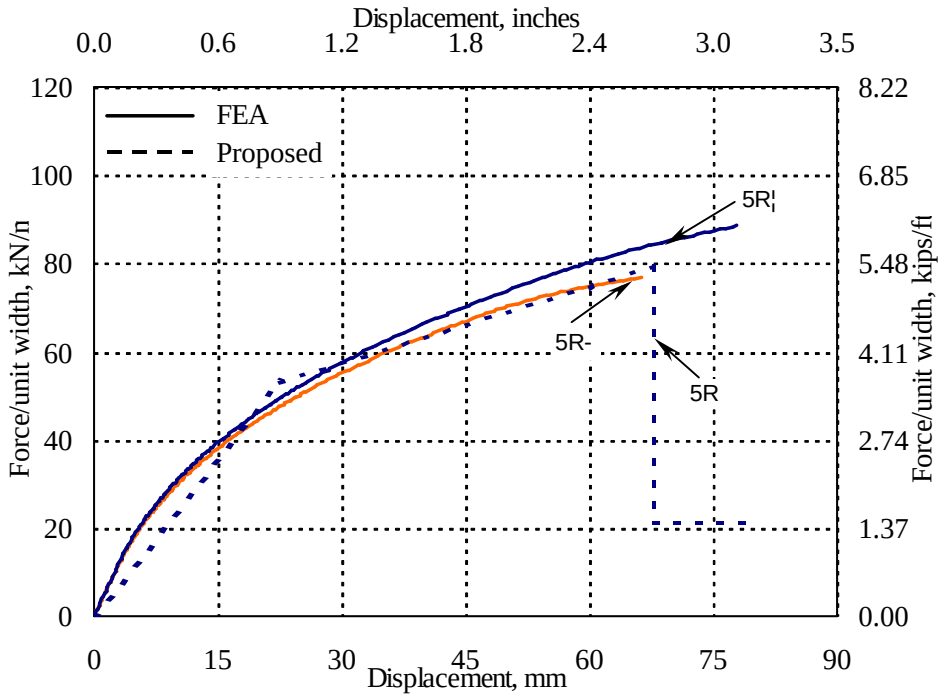

FIG. 7.34 Proposed Modification of FEMA 356 Backbone Curve – Diaphragm 5

7.4 SUMMARY

The analytical lateral in-plane response of straight sheathed wood diaphragms and retrofitted with blocked plywood panel overlay of different aspect ratios and with loading in both main directions has been presented in this section. The prediction of response of these types of diaphragms is based in the finite element method.

The response of an unretrofitted straight-sheathed diaphragm depends on the contribution of the nailed connections distributed over the sheathed surface of the diaphragm and the flexural stiffness of the wood members (i.e., the sheathing boards or the joists, depending on the direction of loading). In the case of the retrofitted diaphragms, the contribution of the panel overlay to the response is quite significant reducing the importance of the original diaphragm response.

Comparing the similarities of the responses of the unretrofitted diaphragms 1U with 4U and 2U with 5U for loading parallel to the joists in terms of force per unit width, the response of diaphragms with equal sheathing board lengths is the same, regardless of the quantity of boards in the diaphragm. For loading perpendicular to the joists, a stiffer response was found in diaphragms with short lengths compared to diaphragms of the same width but longer lengths. Therefore the orientation of the applied loading and the joist direction play an important role in the behavior of the diaphragm.

In the retrofitted square diaphragms with an aspect ratio of 1:1 (diaphragms 1R and 5R) the response tends to be similar in both directions. Small differences can occur which are attributed to the different in-plane lateral bending stiffness of the original diaphragm in each direction of loading. For retrofitted diaphragms 2R and 3R with aspect ratios 2:1 and 3:1, respectively, the responses for loading perpendicular to the joists are about 50% and 100% stiffer than the corresponding responses for loading parallel to the joists, respectively. Diaphragms 2R and 4R have the same overall dimensions, and similar responses for loading parallel to the short direction of the diaphragm were observed for the retrofitted cases. For loading parallel to the long direction, the response in diaphragm 4R is stiffer than the response of diaphragm 2R because the corresponding unretrofitted diaphragm 4U is stronger compared to the unretrofitted diaphragm 2U in that same direction. In general, the lateral response of unretrofitted and retrofitted diaphragms is different in each direction of loading.

For both unretrofitted and retrofitted diaphragms loaded parallel to the joists, it was found that the shorter the diaphragm span, the higher the nail-slip. The opposite is true for both type of diaphragms when loaded perpendicular to the joists. Nail slip values usually did not reach the limiting slip of 12.7 mm (0.5 in.) in the unretrofitted diaphragms. In the retrofitted diaphragms, the slip values usually reached the limiting slip of the nailed connection models.

Modifications are needed to the equation and parameters given in FEMA 356 to determine the response of unretrofitted diaphragms to consider the loading direction for diaphragms with short spans, and to also consider larger displacements. The comparison of FEMA 356 backbone curve with the FE responses for the retrofitted diaphragms has large differences in strength, stiffness and displacement. New values are proposed for the yield shear strength, shear stiffness (through factors listed in Table 7.9). These parameters are used to determine the backbone curve through Eq. 5.3. The displacement ratio at first loss of strength (*d*) is proposed to increase from 2.5 to 3.0. It should be mentioned that these recommendations are made based on experimental testing made on new materials built using pre-1950's construction details. Aging of the nailing and wood should be studied to determine proper values of the material mechanical properties.

It is interesting to compare the backbone curves with the expected demand from an earthquake. For this purpose, a two-story firehouse in St. Louis, Missouri, was selected to show the comparison, similar to a case study developed by Grubbs (2002). In this case the building plan dimensions were hypothetically reduced to the plan dimensions of diaphragm 2 (and diaphragm 4). For this case study the walls consist of 3-wythe brick construction with a total thickness of 33 cm (13 in.). The story heights are 4.42 m (14.5 ft.) and 3.35 m (11 ft.). A linear static procedure from FEMA 273 and FEMA 356 was used to determine the equivalent static horizontal force on the short direction of the diaphragm for an earthquake with 10% probability of exceedance in a 50-year event. Using FEMA 273 a force per unit width of 9.1 kN/m (0.6 kip/ft.) and 13.4 kN/m (0.9 kip/ft.) resulted for the unretrofitted and retrofitted cases, respectively. Using FEMA 356 a force per unit width of 4 kN/m (0.3 kip/ft.) and 7.3 kN/m (0.5 kip/ft.) resulted for the unretrofitted and retrofitted cases, respectively. Comparing the larger forces from FEMA 273 with the backbone curves of unretrofitted diaphragms 2 and 4 (Fig 7.17), we can estimate that the resulting lateral displacement is approximately 38 mm (1.5 in.), and 76 mm (3 in.) for diaphragm 2 and 4, respectively. For the

retrofitted diaphragms 2 and 4 (Fig 7.18) the lateral displacement is reduced to approximately 5 mm (0.2 in.). The plywood panel retrofit reduced the lateral displacement 7.5 and 15 times in diaphragms 2 and 4, respectively.

8. CONCLUSIONS

8.1 SUMMARY

The objective of this research was to investigate the behavior of existing and rehabilitated wood diaphragms in URM buildings under lateral in-plane loads. The focus of the research was on essential facilities, assuming a pre-1950's fire station from the St. Louis area as the prototype building. URM buildings built prior to that time lack most of the details used today for seismic design. To accomplish the research objective, both experimental and analytical research was undertaken.

The experimental research entailed the construction and testing of three specimens, which were representative of wood diaphragms in pre-1950's URM buildings. The specimens included the diaphragm and the anchor connections. Specimens were tested, retrofitted and retested again under quasi-static reversed cyclic load from a single actuator, which was applied through a loading frame connected to the diaphragm sheathing at the third points of the diaphragm span length along the diaphragm width. Different rehabilitation methods were used for retrofit, such as enhanced shear connectors and perimeter strapping, a steel truss attached to the bottom of the joists and connected to the end support frames, and unblocked and blocked plywood overlays added to the existing sheathing.

The lateral displacement response at various points along the diaphragm span, slip displacement between sheathing members and strain response of the anchor connections were measured. Backbone curves corresponding to the diaphragm midpoint were constructed from the measured cyclic curves and used to develop simpler bilinear curves to represent the behavior of the wood diaphragms, which in turn defined the yield force and yield displacement. Comparisons between the response of each unretrofitted diaphragm and their retrofits were made. The results were also compared with the

values obtained from both the FEMA 273 and FEMA 356 guidelines for the shear strength, stiffness and backbone curves of the diaphragms.

Detailed 2D finite element models of the diaphragm specimens (unretrofitted and retrofitted) were developed and calibrated to fit the experimentally measured cyclic behavior. A key part of this stage included the modeling of the nailed connections, which were modeled using nonlinear springs with hysteretic properties. Suitable models for the two types of nailed connections were selected from the literature and adapted in the diaphragm models. The calibration procedure consisted of selecting hysteretic parameters that allowed for strength deterioration and stiffness degradation.

The predicted lateral response for unretrofitted and retrofitted diaphragms with different geometries and length-to-width aspect ratios was determined for monotonic loading using similar FE models and compared with the backbone curves recommended by the FEMA 356 guidelines. The experimental and analytical results were used to develop recommendations for determining backbone curves to represent the lateral in-plane response for similar unretrofitted and retrofitted diaphragms. These recommendations are in the form of adjustments to the current FEMA 356 guidelines.

8.2 CONCLUSIONS

1. Test results show that the existing diaphragms were very flexible under in-plane loading and that all four rehabilitation methods used (steel strapping and enhanced shear connections, steel truss, unblocked plywood overlay and blocked plywood overlay) accomplished the objectives of increasing in-plane lateral shear strength and stiffness. The steel truss retrofit provided the largest increase in shear strength and stiffness, followed by the blocked plywood overlay retrofit.

2. Measured deformations of the diaphragm-to-wall anchor connections indicate that the connections can contribute to the overall lateral displacements of

diaphragms with previously undamaged connections by up to 13% (diaphragm specimen MAE-2A).

3. A comparison of the parameters of the measured response with the predictions from the FEMA 273 and FEMA 356 guidelines for seismic rehabilitation shows the following differences:

   - For the T&G diaphragm and retrofits, the measured shear strength and stiffness of the diaphragm were lower than predicted by both FEMA 273 (64% to 68% for shear and 3% to 12% for stiffness) and FEMA 356 (87% to 90% for shear and 20% to 73% for stiffness). In the straight sheathed diaphragms and retrofits, the measured shear strength was higher than predicted by FEMA 273 (143% to 228%) and FEMA 356 (107% to 228%), except for the case of diaphragm MAE-2C (93% for FEMA 273 and 70% for FEMA 356). The measured effective stiffness was lower than the FEMA 273 value in half of the cases (42% to 76%) and higher for the other half (108% to 119%); the measured stiffness was higher for all of the FEMA 356 values (263% to 478%).
   - The ductility *m* factors are overpredicted for the T&G diaphragm and the plywood panel overlay diaphragm (MAE-1, MAE-2B, MAE-2C, MAE-3B). This can lead to an unconservative design due to overestimating the available ductility.
   - The experimental backbone curves did not show the reduction of shear strength that is given by the predicted backbone curves. For the level of displacements applied, the experimental backbone curves can be represented by a bilinear curve requiring only the definition of the yield point and the ultimate point. However, in design the constraints of the out-of-plane URM walls and its connections must be considered.

4. McLain's lower bound connection model was adopted to represent nail slip behavior of the nails used in the tests. FE analyses using the nailed connection model, predict cyclic behavior with a satisfactory degree of approximation for unretrofitted diaphragm specimens. For the case of the retrofitted diaphragm specimens, the analyses provides a low estimation of dissipated energy because the predicted hysteretic loops were not wide enough.

5. A comparison of the FE responses of the diaphragms with different geometries and aspect ratios with the predictions from the FEMA guidelines shows the following:
   - FEMA 356 provided a better approximation of the backbone curves of diaphragms as compared to FEMA 273. The expression that defines the yield displacement and shape of the curve gives a better prediction of the experimental curves.
   - A modification is needed for the FEMA 356 expressions used to develop the backbone curve for unretrofitted diaphragms to consider the loading direction relative to the joist direction, especially for short span diaphragms. In addition, displacements corresponding to the point of first loss of strength need to be increased. New values of the parameters used in the FEMA expressions are proposed for straight-sheathed diaphragms retrofitted with blocked plywood overlay. These values are given in Section 7.

8.3 RECOMMENDATIONS FOR FUTURE WORK

The following recommendations will provide a better understanding of the interaction of the flexible floor diaphragm, out-of-plane walls and rigid in-plane walls in URM buildings, for assessing rehabilitation methods for better performance of these structures under seismic motions.

1. Dynamic tests on URM building specimens with rehabilitated flexible diaphragms should be performed. Scaled models should be tested on a shaking table to determine the interaction of the diaphragm and wall elements and to determine the failure sequence of the elements of the structure. Simultaneous motion in both orthogonal directions should be applied to the specimen.

2. This testing is limited to 2:1 length-to-width aspectio ratio. Quasi-static reverse cyclic tests on rehabilitated wood diaphragms covering a range of length-to-width aspect ratios should be performed to verify the predicted FE responses and the proposed modifications of the parameters given in FEMA 356 for the construction of backbone curves.

3. Three-dimensional dynamic inelastic analyses of URM buildings with retrofitted flexible diaphagm models should be performed to determine the interaction between the in-plane and out-of-plane walls and the rehabilitated floor and roof diaphragms. Using the results of the experimental data for diaphragms from this research and the measured behavior of URM walls obtained in other projects of the MAE Center, nonlinear element models can be developed for analysis. This study should also verify that stiffening the diaphragm does not amplify the seismic demand on the URM walls and determine whether the diaphragm drives the motion of the out-of-plane walls of a URM building, as stated by previous research (ABK 1984, Tena-Colunga 1992). Simpler two-dimensional models should be developed for design, based on a detailed three-dimensional analysis. A common cause of failure found in past earthquakes, occurred as a result of out-of-plane wall failures. For this reason, it will be important to focus the study on the diaphragm and the out-of-plane-wall behavior, including the connections.

4. A material testing program of the wood and nail components of diaphragms should be conducted considering aging as a factor to determine proper values of the mechanical properties.

REFERENCES

Agbabian, M. S., Barnes, S. B. and Kariotis, J. C. (ABK) (1981). "Methodology for Mitigation of Seismic Hazards in Existing Unreinforced Masonry Buildings: Diaphragm Testing." National Science Foundation, Washington, D.C.

Agbabian, M. S., Barnes, S. B. and Kariotis, J. C. (ABK) (1984). "Methodology for Mitigation of Seismic Hazards in Existing Unreinforced Masonry Buildings: The Methodology." National Science Foundation, Washington, D.C.

American Forest & Paper Association (AF&PA) (1996). "LRFD Manual for Engineered Wood Construction." AF&PA, Washington, D.C.

American Forest & Paper Association (AF&PA) (1997). "National Design Specification for Wood Construction." NDS, Washington, D.C.

American Forest & Paper Association/American Society of Civil Engineers AF&PA/ASCE (1995). "Standard for Load and Resistance Factor Design (LRFD) for Engineered Wood Construction." *AF&PA/ASCE 16-95*, Reston, Virginia.

American Institute of Steel Construction AISC (1995). "Manual of Steel Construction." LRFD 2nd Ed., AISC, Chicago, Illinois.

American Society of Civil Engineers (ASCE) (2000). "Prestandard and Commentary for the Seismic Rehabilitation of Buildings." *FEMA Publication 356*, Federal Emergency Management Agency, Washington, D.C.

APA – The Engineered Wood Association (APA) (1985). "Design/Construction Guide - Residential and Commercial." APA, Tacoma, Washington.

APA – The Engineered Wood Association (APA) (1986). "Plywood Design Specification." APA, Tacoma, Washington.

Applied Technology Council (ATC) (1981). "Guidelines for the Design of Horizontal Wood Diaphragms." *ATC-7*, ATC, Berkeley, California.

Applied Technology Council (ATC) (1997a). "NEHRP Guidelines for the Seismic Rehabilitation of Buildings." *FEMA Publication 273*, Building Seismic Safety Council, Washington, D.C.

Applied Technology Council (ATC) (1997b). "NEHRP Commentary on the Guidelines for the Seismic Rehabilitation of Buildings." *FEMA Publication 274*, Building Seismic Safety Council, Washington, D.C.

Breyer, D. E. (1999). *Design of Wood Structures*,. 4th Ed., McGraw-Hill, New York.

Bruneau, M. (1994). "State-of-the-Art Report on Seismic Performance of Unreinforced Masonry Buildings." *Journal of Structural Engineering*, 120(1), 230-251.

Cheung, C. (1984). "Dynamic Response of Wood Diaphragms in Low-Rise Wood Framed Buildings." Ph.D. dissertation, Department of Civil Engineering, Washington State University, Pullman.

Chopra, A. (1995). *Dynamics of Structures*, 1st Edition, Prentice Hall, Englewood Cliffs, New Jersey.

Countryman, D. (1952). "Lateral Tests on Plywood Sheathed Diaphragms." *Laboratory Report 55*, Douglas Fir Plywood Association, Tacoma, Washington.

Countryman, D. (1955). "1954 Horizontal Plywood Diaphragm Tests." *Laboratory Report 63*, Douglas Fir Plywood Association, Tacoma, Washington.

CUREE (2002). "Recommendations for Earthquake Resistance in the Design and Construction of Woodframe Buildings", Final Review Draft, 15 November.

Consortium of Universities for Research in Earthquake Engineering, CUREE, California Institute of Technology, <www.curee.org>

Foliente, G. (1995). "Hysteresis Modeling of Wood Joints and Structural Systems." *Journal of Structural Engineering*, 121(6), 1013-1022.

Grubbs, A. (2002). "Seismic Rehabilitation of Wood Diaphragms in Unreinforced Masonry Buildings." M.S thesis, Department of Civil Engineering, Texas A&M University, College Station, Texas.

Hamburger, R. O. and McCormick, D. L. (1994). "Implications of the January 17, 1994 Northridge Earthquake on Tilt-up and Masonry Buildings with Wood Roofs." *Northridge Earthquake: Lessons Learned, 1994 SEAONC Spring Seminar*, San Francisco, California.

Hibbitt, Karlsson, Sorensen (2000). *ABAQUS Standard User's Manual – Version 6.1*. Pawtuckett, Rhode Island.

ICBO, (1976). "Uniform Building Code." International Conference of Building Officials, Whittier, California.

ICBO, (1997). "Uniform Code for Building Conservation." International Conference of Building Officials, Whittier, California.

Johnson, J. W. (1956). "Lateral Tests on Full-Scale Lumber and Plywood-Sheathed Roof Diaphragms." *paper no. 56-S-16*, The American Society of Mechanical Engineers (ASME) Spring Meeting, Portland, Oregon, March 19-21, 1956.

Kuenzi, E. W., (1955) "Theoretical Design of a Nailed or Bolted Joint under Lateral Load," *Report No. D1951*, U.S. Dept. of Agriculture, Forest Production Laboratory, Madison, Wisconsin.

Mahin S. and Bertero V. V. (1976). "An Evaluation of Inelastic Seismic Design Spectra." *Journal of the Structural Division*, 107(ST9), 1777-1795.

McLain, T. E. (1975). "Curvilinear Load-Slip Relations in Laterally-Loaded Nailed Joints." Ph.D. dissertation, Department of Forest and Wood Sciences, Colorado State University, Fort Collins.

Paquette, J. and Bruneau, M. (2000). "Pseudo-Dynamic Testing of Unreinforced Masonry Buildings with Flexible Diaphragm." *Proceedings of the 12th World Conference on Earthquake Engineering*, Auckland, New Zealand, paper 1367, 1-7, available on CD-ROM only.

Park, Y., Reinhorn, A. and Kunnath, S. (1987). "IDARC: Inelastic Damage Analysis of Reinforced Concrete Frame – Shearwall Structures." *Technical Report NCEER-87-0008*, National Center for Earthquake Engineering Research, State University of New York at Buffalo.

Pellicane, P., Stone, J. and Vanderbilt, M. D. (1991). "Generalized Model for Lateral Load Slip of Nailed Joints." *Journal of Materials in Civil Engineering*, 3(1), 60-77.

Sathyamoorthy, M. (1997). *Nonlinear Analysis of Structures*, 1st Edition, CRC Press, Boca Raton, Florida.

Stelzer, C. D. (1999). "On Shaky Ground." *St. Louis Riverfront Times*. December 15, <www.riverfronttimes.com/issues/1999-12-15/feature.html>

Tena-Colunga, A. (1992). "Seismic Evaluation of Unreinforced Masonry Structures with Flexible Diaphragms." *Earthquake Spectra*, 8(2),.305-318.

Tissell, J. R. (1967). "1966 Horizontal Plywood Diaphragm Tests." *Laboratory Report 106*, American Plywood Association, Tacoma, Washington.

Tissell, J. R. and Elliott, P. E. (1997). "Plywood Diaphragms." *Report 138*, The Engineered Wood Association (APA), Tacoma, Washington.

White, D. and Kim, S. (2000). "Diaphragm and Wall Elements for Analysis of Low-Rise Building Structures: ABAQUS User Element Manual." Georgia Institute of Technology, Atlanta, Georgia.

Wilkinson, T. L. (1971). "Theoretical Lateral Resistance of Nailed Joints." *Journal of the Structural Division*, 97(ST5), 1381-1398.

Wilkinson, T. L. (1972). "Analysis of Nailed Joints with Dissimilar Members." *Journal of the Structural Division*,.98(ST9), 2005-2013.

Winistorfer, S. and Soltis, L. (1994). "Lateral and Withdrawal Strength of Nail Connections for Manufactured Housing." *Journal of Structural Engineering*, 120(12), 3577-3594.

Yi, T., Moon, F., Leon, R., Kahn, L. (2002). "Performance Characteristics of Unreinforced Masonry Low-rise Structure before and after Rehabilitation," Urban Earthquake Risk - *Proceedings of the Seventh U.S. National Conference on Earthquake Engineering (7NCEE)*, EERI, Boston, Massachusetts, July, available on CD-ROM only.

Zagajeski, S., Halvorsen, G. T., Ganga Rao, H.V.S., Luttrell, L. D., Jewell, R. B., Corda, D., N. and Roberts, J. D. (1984). "Theoretical and Experimental Studies on Timber Diaphragms Subject to Earthquake Loads," *Final Summary Report*, Department of Civil Engineering, West Virginia University, Morgantown.

APPENDIX

The following calculations are required to determine parameter B as given in Eq. 6.4. The equations were developed by Kuenzi (1955), based on the theory of beams on elastic foundations. The given equations are used to determine the load that produces a joint slip of 0.015 in. The following expressions were taken from Wilkinson (1972).

Theoretical Derivations

The differential equation for the deflection curve of a beam supported on an elastic foundation is:

$$EI\frac{d^4y}{dx^4} = -ky \tag{A.1}$$

where:

E = Modulus of elasticity of the nail
I = Moment of inertia of the nail
y = Deflection at point x
k = Foundation modulus

The foundation modulus can be expressed as:

$$k = k_o d \tag{A.2}$$

where:

k_o = elastic bearing constant
d = nail diameter

Wilkinson gives a relationship between the elastic bearing constant and the specific gravity, in kips/in.^{3}:

$$k_o = 2144(SG) \tag{A.3}$$

where SG is the specific gravity.

The solution of Eq. A.1 results in expressions involving a characteristic

$$l = \sqrt[4]{\frac{k}{4EI}} \tag{A.4}$$

Kuenzi developed a relationship between the load and the slip for a two-member wood joint.

$$d = P\left[2(L_1 + L_2) - \frac{(J_1 - J_2)^2}{K_1 + K_2}\right] \tag{A.5}$$

where

d = joint slip
P = load

The expressions for factors L_1, L_2, J_1, J_2, K_1 and K_2 are listed in Table A.1.

Table A.1 Expressions for Factors in Eq. A.5

Factor	Expression
L_1	$\frac{l_1}{k_1}\left[\frac{\sinh l_1 a \cosh l_1 a - \sin l_1 a \cos l_1 a}{\sinh^2 l_1 a - \sin^2 l_1 a}\right]$
L_2	$\frac{l_2}{k_2}\left[\frac{\sinh l_2 b \cosh l_2 b - \sin l_2 b \cos l_2 b}{\sinh^2 l_2 b - \sin^2 l_2 b}\right]$
J_1	$\frac{l_1^2}{k_1}\left[\frac{\sinh^2 l_1 a + \sin^2 l_1 a}{\sinh^2 l_1 a - \sin^2 l_1 a}\right]$
J_2	$\frac{l_2^2}{k_2}\left[\frac{\sinh^2 l_2 b + \sin^2 l_2 b}{\sinh^2 l_2 b - \sin^2 l_2 b}\right]$
K_1	$\frac{l_1^3}{k_1}\left[\frac{\sinh l_1 a \cosh l_1 a + \sin l_1 a \cos l_1 a}{\sinh^2 l_1 a - \sin^2 l_1 a}\right]$
K_2	$\frac{l_2^3}{k_2}\left[\frac{\sinh l_2 b \cosh l_2 b + \sin l_2 b \cos l_2 b}{\sinh^2 l_2 b - \sin^2 l_2 b}\right]$

Note: *a*, and *b* are the member thicknesses, or if the nail does not completely penetrate the member, then *a* or *b* is the depth of penetration. The subscripts refer to either member 1 or member 2.